Politechnika Wrocławska

FIELD OF SCIENCE: Natural sciences

DISCIPLINE OF SCIENCE: **Chemical Sciences (Nauki Chemiczne)**

DOCTORAL DISSERTATION

New fluorescent markers for one- and two-photon microscopy with emphasis on amyloid detection

Nowe znaczniki fluorescencyjne do mikroskopii jedno- i dwufotonowej ze szczególnym uwzględnieniem wykrywania amyloidów

Agata Hajda, MSc Eng.

Supervisor:

Dr hab. Joanna Olesiak-Bańska, prof. uczelni

Keywords: two-photon absorption, amyloids, nanoclusters, fluorescence, BF-functionalized dyes

WROCŁAW 2026

Funding and Doctoral Institution

The part of the research was financed by the project NCN OPUS-22 (2021/43/B/ST5/00753): „Nowe dwufotonowe absorbery o architekturze dipolowej i kwadrupolowej: od syntezy po zastosowania.”

The research was mainly performed in the laboratories of the Institute of Advanced Materials at the Chemistry Faculty of Wroclaw University of Science and Technology.

List of the author's scientific publications completed as part of her doctoral dissertation:

1. **Agata Hajda,** Lizaveta Petrusevich, Robert Zaleśny, Borys Ośmiałowski, Joanna Olesiak-Bańska. Novel O,N,O-coordinated organofluoroboron probe for amyloid detection: insight from experiment and theory. Chemical Communications. 2025, vol. 61, nr 20, s. 3990-3993
   DOI: 10.1039/d5cc00243e
2. **Agata Hajda**, Rweetuparna Guha, Stacy Marla. Copp, Joanna Olesiak-Bańska. Two photon brightness of NIR-emitting, atomically precise DNA-stabilized silver nanoclusters. Chemical Science. 2025, vol. 16, nr 4, s. 1737-1745
   DOI: 10.1039/d4sc05853d
3. **Agata Hajda**, Manuela Grelich-Mucha, Patryk Rybczyński, Borys Ośmiałowski, Robert Zaleśny, Joanna Olesiak-Bańska. BF2-Functionalized Benzothiazole Amyloid Markers: Effect of Donor Substituents on One- and Two-Photon Properties. ACS Appl. Bio Mater. 2023, 6, 12, 5676–5684.
   DOI: 10.1021/acsabm.3c00815

Other publications in scientific journals:

1. Patryk Rybczyński*, **Agata Hajda***, Robert Zaleśny, Borys Ośmiałowski, Joanna Olesiak-Bańska. Thioflavin T inspirations: on the photophysical and aggregation properties of fluorescent difluoroborates based on the benzothiazole core. Journal of Physical Chemistry A. 2025, vol. 129, nr 15, s. 3663-3671.
   DOI: 10.1021/acs.jpca.5c01254
   *P.R. and A.H. contributed equally to this work.
2. Malavika KayyilVeedu , **Agata Hajda** , Joanna Olesiak-Bańska , Jérôme Wenger . Threspecies multiplexing of fluorescent dyes and gold nanoclusters recovered with fluorescence lifetime correlation spectroscopy. BBA - General Subject. 2024, 1868, Issue 6.
   DOI: 10.1016/j.bbagen.2024.130611
3. Dipankar Bain, Hao Yuan, Anna Pniakowska, **Agata Hajda**, Charlène Bouanchaud, Fabien Chirot, Clothilde Comby-Zerbino, Virginie Gueguen-Chaignon, Vlasta Bonačić-Koutecký, Joanna Olesiak-Banska, Željka Sanader Maršić and Rodolphe Antoine , One- and two-photon brightness of proteins interacting with gold. A closer look at gold–insulin conjugates. Nanoscale, 2024,16, 14953-14958.
   DOI: 10.1039/D4NR01697A
4. Malavika Kayyil Veedu, Julia Osmólska, **Agata Hajda**, Joanna Olesiak-Bańska, Jérôme Wenger. Unveiling the photoluminescence dynamics of gold nanoclusters with fluorescence correlation spectroscopy. Nanoscale Advances. 2024, vol. 6, nr 2, s. 570-577.
   DOI: 10.1039/D3NA00869J
5. Dorota Dudek, Emilia Dzień, Joanna Wątły, Agnieszka Matera-Witkiewicz, Aleksandra Mikołajczyk, **Agata Hajda**, Joanna Olesiak-Bańska, Magdalena Rowińska-Żyrek, Zn(II)

binding to pramlintide results in a structural kink, fibril formation and antifungal activity. Sci Rep 12, 20543 (2022).
DOI: 10.1038/s41598-022-24968-y

Publications under review in scientific journals:

1. **Agata Hajda**, Patryk Rybczyński, Weronika Andrzejczak, Borys Ośmiałowski, Joanna Olesiak-Bańska. Thioflavin-T derivatives with controlled AIE and ACQ properties as potential one-photon and two-photon amyloid markers. **DOI: 10.26434/chemrxiv-2025-spn41** (text available on ChemRxiv)
2. **Agata Hajda**, Patryk Obstarczyk, Joanna Olesiak-Bańska. NIR excitation in atomically precise nanoclusters via 2-photon and 3-photon absorption. (review)

Acknowledgements

I would like to begin these acknowledgements to express my sincere gratitude to my Supervisor Prof. Joanna Olesiak-Bańska for her invaluable guidance, support, and encouragement throughout my doctoral studies. Her insightful advice, patience, and continuous belief in my work were essential to the completion of this dissertation. I am deeply grateful for the opportunity to participate in the international conferences, internships and be part of international cooperation with other scientists, which have significantly contributed to my development as a researcher. It has been a privilege to learn from and work with such an inspiring mentor.

I would like to thank my colleagues from the NONA group - Anna Pniakowska, Patryk Obstarczyk, Maciej Lipok, Manuela Grelich-Mucha. They taught me new techniques, syntheses and were helpful at every step when I had problems as a beginner in the lab. Thank you for amazing atmosphere in the laboratory. I also want to thank my friend from other group - Olga Kaczmarczyk, which was emotional support thought this PhD journey. She was always helpful with Transmission Electron Microscopy of amyloids. I want to thank also Patryk Rybczyński from UMK, who synthesized most of the compounds I was working on.

My sincere thanks goes to colleges and supervisor during my internships abroad. Firstly, I want to thank Prof. Vladimir Torbev from University of Strasbourg, where I learned Solid Phase Peptide Synthesis. This internship also taught me determination and showed me a different scientific perspective. During that time extremely helpful was Thomas Bachelart, which helped me with experiment in the laboratory and thought me foundation of synthesis and purification of peptides. Secondly, I want to thank Prof. Rodolphe Antoine from CNRS - Institute for Light and Matter, Lyon, where I could gain knowledge about Mass Spectrometry of metal nanoclusters. Every colleges in Lyon were supportive, however one person I want to thank the most - Hao Yuan.

There are also many scientists, who impacted my research. I would like to specially thank Professor Rober Zaleśny and Professor Borys Ośmiałowski during collaboration regarding organic dyes for 2PFM. I want to also thank PhD Aneta Tarczewska for overcoming my problems with electrophoresis.

I want to thank my fiancé – Paweł Szmalcel, who has been supportive of me since the beginning of my doctorate, thank you for your understanding and support in the further development of my scientific career. I want too also thank my brother Paweł Hajda, who wishes me a Nobel Prize, or at least to become a Professor (I don't know if I can handle such a challenge).

I would like to dedicate this dissertation to my parents – Teresa and Krzysztof Hajda, who have always supported me and they encouraged me to develop my scientific interests. Even when I felt something was too difficult, they trusted in my abilities and encouraged me to

keep going. I know how important education is to you, because it has opened many paths in your life, and therefore in mine.

I. CONTENTS

LIST OF ABBREVIATIONS:

GM –Göppert Mayer (unit)

FQY – Fluorescence quantum yield

2PFM - Two-Photon Fluorescence microscopy

1PFM- One-Photon Fluorescence microscopy

2PA – two-photon absorption

1PA- one-photon absorption

2PE- two-photon excitation

NIR – near infrared

Ag_NDNA - DNA-templated silver nanoclusters

TEM- Transmission Electron microscope

AFM- Atomic Force Microscope

CT - charge transfer

ICT - intramolecular charge transfer

TICT - Twisted Intramolecular Charge Transfer

ThT- Thioflavin-T

2PEL - Two-photon excited luminescence

PET - Positron emission tomography

MeO-X04 - Methoxy-X04

ML- Machine Learning

ABSTARCT:

The subject of the dissertation is fluorophores for potential use in microscopy and spectroscopy, with an emphasis on fluorophores that can be effectively excited by two photons.

This doctoral dissertation is divided into two main sections: a literature review and an experimental section. The literature section consists of four main chapters: 1) Two-photon absorption, including a subsection on Two-photon Fluorescence Microscopy (2PFM); 2) Fluorophores for 2PFM; 3) Amyloids, including a subsection on two-photon fluorescent probes for amyloid detection. Its purpose is to outline the motivations and scientific gap addressed by the dissertation. The literature review aims to explain the importance of research on specific fluorescent markers, as well as the broader scientific and social context: 1) The importance of fluorescence microscopy with an emphasis on 2PFM in medical and biological sciences; 2) How to respond to the limitations of organic fluorophores in bioimaging with DNA-stabilized silver nanoclusters (Ag_N-DNA); 3) The importance of 2PFM in amyloid research; 4) The current state of knowledge on the principles of constructing markers for amyloids, with an emphasis on two-photon probes; 5) The importance of research on amyloids, which is related to their connection with human diseases. It was important for the author of the dissertation to demonstrate how fundamental studies on the optimization of two-photon absorbers, as well as a deeper understanding of their optical properties upon binding to amyloids, can be effectively translated into preclinical research — the driving force behind clinical studies and the development of effective medical therapies. Fluorescent probes are designed either to find direct application or to serve as a starting point for further modification. The hypotheses of this doctoral dissertation are as follows: **Hypothesis 1:** BF2-functionalized benzothiazoles can serve as fluorescent amyloid probes. Modification of the localization of functional groups in the molecules has an impact on optical properties of studied fluorophores bound to amyloid fibrils; **Hypothesis 2:** 2PA of fluorophores bound to amyloids is different than the one of free molecules and can be modulated based on their chemical and consequently electronic structure; **Hypothesis 3**: Atomically-precise nanoclusters Ag_N-DNA can have high two-photon absorption cross-section (σ_2) and two-photon brightness ($\sigma_{2,B}$) exceeding 50 GM, which will make them competitive potential probes for bioimaging. In addition to the hypotheses, the goals of the doctoral dissertation were also formulated: **Goal 1**: Prove that new fluorophore scaffold based on BF moiety interact with amyloids and have improved optical properties (red-shifted absorption and emission and high values of σ_2), as compared to commercially available standard Methoxy-X04; **Goal 2**: Determine relationship between the modulation of 2PA of studied fluorophores bound to amyloid with the structure of fluorophores; **Goal 3**: Proposing new NIR-emitting nanoparticles, which are water-soluble two-photon absorbers and confirm their optical properties.

The second part of the dissertation, i.e., the experimental part, refers to the specific objectives and hypotheses of the dissertation, with a final paragraph on the summary and further prospects resulting from the research conducted as part of this dissertation. Experimental part focuses on

three articles, two of which concern organic markers for amyloids, and one focuses on silver nanoclusters as new potential two-photon markers. Each article is a separate subsection, which presents a description of the research objective, a discussion of key results, and a summary. Each summary indicates which hypotheses and goals of the doctoral dissertation are addressed by a given scientific article. A detailed description of all results, discussions, and the experimental part is included in the attached articles and supplementary materials.

Answering the hypotheses and achieving the goals of this dissertation required the use of a number of spectroscopic methods, such as one-photon absorption measurements, fluorescence and fluorescence excitation spectra, Fluorescence Quantum Yield (FQY), and fluorescence lifetime. Fluorescence techniques were also used to determine specific parameters such as dissociation constant (K_d), photostability of systems, and interactions of organic dyes with amyloids. Nonlinear optical measurements, i.e., two-photon excited luminescence, were used to determine σ_2 and $\sigma_{2,B}$. Atomic force microscopy (AFM) and transmission electron microscopy (TEM) were used to confirm the formation of amyloids from native proteins.

Article 1, entitled "BF2-Functionalized Benzothiazole Amyloid Markers: Effect of Donor Substituents on One- and Two-Photon Properties" presented in section III “Published Work - Description of own research” describes the effect of the position of the electron donor group (-methoxy) in the core composed of BF2-functionalized benzothiazole on one- and two-photon properties after binding with amyloids. The research addresses the limited understanding of the influence of the structure of the fluorophore on the modulation of optical properties after binding with amyloids. In particular, in the field of two-photon absorption modulation, there is a lack of systematic work addressing this issue. An innovative aspect of the work is the determination of cross sections for two-photon absorption before and after binding with amyloids, as the literature presents measurements of cross sections determined only in solvents. The work responds to **hypotheses 1** and **2**, and **goal 2**.

Article 2, entitled “Two-photon brightness of NIR-emitting, atomically precise DNA-stabilized silver nanoclusters”, presented in section III “Published Work - Description of own research”, focuses on the two-photon absorption of four representatives of silver nanoclusters stabilized with DNA oligonucleotides (Ag_N-DNA). For the first time in the literature, I presented two-photon absorption cross-section and two-photon brightness of atomically precise Ag_N-DNA. The research addresses the limitations of organic two-photon absorbers, such as NIR emission (>700 nm) characterized by high fluorescence quantum yields and water solubility. The work addresses **hypothesis 3** and **goal 3**, that Ag_N-DNA have two-photon brightness above 50 GM, which provides a basis for their use in bioimaging.

Article 3, entitled “A novel O,N,O-coordinated organofluoroboron probe for amyloid detection: insight from experiment and theory,” presented in section III “Published Work - Description of own research”, focuses on presenting a new structure that interacts with amyloids and has better optical properties such as fluorescence shifted towards longer

wavelengths, higher cross sections for two-photon absorption, and a wider range of two-photon excitation, even in the range above 1000 nm, than the commercially available standard for two-photon microscopy for staining amyloids – Methoxy-X04. The work also presents a solution for modifying the structure based on O,N,O-coordinated organofluoroborane in order to increase fluorescence quantum yield and two-photon absorption cross-section. The research responds to **hypothesis 2** and **goal 1**of developing a new marker for amyloids that would be competitive with the commercially available standard.

At the end of the dissertation, a possible perspective for the further development of the research contained in this doctoral dissertation is presented, as well as a general overview of the topics discussed.

ABSTRACT IN POLISH (STRESZCZENIE PRACY):

Tematyką rozprawy są fluorofory do potencjalnego zastosowania w mikroskopii, z akcentem na fluorofory, które mogą być efektywnie wzbudzane dwufotonowo.

Niniejsza rozprawa doktorska jest podzielona na dwie główne sekcje: część literaturową oraz część eksperymentalną. Część literaturowa składa się z 4 głównych rozdziałów: 1) Absorpcja dwufotonowa (2PA), w tym podrozdział o mikroskopii dwufotonowej; 2) Fluorofory do zastosowań w mikroskopii dwufotonowej; 3) Amyloidy, w tym podrozdział o znacznikach fluorescencyjnych wzbudzanych dwufotonowo do znakowania amyloidów. Ma ona na celu przybliżyć motywacje oraz lukę naukową na którą odpowiada rozprawa doktorska i zawarte w niej badania. Przegląd literatury ma na celu przybliżenie znaczenia badań nad konkretnymi znacznikami fluorescencyjnymi, jak i również zaprezentować szerszy kontekst naukowy oraz społeczny: 1) Znaczenie mikroskopii fluorescencyjnej z naciskiem na mikroskopię dwufotonową w naukach medycznych, biologicznych; 2) Jak na ograniczenia fluoroforów organicznych w bioobrazowaniu odpowiadają nanoklastry srebra stabilizowane DNA ; 3) Znaczenie mikroskopii dwufotonowej w badaniach nad amyloidami; 4) Aktualny stan wiedzy na temat zasad konstrukcji znaczników fluorescencyjnych dla amyloidów z akcentem na sondy dwufotonowe; 5) Znaczenie badań nad amyloidami, co wiąże się z ich związkiem z chorobami cywilizacyjnymi. Istotne dla autorki rozprawy było pokazanie jak badania podstawowe nad optymalizacją absorberów dwufotonowych, oraz głębszym zrozumieniem ich właściwości optycznych po związaniu z amyloidami, mogą realnie przełożyć się na badania przedkliniczne, które są motorem napędowym badań klinicznych oraz konstrukcji efektywnych terapii medycznych. Do hipotez rozprawy doktorskiej należą: **Hipoteza 1:** Benzotiazole funkcjonalizowane grupą BF_2 mogą służyć jako fluorescencyjne znaczniki dla amyloidów. Modyfikacja rozmieszczenia grup funkcyjnych w cząsteczkach wpływa na właściwości optyczne badanych fluoroforów związanych z włóknami amyloidowymi; **Hipoteza 2:** Absorpcja dwufotonowa (2PA) fluoroforów związanych z amyloidami, różni się od 2PA niezwiązanych fluoroforów i może być modulowana w zależności od struktury chemicznej, a

w konsekwencji także struktury elektronowej ; **Hipoteza 3**: Atomowo precyzyjne nanoklastry Ag_N-DNA mogą charakteryzować się wysokim przekrojami czynnymi na absorpcje dwufotonową (σ_2) i przekrojami efektywnymi na absorbcje dwufotonową ($\sigma_{2,B}$) przekraczającym 50GM, co uczyni je atrakcyjnymi znacznikami do zastosowania w bioobrazowaniu dwufotonowym. Oprócz hipotez sformułowano również cele rozprawy doktorski: **Cel 1**: Zaproponowanie cząsteczki z nowym rdzeniem opartym na grupie funkcyjnej BF oddziałowującej z amyloidami oraz charakteryzuje się lepszymi właściwościami optycznymi (przesunięta ku dłuższym falą absorpcja i emisja oraz wyższe wartości σ_2) w porównaniu ze standardowym, komercyjnie dostępnym znacznikiem fluorescenycjnym dla amyloidów: Methoxy-XO4; **Cel 2**: Określić związek pomiędzy modulacją 2PA badanych fluoroforów związanych z amyloidem a strukturą fluoroforów. **Cel 3:** Zaproponowanie nowych nanocząstek emitujących fotoluminescencje w zakresie bliskiej podczerwieni (NIR), które są rozpuszczalnymi w wodzie absorberami dwufotonowymi i określenie ich właściwsi optycznych.

Druga część rozprawy, czyli część eksperymentalna odnosi się do konkretnych celów i hipotez rozprawy, z końcowym akapitem na temat podsumowania i dalszych perspektyw, wynikających z badań przeprowadzonych w ramach tej rozprawy. Skupia się ona na 3 artykułach, z czego dwa dotyczą organicznych znaczników dla amyloidów, a jeden skupia się na nanoklastrach srebra jako nowych potencjalnych znacznikach dwufotonowych. Każdy artykuł to osobny podrozdział, w którym przedstawiono opis celu badań, dyskusję kluczowych wyników oraz podsumowanie. W każdym podsumowaniu zawarto na jakie hipotezy i cele rozprawy doktorskiej odpowiada dany artykuł naukowy. Szczegółowy opis wszystkich wyników, dyskusji oraz części eksperymentalnej jest zawarty w dołączonych artykułach i materiałach uzupełniających.

Odpowiedź na zadane hipotezy i realizacja celów tej rozprawy wymagało użycia szeregu metod spektroskopowych takich jak: pomiary absorpcji jednofotonowej, widm fluorescencji i wzbudzania fluorescencji, wydajności kwantowej fluorescencji, czasów życia fluorescencji. Techniki fluorescencyjne służyły również do wyznaczenia konkretnych parametrów takich jak: stała dysocjacji (K_d), fotostabilności układów, odziaływań barwników organicznych z bioanalitami. Wykorzystano pomiary z zakresu optyki nieliniowej czyli technikę dwufotonowo wzbudzanej luminescencji, aby wyznaczyć przekroje czynne na absorpcję dwufotonową (σ_2) oraz przekroje efektywne dwufotonowe ($\sigma_{2,B}$). W celu potwierdzenia otrzymania amyloidów z natywnych białek użyto obrazowania na mikroskopie sił atomowych (AFM ang. *Atomic Force Microscope*) oraz transmisyjnym mikroskopie elektronowym (TEM, z ang. *transmission electron microscope*).

Artykuł 1 o tytule „BF2-Functionalized Benzothiazole Amyloid Markers: Effect of Donor Substituents on One- and Two-Photon Properties" przedstawiony w sekcji III „ Opublikowane prace – opis własnych wyników" opisuje wpływ położenia grupy donorowej (-metoksy) w rdzeniu złożonym z BF_2-sfunkcjonalizowanym benzotiazolem na właściwości jedno- oraz

dwufotonowe po związaniu z amyloidami. Badania odpowiadają na ograniczone zrozumienie wpływu struktury chemicznej fluoroforu na modulacje właściwości optycznych po związaniu z amyloidami. W szczególności w zakresie modulacji absorpcji dwufotonowej, brak systematycznych prac, które poruszałyby ten wątek. Innowacyjnym aspektem pracy jest wyznaczenie σ_2 przed i po związaniu z amyloidami, ponieważ w literaturze prezentowane są pomiary σ_2 tylko w rozpuszczalnikach. Praca odpowiada na hipotezę nr. 1 oraz 2, cel nr. 2.

Artykuł 2 o tytule „Two-photon brightness of NIR-emitting,atomically precise DNA-stabilized silver nanoclusters" przedstawiony w sekcji III „ Opublikowane prace – opis własnych wyników", koncentruje się na absorpcji dwufotonowej czterech przedstawicieli nanoklastrów srebra stabilizowanych oligonukleotydami DNA (Ag_N-DNA). Po raz pierwszy w literaturze, zaprezentowano przekroje czynne na absorpcję dwufotonową atomowo precyzyjnych Ag_N-DNA. Badania odpowiadają na ograniczenia organicznych absorberów dwufotonowych, takie jak emisja w NIR (>700nm) charakteryzująca się wysokimi wydajnościami kwantowymi fluorescencji oraz rozpuszczalność w wodzie. Praca odpowiada na hipotezę nr. 3 oraz cel nr. 3, że Ag_N-DNA mogą mieć $\sigma_{2,B}$ powyżej 50 GM, co stanowi podstawę do wykorzystania ich w biobrazowaniu.

Artykuł 3 o tytule „A novel O,N,O-coordinated organofluoroboron probe for amyloid detection: insight from experiment and theory" przedstawiony w sekcji III „ Opublikowane prace – opis własnych wyników" skupia się na zaprezentowaniu nowej struktury, która oddziaływuje z amyloidami i ma lepsze właściwości optyczne od komercyjnie dostępnego standardu dla dwufotonowej mikroskopii dla amyloidów – Methoxy-X04, tzn. fluorescencję przesuniętą ku dłuższym długościom fali, wyższe przekroje czynne na absorpcję dwufotonową, szerszy zakres wzbudzenia dwufotonowego, nawet w zakresie powyżej 1000 nm. Praca prezentuje, również rozwiązanie na modyfikacje struktury opartej na organofluoroboranie skoordynowanym przez O,N,O w celu zwiększenia wydajności kwantowej fluorescencji i przekrojów czynnych na absorpcje dwufotonową. Badania odpowiadają na hipotezę nr. 2 oraz cel nr. 1 opracowania nowego znacznika dla amyloidów, który byłby konkurencyjny dla komercyjnie dostępnego standardu.

Na końcu rozprawy przedstawiono możliwą perspektywę na dalszy rozwój badań zawartych w tej rozprawie doktorskiej, jak i ogólne spojrzenie na omawiane tematy.

II. INTRODUCTION

Chapter 1. SCOPE AND AIMS OF THE DISSERTATION:

Fluorescent markers are widely used in biological research, medical diagnostics, pharmaceuticals, and healthcare. They have gained popularity in both *in vitro* and *in vivo* studies due to their ability to detect targeted molecules in real time without disrupting biological structures, making them essential tools for both fundamental science and applications. The first fluorescent process was observed for organic fluorophore—quinine—at the end of the 19th century. Since then, the portfolio of fluorophores has progressively expanded, initially including only organic fluorophores. The introduction of fluorophore families such as rhodamines, fluorescein, coumarins, cyanine dyes, and BODIPYs was followed by the groundbreaking discovery of fluorescent proteins, which are now widely used as genetically encoded probes. A third wave of fluorophores includes nanomaterials such as quantum dots, noble metal nanoclusters, lanthanide-doped nanoparticles and many more. The ongoing advancement in fluorophore design and technology enables pushing fluorescence-based techniques such as microscopy and spectroscopy for advanced studies. **The optimization of the fluorophores for certain application is still an ongoing process.** Fluorescent probes might be dedicated to detect certain analytes and simultaneously present proper optical properties, which enable detection by special type of spectroscopy technique or microscopy. To design fluorescent probes for a specific application, it is crucial to understand the relationship between chemical structure and optical properties as well as potential interactions with targeted structures. This thesis focuses on characterization and optimization of two types of fluorescent probes: 1) Dedicated to have proper optical properties for Two-photon fluorescent microscopy (2PFM) like high two-photon absorption cross-section (σ_2), emission above 700 nm (NIR-I region) without a need of detection of certain analytes; 2) Dedicated to have proper optical properties for 2PFM like high σ_2 and simultaneously detect amyloid fibrils. The 1st group of fluorophores for 2PFM expands the palette of two-photon absorbers with properties like NIR-emission, high FQY, water-solubility, which are highly desirable for *in vivo* applications. Since they do not have any specific chemical modifications to stain chosen biostructures, they might be used e.g to measure blood flow or might be a great platform for further modifications to gain some selectivity toward selected biostructures. For this purpose I investigated 2PA of atomically precise DNA-templated silver nanoclusters (Ag_N-DNA). Their optical properties like emission above 700 nm, high FQY (up to 73%) and water-solubility were in line with the goals of the PhD thesis, which are listed below. The 2nd group of fluorophores are organic dyes based on BF/BF2 moiety: BF_2-functionalized benzothiazoles and N,O-coordinated BF dye. This area of thesis focuses on: 1) Proposing a marker for amyloids that would have competitive optical properties (red-shifted emission, higher σ_2, longer wavelengths of excitation) compared to the commercially available markers for 2PFM;

2) Investigation of structural modification impact on optical properties (one- and two-photon) of fluorescent dyes based on BF_2-functionalized benzothiazole core for amyloid detection.

Summary of research gaps, main hypotheses and goals for studied fluorophores is presented in Figure 1. **Due to the fact that, studies of fluorophores based on BF/BF_2 moiety and Ag_N-DNA respond to different research gaps, goals and hypotheses of the thesis were specified depending on the material tested.**

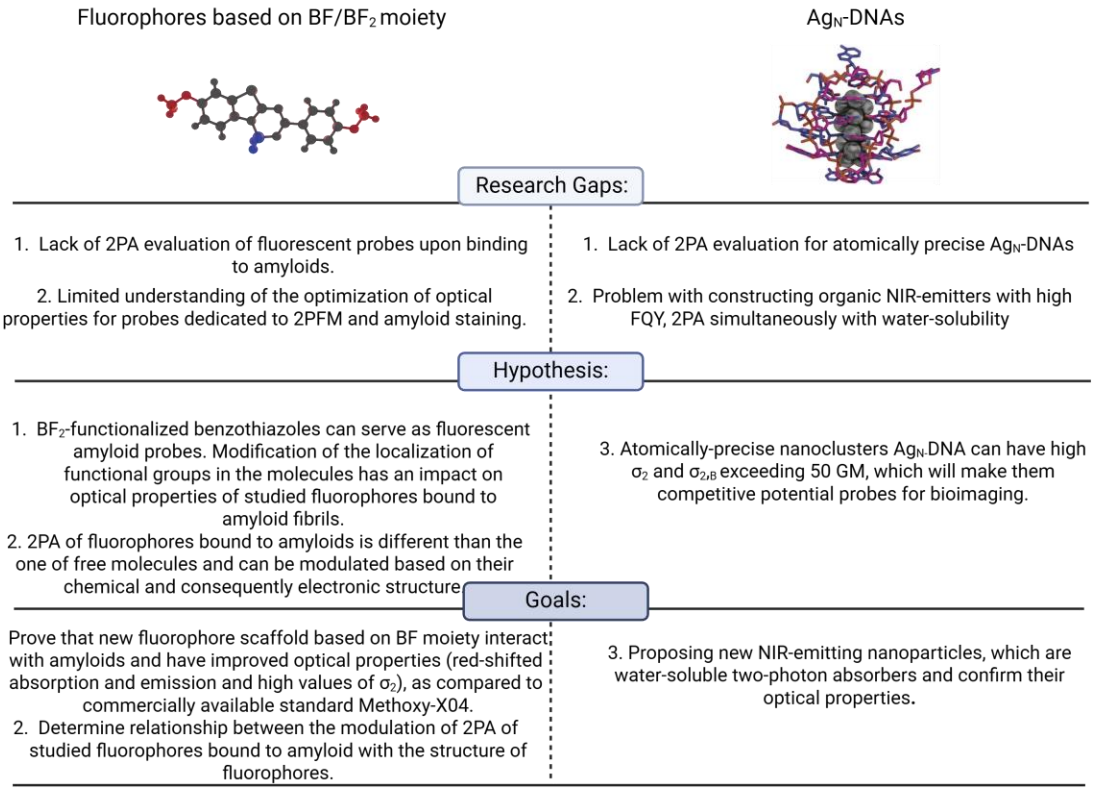

Figure 1. *Summary of research gaps, main hypotheses and goals for studied fluorophores.*

Main hypotheses are:

- **Hypothesis 1:** BF_2-functionalized benzothiazoles can serve as fluorescent amyloid probes. Modification of the localization of functional groups in the molecules has an impact on optical properties of studied fluorophores bound to amyloid fibrils.
- **Hypothesis 2:** 2PA of fluorophores bound to amyloids is different than the one of free molecules and can be modulated based on their chemical and consequently electronic structure.
- **Hypothesis 3:** Atomically-precise nanoclusters Ag_N-DNA can have high two-photon absorption cross-section (σ_2) and two-photon brightness ($\sigma_{2,B}$) exceeding 50 GM, which will make them competitive potential probes for bioimaging

Main Goals are:

- **Goal 1:** Prove that new fluorophore scaffold based on BF moiety interact with amyloids and have improved optical properties (red-shifted absorption and emission and high values of σ_2), as compared to commercially available standard Methoxy-X04.
- **Goal 2** Determine relationship between the modulation of 2PA of studied fluorophores bound to amyloid with the structure of fluorophores
- **Goal 3:** Proposing new NIR-emitting nanoparticles, which are water-soluble two-photon absorbers and confirm their optical properties.

All presented hypotheses were verified and confirmed in articles included in this thesis.

Chapter 2. LITERATURE REVIEW

2.1 Two-photon absorption – principles and application

2.1.1 Two-Photon absorption:

2PFM relies on a non-linear optical phenomenon called two-photon absorption (2PA) predicted by Maria Goeppert-Mayer in 1930s, long time before experimental evidence of this phenomenon was presented. 2PA is a simultaneous absorption of two photons, usually of double the wavelength (degenerate 2PA) required for one-photon absorption (1PA). 2PA is a third-order **non-linear optical process**, which depends quadratically on incident light intensity ($\sim I^2$), in contrast to 1PA, which has linear dependence. First experimental evidence of 2PA was made by Kaiser and Garret on europium doped calcium fluoride crystals ($CaF_2:Eu^{2+}$) shortly after the invention of pulsed lasers.[1] The physical principles of 2PA rely on the fact that this process requires a very high photon density within a small volume, which is achieved by short-pulsed lasers.

To better understand physical principles of 2PA, light-matter interactions have to be considered. For this purpose, the effect of magnetic field in the electromagnetic wave (light) is neglected and only electric field (E) will be described. When the incident light interacts with the sample, it induces a macroscopic polarization **P,** **P** can be spread out into a power series of E, which is presented in equation (1):

(1) $P = \varepsilon_0 \chi^{(1)} E_j + \varepsilon_0 \chi^{(2)} E_j E_k + \varepsilon_0 \chi^{(3)} E_j E_k E_l \ldots.$

Where ε_0 is electric permittivity of free space and $\chi^{(n)}$ is n-th order susceptibility.

The polarization **P** can be expressed as the sum of a linear and a nonlinear component. The nonlinear part consists of higher-order terms of the polarization and is referred to as the nonlinear polarization, denoted by $\mathbf{P_{NL}}$, expressed by equation (2):

(2) $\boldsymbol{P}_{NL} = \varepsilon_0 \chi^{(2)} E_j E_k + \varepsilon_0 \chi^{(3)} E_j E_k E_l + \cdots.$

As described by equation (2), non-linear polarization do not depend linearly on the electric field.

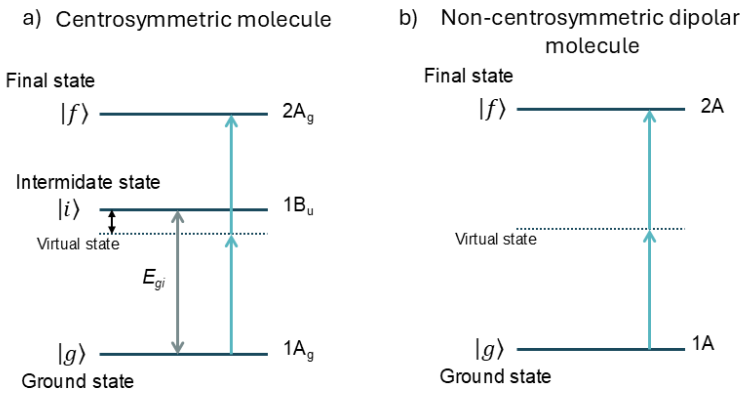

Figure 2. *Schematic representation of energy diagrams for: a) centrosymmetric chromophore and b) non-centrosymmetric dipolar chromophore upon two-photon absorption. Made based on energy diagrams presented in [Angewandte Chemie International Edition 2009, 48 (18), 3244-3266].*

Now, let's move on to the description of molecular physical quantities relating to 2PA, which are important in the frame of constructing two-photon absorbers. Coefficient σ_{max} is described as the molecular 2PA cross-section, which is expressed in Göppert-Mayer units (1GM =10^{-50} cm^4 s $photons^{-1}$ $molecule^{-1}$). For plane-polarized light, the value of σ_{max} corresponding to a transition from the ground state (*g*) to the final state (*f*) **at the maximum of a 2PA** with a Lorentzian- line shape is determined by Equation (3)[2]:

$$(3)\ \sigma_{max} = \frac{2\pi h\nu^2 L^4}{\varepsilon_0^2 n^2 c^2}\left(\frac{1}{\Gamma}\right) S_{fg}$$

$$(4)\ S_{fg} = \left[\sum_i \frac{\langle \mu_{gi}\mu_{if}\rangle}{(E_{gi}-h\nu)}\right]^2$$

Where, $h\nu$ is the photon energy, ε_0 is electric permittivity of vacuum; Γ is the half-width at half maximum of the 2PA band and E_{gi} is the energy gap between the ground state and an intermediate state *i; n* is refractive index; factor $L= (n^2+2)/3$ denotes the enhancement of the optical field in the medium relative to that in a vacuum.

Equation (3) describes the value of 2PA cross-section at the maximum of a 2PA band. This expression can be simplified since, for most strong two-photon absorbers the orientational average of the transition dipole moments equals 1/5. As a result, the vector notation can be omitted and, after rearrangement, the simplified form given by Equation (5) is obtained:

$$(5)\ S_{fg} = \frac{1}{5}\left[\left(\frac{\Delta\mu_{gf}\mu_{gf}}{h\nu}\right)^2 + \sum_{i\neq f,g}\left(\frac{\mu_{gi}^2\mu_{if}^2}{E_{gi}-h\nu}\right)\right]$$

Where $\Delta\mu_{gf}$ is the difference in the static dipole moment in the final state relative to the ground state; μ_{gi} dipole moment between ground and intermediate state;μ_{if} is a dipole moment between intermediate and final state. The equation (5) can be divided into two terms: dipolar

term (D), which stands for $\left(\frac{\Delta\mu_{gf}\mu_{gf}}{h\nu}\right)^2$ and two-photon (T) term, which stands for $\sum_{i\neq f,g}\left(\frac{\mu_{gi}^2\mu_{if}^2}{(E_{gi}-h\nu)^2}\right)$. Equation (5) is a starting point in understanding the principles of constructing organic compounds as two-photon absorbers. However, before moving on to specific examples of molecular architecture, it is necessary to introduce a general energy diagram for the principal states involved in two-photon absorption, which is presented in Figure 2. There are two states: ground-state $|g\rangle$ and the final-state $|f\rangle$ wavefunctions. In the Figure 2 were compered energy diagrams during 2PA process for two types of molecules: centrosymmetric with D_{2h} symmetry (quadrupoles) and non-centrosymmetric with C_2 symmetry (dipolar molecules). Firstly, molecules with centrosymmetric architecture will be discussed. Both transitions $g \leftrightarrow i$ and $i \leftrightarrow f$ are 1P electric-dipole-allowed. However, during 2PA, the optical frequency ν does not match the resonance condition for both of these transition. The non-stationary (virtual) state is created, which is superposition of $|g\rangle$ and $|f\rangle$ wavefunction, where the induced polarization is shifted relative to the intermediate state by a frequency difference corresponding to an energy $\Delta = E_{gi} - h\nu$. Virtual state exist for extremely short period of time (around 5 fs), while chromophores faces the electric field of first photon[3]. In centrosymmetric molecules, the 1Ag → 2Ag transition is forbidden in 1PA, but allowed in 2PA. Opposite selection rules for 1P and 2P occurs from the presence of transient state $|i\rangle$ with *ungerade* symmetry, which in this superposition enables a second photon at frequency *ν* to induce an electric-dipole transition to the final *gerade* state $|f\rangle$. Transitions, which are the most dominant in 1PA, are not the most dominant in 2PA. Considering S_{fg} for centrosymmetric chromophores, term D in equation (5) is zero, due to zero value of the static dipole moments.

The dipolar non-centrosymmetric chromophores present distinct energy diagram from centrosymmetric molecules, which reflects in allowed transitions. The $g \leftrightarrow f$ transitions are electric dipole allowed in 1PA and 2PA, which gives rise to usually the same observed dominant transitions in 1P and 2P regime. **For non-centrosymmetric molecules $|f\rangle$ operates as virtual state $|i\rangle$.** For these molecules D term contributes to S_{fg} value, contrary to centrosymmetric chromophores. However, T term makes now smaller contribution than for centrosymmetric molecules and is intrinsically smaller than D. This partially explains higher two-photon absorption cross sections for centrosymmetric molecules like quadrupoles, than for non-centrosymmetric dipolar chromophores. More details regarding molecular and electronic architecture for two-photon absorbers organic molecules, will be presented in section "2PA in organic molecules".

There are two main quantities important for evaluation of two-photon properties for fluorophores, which are experimentally measured or can be simulated, two-photon absorption cross-section (σ_2) and two-photon brightness ($\sigma_{2,B}$)**.**

Mentioned quantity σ_2 is a concentration independent quantity, which can be expressed by (6):

(6) $\sigma_2 = \frac{\hbar\omega\alpha_2}{N}$

where *N* stands for the number density of the absorbing molecules and $\hbar\omega$ for the energy of absorbed photons, and α_2 is two-photon absorption coefficient.

If two-photon absorption (and so on excitation) is followed by luminescence, this process is called two-photon excited luminescence (2PEL). Due to the fact that 2PA depends quadratically on laser intensity, the highest probability of the process is in the point of the highest density of photons, which is a focal point. Based on this principle, not all fluorophores are excited in the light path, but only those at the focal point, making possible 3D sectioning. For 2P excited fluorophores $\sigma_{2,B}$ is used to express how effective is emission upon two-photon excitation, which is described by equation (7):

(7) $\sigma_{2,B} = \sigma_2 * FQY$

Where FQY stands for fluorescence quantum yield.

For fluorophores, one of the most popular experimental techniques to measure σ_2 is 2PEL technique. It is an indirect method of probing 2PA, where intensity of luminescence after 2PA is measured. In this thesis 2PEL reference method was used, which relies on a reference compound with known σ_2 which is measured in the same experimental conditions as sample with unknow σ_2.[4] Sample and reference should also emit in similar spectral region, to keep exactly the same experimental conditions during measurements. Due to the fact that this methods relies on emission, information about transitions, which leads to luminescence is obtained. In materials, which have various 1PA and 1PE spectra, comparison of σ_2, should be to 1PE, not 1PA. Luminescence of both samples is collected and then σ_2, is calculated based on the formula (8):

(8) $\sigma_{2,s} = \frac{F_S C_r FQY_r {n_r}^2}{F_r C_s FQY_s {n_s}^2}\sigma_{2,r}$

Where *C* is the fluorophore molar concentration, *n* the refractive index of the solvent, FQY the fluorescence quantum yield, and *F* the integral over the whole two-photon excited emission band. The letters *s* and *r* correspond to a sample and a reference, respectively.

2.1.2 Two-photon fluorescence microscopy:

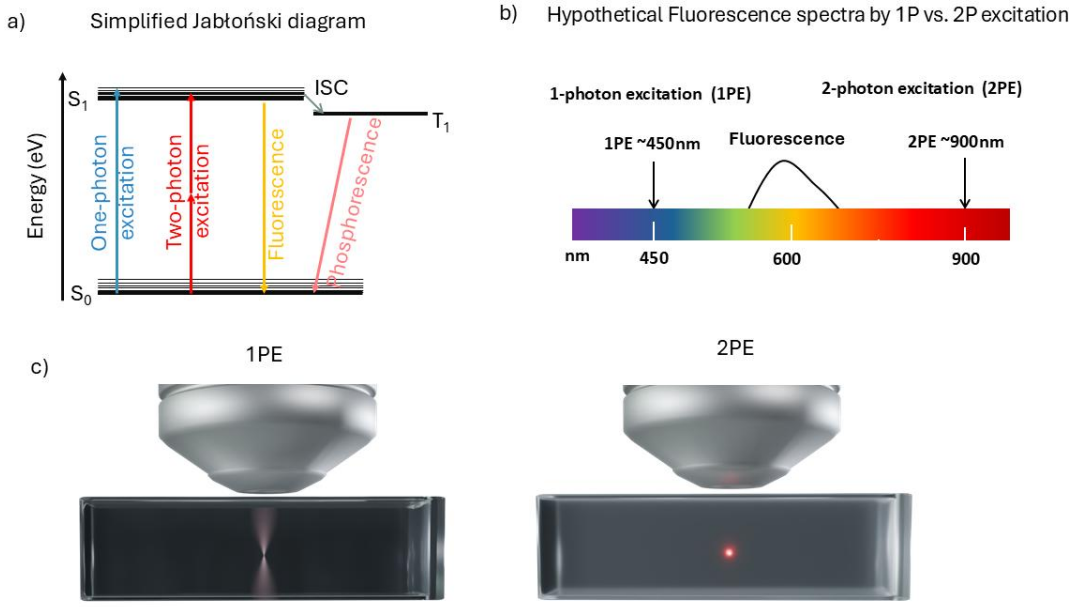

Figure 3. *a) Simplified Jablonski diagram with comparison one- and two-photon excitation, with the ground state (S_0), first excited state (S_1), triplet state (T_1) and vibrational states (thin lines), grey arrow stands for Intersystem crossing (ICS); b) Hypothetical comparison of emission obtained from 1P and 2P excitation; c) Profiles of 1PE and 2PE on cuvettes with fluorophore. Emission upon 2PE is only visible on the focal plane.*

Fluorescence microscopy is a visualization technique based on detection of fluorescence emission from fluorophores. It is widely used in physiological conditions to better understand biological processes origin in the cells, organisms, but also in studies regarding pathophysiological conditions.[5] There are plenty types of optical microscopic techniques, which relies on fluorescence detection. One of the possible distinction is type of excitation that is used to excite fluorophores – one-photon or multiphoton (two- or three-photon are the most popular). One photon fluorescence microscopy (1PFM) is versatile in terms of resolution or imaged samples e.g. confocal microscopy, light-sheet microscopy, super-resolution microscopy, wide-field microscopy. The popularity of 1PFM has led to the extensive work on development of fluorescent probes with intended properties, which resulted in numerous commercial fluorescent probes suitable for various applications[6-7]. It is worth mentioning that the development of fluorophores, is still an important branch of chemistry and materials science[8-9], also contributed to the development of microscopy itself. In terms of *in vivo* imaging especially useful are NIR biological windows– ranges of wavelengths >700 nm, where tissues absorb and scatter less light, than in shorter wavlenghts.[10-11] It translates into deeper penetration

of light into the sample. We can distinguish three biological windows: NIR-I (700-950 nm), NIR-II (1000-1400nm), NIR-III (1600 to 1870 nm).[12-13] Since small-organic fluorophores with absorption in these regions are rare, a problem might be solved by two-photon excitation (2PE). Comparison of one-photon excitation (1PE) and 2PE is schematically presented on simplified Jablonski diagram on Figure 3a. The sum energy of two photons have to match with the energy gap corresponding to one-photon excitation. Produced fluorescence or phosphorescence by 1P or 2P excitation is usually the same in energy, which is presented schematically in Figure 3b. 2PFM, also relies on fluorescence detection, but excitation is operated via 2P. In the case of 1PFM, all fluorophores in the light path are excited, and produce photoluminescence, while in 2PFM only molecules which are in the focal point, as it is presented in Figure 3c. Excitation in biological windows provides better resolution and penetration depth than in the visible range of excitation, additionally if 2PE is also followed by NIR emission, it provides even 4 times deeper penetration into the tissues than using visible-wavelength emissions[14]. 2PFM was introduced in 1990 by Winfried Denk and his coworker James H. Strickler in the Webb lab.[15] Advantages of 2PFM like using lower energy photons in the NIR-I or NIR-II region, three-dimensional (3D) sectioning, excitation in femtoliter volume and low photodamage contributed to its use in more specialized applications[16], compared to 1PFM. It is widely used in visualization of deep laying structures e.g brain (deeper penetration of excitation wavelength)[17], dynamic processes over long period of time e.g amyloid plaques formation in the brain[18] or blood flow in the vessels[19]. Importantly, in 2PFM the same type on microscopes as in 1PFM can be used, the key difference is an excitation source, which in 2PFM is a pulsed laser.[20-21] One of the important application of 2PFM in the light of this thesis is amyloid detection. 2PFM contributed significantly, in understanding the role of amyloids in neurodegenerative diseases. It allowed, for the first time, visualization of single senile plaques in the brain of living transgenic mice over long period of time[22]. Due to the use of 2PFM, the same plaques could be re-imaged after 5 months. Research revealed that the majority of deposits remain unchanged over time. Up to the present, a number of studies applied 2PFM with amyloid staining probes in longitudinal imaging of *denovo* formation of plaques.[23-25] Innovative 2PFM allows monitoring individual cells and their activity in the brain of awake rodents, providing a powerful tool for neuroscience research[26-27]. Recently, some papers focused on the impact of amyloid-β deposits on activity of individual neurons.[28-29] Use of 2PFM gives higher spatial resolution, than 1PFM imaging and is favorable in observation of dynamic changes over longer period of time. Visualization of interactions of single cells with amyloids or growth of single plaques in the brain is irreplaceable tool in pre-clinical research on amyloids formation. Other technique used *in vivo* in amyloid research in the brain[30] - Positron emission tomography (PET) has detection resolution on milimeters scale, which gives more global information regarding the whole organ e.g brain[31]. It cannot be used in studies on single cell level, as 2PFM. These techniques are considered as complementary approaches in preclinical research rather than substitutes for each other. 2PFM is also used as a tool in PET amyloid tracer evaluation.[32] Amyloid research is only a tip of the iceberg in the brain research

using 2PFM. One of the greatest achievements in the development of 2PFM is the design of systems that allow for imaging the brain of freely moving organisms like rodents[33-35], *Drosophila* larvae[36], which is mostly used for neuronal activity monitoring during natural behavior of animals. Neurovascular dynamics imaging is another interesting application of 2PFM. It is possible to visualize the full range of brain vasculature, from large arteries and veins down to individual capillaries[37] and record 3D blood flow speeds up to ~3 mm/s[37]. 2PFM also helps to monitor in real-time movement of red blood cells through cortical vessels[38]. 2PFM supported by computational simulation helped to revel that red blood cells contribute to stabilization of blood flow in brain vascular system[39], which might be important in the light of pathologies with disturbed microcirculation such as stroke, dementia, or traumatic brain injury.

This paragraph **highlights the importance of 2PFM** in understanding biological processes, which is the basis for creating improved medical therapies, understanding the etiology of diseases and discovering the world in general. However, to take a full advantage of the benefits of 2PFM, **proper fluorescent markers are required**. This explains why investigating construction of new fluorescent markers for 2PFM intended for amyloids or for more general purpose e.g examination of blood flow in the brain is needed.

2.2. Fluorophores for 2PFM

2.2.1 2PA in organic molecules:

The principle of construction of effective two-photon absorbers has foundation in the description of molecular two-photon absorption cross-section, (see equation (3)). There are rules grounded on experimental and theoretical works, which help to predict, which organic molecules can have elevated σ_2. High values of μ_{gi}, μ_{if}, μ_{gf} and $\Delta\mu_{gf}$ are crucial, as based on equation (5). Molecules with extended intramolecular charge transfer (ICT), which present architecture like the electron donor−acceptor (D−A) dipoles, D-π-D, D-π-A-π-D, DAD, quadrupoles meet those requirements.[40-41] Apart from general electronic architecture important factors are: increasing intramolecular conjugation length, linker between donor and acceptor part of a molecule, strength of electron donor and acceptor groups. Examples of strong donor groups are: – *N,N*-dimethylamine (-NMe_2); *N,N*-diphenylamine (-DPA); and other substituted amines with scheme -NR_2 or -NHR (R-substituted group); hydroxy group (-OH); aloxy group -OR (e.g., –OCH_3). Strong electron acceptor groups are: cyano group (-CN); nitro group (-NO_2); trifluoromethyl group (-CF_3); carbonyl-containing groups: aldehyde, ketone, carboxylic acid, ester (–CHO, –COR, –COOH, –COOR). The placement of donor and acceptor groups inside architecture of a molecule is a crucial factor and most effective are architectures with donor/acceptor groups at the center and ends of the chromophore[2]. Theoretical predications of σ_2 using Time-Dependent Density Functional Theory (TD-DFT) can serve as initial screening

for large number of compounds, which was presented by Knysh *et al*[42]. Systematic change in the core, addition of different donor and acceptor groups, in the π-linker have impact on 2PA and the best candidates can be extracted from a large set of compounds for experimental evaluation.

For bioimaging proposes, not only σ_2 is important, but also FQY, since detection is based on intensity of fluorescence signal. In the literature values of $\sigma_{2,B}$ which are recommended for appropriate signal-to-noise ratio during imaging procedure[43] should exceed 50 GM. Selection rules for 2PA and 1PA are different[44]. Molecule, which effectively absorbs and emits under one-photon excitation, does not have to have the same response upon two-photon excitation, which was explained in the subsection 2.1.1 "Two-photon absorption" (especially for centrosymmetric molecules). However, this phenomenon does not correspond only to centrosymmetric chromophores, and prediction of 2PA theoretically for structures with complex energy landscapes like nanomaterials or fluorescent proteins is extremely challenging. Due to this fact experimental evaluation is often the only way to obtain an insight into 2PA.

One of the strong electron acceptor groups is boron difluoride (BF_2) moiety, which is widely used for constructing dyes with high σ_2[45-47], up to few thousands GM[48-49]. 4,4-difluoro-4-borata-3a-azonia-4a-aza-s-indacene (BODIPy) was introduced in 1968 by Treibs and Kreuzer.[50] Now, BODIPy family is one of the main classes of the fluorescent probes, which is described in many reviews.[51-54] There are several main advantages, which impacted expansion of BODIPy research and application – robust photostability, obtaining high FQY and molar absorption coefficients. In BODIPy group BF_2 is coordinated by two nitrogens, however there are also N,O-coordinated or O,O-coordinated BF derivatives. Modifications in coordination atoms impact bond angles and electronic distribution, which translate to optical properties of molecules. Fluorophores with N,O- coordinated BF_2 moiety can have extremely high FQY – 90%[55];98%[56]. These are interesting fluorescent dyes to study in the context of two-photon probes due to the mentioned values of FQY and σ_2, but also due to their interaction with amyloids, which will be discussed in the chapter "Fluorescent probes for Amyloids in 2PFM".

It is worth presenting the limitations of organic two-photon excited fluorophores. As mentioned in the subsection 2.1.2 "two-photon fluorescence microscopy" probes, which emit in NIR regions increase light penetration depth, as compared to probes with fluorescence emission below 700 nm.[50-52] However, construction of NIR-to-NIR two-photon (emission in NIR and excitation by 2P in NIR) probes is not a trivial task. In order to construct effective 2P absorbers large number of aromatic rings and conjugated bonds have to be places in the molecule, which results in weak water-solubility. It can limit some biological applications. Additionally, obtaining emission in NIR often results in low FQY, due to the fact, that by shifting the emission towards red region of the electromagnetic waves, the energy gap between the ground state and the excited state decreases, which favors non-radiative process. To summarize, simultaneous enhancement of the three properties: 1) fluorescence in NIR region;

2) two-photon absorption; 3) water solubility, is limited in small organic molecules. To overcome this obstacle, new materials are proposed. One of the group of nanomaterials, which have NIR-emission with high FQY and are water-soluble are **DNA templated silver nanoclusters.**

2.2.2 DNA templated silver nanoclusters:

DNA-stabilized silver nanoclusters (Ag_N-DNAs) are novel atomically precise fluorescent nanomaterials combined of silver core and stabilizing DNA oligomers. They link achievements of metal nanocluster chemistry and DNA nanotechnology, which contributes to the increase in research on these nanomaterials in recent years[57]. Nucleotide bases present in DNA have different affinity toward silver ions (Guanine ~ Cytosine > Adenine > Thymine), due to this fact DNA is sequence-dependent ligand for silver atoms. DNA oligomer sequence controls properties of Ag_N-DNAs including emission wavelengths, shape and their size.[57-59] In this thesis are only discussed nanoclusters, which are stabilized by single-stranded DNA (ssDNA). Since the optical properties of materials are the core of this dissertation, they will be discussed in greater detail in the following section. First report on Ag_N-DNAs nanoclusters was presented in 2004[60], indicating emissive species made from 1-4 silver atoms bound to 12-base oligonucleotide. After this discovery, interest in DNA- and oligonucleotide-stabilized silver nanoclusters grew rapidly, leading to extensive research efforts, which point out their tunable optical properties.[61-64] Shortly, after introduction of Ag_N-DNAs their 2PEL was evaluated[65], exhibiting large σ_2 reaching 50 000 GM. In time of reporting, these nanoclusters had σ_2 exceeding the values characteristic for known water-soluble two-photon absorbers. It positioned them as interesting fluorophores that may be a foundation to a new generation of water-soluble two-photon fluorophores with some of the largest σ_2, small size, and excellent one- and two-photon brightness. However, at the beginning of exploring Ag_N-DNAs, end-products of syntheses were a mixture of various species (emissive and non-emissive ones) and for many years purity was a great difficulty and homogeneous size of Ag_N-DNAs was not obtained for these samples. Therefore, it is not possible to assign specific optical properties determined at that time to a specific molecular formula (chemical composition like number of silver atoms, number of ligands per one nanocluster and oxidation state) of Ag_N-DNAs. The use of High-Performance Liquid-Chromatography (HPLC) to purify products after synthesis and determination of molecular formula based on electrospray ionization (ESI) Mass Spectrometry (MS) opened the door for atomically precise Ag_N-DNA[66-67] and assignments of optical properties to specific structure. In order to deeply understand modulation of optical properties of Ag_N-DNAs by oligonucleotides sequence, high-throughput synthesis combined with Machine Learning (ML) was employed.[68-70] ML helped to understand these materials and also predicted hundreds of new emitters, which significantly expanded the family of Ag_N-DNAs. They have interesting optical properties since many of them emit in the NIR-I region[57, 71] or even at the border NIR-I/NIR-II [72-73], have high FQY (up to 73%)[74], presents dark states[75]

and Optically Activated Delayed Fluorescence (OADF)[76-77]. Recently, the first examples of application of Ag_N-DNAs in the cell staining through copper-free click chemistry method were presented[78] and *in vivo* 2PFM for measuring cerebral blood flow[79]. However, till today only 3 nanoclusters have known crystal structure[72, 80-82], which hampers theoretical calculation of their optical properties, and in depth understanding of electronic levels and optical properties relationship.

2.2.2.a Structure and chemical composition of Ag_N-DNAs:

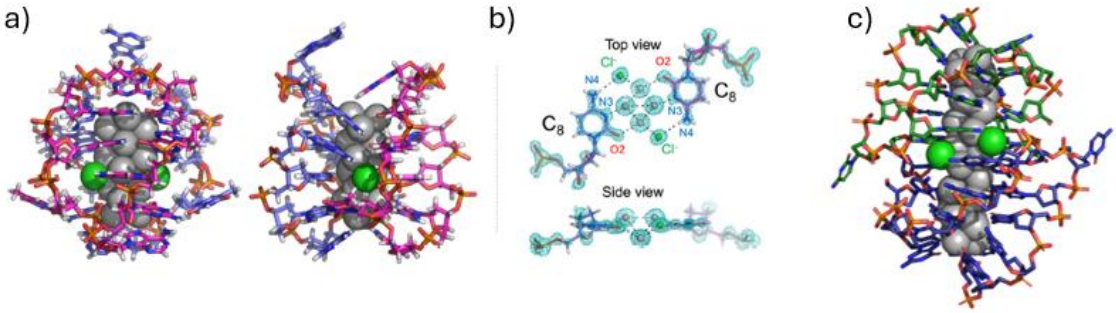

Figure 4. *a) Crystal structure of $(DNA)_2[Ag_{16}Cl_2]^{8+}$; b) $2|F_o| - |F_c|$ map around an Ag-mediated C8–C8 base pair contoured at the 1.5 σ level. (Silver: Ag atoms; green: Cl^- ions.) PDB number: 6M2P. Reproduced from [J. Am. Chem. Soc. 2023, 145, 19, 10721–10729]; c) Crystal structure of $DNA_2(Ag_{28}Cl_2)^{14+}$. PDB number: 9KHW. Reproduced from [Small Struct. 2025, 2500022].*

Synthesis of most Ag_N-DNA is a simple procedure, where borohydride reduction ($NaBH_4$) of a solution of Ag^+ (obtained from $AgNO_3$) and ssDNA is carried out in neutral pH.[59] Reaction solution has to age for a few days (depends on the protocol), the end product is a mixture of silver-DNA products. Obtaining pure product requires extensive purification on HPLC.

Ag_N-DNA are characterized by numbers of silver atoms N_{tot} and DNA strands x_s .N_{tot} can be divided into a number of neutral (N_0) and cationic (N_+) silver atoms. Not all silver atoms in an Ag_N–DNA nanocluster contribute to the valence electron count, as some are coordinated to nucleobases. The effective valence electron can be calculated based on a formula: $N_0 = N_{tot} - N_+$. Most of characterized nanoclusters by ESI-MS have N_{tot} between 8-30, and are mostly stabilized by ssDNA with 10-20 nucleotide bases. Effective valence electrons value is one of the key parameters, since numerous metal nanoclusters can be explained by "superatom" model, where the effective valence electrons within the cluster core adopt an electronic shell structure comparable to the shell structure of a nuclei[83]. In this prediction Ag_N-DNA with N_0 = 2 or 8, which is considered a magic number should have spherical shape. However, in experimental data, Ag_N-DNA with N_0 =4 and 6 are dominant[84], and have assigned rod-like geometry. Scarce examples of crystallographic data seem to support dominance of rod-like Ag_N-DNA. In 2019 X-ray crystal structure of DNA_2Ag_{16} was reveled, where silver core had rod-like geometry with two DNA decamers stabilizing the structure. It presented, which DNA

nucleobases are involved in silver complexation[81]. 4 years after revealing crystal structure of DNA_2Ag_{16} Gonzàlez-Rosell *et al.* discovered that initially proposed structure is not fully correct[85], since there are 2 chloride ions, which were firstly assigned as low-occupancy silvers by X-ray crystallography (they were even excluded from overall chemical formula). The correct chemical formula is **$DNA_2[Ag_{16}Cl_2]^{8+}$**, which was also proved by ESI-MS and calculations – see correct structure in Figure 4a,4b [85]. Characteristic feature is, that silver core is shielded by the DNA from the solvent, only the area near the two chloride ions remains exposed.[85] Recently, similar structure was proposed for presented Ag_N-DNA with 28 silver atoms – see Figure 4c [72]. It had rod-like geometry with around 2 nm length, intriguingly in the crystal structure molecular formula was assigned as **$DNA_2(Ag_{28}Cl_2)^{14+}$** by X-ray structure, which was also supported by energy-dispersive X-ray (EDX) spectra. However, in the solution presence of chlorido ligands was not confirmed using ESI-MS. Despite the isolated cases of crystal structures of Ag_N-DNA, the interpretation of the data is not trivial.

2.2.2.b Optical properties:

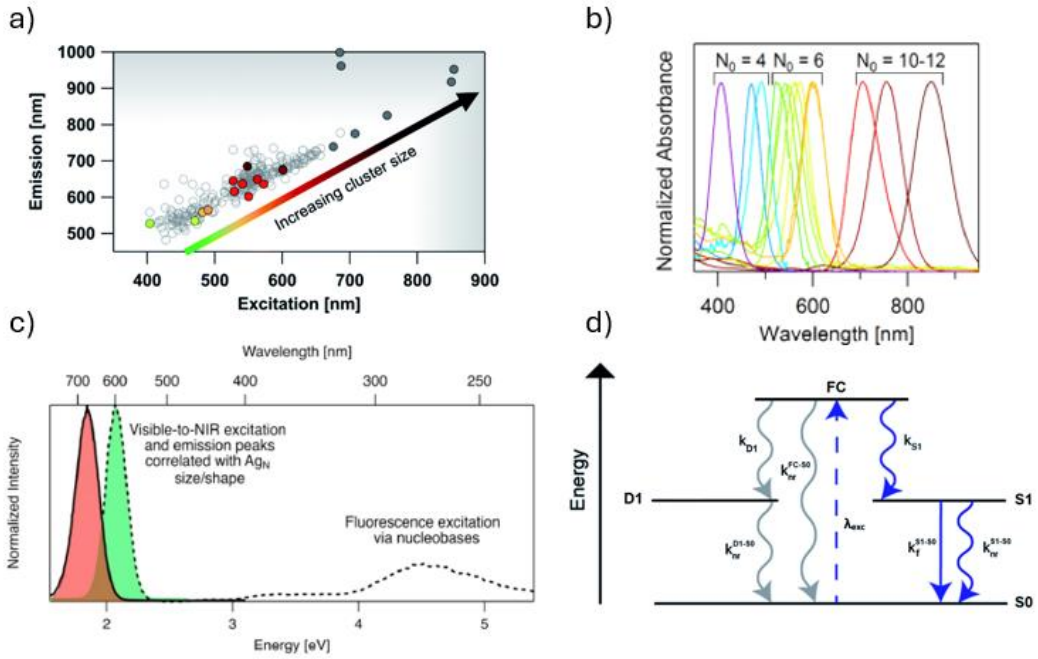

Figure 5. a) In Ag_N-DNAs, the DNA sequence defines the fluorescence wavelengths, spanning from visible to NIR wavelengths, and this behavior is associated with the cluster dimensions. Reproduced from [Nanoscale Adv., 2021, 3, 1230–1260].; b) Peak absorbance wavelength of Ag_N-DNAs scales with N_0. Reproduced from [Acc. Chem. Res. 2024, 57, 2117−2129]; c) Schematic depiction of excitation (dashed) and emission (solid) spectra characteristic of Ag_N-DNAs. Reproduced from [Acc. Chem. Res. 2024, 57, 2117−2129]; d) Schematic electronic structure of the Ag_N-DNAs. Reproduced from [C. Cerretani, M. R. Carro-Temboury, S. Krause, S. A. Bogh and T. Vosch, Chem. Commun., 2017, 53, 12556–12559].

Most of the Ag_N-DNAs present emission between blue and NIR ranges with fluorescence lifetime between 1-4 ns and high FQY (above 10%). Their excitation and emission are

characterized by a high degree of polarization, which results from defined and directional transition dipole moments.[86] In the Figure 5a dependency of cluster size on emission and excitation wavelength is presented. Since size of the cluster is determined by DNA sequence, we can call them programmable fluorophores. The effective valence electron also impacts position of absorption peak, higher value of N_0 is linked with longer wavelengths of absorption – see Figure 5b. Excitation and absorption usually have one gaussian shape band in the longer wavelengths range, higher energy transitions with low intensity and transition around 260 nm characteristic for DNA bases – see Figure 5c. Upon excitation at 260nm and at longer wavelengths the same emission is obtained, which is not fully understood.[87] Photophysics of these nanomaterials based on experimental data is more complicated than organic fluorophores, and have to be described out of simple Jabloński diagram. There is proposed general phenomenological model of energy relaxation for Ag_N-DNAs upon excitation, based on ultrafast transient absorption experiments – see Figure 5d. Initially, upon excitation Ag_N-DNAs populate the excited state (Franck-Condon state), later fraction of nanoclusters return to ground state within time range of hundreds of fs. In a similar time range formation of emissive state occurs and nanoclusters relax by radiation of emission in nanoseconds regime. However, there is also additional state formation possibility, called dark state, with a millisecond-scale decay time. Reported values for the quantum yield formation of a dark state fluctuating between a few percent to 25%. Presence of this state have broad implications for observed optical phenomena in Ag_N-DNAs. Excitation of the dark state can shift the Ag_N-DNA to the emissive state, resulting in OADF phenomena.[76-77, 88] In OADF, firstly dark state is formed upon primary excitation, later long-lived dark states can absorb secondary excitation in NIR region, which results in emission. Ag_N-DNAs can emit upconversion fluorescence similar to lanthanide doped nanomaterials.[77] All of the mentioned optical phenomena present Ag_N-DNAs as emitters with complex photophysics. There is one representative of Ag_N-DNAs, which is the most extensively studied due to stability and known crystal structure - $DNA_2[Ag_{16}Cl_2]^{8+}$.[82, 89-90] For $DNA_2[Ag_{16}Cl_2]^{8+}$ there are a few theoretical works, which revealed the electronic ground state of nanocluster in a solvent[91], orbitals involved in electronic transitions forming absorption spectra[91], theoretical circular dichroism[91]. Another work explained mechanism of dual emission[90], where nanosecond emission with $\lambda_{EM} \sim 690$ nm comes from spin-allowed $S_1 \rightarrow S_0$ transition, while delayed microsecond emission originates from spin-forbidden $T_1 \rightarrow S_0$ transition. Additional changes in structure after excitation were presented, where bond between the Ag–guanines is weaken and the length of the silver core expands[90].

As stated in the introduction to Ag_N-DNAs, they were promising candidates as two-photon probes. However, since introduction of atomic precision in Ag_N-DNAs, no investigation regarding two-photon absorption was done. In the light of preliminary studies on mixtures showing great potential as two-photon excited emitters, and considering their high FQY for NIR emitters, **the evaluation of their two-photon properties seems well justified,** especially since atomically precise thiol stabilized gold and silver nanoclusters are known to exhibit very high two-photon absorption cross-sections (above 1000 GM).[92-95] An advantage of Ag_N-DNAs

over other atomically precise thiol stabilized gold and silver nanoclusters with high σ_2 can be water-solubility, which is important in terms of bioimaging application.

2.3. Amyloids

2.3.1 Definition of amyloids:

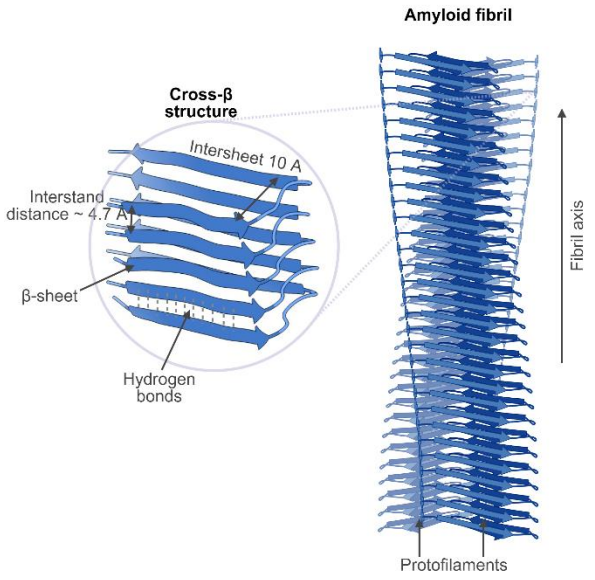

Figure 6. *Schematic representation of amyloid fibrils. Cross-β structure was done based on 3D Structure of Alzheimer's Abeta(1-42) fibrils using PDB: 2BEG. Figure was made using Bioreder® with Publication and Licensing Rights.*

In the mid-19th century, Rudolf Virchow introduced the term "amyloid" to describe abnormal extracellular deposits in tissues that exhibited a starch-like reaction when treated with iodine and sulfuric acid.[96-97] He concluded, that this deposits are composed of cellulose. Later, in 1859 Friedreich and Kekule discovered, that extracellular deposits lack carbohydrate, and have a presence of proteins. Although new insights into these structures were gained, the term *amyloid*—derived from the Greek word *amylon*, meaning starch – stayed. From 19th century till around 1950 structure of amyloids was elusive[98]. From that time, amyloids were extensively studied and the most important information regarding their characteristic will be presented. Amyloids are aggregates composed of thousands of peptide or protein monomers arranged in a highly ordered cross-β architecture – schematic representation in Figure 6. Inside fibrils, β-strands align perpendicularly to the fibril axis, forming extended β-sheets that stack parallel to the axis and are stabilized by a continuous hydrogen-bonding network[99] - see Figure 6. One mature amyloid fibril might be composed of few smaller building blocks called protofilaments. This supramolecular organization implicates exceptional chemical and thermodynamical stability of this structures. The most general morphology of amyloids is long, non-branched fibrils with diameters of 6–12 nm. They have a characteristic X-ray diffraction pattern showing a meridional reflection at ~4.7 Å and an equatorial reflection at ~6–11 Å[100-101], corresponding to inter-strand and inter-sheet spacings, respectively – see Figure 6 inset. **Amyloids from various proteins have common structure, as described above.** However one of the feature of amyloids is also polymorphism – diversity in morphology on mesoscopic and atomic level. The most simple, yet the essential definition of polymorphism was written by Liisa Lutter *et al*: "From one amino-acid sequence to many three-dimensional structures"[102]. The polymorphism can also be considered in hierarchical manner, since amyloids are hierarchically organized on many levels. Starting from the largest organizational unit: 1) differences in

mesoscopic arrangement like fibril length, helical pitch, handedness of fibril twist, number of protofilaments per fibril; 2) assembly of protofilaments inside the fibrils; 3) protofilament fold; 4) amino acid sequence changes by e.g post translational modifications, mutations. Polymorphism translates to various biological response, which will be explained in the next chapter "Amyloid links with disease". Polymorphism might play a crucial role in binding of ligands to amyloids[103] e.g PET tracers, inhibitors of growth, fluorescent probes. However, prediction of amyloid 3D-structures is a challenging process, various polymorphs coexist in a laboratory tube and their separation in most cases is impossible. The recent studies used high-throughput experiments to select fluorophores, which selectively binds to tau polymorphs[104]. The use of high-throughput experiments, which give large amount of data with ML approaches might be a future successful method in selection of proper drugs and probes targeting amyloids.

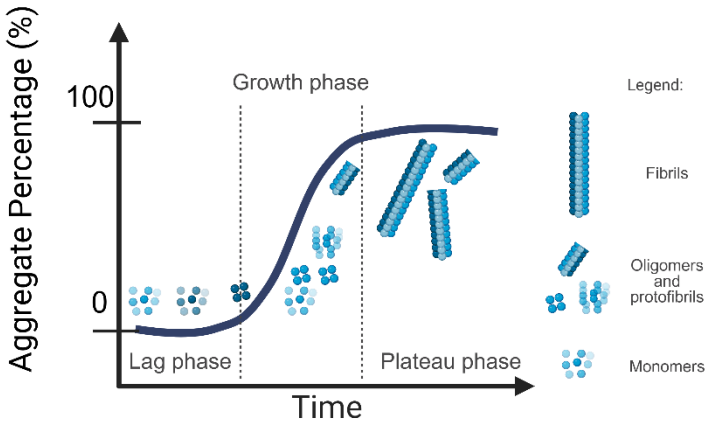

Figure 7. *Schematic representation of primary pathway of amyloids growth from monomers of peptides. Figure was made using Biorender® with Publication and Licensing Rights.*

When discussing amyloids, their growth mechanism is a key feature. Amyloids are formed in a polymeric type growth.[105-106] There are two type of pathways of amyloid growth[107-108]: 1) primary pathway, when new aggregates are formed from monomeric peptides and 2) secondary pathways, when new fibrils might be created from fragmentation of already existing fibrils or through the process called secondary nucleation[109], when on already existing fibrils new fibrils are formed from monomers. Let focus on a primary pathway, which is presented in Figure 7. Starting from a monomeric unit, nuclei is formed, then peptide oligomers are formed, which with proper amount of monomer-subunits form β-sheet rich structure and elongate into protofibrils and later mature fibrils. The kinetic profile is typically sigmoidal shape with three phases – lag phase, growth phase and plateau phase. In fluorescence-based experiments, a dye whose fluorescence emission is enhanced upon interaction with fibrils, rather than the monomeric form of the peptide, is added. Due to this phenomena, fluorescence signal is detected, which increases when number of fibrils in growing. During lag time, nuclei are formed and no signal is detected.[110] When numerus nuclei will grow and proliferate to give detectable signal, growth phase starts to appear. In a growth phase oligomers are formed, which elongate and giving rise to elongated structures called protofibrils. This is also the phase rich in amyloid oligomers. In the literature, the term "amyloid oligomers" has wide and ambiguous definition.[111-112] Oligomers of amyloids represents diverse group of soluble or insoluble aggregates formed by few to thousands of monomeric peptide subunits. They spark attention

due to their biological activity and neurotoxicity[113-114]. The last phase – plateau is state, where concentration of monomer form of peptide is in an equilibrium.[110] Study of the kinetic growth of amyloids *in vitro* is mostly done using fluorescent probes like Thioflavin-T, which increases their fluorescence response upon binding to amyloids, not soluble native proteins (it will be described in the chapter "Fluorescent probes for amyloid detection"). However, investigation of amyloid deposits buildup *in vivo* is more challenging task, there is also a possibility to use of proper fluorescent staining probes and visualize brain of model organisms for weeks or months. For this purpose 2PFM is used, due to advantages, which were mentioned in the chapter "Two-photon fluorescence microscopy".

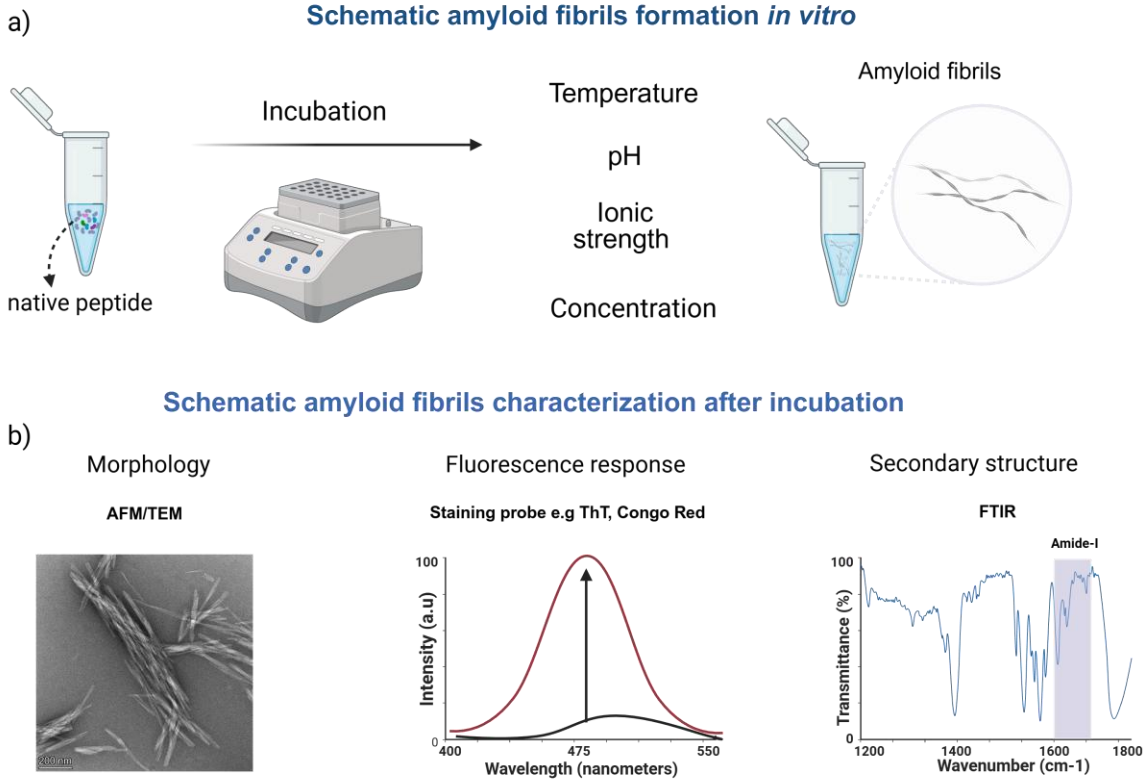

Figure 8. *a) Scheme of amyloid fibrils formation from native protein in laboratory conditions; b) representation of complementary techniques of amyloid characterization after incubation. Figure made using Biorender® with Publication and Licensing Rights.*

Since not all amyloid-related processes can be investigated *in vivo*, and a deeper understanding of the fundamental dynamics and properties of amyloids is required, the majority of amyloid studies are carried out *in vitro*, under controlled conditions in laboratory tubes etc. To study amyloids in laboratory (*in vitro*), native proteins are incubated in specific conditions like elevated temperature, proper (high) concentration, ionic strength and pH (schematic illustration in Figure 8a). The incubation conditions depend on used native proteins, however usually low pH, higher temperature and ionic strength induce faster aggregation. There are proteins, which are used as amyloid-model systems due to their simple incubation and

relatively low price compared to disease related proteins e.g bovine insulin[115], hen egg white lysozyme[116] and β-lactoglobulin[117]. For bovine insulin, which was used in this thesis as a model amyloidogenic protein, conditions of incubation are: pH 1.5-3, with elevated temperature above 37°C, additionally extra salt content e.g NaCl can impact obtained morphology of amyloids. To confirm presence of fibrils in solution after incubation and obtaining their characteristics features, several techniques might be used. They gives various information regarding amyloid structure – as presented in Figure 8b. To confirm the presence and morphology of fibrils: Transmission Electron microscope (TEM) or Atomic Force Microscope (AFM) imaging is performed. TEM gives more reliable information about the sizes in the sample plane (X and Y axis), while AFM can give precise information in Z-axis, which is not possible under TEM. AFM is widely used in amyloid morphology studies[117-118], it can be also harvested to give more detailed information, like polymorphism studies[119]. TEM can also be used routinely to confirm presence of amyloids. However, it should be remembered that the sample preparation procedure uses heavy isotope salts like uranyl acetate to obtain suitable image contrast. Cryo-EM, which is a type of TEM applied to samples with cryogenic temperature revolutionized amyloid research. This is not a technique used in routine research, but rather to answer fundamental questions regarding 3D models of fibrils on atomic level[120-122]. Other detection methods are techniques based on fluorescence using proper fluorescent amyloid-staining agents like Thioflavin-T or Congo-Red. They are fast and widely available methods in any (bio)chemical laboratory. Fluorescence application to detect amyloids will be in details described in the chapter “Fluorescent probes for amyloid detection”. To observe characteristic changes in secondary structure of proteins upon aggregation, Fourier Transform InfraRed (FTIR) spectroscopy measurements might be performed. Changes in Amide-I region (1600-1700 cm^{-1}) characteristic for β-sheets are an indicator of amyloid formation[123].

2.3.2 Amyloids links with diseases:

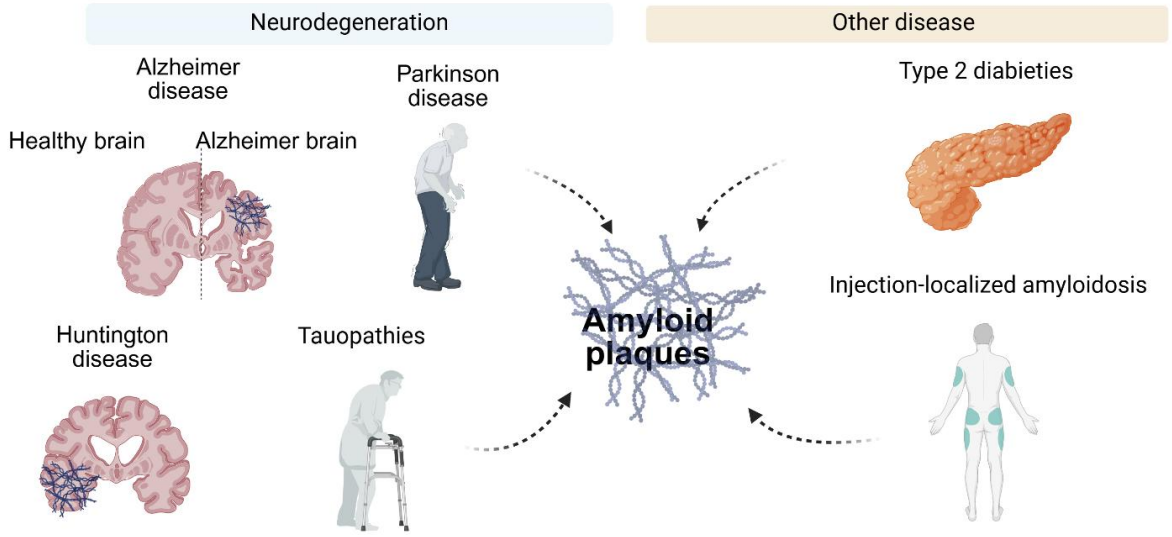

Figure 9. *Examples of neurodegeneration disease and other type of disease related to amyloid plaques formation. Figure made using Biorender® with Publication and Licensing Rights.*

Amyloids association with diseases dates back to Alois Alzheimer discoveries in 1906, when he documented first case of AD in his patient - Auguste Deter.[124] In postmortem tissues Alzheimer visualized plaques in the brain, which contained amyloids stained with dye called Congo-Red. Amyloid fibrils can aggregate into bigger structures called amyloid plaques in the human body, which in histopathological evaluation can be even see with naked eye. To this day presence of amyloids is associated with over 50 diseases[108], which the most popular are neurodegeneration diseases, but also other like Type 2 Diabetes (T2D), Injection-localized amyloidosis or Senile systemic amyloidosis.[125] There are also "functional amyloids", which have physiological activities in bacteria or humans.[126-128] However, they will not be discussed here. In humans or model organisms specific native protein, which plays important physiological role in healthy individuals can abnormally aggregate. In the Figure 9 examples of diseases are shown, which are related with amyloid plaques accumulation. **IAPP – islet amyloid polypeptide or amylin is** a peptide hormone co-secreted with insulin by pancreatic β-cells, contributing to glucose homeostasis, formation of amyloids by IAPP is a factor in development of **Type 2 Diabetes (T2D)**[129]. **Tau protein**, which participate in microtubule assembly and stabilization, can form inclusions in the brain, which are related with a group of neurodegenerative pathologies called **Tauopathies**[130]**, including Alzheimer's disease (AD)**; **α-synuclein** is mainly responsible for regulating synaptic vesicles and neurotransmitter release, its abnormal aggregation is related with **Parkinson disease and dementia with Lewy bodies**[131]; **Huntingtin (HTT)** has many functions in a healthy organism, simply it can be summarized as a protective and regulatory role in the nervous system, its aggregation is

associated with **Huntington disease**[132]. However, the most famous representative of disease-related amyloid is **Amyloid-β (Aβ) protein**, which is more considered as a byproduct of the metabolism of a larger protein called amyloid precursor protein (APP). Upon aggregation forms amyloid plaques in the brain, which are hallmarks of **AD development**[117]. The *amyloid-cascade-hypothesis* is one of the possible explanation of the pathogenesis of AD - as cause of accumulation of Aβ plaques in the brain. It sparks a lot of attention in scientific community, which confirms number of publications: **1,750** in WoS (till 02.09.2025) for keywords : amyloid-cascade-hypothesis or amyloid hypothesis. Hypothesis formulated in 1992 present linear cause (amyloid formation and accumulation in the brain) and effect (AD development) mechanisms[133]. Based on this hypothesis amyloids became main target in research and therapeutics regarding AD. A major problem in the study of the influence of amyloids on organisms physiology is the fact that in a disease state several native proteins may aggregate e.g in AD besides Aβ plaques in the brain, hyperphosphorylated tau protein as neurofibrillary tangles (NFTs) are also present [134-135]; there is also more evidence of cooperation between Aβ plaques and IAPP aggregates in the individuals who suffer from T2D and AD[136-137]. Additionally, polymorphism[138-139] and various conformers of amyloids[140] from the same native peptide complicate the study of amyloid effect on pathology development. It has a real implication in human health, since distinct polymorphs translate to development of different disease[120, 141-142] - specific folds of tau protein define distinct tauopathies. Determined structure of tau polymorphs by Cryo-EM from the postmortem brains from the individuals having different types of tauopathies e.g Pick's disease, Chronic Traumatic Encephalopathy (CTE) reveled that specific filament fold indicated certain pathologies[143]. Similar scenario is for Amyloid-β, individuals with sporadic Alzheimer's disease had domination of Type-1 filaments, while patients with familial Alzheimer's disease had domination with so-called Type-II filaments[144]. This shows the complex molecular picture of amyloids and explains, why despite thousands of studies, scientists are still working intensively on them.

Over the years some concerns regarding *amyloid-cascade-hypothesis* hypothesis were raised[145-146], due to the extensive *in vivo* studies in laboratories on animal models and also based on data taken from patients. Nowadays, medical community considers it more as a working hypothesis[147] and AD and other amyloid-related diseases is still not well understood [148]. Even thou linear correlation between cause and effect seems to be far from the true, new therapies targeting formation of amyloids were approved by US Food&Drugs Administration (FDA)[149-151]. Due to population aging in developed countries, which is related with high percentage of dementia patients, lack of effective therapies can lead to hundreds of billions of dollars cost (based on data provided by The Alzheimer's Association). Without a doubt, there is still a need to better understand the role of amyloids in diseases since it can impact development of new therapeutics, which has health consequences for millions of people around the world as well as financial consequences for government and medical institutions. One of the approaches to understand in details the role of amyloids in development and progression of diseases is detection and visualization on molecular level preferably in model organisms, as

well the study of amyloid *in vitro*. It can be realized by techniques based on fluorescence like spectroscopy or microscopy, which are standard methods in pre-clinical studies. To obtain fluorescent signal fluorescent probes, which will bound to target (in the case of this dissertation - amyloids) are needed. In the next chapter fluorescent probes for amyloid detection will be presented.

2.3.3 Fluorescent probes for amyloid detection:

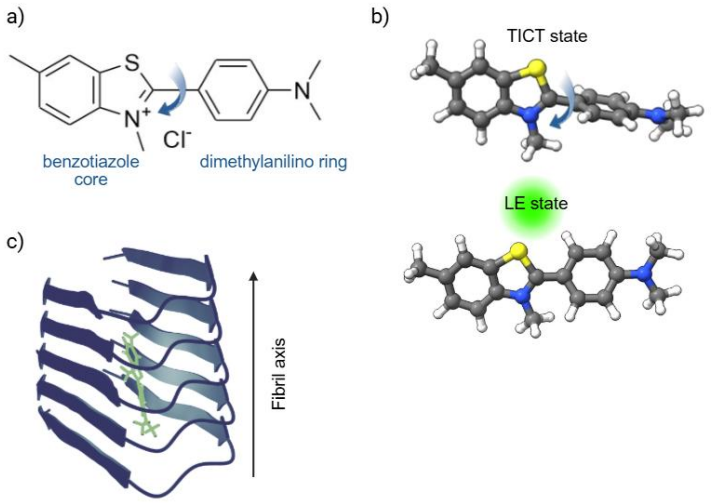

Figure 10. *a) Structure of ThT, arrow indicate rotating C-C bond; b) Structure conformation of ThT in the TICT and LE state. LE state is highlighted to point out its emissive nature; Taken from PubChem and modified using ChimeraX. c) Location of ThT inside the fibril, 3D Structure of Alzheimer's Abeta(1-42) fibrils using PDB: 2BEG. Modified using ChimeraX and Blender 4.3.*

One of the most popular amyloids detection methods *in vitro* and *in vivo* rely on fluorescent probes, which selectively binds to amyloids fibrils. Fluorescent probes can be used to visualize amyloids in the imaging procedure, which was mentioned before. However, they can also be applied in spectroscopic techniques when it is necessary to determine whether amyloids are present in solution e.g study kinetics of amyloid formation, study the formation of amyloids in certain incubation conditions.

The gold standard in fluorescent probes for amyloid detection is Thioflavin-T (ThT) - 2-[4-(dimethylamino)phenyl]-3,6-dimethyl-1,3-benzothiazol-3-ium chloride (IUPAC name) – see structure in Figure 10a. Since being introduced for amyloid staining in 1965[152], the dye has been routinely used for the *in vitro* quantification of amyloid formation. ThT upon binding to amyloids have fluorescence emission maximum (λ_{EM}) around 485 nm and its intensity increases few orders of magnitude upon binding to amyloids, as compared to free dye in the solution. It was proven that ThT binds to the amyloid fibrils parallel to their long axes (Figure10c)[153]. ThT belongs to the group of so-called molecular rotors[154-155], the C-C bond between benzothiazole core and the dimethylanilino ring can rotate in the solution. Due to this fact upon excitation formation of Twisted Intramolecular Charge Transfer (TICT) take place, where the angle between benzothiazole and dimethylanilino rings changes from 37° to 90°, which leads to non-radiative processes domination and almost non-fluorescence response[156]. On the other hand, when molecule is immobilized in the high viscosity medium or inside fibrils, it results in formation of emissive locally excited (LE) state[157]. Comparison of

conformation for this two states is presented in Figure 10b. Non-bound ThT gives low background signal and high enhancement of FQY upon binding is used to detect fibrils[158], especially in amyloid growth kinetics (see subsection 2.3.1 Definition of amyloids). The works from Prof. Sara Linse and Prof. Tuomas P J Knowles made a major contribution in the development of amyloid growth kinetics protocols and mathematical models of the kinetics of amyloid growth using ThT[106-107,110,159], but also revealed new pathways of growth like secondary nucleation[109,160] or differences in growth of amyloids from Aβ40 and Aβ42 peptides.[161] ThT most often possess a few types of binding modes with various affinities to amyloids from different proteins e.g insulin[162-163], Aβ42[164-165], alfa-synuclein[166]. Also adding dye to mature fibrils or during incubation procedure might impact a type and number of binding modes.[167]

The number of publications focusing on ThT or employing it in various applications clearly reflects the popularity of this dye, however it has also disadvantages, which encourage scientists to develop new fluorescent probes for amyloid detection. Presence of additional exogenous compounds in solution can give false results monitoring aggregation process[168]. Ionic strength has impact on the performance of ThT[169], by modification of the dye's binding affinity and fluorescence intensity upon interaction with amyloids. Additionally, pH plays an important role in ThT interactions with amyloids, since it is a cationic dye (has a positive charge on nitrogen in benzotiazole core). On the surface of amyloids, there are amino acid residues with variable protonation, with pH change, protonation of this groups also change and when the surface of the fibril may be positively charged, electrostatic repulsion limits the binding of positively charged ThT (opposite effect is when the surface of the fibril is negatively charged). Incubation of peptides occurs often at low pH, which lowers fluorescence response of ThT[170] and can give false results[171]. Furthermore, charged nature with low lipophilicity limits its use in *in vivo* studies, since it has poor blood-brain barrier penetration[172]. Another disadvantage is limited selectivity toward amyloids, ThT also binds to DNA[173-174] and RNA[175-176]. ThT binds to fibrils formed from various peptides. While the binding induces a characteristic fluorescence signal, the emission maximum remains largely unchanged regardless of the amyloid type. Consequently, ThT assays cannot distinguish between different amyloid species, which can be considered a limitation depending on the intended application. To answer mentioned disadvantage many derivatives of ThT were proposed. Derivative called **ThN** addressed hydrophobicity of ThT, emission position (red-shifted), enhanced binding affinity toward Aβ amyloids[177]. Analog **DMASEBT** has red-shifted emission by over 100 nm[178-179], which increases its attractiveness for *in vivo* studies. There are derivatives dedicated for detection of certain amyloids- Amylin[180] ; α-synuclein[181]. Lisa-Maria Needham *et al.* addressed detailed photophysical characterization and comparison of library of derivatives, differing in one modification in the structure, e.g. a functional group[182].

Most of derivatives of ThT use ability of molecular rotors, where the non-restricted structure is non-fluorescent, however after binding, intense emission occurs due to the rigidification of

the dye structure inside fibrils. To note, ThT derivatives are not only representatives of molecular rotors for amyloid detection[183]. However, there are more mechanism of modulating fluorescence properties of probes interacting with fibrils. Another family of fluorophores are so-called "environment sensitive" dyes, which upon changes in polarity[184-185] or simultaneously polarity and viscosity modulate emission[186-188]. This type of molecules often have charge-transfer (CT) character, which means that during electronic excitation (via light) electron density moves from electron-donating part of the molecule to an electron-accepting part. This excited state with redistributed electron density have stronger dipole moment, than ground state. Polar solvents/microenvironment stabilize excited state more strongly, leading to solvent-dependent shifts in emission spectra, which is called solvatochromism. It is especially useful, since environment inside binding pockets of amyloids is usually less-polar, which can be probed by emission of this type of dyes. Binding pockets in fibrils formed from different native proteins or even between conformers of amyloids also have various microenvironment, which can be detected. **Aminonaphthalene 2-cyanoacrylate (ANCA)** dye was used to discriminate Amyloid-β and Prion Plaques in brain thanks to distinct fluorescence spectra upon binding to various amyloids, additionally static relative permittivity of binding pockets of Aβ and PrP^{Sc} were estimated.[189] Another, group are probes based on N,O-benzamide difluoroboron moiety (- N,O-BF_2) which is strong electron acceptor group connected with electron donor group - N,N'-dimethylaminobenzene. It creates intramolecular CT character in order to reach the emission in NIR region. They also presents solvatochromic properties, which were used in Aβ and tau fibrils detection.[190-191] The best candidate called **4PmNO-2** had 174 nm bathochromic shift from n-hexane (562 nm) to PBS (716 nm). Its environmentally sensitive fluorescence was also reflected upon binding, since in $A\beta_{1-42}$ λ_{EM}= 632 nm, and for Tau λ_{EM}=654nm[190].

2.3.4 Fluorescent probes for Amyloids in 2PFM:

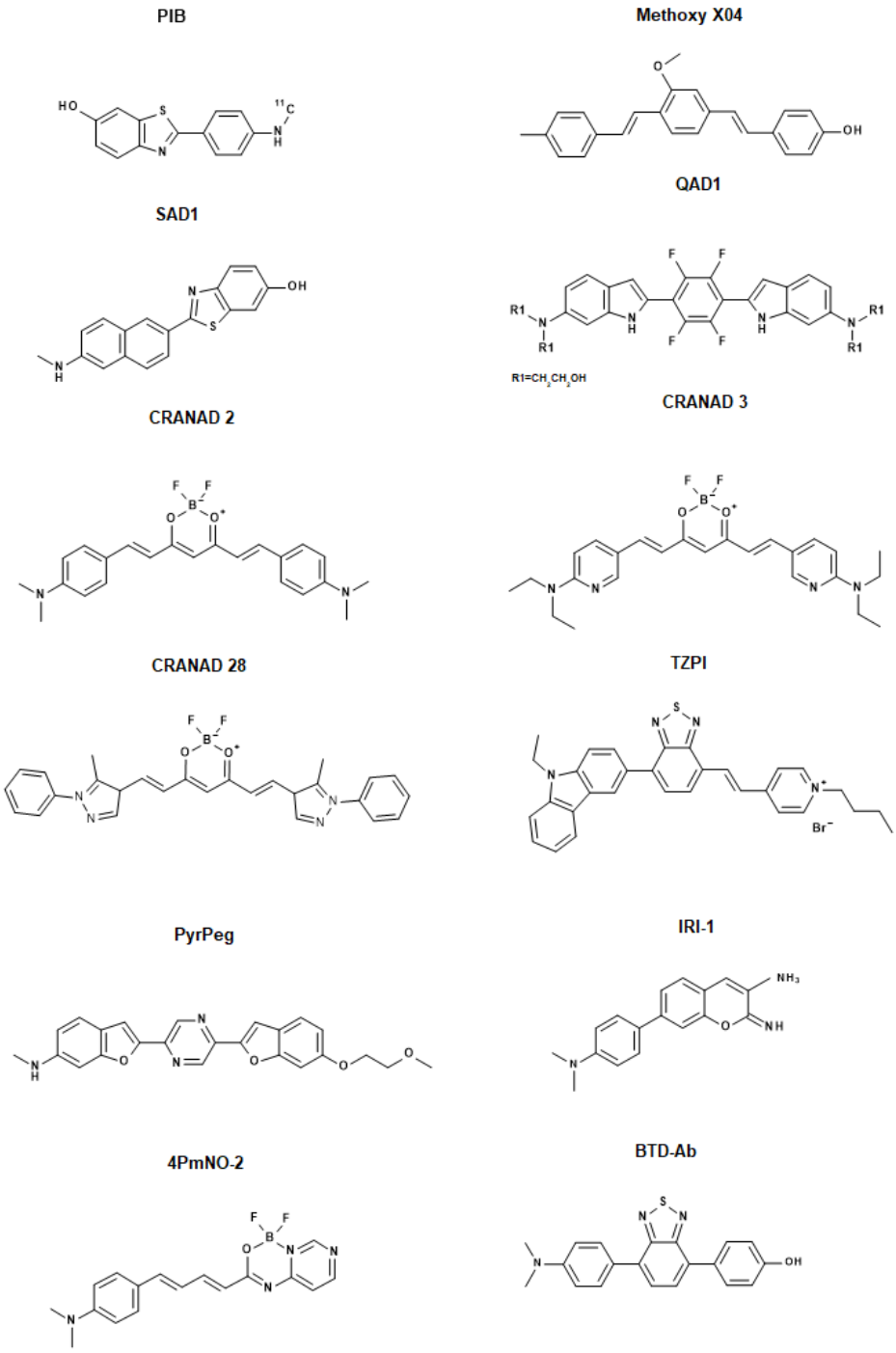

Figure 11. *Structure of dyes presented in section " 2.3.4 Fluorescent probes for Amyloids in 2PFM.".*

This section focuses **only on fluorescent probes used for two-photon microscopy/multiphoton microscopy in amyloid detection**. All of the structures of mentioned probes are presented in Figure 11. The same mechanisms of fluorescence enhancement upon binding to amyloids as discussed earlier are also valid for two-photon excited fluorescence. However, properties of fluorescent probes required for two-photon excited amyloid detection are: high σ_2 and $\sigma_{2,B}$. Additionally since 2PFM is used mostly *in vivo* properties for this type of imaging should be considered: NIR emission; reasonable lipophilicity (log *P* between 1 and 3); molecular mass less than 600 Da; high-affinity binding, stability in blood and low-affinity binding with bovine serum albumin (BSA).[192]

In 2002 William E. Klunk *et al.* proposed one of the fluorescent probes for amyloid detection in 2PFM called **Methoxy-X04 (MeO-X04)**.[193] **MeO-X04** was IV generation of Congo Red (CR)[193] derivative with improved brain entry, which was at that time rarely achieved property. Authors presented detection of individual amyloid plaques in the brain on living PS1/APP mice (one of Alzheimer's disease transgenic mouse model) by multiphoton microscopy. However, optical properties like fluorescence, absorption spectrum, FQY, σ_2 were not presented. Nevertheless the molecule become a standard in postmortem tissues, as well as *in vivo* 2PFM. Later, other publications reveled optical properties of **MeO-X04**, which had some disadvantages like λ_{EM} below 600 nm, which limits light penetration into the tissues; a maximum $\sigma_{2,B} = 75$ GM[194]. Additionally, MeO-X04 have a not-specific staining of various forms of amyloids – Aβ plaques, NFTs and cerebrovascular amyloids. Since the introduction of **MeO-X04**, other two-photon probes with more optimized properties like higher $\sigma_{2,B}$ [194-195] or red-shifted emission[192, 196-198], broader excitation ranges, higher selectivity toward specific type of amyloids[190,199] were proposed. **Pittsburgh Compound-B (PIB)** is based on hydroxybenzothiazole, which was designed for amyloid-imaging PET[200]. However, despite the lack of optimization in two-photon properties (maximal $\sigma_{2,B} \sim 50$GM) and emission below 600 nm, was used for multiphoton microscopy[200]. **PIB** can be used as reference dye for two-photon evaluation.[194]

6-(6-hydroxy-benzo[d]thiazol-2′-yl)-2-(N,N-dimethyl amino)naphthalene, in short **SAD1,** was presented as effective 2P probe that can be used in deep tissue imaging to 3D monitor Aβ plaques *in vivo*[194]. Its performance was compared to other used probes like MeO-X04, PIB. **SAD1** had red-shifted λ_{EM} (497 nm with FQY = 24%), compared to PIB (431 nm) and MeO-X04 (452 nm) in phosphate buffered saline (PBS). **SAD1** had significantly higher $\sigma_{2,B}$ within 720-880 nm 2PE range in contrast to PIB or MeO-X04. Maximum of $\sigma_{2,B}$ for **SAD1** was 170 GM at 750 nm, while PIB 40 GM and MeO-X04 75 GM. **SAD1** was evaluated in transgenic 5xFAD mice (genetically modified model carrying human Alzheimer's-related genes that rapidly develops disease-like symptoms[201]) and allowed for high-resolution 3D imaging of single Aβ plaques *in vivo*, at depths greater than 380 μm, with low background fluorescence and minimal photobleaching. Progress in two-photon absorption cross-sections was visible at that time, however emission was still in the range of high autofluorescence and scattering.

The same group few years later, proposed another 2P probe called **QAD1**, which was quadrupole dye based on tetrafluorobenzene (electron acceptor).[195] Fluorescence emission was between 450-650 nm upon binding to Aβ amyloids and $\sigma_{2,B}$ was improved, with value 420 GM at 750 nm. **QAD1** was also evaluated *in vivo* on the transgenic 5xFAD mice and 3D visualization of the individual plaques was obtained. $\sigma_{2,B}$ was significantly improved compared to SAD1, emission ranges were slightly red-shifted. However, excitation range was the same as in the case of SAD1, MeOX-4 or PIB, not exciding 880 nm.

Interesting scaffold based on boron-containing curcumin derivative for amyloid detection was presented by Chongzhao Ran *et al.* (called **CRANAD)**[192]. It was one of the first dyes that had emission in NIR along with 70-fold fluorescence intensity increase upon binding to Aβ aggregates and suitable properties for studying amyloids *in vivo* as stability in serum, high affinity towards Aβ amyloids (K_d = 38.0 nM) and proper brain entry. The first generation of CRANADs laid the foundation for the broad group of derivatives, some of them were more intended for two-photon microscopy. CRANADs due to their electronic architecture with strong ICT character, present environment sensitive emission in the NIR range, which contributed to their versatile applications. In **CRANAD-3** the two phenyl rings were replaced by pyridyls in order to promote hydrogen bond formation between the interacting Aβ fragment and the pyridine nitrogen atoms[198]. **CRANAD-3** showed λ_{EM} ~ 730 nm in PBS and various response like fluorescence enhancement and peak of emission toward soluble species (monomers, dimers, and oligomers) and insoluble (aggregates) Aβ species. 2PFM imaging of Aβ deposits with **CRANAD-3** was performed, co-staining of amyloid plaques with Thioflavin-S (derivative of ThT used in histopathology) confirmed its applicability. However, authors did not present two-photon properties of this dye (σ_2, or $\sigma_{2,B}$), in this meter it's impossible to compare it quantitatively to previously mentioned two-photon probes. **CRANAD-28** with phenyl rings replaced with phenyl substituted N-1 position of pyrazole was also tested for 2PFM[197]. Due to this substitution, FQY of **CRANAD-28** was improved compared to other derivatives from this family – with values of FQY in PBS equal 29%, while in EtOH 47%. It also stained Aβ aggregates in APP/PS1 mouse, which was image by 2PFM. However, as for **CRANAD-3,** authors did not presented two-photon properties of studied molecule. In general, CRANAD derivatives are known for NIR emission and optimized properties for *in vivo* imaging. Unfortunately, their quantitative 2P properties have not been demonstrated, which minimizes the understanding of the influence of structure changes in derivatives on their non-linear properties. Based on the structures and use in 2PFM, it can be assumed that σ_2 might be high due to the donor-acceptor-donor electronic architecture. Incorporated BF_2- moiety is a strong acceptor, impacts σ_2, which was discussed preciously.

Molecular rotor probe called **intramolecular rotation-enabled iminocoumarin 1 (IRI-1)** based on coumarin core and rotating dimethylaniline group was introduced for 2PFM.[202] Inspired by ThT, **IRI-1** presented conformational restriction upon binding to amyloids[202], which resulted in fluorescence intensity increase of ~167-fold in the presence of Aβ fibrils.

Low signal-to-noise ratio resulted from TICT state formation of excited non-bound dye. Optical properties were : λ_{EM}=566 nm in the presence of Aβ fibrils and $\sigma_{2,B}$ reached values up to 111 GM at an excitation 880 nm. To confirm visualization of Aβ plaques in transgenic mice 5xFAD by **IRI-1** using 2PFM, co-staining with MeO-X04 was performed**.** High degree of signal overlap coming from two dyes, confirm that **IRI-1** can detect plaques *in vivo* by 2PFM. Example of **IRI-1** shows, that class of molecular rotors can be effective two-photon probes for amyloid detection, however one of the disadvantage was less red-shifted emission compared to e.g CRANADs family.

Dye called **PyrPeg**, fusion of a pyrazine derivative and poly(ethylene glycol),[203] reached record high $\sigma_{2,B}$ for amyloid probes - 543 GM in 1,4-dioxane. Its fluorescence emission is located on the border of 600 nm (in 1,4-dioxane). High $\sigma_{2,B}$ resulted in higher signal in the imaging procedure upon staining amyloid plaques, than for Thioflavin-S and MeO-X04. In AD model mouse brains and human post-mortem tissues, the novel probe shows selective affinity for insoluble Aβ over tau or α-synuclein aggregates. Additionally, **PyrPeg** was used in Aβ staining in metabolic studies.[204] Missing information in the article is fluorescence properties of **PyrPeg** upon binding to amyloids (like emission ranges, FQY, or enhancement of fluorescence). Therefore, despite the record high cross sections in 1,4-dioxane, some of the optical properties cannot be compared to other dyes presented in this section.

Fluorescent benzothiadiazole (BTD) derivatives are gaining more and more interest as novel probes[205] due to strong electron acceptor effect and relatively simple modifications in the structure. Polarity-sensitive dye with D–A-ion architecture based on BTD scaffold called **TZPI** was presented for insulin amyloid detection[185]. In **TZPI** the dominant mechanism of enhancement of fluorescence is the change of polarity in the environment (restriction of conformation was excluded). **TZPI** exhibits a large σ_2= 467.6 GM at 890 nm excitation upon binding to amyloids**, it is first and only σ_2 presented in this chapter upon binding to amyloids. All other values were measured for unbound dyes in the solvents. TZP**I also had high photostability and λ_{EM} =648 nm with insulin amyloids. Another BTD-based probe is the so-called **BTD-Aβ**.[206] It is a molecular rotor with D-A-D architecture. **BTD-Aβ** presented σ_2=240 GM, red emission with λ_{EM}=630 nm, and large Stokes shift of 200 nm, which is also beneficial in bioimaging. The probe was successfully used for *in situ* observation of Aβ42 aggregating in brain-derived endothelial cells and *in vivo* brain imaging in AD mice.

Another interesting family of fluorophores is organoboron compounds, which includes N,O-coordinated or N,N- coordinated organo-BF_2/BF dyes. Many derivatives were proposed for amyloid detection, however most of them are intended for one-photon detection. Y. Chen *et al.* presented series of new N,O-coordinated organo-difluoroboron probes with D-A architecture.[190] The optical properties of the dyes made them suitable for 1P and 2P NIR imaging. Upon binding to Aβ aggregates and NFTs, their emission maxima differed between synthetic protein preparations and aggregates obtained from AD patient tissues and transgenic

mice. For probe called **4PmNO-2**, σ_2 reached 234 GM at the excitation wavelength of 810 nm. Unfortunately, 2PA of other presented molecules was not evaluated.

There is a progress in development of two-photon probes in terms of fluorescence emission ranges, values of σ_2, $\sigma_{2,B}$ and selectivity. It is worth noting, that some of the markers, despite their use in imaging, lacked the information about key optical parameters like σ_2, FQY, λ_{EM} for two-photon markers. This does not remove their ability to be used in two-photon microscopy, although it significantly complicates comparing the markers with each other and understanding how the structure affects the properties. There are aspects regarding two-photon probes for amyloids which are not addressed in the literature. One of them is a change of values of σ_2 or $\sigma_{2,B}$ upon binding to amyloids. Only in study on **TZPI** authors measured σ_2 upon binding to insulin amyloids, other works present σ_2 only in solvent (usually organic ones). Two-photon absorption cross-sections can be influenced by surrounding microenvironment, which was used in sensing K+ ions[207], viscosity[208], polarity[209], localization inside DNA[210]. It is important due to the fact that higher σ_2 correlates with obtaining higher signal upon 2PE. Potential changes between σ_2 in solvents and upon binding may give a false representation of the possibilities of a given dye. Second, there are no studies addressing correlation between structure- two-photon properties and amyloid binding. In terms of one-photon probes, creating library of structures and comparing their relationship between structure – optical properties e.g FQY, λ_{EM}, simultaneously with amyloid binding is a known approach. However, for two-photon probes even if library of molecules is created, evaluation is done only for one-photon properties and only the best candidate is evaluated in terms of σ_2 and 2PFM, which was the case for N,O-coordinated organo-difluoroboron dyes[190]. Lack of correlation between structure-two-photon properties-amyloid interactions limits design of fluorescent probes with intended properties, which I address in this thesis.

III. PUBLISHED WORK - DESCRIPTION OF OWN RESEARCH

Chapter 3. BF2-FUNCTIONALIZED BENZOTHIAZOLE AMYLOID MARKERS: EFFECT OF DONOR SUBSTITUENTS ON ONE- AND TWO-PHOTON PROPERTIES.

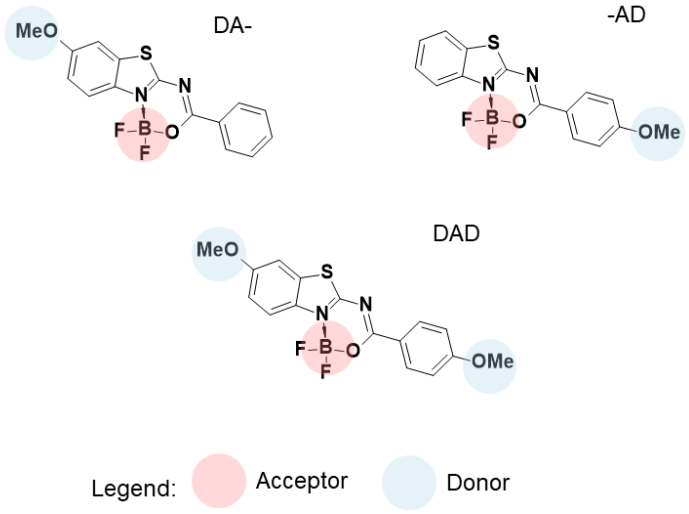

***Figure 12**. Structures of studied molecules with highlighted donor and acceptor part of the molecules. Blue circles indicates electron donor groups; red circles indicates electron acceptor groups.*

3.1 Research purpose:

9 BF_2-functionalized benzothiazoles with structural core inspired by ThT, were previously proposed by Rybczyński et *al.*[56] The systematic change of functional groups in the two substitution points (R and R'), where R is benzothiazole fragment and R' is the *para* position of the phenyl ring (R′) resulted **in tunning FQY between 0.4 and 98%.** Substitution in R and R' points were done by two functional groups: mild electron donating group – methoxy (-MeO) and inductive electron acceptor (-CF_3). Single C−C bond between the benzothiazole core and phenylene group, is similar as in ThT, resulted in rotational freedom. To systematically evaluate how dye structure relates to its **optical properties upon interaction with amyloids**, I selected three dyes from the work of Rybczyński et *al* [56], which had varying position of donor group in the R,R' positions. Studied dyes with architecture: (1) donor-acceptor (**DA-**) (IUPAC

name: ((*Z*)-[(difluoroboryloxy)-phenylmethylene](6-methoxy-1,3-benzothiazol-2-yl)amine); (2) acceptor-donor (**-AD**) (IUPAC name: (*Z*)-[(difluoroboryloxy)(4-methoxyphenyl)-methylene]-1,3-benzothiazol-2-ylamine); (3) donor-acceptor-donor (**DAD**) (IUPAC name: (*Z*)-[(difluoroboryloxy)(4-methoxyphenyl)methylene](6-methoxy-1,3-benzothiazol-2-yl)amine)) are presented in Figure 12. They have dipolar electronic architecture with a mild-donor agent and strong acceptor group - BF_2.

From studies by Rybczyński *et al* [56] it is known, that the FQY of **DA-** dye is mainly sensitive to viscosity; **-AD** dye was robust emitter and exhibited low sensitivity to environmental factors (hydrogen-bonding network, polarity, and viscosity); **DAD** dye fluorescence was responding to changes in hydrogen-bonding, polarity as well as viscosity. I wanted to investigate whether these dependencies obtained in solvents could be translated into interactions with more complex structures like amyloids. This approach was beneficial in terms of understanding optical properties such as the fluorescence lifetime (τ), FQY, 2PA, λ_{EM} change upon binding to amyloid fibrils. One of the main goals of the research was **to evaluate σ_2 of dyes before and after binding to amyloids**. This could give an insight into modulation of 2PA and 2PEL in the same manner as one-photon properties, which is an innovative aspect of the research. σ_2 or $\sigma_{2,B}$ are determined mostly in pure solvents such as ethanol, chloroform, methanol, *N*,*N*-Dimethylformamide, which mimic more hydrophobic environment in the core of amyloids. However, scarce examples presented in the literature investigating dyes bound to biopolymers such as DNA or peptides indicate that the fluorophore orientation and localization inside biomolecules module their two-photon response[210-211]. Thus, determination of σ_2 upon binding should predict more accurately performance of probe for 2PFM, than evaluation only in pure solvents. Additionally, it can lay the foundation for future investigation of fluorescent probes, where modulation upon binding will play a role in the design of not only fluorescence properties, but also 2PA.

3.2 Results:

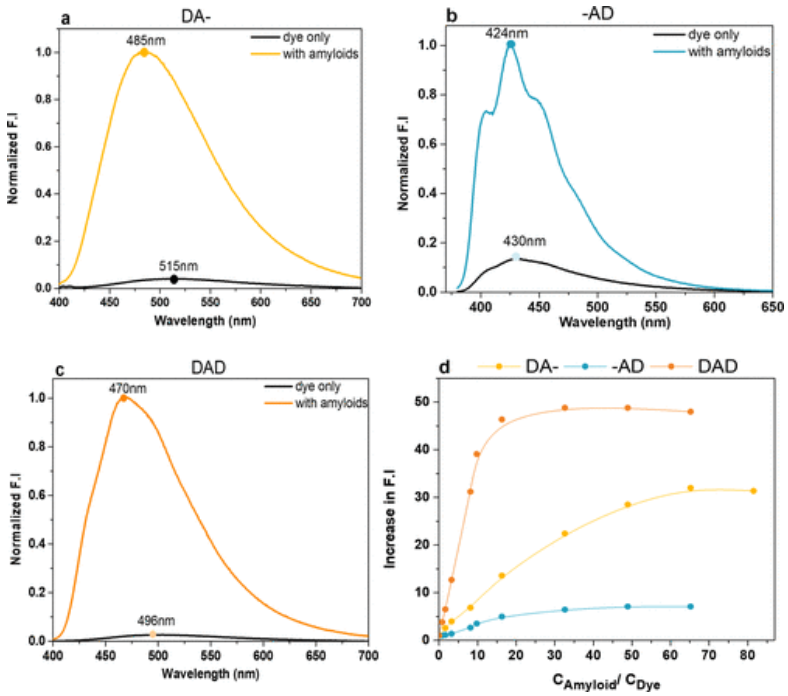

Figure 13. *Fluorescence intensity of dyes upon interaction with insulin amyloids for: (a) DA- dye (b) AD dye (c) DAD dye; (d) Comparison of fluorescence intensity (F.I) increase with increasing concentration of insulin amyloids. Figure reproduced from [Hajda A., Grelich-Mucha M., Rybczyński P., Ośmiałowski B., Zaleśny R., Olesiak-Bańska J. (2023). BF2-Functionalized Benzothiazole Amyloid Markers: Effect of Donor Substituents on One- and Two-Photon Properties. ACS Appl. Bio Mater. 6, 12, 5676–5684.]*

Dyes were synthesized by Patryk Rybczyński and Prof. Borys Ośmiałowski at the University of Mikolaj Kopernik, Toruń. Model amyloid system was bovine insulin amyloids, where I confirmed the presence of fibrils after incubation of native protein by AFM, which is presented in Figure S1 of Supporting Information on page 62. Firstly, I evaluated one-photon optical properties like FQY, one-photon excited fluorescence (1PEF), τ_{ave}, of fluorophores before and after insulin amyloid binding and compared to values in glycerol – which represents a viscous medium, and in $CHCl_3$, which represents a hydrophobic medium. Restricted motion of a dye in glycerol relates to immobilization of a dye inside the amyloids, while $CHCl_3$ hydrophobic environment resembles usually hydrophobic binding pockets of amyloids. **Note that it is an approximation of certain properties of microenvironment in amyloids.** Fluorescence spectrum before and after amyloid binding for all dyes is presented in Figure 13. I measured fluorescence spectra at various concentration of amyloids (dye concentration was constant) and increase in fluorescence intensity at $\lambda_{EM.}$ is plotted in Figure 13d, to obtain information at what ratio of concentration between amyloids and dyes saturation of fluorescence is observed. Based on this data concentration of amyloids for each dye was

chosen, which was later used in detailed studies for FQY, τ_{ave} and 2PA. The value of FQY increased in the following order upon binding to amyloids: **DA-** (27.5%) < **DAD** (75.2%) < **AD** (94.4%). It also followed the trend observed in glycerol and $CHCl_3$, which confirms that chosen environmental models reproduce the effects present upon amyloid binding. The highest ratio between FQY for solution before and after amyloid addition (Φ_{rat}) was for **DAD** fluorophore (Φ_{rat} =57.9), which has emission dependent on a few factors: hydrogen-bonding, polarity, viscosity. For **DA-** change in FQY upon binding to amyloids (Φ_{rat} =25) and for high viscosity medium (Φ_{rat}=27.1) is very similar, which suggests mechanism of fluorescence enhancement upon binding coming mostly from immobilization inside amyloid fibrils, similar to ThT. Due to the efficient emission of **-AD** in various environments already in the free for of the dye, the fluorescence enhancement upon binding is low and ratio between FQY before and after binding is the smallest for this dye **(Φ_{rat}=7.4).**

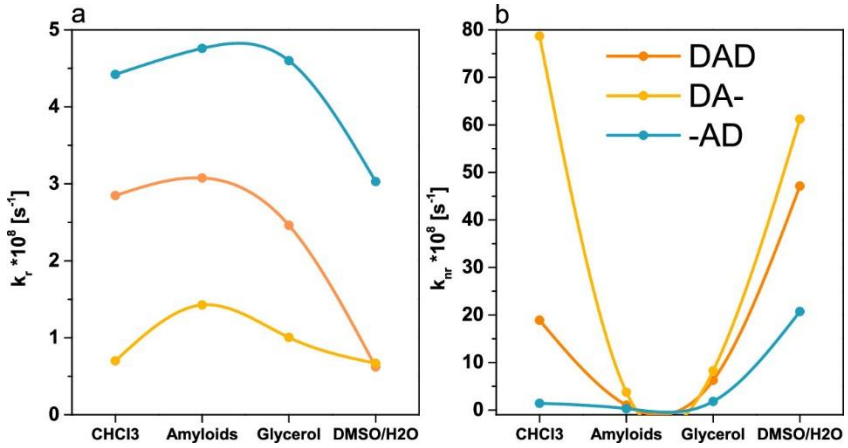

Figure 14. *(a) Comparison of kr values for dyes in $CHCl_3$, amyloid solution, glycerol, DMSO/H2O (solution before amyloid addition). (b) Comparison of knr values for dyes in CHCl3, amyloid solution, glycerol, DMSO/H2O. Figure reproduced from [Hajda A., Grelich-Mucha M., Rybczyński P., Ośmiałowski B., Zaleśny R., Olesiak-Bańska J. (2023). BF2-Functionalized Benzothiazole Amyloid Markers: Effect of Donor Substituents on One- and Two-Photon Properties. ACS Appl. Bio Mater. 6, 12, 5676–5684.].*

For all dyes upon amyloid binding, life times increased from values below 0.5 ns to 1.93 1.98, 2.45 ns for **-DA**, **-AD**, **DAD**, respectively. Measured τ and FQY were used to calculate the radiative (k_r) and nonradiative (k_{nr}) decay constants. Trends of k_r and k_{nr} in various media like $CHCl_3$, glycerol, amyloids, solution before binding (mixture of H_2O and DMSO) were evaluated and are presented in Figure 14. I concluded that position of a donor group is linked with the changes of k_r and k_{nr}. **k_r is influenced by substitution of the donor on rotating phenyl ring**, **while k_r, is influenced by the donor attached to the benzothiazole core**. Additionally, I studied fluorescence enhancement of dyes upon binding to other types of amyloid, obtained from hen egg white lysozyme (HEWL). Fluorescence intensity for dye **DAD** and **DA-** is smaller for the same content of amyloids in HEWL as compared to insulin. However, position of $\lambda_{EM.}$ and shape of the spectrum is almost the same. Interestingly, **-AD** dye

mixed with HEWL amyloids decreased intensity, even in comparison to free dye. Quenching is increasing with increasing amyloid content – see Figure S9 in Figure 72. Higher content of arene groups due to the six Tryptophan (Trp) residues in HEWL were attributed to this phenomena.

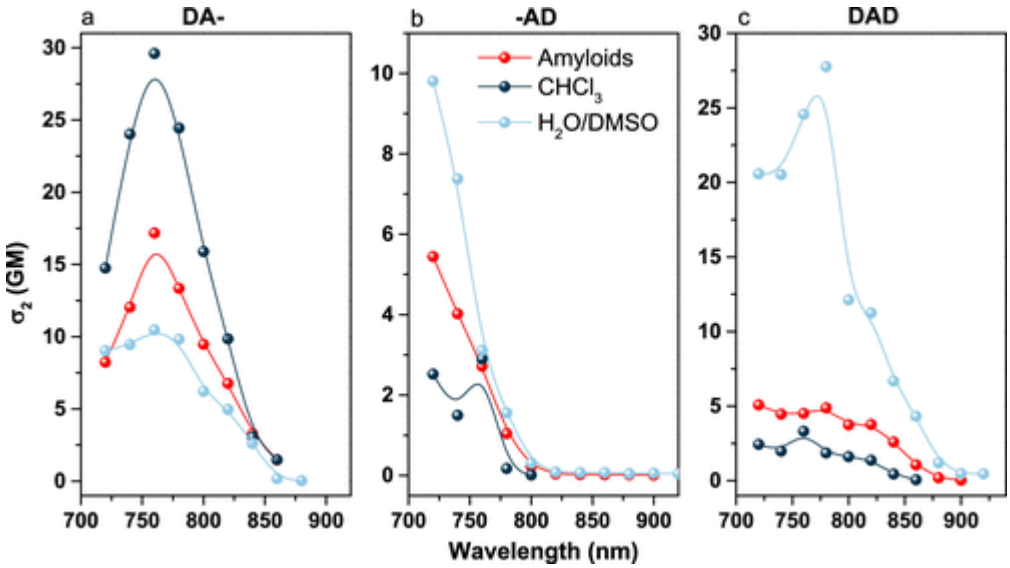

Figure 15. *Two-photon absorption cross section for dyes in various environments: H_2O/DMSO mixture,$CHCl_3$, and amyloid solution (concentration presented in the Experimental Section of article). (a) DA- dye, (b) -AD dye, and (c) DAD dye. The uncertainty of the calculated values was ±15%. Figure reproduced from [Hajda A., Grelich-Mucha M., Rybczyński P., Ośmiałowski B., Zaleśny R., Olesiak-Bańska J. (2023). BF2-Functionalized Benzothiazole Amyloid Markers: Effect of Donor Substituents on One- and Two-Photon Properties. ACS Appl. Bio Mater. 6, 12, 5676–5684.]*

I measured 2PA of dyes in $CHCl_3$, upon binding to amyloids and in the same solvent before amyloid binding (H_2O/DMSO) by 2PEL technique. Comparison of measured σ_2 for all probes is presented in Figure 15. In H_2O/DMSO solution the highest σ_2 was for the **DAD** dye (28 GM), while the lowest for **-AD** (~10 GM). For **-AD** and **DAD** σ_2 decreased upon binding to amyloids, while for **DA-** it increased. Since there are various trends in changes of σ_2, I wanted to understand possible explanation. Microenvironment inside binding pockets of amyloids is usually hydrophobic. In order to evaluate σ_2 in a hydrophobic environment, 2PA was measured in a more hydrophobic and less polar solvent ($CHCl_3$) than H_2O/DMSO solution. In evaluation of one-photon properties $CHCl_3$ turned out to be a sufficient approximation. For σ_2 the same trends were observed in $CHCl_3$ as in amyloids. **DA-** had σ_2 higher than in H_2O/DMSO solution, while in **-AD** and **DAD** it had smaller values – see Figure 15. This provides an information, that polarity is one of the modulator of σ_2 upon binding to amyloids. At the end, values of $\sigma_{2,B}$ were compared for all investigated dyes and $\sigma_{2,B}$ with amyloids increased in comparison to not-bounded dyes.

3.3 Summary:

I presented, that fluorophores based on benzothiazole core with incorporated N,O-coordinated BF2 moiety interact with amyloids. I confirmed **hypothesis 1** "BF2-functionalized benzothiazoles can serve as fluorescent amyloid probes. Modification of the localization of functional groups in the molecules has an impact on optical properties of studied fluorophores bound to amyloid fibrils". Dyes upon binding presented FQY even up to ~ 94%, without a strong electron donor in the structure. Probe **DAD**, which exhibited sensitivity of FQY to more than one environmental factor, had the highest increase in FQY with insulin amyloids. **-AD** was the least sensitive to viscosity, and it displayed the largest variations in fluorescence detected upon binding to HEWL *vs* insulin amyloids. It might give a hint in construction of probes, which can discriminate amyloids from various native peptides and proteins. They should have limited fluorescence response on viscosity and thus higher sensitivity to other environmental factors.

Two-photon properties of the dyes were also investigated, and we presented for the first time σ_2 before and after amyloid binding. Evaluation of 2PA in the solvents may demonstrate a trends, however is not sufficient for the prediction of σ_2 and $\sigma_{2,B}$. The increase in σ_2 upon binding was observed only for **DA- dye,** while values of $\sigma_{2,B}$ increased for all the dyes. In general, all dyes presented relatively low values of σ_2, and $\sigma_{2,B}$ ~5 GM due to the mild donor in the structure. Since dyes present potential in amyloid detection, incorporation of a stronger donor in the structure should increase σ_2.

This studies determine the goal of deeper understanding relationship between modulation of 2PA of a dye bound to amyloid with structure of studied fluorophore. **Hypothesis 2** "2PA of fluorophores bound to amyloids is different than the one of free molecules and can be modulated based on their chemical and consequently electronic structure" was confirmed. BF2-functionalized benzotiazoles can be a new scaffold for further application in amyloid detection. My studies answered the **goal 2** "Determine relationship between the modulation of 2PA of studied fluorophores bound to amyloid with the structure of fluorophores". The studies also give information on modulation of k_r and k_{nr} for fluorophores intended for amyloid detection.

3.4 **Research contribution of PhD candidate:**

Contribution of PhD candidate

Agata Hajda
Institute of Advanced Materials
Wroclaw University of Science and Technology
ul. Gdańska 7/9
50-344 Wrocław

Author Contribution Statement

I, Agata Hajda hereby declare that in the article: BF2-Functionalized Benzothiazole Amyloid Markers: Effect of Donor Substituents on One- and Two-Photon Properties. *ACS Appl. Bio Mater. 2023, 6, 12, 5676–5684* , I was responsible for:

- Methodology
- Investigation
  - Incubation and characterization of amyloid fibrils.
  - One-photon measurements of dyes in solvent and upon biding to amyloids: absorption, emission, fluorescence lifetime, fluorescence quantum yield, photostability.
  - Two-photon measurements: two-photon excited fluorescence.
- Data analysis.
- Writing – orginal draft.

Agata Hajda

3.5 Article and supporting information:

ACS APPLIED BIO MATERIALS

www.acsabm.org

Article

BF_2-Functionalized Benzothiazole Amyloid Markers: Effect of Donor Substituents on One- and Two-Photon Properties

Agata Hajda, Manuela Grelich-Mucha, Patryk Rybczyński, Borys Ośmiałowski, Robert Zaleśny, and Joanna Olesiak-Bańska*

Cite This: *ACS Appl. Bio Mater.* 2023, 6, 5676−5684

Read Online

ACCESS | Metrics & More | Article Recommendations | Supporting Information

ABSTRACT: Investigation of amyloids with the aid of fluorescence microscopy provides crucial insights into the development of numerous diseases associated with the formation of aggregates. Here, we present a series of BF_2-functionalized benzothiazoles with electron-donating methoxy group(s), which are tested as amyloid fluorescent markers. We evaluate how the position of donor functional group(s) influences optical properties (fluorescence lifetime (τ) and fluorescence quantum yield (FQY)) in a solution and upon binding to amyloids. We elucidate the importance of surrounding environmental factors (hydrogen-bonding network, polarity, and viscosity) on the observed changes in FQY and evaluate how the localization of a donor influences radiative and nonradiative decay pathways. We conclude that a donor attached to the benzothiazole ring contributes to the increment of radiative decay pathways upon binding to amyloids (k_r), while the donor attached to the flexible part of a molecule (with rotational freedom) contributes to a decrease in nonradiative decay pathways (k_{nr}). We find that the donor−acceptor−donor architecture allows us to obtain 58 times higher FQY of the dye upon binding to bovine insulin amyloids. Finally, we measure two-photon absorption (2PA) cross sections (σ_2) of the dyes and their change upon binding by the two-photon excited fluorescence (2PEF) technique. Measurements reveal that dyes that exhibit the increase/decrease of σ_2 values when transferred from highly polar solvents to $CHCl_3$ present a similar behavior upon amyloid binding. Our 2PA experimental values are supported by quantum mechanics/molecular mechanics (QM/MM) simulations. Despite this trend, the values of σ_2 are not the same, which points out the importance of two-photon absorption measurements of amyloid−dye complexes in order to understand the performance of 2P probes upon binding.

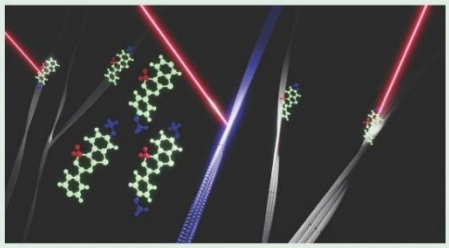

KEYWORDS: *fluorescence probes, amyloids, two-photon absorption, BODIPY, thioflavin T*

1. INTRODUCTION

Amyloids are misfolded proteins with a characteristic fibrillar morphology and a β-sheet-rich secondary structure. According to one of the hypotheses, their presence in tissues is one of the hallmarks of over 50 diseases, including various neurodegenerative disorders, such as Parkinson's disease (PD) and Alzheimer's disease (AD), and type 2 diabetes (T2D).[1] The mentioned pathologies are incurable, and their etiology is still not fully understood.[2] Accurately tracking the development and localization of amyloids inside cells is crucial for understanding disease progression and the development of therapeutic agents. Techniques such as magnetic resonance imaging (MRI),[3] positron emission tomography (PET),[4] and fluorescence microscopy enable the detection of amyloids *in vivo*.[5] Fluorescence microscopy attracts broad attention, mainly due to its simplicity and higher spatial resolution compared to other mentioned techniques. Another type of microscopy, widely used *in vivo*, is two-photon microscopy (2PM). 2PM enables excitation in the near-IR region (>700 nm), which is beneficial due to its deeper tissue penetration, low phototoxicity, minimalized photobleaching, and imaging of small objects.[6,7] 2PM has already been successfully employed in the visualization of Aβ amyloids located in the deep brain region.[8,9] However, fluorescence microscopy requires fluorescent amyloid-binding agents to obtain a high signal-to-noise ratio. From the spectroscopic point of view, perfect markers should present the following features: (1) increase in FQY upon amyloid binding and/or shift in the maximum emission/absorption wavelength upon binding to differentiate between a dye in the bound and unbound states; (2) high photostability; and (3) emission and absorption in the first biological window

Received: September 14, 2023
Revised: November 15, 2023
Accepted: November 23, 2023
Published: December 7, 2023

https://doi.org/10.1021/acsabm.3c00815
ACS Appl. Bio Mater. 2023, 6, 5676−5684

(700−950 nm). When it comes to markers for 2PM, a high value of the product of two-photon absorption cross section (σ_2) and FQY (ϕ), $\sigma_{eff} = \sigma_2 \times \phi$, is additionally required. The latter quantity (σ_{eff}) is also termed the two-photon action cross section.

The smart construction of new fluorescent dyes for amyloid detection is a challenging process. Most existing probes are based on popular fluorophores: benzothiazoles,[10−12] BODIPY,[13−15] curcumin,[16,17] and thiophene.[18−20] Moreover, various mechanisms of enhancing FQY of probes upon binding to amyloids are explored: (1) restriction of rotation of structural parts of a dye upon binding, which occurs in molecular rotors such as thioflavin T (ThT),[21] (2) transition from a hydrophilic to a hydrophobic environment (e.g., Acedan derivatives),[22] (3) dual mechanism of restriction and environment (e.g., ANCA),[23] or (4) aggregation-induced emission.[24] Recently, our group has synthesized a series of BF_2-functionalized dyes with structural core inspired by ThT.[25] By and large, dyes carrying the BF_2 moiety attracted the attention of the scientific community as fluorescent probes due to their outstanding photophysical properties: high FQY, large molar extinction coefficients, tunable emission wavelength and narrow emission bands, high chemical stability, and high two-photon absorption cross sections.[26−28] The difluoroborate (BF_2) moiety acting as an electron acceptor can lead to strong intramolecular charge transfer (ICT) when combined with the electron donor group. The same moiety is also responsible for the rigidification of the molecular skeleton. The largest group of BF_2-containing dyes is 4,4-difluoro-4-bora-3a,4a-diaza-s-indacenes (BODIPYs). In BODIPYs, two nitrogen atoms coordinate with an atom of boron; however, in some similar derivatives, nitrogen is replaced by oxygen. It is worth mentioning that N,O-coordinated BF_2 probes were already used to detect Aβ plaques and neurofibrillary tangles in 1PM and 2PM, but there were no systematic studies of two-photon properties of probes before and after amyloid binding.[29,30] Examination of multiphoton properties can provide new information about the relationship between the structure of the probe and amyloid interactions, which might differ from one-photon optical changes. In this paper, we investigate the potential of BF_2-functionalized benzothiazoles with electron-donating methoxy group(s) as amyloid fluorescent markers. To gain systematic knowledge about the relationship between the dye structure, its optical properties, and their modification by binding to amyloids, we investigate three dyes with a weak electron donor located on one or both terminals of the fluorescent core (see Figure 1): (1) **DA-** ((*Z*)-[(difluoroboryloxy)-phenylmethylene](6-methoxy-1,3-benzothiazol-2-yl)amine), (2) **-AD** ((*Z*)-[(difluoroboryloxy)(4-methoxyphenyl)-methylene]-1,3-benzothiazol-2-ylamine), and (3) **DAD** ((*Z*)-[(difluoroboryloxy)(4-methoxyphenyl)methylene](6-methoxy-1,3-benzothiazol-2-yl)amine). Using the same benzothiazole core, it was possible to modulate the FQY between 0.4 and 98%[28] by changing the position of the donor and acceptor units only. In the current study, changes in optical properties such as the fluorescence lifetime (τ), FQY, 2PA, 1P, and 2P excited fluorescence upon binding to amyloid fibrils are investigated. The discussion is focused on differences in the architecture of dyes, as well as different dependencies of FQY on surrounding environmental factors (hydrogen-bonding network, polarity, and viscosity) and the performance of dyes upon binding to amyloids. We indicate general principles in the evaluation of one- and two-photon optical properties of fluorescent amyloid markers. That is mainly based on their σ_2 or σ_{eff} in moderate polarity media such as EtOH, DMF, and DCB, as the core of amyloids is similar in polarity to the mentioned solvents. Although scarcely presented in the literature, investigations of dyes bound to biopolymers such as DNA or proteins show that the orientation and localization of fluorophores inside biomolecules influence their 2PA cross sections.[31,32] Thus, 2PA cross-sectional determination of free dyes in organic solvents may not be sufficient to predict their two-photon absorption upon binding to amyloids, which are complex biopolymers. Here, we evaluate the need for the determination of σ_2 not only in solution but also after binding to amyloids for a reliable discussion on the structure−property relation in the design of two-photon amyloid markers.

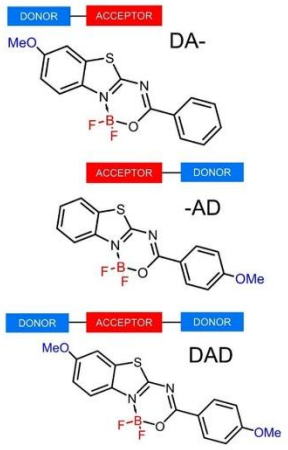

Figure 1. Structures of the investigated dyes.

2. EXPERIMENTAL SECTION

2.1. Synthesis of Dyes. The synthesis of dyes was described in our previous article.[1]

2.2. Incubation of Bovine Insulin Amyloids. Bovine insulin (BI) was purchased from Sigma-Aldrich (I5500) and dissolved in HCl solution (pH ~ 1.5), yielding the final concentration of 2 mg/mL. The samples were incubated in an Eppendorf ThermoMixer C for 40 h at 45 °C, with agitation set to 700 rpm.

2.3. Incubation of the Hen Egg White Lysozyme (HEWL) Amyloids. HEWL was purchased from Sigma-Aldrich (L6876) and dissolved in HCl solution (pH ~ 1.5) to yield a final concentration of 20 mg/mL (1.4 mM). The samples were incubated in an Eppendorf ThermoMixer C for 20 h at 85 °C, with the agitation set to 1400 rpm.

2.4. Atomic Force Microscopy (AFM). The full procedure is published elsewhere.[14] In brief, samples were diluted to 0.01 mg/mL. The droplets of the samples were deposited on a mica layer, rinsed with Milli-Q water after 5 min, and dried afterward. Measurements were conducted by using a Veeco Dimension V atomic force microscope in tapping mode with the SuperSharpSilicon probe mounted (Manufacturer: NANOSENSORS).

2.5. Absorption and Fluorescence Spectroscopies. One-photon absorption spectra were measured with a Jasco V-670 spectrophotometer in quartz cuvettes within the range of 280−700 nm. Stock solutions of dyes were prepared by dissolution in DMSO (500 μM), and all solutions were prepared before use. For samples of mixtures of water and DMSO, the appropriate volume of the stock solution was withdrawn and diluted so the volume of DMSO reached 40%; then,

https://doi.org/10.1021/acsabm.3c00815
ACS Appl. Bio Mater. 2023, 6, 5676−5684

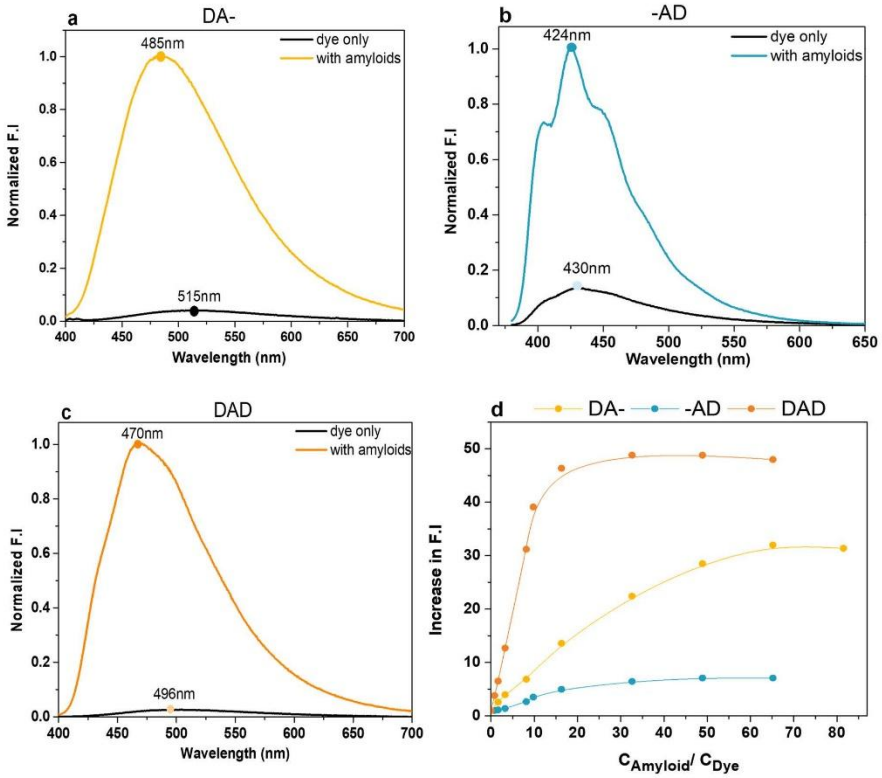

Figure 2. (a) Fluorescence intensity of **DA-** upon interaction with BI amyloids (122 μM). (b) Fluorescence intensity of **-AD** upon interaction with BI amyloids (122 μM). (c) Fluorescence intensity of **DAD** upon interaction with BI amyloids (82 μM). (d) Comparison of fluorescence increase with increasing concentration of BI amyloids.

Milli-Q water was added. For samples with amyloids, the order of addition to prepare samples was as follows: DMSO, the stock solution of dye, the stock solution of amyloids, and Milli-Q water. The final concentration of the dye in fluorescence enhancement measurements upon amyloid binding was 2.5 μM. Fluorescence emission and excitation spectra were recorded using an FS5 Spectrofluorometer (Edinburgh Instruments) equipped with a xenon lamp.

2.6. Selectivity toward Biomolecules and Bovine Serum Albumin (BSA). Measurements of fluorescence changes of dyes (2.5 μM) upon binding to various bioanalytes and BSA were measured on a clarioSTAR Plus plate reader in a 96-well black plate. Fluorescence spectra were measured 10 min after the incubation of dyes with biomolecules at room temperature. To compare changes before and after binding, the fluorescence intensity (FI) at maximum wavelength before and after binding in the same solvent were divided by each other ($FI_{after\ binding}/FI_{dye\ alone}$).

2.7. Fluorescence Quantum Yield. The FQY was measured by using the SC-30 Integrating Sphere Module for an FS5 spectrofluorometer from Edinburgh Instruments. The concertation of dyes was set to obtain a high signal on a two-photon microscope, as the FQY is used to calculate the 2PA cross section. For measurements before and after amyloid binding, the DMSO content was the same as that described in Section 2.5. The final concentration of dyes with and without amyloids was 2.5 μM. The amyloid concentrations were 122 μM for **DA-**, 82 μM for **-AD**, and 82 μM for **DAD**. These concentrations provided the best enhancement in fluorescence.

2.8. Fluorescence Lifetime Characterization. One-photon excited fluorescence decays were acquired by time-correlated single-photon counting (TCSPC), the setup containing an Acton SpectraPro SP-2300 monochromator (Princeton Instruments) and a high-speed hybrid detector HPM-100-50 (Becker & Hickl GmbH) controlled by a DCC-100 card. As an excitation source, a BDL-375-SMN picosecond laser diode (20 MHz, λ_{exc} = 377 nm) was used. For each measurement, 6 scans were performed, which were later fitted in SPCImage software. For the fitting of data, synthetic IRF was used. The mean value of the fluorescence lifetimes from 6 scans was calculated to obtain the most reliable result. The mean value was used as the "real" data in the calculation of k_{nr} and k_r. Decays were measured at λ_{em} = 430 nm (**-AD**), λ_{em} = 490 nm (**DA-**), and λ_{em} = 475 nm (**DAD**). Samples had the same concentrations of dyes and amyloids as those in FQY measurements.

2.9. Calculation of k_r and k_{nr}. To calculate k_r and k_{nr}, the fitted average lifetime and measured FQY were used, as described in eqs 1 and 2

$$\varphi = \frac{k_r}{k_r + k_{nr}} \quad (1)$$

https://doi.org/10.1021/acsabm.3c00815
ACS Appl. Bio Mater. 2023, 6, 5676−5684

$$\tau = \frac{1}{k_r + k_{nr}} \quad (2)$$

2.10. Characterization of Nonlinear Optical Properties. Two-photon excited luminescence was measured using a custom-built multiphoton microscope consisting of a femtosecond mode-locked Ti:sapphire laser (~100 fs, 80 MHz, Chameleon, Coherent Inc.) with an incident wavelength range tunable within λ = 700−1050 nm. Luminescence was recorded through a microscope objective (Nikon Plan Fluor, 40×, NA 0.75), and 2PEF signals were recorded in the epifluorescence mode. 2PEF spectra were measured with a Shamrock 303i spectrometer (Andor) equipped with an iDus camera (Andor). Samples and references were illuminated with the output power set between 40 and 70 mW depending on the measured dye (reference always was measured with the same power as the sample). Experimental conditions were chosen to prevent photobleaching and achieve a high signal-to-noise ratio. Two-photon absorption cross sections were calculated with eq 3

$$\sigma_{2,s} = \frac{F_s C_r \varphi_r n_r^2}{F_r C_s \varphi_s n_s^2} \sigma_{2,r} \quad (3)$$

Effective two-photon absorption cross sections were calculated with eq 4

$$\sigma_{2,\mathrm{eff}} = \varphi \sigma_{2,s} \quad (4)$$

where C is the fluorophore molar concentration per cubic centimeter, n the refractive index of the solvent, φ the fluorescence quantum yield, and F the integral over the whole two-photon excited emission band. The letters s and r correspond to the sample and reference, respectively. The chosen reference was a fluorescein solution in 0.1 M NaOH. The two-photon absorption cross section of fluorescein was obtained from elsewhere.[45] Samples prepared in $CHCl_3$ and H_2O/DMSO before and after amyloid binding had the same concentrations of dyes and amyloids as in FQY measurements.

2.11. Power Dependence of the Fluorescence Intensity. To confirm that the observed fluorescence excited by laser pulses had a two-photon nature, we measured the intensity versus excitation power dependence and determined the power exponent n (eq 5).

$$n = \frac{\log(\text{PL intensity})}{\log(\text{power})} \quad (5)$$

where the PL intensity is a 2P excited photoluminescence intensity, and the power is the average incident laser power.

2.12. Computer Simulations. The studied dyes were solvated with chloroform or water molecules, resulting in spherically symmetric clusters. Two-layer ONIOM calculations were performed for the clusters.[46] The composition of layers was determined based on the following criteria:

$$\text{layer 1: } 0\ \text{Å} < |R_{COM}^{solvent} - R_{COM}^{solute}| \leq 8\ \text{Å}$$

$$\text{layer 2: } 8\ \text{Å} < |R_{COM}^{solvent} - R_{COM}^{solute}| \leq 30\ \text{Å}$$

where R_{COM}^{i} refers to the position vector of the center of mass (COM) of the i-th molecule. Subsequently, the optimization of the geometry was performed using GAUSSIAN program.[47] In so doing, layer 1 was described at the B3LYP/6-31+G(d) level of theory with D3 version of Grimme's dispersion model,[48] while layer 2 was described by the AMBER force field.[49] The optimized clusters were subsequently used in electronic structure calculations to determine one- and two-photon absorption spectra. These calculations were performed using TURBOMOLE program[50] at the RI-CC2/aug-cc-pVDZ level of theory,[51] and all solvent molecules were represented by point charges.

3. RESULTS AND DISCUSSION

BF_2-functionalized benzothiazoles with additional electron-donating functional methoxy groups were synthesized according to a protocol described elsewhere.[25] These probes possess a single C−C bond between the benzothiazole core and phenylene group, which introduces rotational freedom—a feature resulting in the linear dependency of FQY on viscosity.[25] However, the sensitivity of FQY to viscosity changes differs between dyes. It was proven that the FQY of **DA-** is mainly sensitive to viscosity, **-AD** is weakly sensitive to environmental factors (hydrogen-bonding network, polarity, and viscosity), and **DAD** is simultaneously sensitive to the hydrogen-bonding/polar environment and viscosity.[25]

The dyes present a low intensity of fluorescence in H_2O/DMSO mixture, with FQY values equal to 1.3, 1.1, and 12.8% for **DAD**, **DA-**, and **-AD**, respectively. These values can be largely increased upon binding with amyloids, as shown in Figure 2a−c. We prepared bovine insulin (BI) amyloids and confirmed their presence by atomic force microscopy (AFM) (Figure S1a). Details about the preparation of samples are described in the Experimental Section. Values of the fluorescence intensity (FI) for amyloid solutions were compared before and after binding. As shown in Figure 2d, a strong increase in FI, from 7 for **-AD** dye to 49-fold for the **DAD** dye, was observed upon binding to amyloids. To determine whether the increase in FI is equally sensitive to protein monomers, the fluorescence of dye solutions with the monomeric form of bovine insulin was measured. A lack of intensity changes confirmed that the enhancement of FI is specific for the interaction with amyloid fibrils (Figure S6). As shown in Figure 2d, **DAD** achieves the highest fluorescence increase and **-AD** the lowest fluorescence increase for the same ratio between the amyloid and dye concentration. In order to evaluate the potential usage of dyes *in vivo*, the fluorescence response in a range of concentrations of bovine serum albumin (BSA) was determined (Figure S5). The smallest interactions seem to occur for the **-AD** dye, as with increasing BSA concentration, the fluorescence remains almost constant. For dyes **DAD** and **DA-**, we observed similar responses between 10 and 12.5 μM BSA. We clearly observed the interactions of BSA with these two dyes. It is worth mentioning that in the same instrumental settings, dyes with amyloids present higher intensities at lower concentrations compared to BSA. To conclude, there is a small chance of a background signal from the BSA−dye complex, especially for the **DAD** dye. However, the interactions suggest that it might be efficiently transported through the bloodstream.

For all dyes, the emission maximum was blue-shifted upon binding as compared to the solution without amyloids. One-photon optical properties such as the emission maximum wavelength (λ_{em} [nm]), absorption maximum wavelength (λ_{abs} [nm]), and average fluorescence lifetime (τ_{avr} [ns]) were also measured in H_2O/DMSO mixtures as well as in solvents of low polarity ($CHCl_3$) and high viscosity (glycerol), as presented in Table S1. For ease of comparison, we present the position of fluorescence emission for all dyes in used solvents in one spectrum (Figure S2). The smallest changes are observed for **-AD**. To examine the photostability of dyes, we measured the fluorescence intensity changes upon irradiation of 370 nm wavelength (Figure S3). The **DA-** and **-AD** intensities did not change, which indicates that they are highly photostable, while the **DAD** intensity decreased by around 10% after 1h of irradiation.

Amyloids possess a hydrophobic core and hydrophilic side groups exposed to the aqueous solution, and binding of dyes may occur in either of the locations. Dissolving dyes in $CHCl_3$ is intended to show the optical properties of dyes in a

https://doi.org/10.1021/acsabm.3c00815
ACS Appl. Bio Mater. 2023, 6, 5676−5684

hydrophobic medium, whereas glycerol is used to evaluate the influence of immobilization of dyes in the amyloid fibrils.

FQY and τ values were evaluated before and after amyloid binding in the same solvent. The highest FQY in the presence of amyloids was achieved for **-AD** (94%). This value is similar to the best FQY standards, such as Rhodamine 6G or fluorescein.[33] The second highest value in the presence of amyloids was obtained for **DAD** and was equal to 75%. The least emissive is **DA-**, with an FQY equal to 27.5%. The decrease of FQY values in the series **-AD**, **DAD**, and **DA-** observed in amyloid solutions corresponds to the order found for solutions in chloroform (Table S1; note that the values are not the same).

First, we compared the FQY in the same solvents before and after binding to amyloids, and subsequently, we compared changes in FQY with the values in high-viscosity media (glycerol) as the dyes exhibited different sensitivity to viscosity. **DA-** showed a 25-fold increase in FQY (ϕ_{rat}) upon binding to amyloids, with similar changes of FQY in amyloids and glycerol (Table 1). This suggests that the improved FQY comes mainly from the immobilization of the molecule upon binding to amyloids. The same behavior is observed for ThT, which belongs to the class of molecular rotor probes. In **-AD**, ϕ_{rat} upon adding amyloids was 7.4, which is higher than the change observed in glycerol in comparison to the much less viscous methanol. In any other solvent, this probe does not exhibit equally high FQY, even though it has similar values in $CHCl_3$ and glycerol (Table S1).

Table 1. Selected Spectroscopic Data for the Dyes in Different Solvents

probe	solution	Φ [%]	Φ_{rat}[a]	τ_{avr} [ns]
DA-	H_2O/DMSO[b]	1.1		0.16
	amyloids[b]	27.5	25	1.93
	glycerol	11.4	27.1	1.08
-AD	H_2O/DMSO[b]	12.8		0.42
	amyloids[b]	94.4	7.4	1.98
	glycerol	73.3	2.7	1.58
DAD	H_2O/DMSO[b]	1.3		0.21
	amyloids[b]	75.2	57.9	2.45
	glycerol	28.4	11.8	1.15

[a]Φ_{rat} for the amyloid solution is Φ of the dye with amyloids divided by Φ of the dye in H_2O/DMSO mixture. Φ_{rat} for glycerol is Φ of the dye in glycerol solution divided by Φ of the dye in methanol. Data for glycerol are taken from ref 26. [b]Details on concentrations and v/v ratios between solvents for each dye are presented in the Experimental Section in the Supporting Information file.

The highest increase in FQY of the presented dyes (58-fold) upon the addition of amyloids was observed for **DAD** (Table 1). Its FQY with amyloids (75%) was almost two times higher than that for ThT with amyloids (42%),[34] while the FQY was found to be lower for glycerol (viscous media) than for the solution of amyloids. This confirms our previous finding that the dye is sensitive to viscosity, and polarity/hydrogen bonding can translate into an interaction with amyloids.

DAD and **-AD** both have a methoxy group on the phenyl side. Some of the present authors have previously proved that such a location of the donor is crucial for achieving a high value of FQY.[25] The methoxy moiety attached to the benzothiazole core present in **DAD** and **DA-** has already been used in ThT derivatives to increase the electron density on the benzothiazole core.[35,36] ThX, one of the ThT derivatives, had an FQY 3.4 times higher than that of the parent ThT upon binding to α-synuclein and showed increased binding affinity. Another publication presented a comparison of a novel library of 12 ThT-inspired fluorescent probes for amyloid protein with the methoxy moiety attached to the benzothiazole core (with or without a positive charge in their structure).[36] In general, charged molecules exhibit a higher FQY after binding to α-synuclein. Our studies show that the introduction of the BF_2 moiety as the acceptor serves as a possible solution for achieving high FQY without using charged species, which is an interesting alternative in the design of probes for amyloid aggregates. Moreover, it should not be overlooked that the dyes carrying a quaternary/charged nitrogen atom would rather interact with polar groups within the protein, while BF_2-carrying ones provide a chance to bind in hydrophobic parts.

Determination of τ and FQY values allowed us to calculate the radiative (k_r) and nonradiative (k_{nr}) decay constants and their changes upon dye binding to amyloids. Fluorescence lifetime values after binding were equal to 1.93, 1.98, and 2.45 for **DA-**, **-AD**, and **DAD**, respectively (Figure S3). In order to link the effect of binding to amyloids with changes in fluorescence, we compared the values of k_r and k_{nr} in $CHCl_3$,

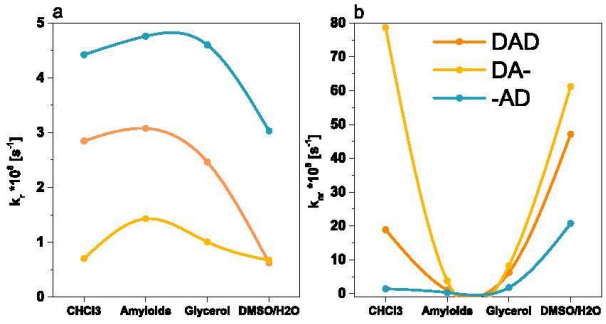

Figure 3. (a) Comparison of k_r values for dyes in $CHCl_3$, amyloid solution, glycerol, DMSO/H_2O. (b) Comparison of k_{nr} values for dyes in $CHCl_3$, amyloid solution, glycerol, DMSO/H_2O. Details of the calculations are given in the SI.

https://doi.org/10.1021/acsabm.3c00815
ACS Appl. Bio Mater. 2023, 6, 5676−5684

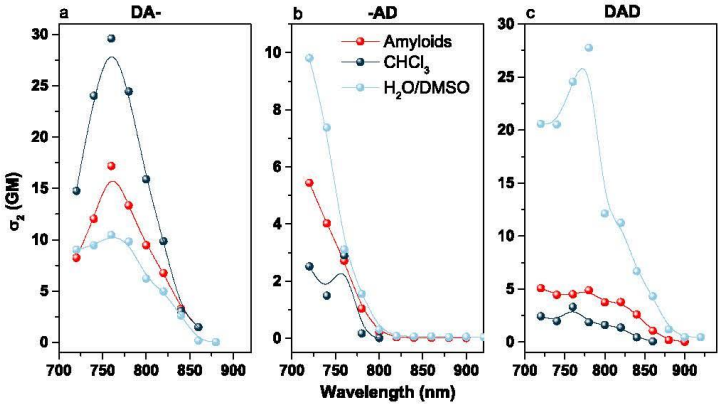

Figure 4. Two-photon absorption cross section for dyes in various environments: H_2O/DMSO mixture (ratios for all dyes are presented in the Experimental Section), $CHCl_3$, and amyloid solution (concentration presented in the Experimental Section). (a) **DA-** dye, (b) **-AD** dye, and (c) **DAD** dye. The uncertainty of the calculated values was ±15%.

glycerol, and H_2O/DMSO solutions before and after amyloid addition for all probes.

DA- presents a decrease in values of k_{nr} after amyloid binding (Figure 3b). There are similarities in k_{nr} in a high-viscosity medium and amyloids. There is additional confirmation that the restriction of the conformational freedom of a dye takes place, which translates into the suppression of the nonradiative processes. In the case of **DA-**, there is also an increase in k_r after binding to amyloids, with higher k_r in amyloids than in glycerol (Figure 3b).

-AD also presents suppression of nonradiative processes after amyloid binding. However, the dye presents similar values of k_{nr} in $CHCl_3$, glycerol, and upon binding to amyloids. Thus, it is not possible to point out a single dominant environmental factor that contributes to the suppression of these processes. The FQY of **-AD** slightly changes with viscosity; thus, the immobilization of the dye contributes to a decrease of nonradiative decay pathways upon binding to amyloids. The contribution of k_r in an amyloid solution is the highest for this dye among all investigated dyes. The localization of the donor group may reduce the rotation capacity around the bond between the benzothiazole core and phenylene group,[37] leading to an initial high FQY of a free dye. Then, upon dye binding to amyloids, further immobilization and hydrophobicity of grooves in amyloids, where the dye is located, allow us to achieve an FQY above 90%.

The **DAD** dye presents high suppression of nonradiative processes after amyloid binding. On a comparison, the k_{nr} values of different solvents were found to be the most similar to the k_{nr} value measured in glycerol. This proves that the immobilization of a molecule takes place, which results in a decrease of k_{nr}. The acceleration of radiative pathways upon binding to amyloids is the highest for this system compared to other dyes (Table S3), which translates into the highest $\Delta\phi$ upon binding to amyloids. As shown in Figure 3a, k_r has similar values in a hydrophobic solvent and amyloids; thus, the polarity may have a significant influence on the radiative decay pathways.

Based on a comparison between dyes, we link particular moieties with the changes of k_r and k_{nr}. The localization of the donor on the part of a molecule exhibiting rotational freedom influences k_r, while the donor attached to the benzothiazole core has a stronger influence on k_{nr}. The highest FQY was obtained for **-AD** upon binding to amyloids, thus achieving a high FQY depending on electron density on the moiety exhibiting rotational freedom. The donor group attached to the benzothiazole core increases the sensitivity of FQY to the immobilization of dyes. **DAD** and **DA-** exhibit FQY sensitivity to viscosity and more "molecular rotor probe"-like behavior. For **DAD** and **-AD** dyes, k_r values in samples with amyloids correspond better with values in a hydrophobic environment than in glycerol. This suggests that dyes are located inside the hydrophobic amyloid structure, which is supported by the hydrophobic character of the dyes determined from log *P* values (see Table S4) and the mentioned earlier presence of fluorine atoms.

We also studied the optical properties of dyes in amyloids of other proteins. The fluorescence intensity of the compounds upon the addition of amyloids formed from hen egg white lysozyme (HEWL) was lower compared to that of BI amyloids (Figure S8), which we attribute to various amyloid environments, e.g., a higher content of arene groups in HEWL compared to BI. A detailed discussion regarding the probe performance upon binding to HEWL is presented in the SI. Overall, trends in intensity increase are the same for dyes upon binding to HEWL and BI amyloids. However, **-AD** in HEWL amyloids presented quenching, and no increment of FI upon binding was observed (Figure S9).

As **DAD** presented the highest increment of FQY upon binding and exhibited the best application potential, we also investigated interactions with various endogenous biomolecules (Figure S4). To summarize, we did not observe any changes in fluorescence upon interaction with to L-cysteine, L-methionine, glycine, glutathione, ascorbic acid, and H_2O_2.

Nonlinear optical properties of the analyzed chromophores were studied in terms of their multiphoton absorption and the corresponding fluorescence processes, with a femtosecond pulsed laser as an excitation source. First, the two-photon nature of absorption processes was confirmed with fluorescence response *vs* the input laser power (Figure S10). σ_2 values

https://doi.org/10.1021/acsabm.3c00815
ACS Appl. Bio Mater. 2023, 6, 5676−5684

of the dyes before and after amyloid binding were measured. The σ_2 value in H_2O/DMSO solution was found to be the highest for the **DAD** dye (28 GM at 780 nm) while the lowest was for **-AD** (~10 GM at 720 nm; Figure 4). For **DA-**, σ_2 increased upon binding to amyloids, whereas for **-AD**, a minor difference was observed, and for **DAD**, we noticed a decrease of the σ_2 value. We also compared the two-photon absorption (2PA) spectra of all chromophores with their one-photon absorption (1PA) spectra (Figure S11). The 2PA spectra of free dyes overlap with the 1PA bands plotted at a double wavelength. On the other hand, probes with amyloids have slightly shifted 2PA bands compared to the doubled positions of the 1PA spectra (Figure S11). In order to assess the effect of polarity on σ_2, we performed 2PA measurements in a more hydrophobic and less polar solvent—$CHCl_3$. For **DAD** and **-AD** in $CHCl_3$, σ_2 decreased compared to that in the H_2O/DMSO solution, while for **DA-**, σ_2 was higher (Figure 4). The presented tendency of σ_2 in $CHCl_3$ correlates to changes upon adding amyloids. The dependence of σ_2 on the solvent polarity is a well-known phenomenon.[38,39] Binding pockets of amyloids are mostly hydrophobic,[40,41] which translates to the observed correspondence between the two-photon performance of dyes in amyloids and $CHCl_3$ solutions. However, values in these two solutions for all probes are not the same: for **DA-**, σ_2 at 760 nm in $CHCl_3$ is 29 GM, which is almost two times higher than that in the solution of amyloids. In complex biopolymers such as amyloids, additional factors influence 2PA, e.g., the local electric field.[31,42,43] Previously presented differences between dyes in BI and HEWL amyloids indicate that interactions with amino acid residues present in fibrils significantly modulate the optical properties of dyes. Similarly, the modulation of nonlinear optical properties is expected.

The experimental investigation of two-photon properties of dyes in solutions was supported by quantum mechanics/molecular mechanics (QM/MM) simulations of dyes in $CHCl_3$ and water (mimicking a water/DMSO mixture). Details of the simulations are provided in the Experimental Section, and a summary of the results is presented in Table S6. The results of simulations are in line with experimental findings and clearly indicate that σ_2 of **DA-** in $CHCl_3$ is much larger than those of **DAD** and **-AD**. Electronic structure calculations also indicate that a more polar environment (water *vs* $CHCl_3$) increases the σ_2 values of the studied dyes.

σ_{eff}, which is a product of σ_2 and FQY, is the quantity that is the most relevant for evaluating the potential of two-photon probes in imaging applications. Values of σ_{eff} increased upon binding for all investigated dyes (Figure S12) due to increasing FQY of these systems, with the value around 4−5 GM, for all dyes. However, the highest difference in the σ_{eff} value between the bound and unbound dyes was observed for **DA-** molecules, which presented the lowest FQY upon binding. In the case of sufficiently large values of σ_{eff}, the increase of the two-photon excited fluorescence intensity upon incorporation into fibrils may be the fundamental factor determining the utility of a dye in bioimaging applications.

4. CONCLUSIONS

In conclusion, we presented a systematic study of the optical properties of three fluorophores with a structure based on ThT and an N,O-coordinated BF_2 moiety, with a donor group located on both or one of the termini of a molecule (**DAD**, **DA-**, and **-AD**). We show that probes with an N,O-coordinated BF_2 acceptor, while incorporated into amyloid fibrils, exhibit FQY values exceeding 70% even without the presence of a strong electron-donating moiety, like the frequently used *N,N*-dimethylamino group. The highest increase in fluorescence upon binding with amyloids was observed for the **DAD** dye, which exhibits an FQY sensitive to a range of environmental factors such as the hydrogen-bonding network, polarity, and viscosity. The results reveal that probes that are sensitive to more than one environmental factor might be the best choice in amyloid detection. Our data show that a crucial aspect in tuning the FQY is the donor location in the molecule. The best performance was obtained for a donor attached to the aromatic ring with a single C−C bond connected to the core with the acceptor. The methoxy group, as a hydrogen bond acceptor, enhances the interaction with amyloids in parallel with increasing FQY, while this group is attached to the benzothiazole ring.

The probes studied here presented various responses to HEWL and BI amyloids. It is beneficial as discrimination between various amyloid structures is important in bioimaging studies of protein aggregates. The probe **-AD** has an FQY that is the least sensitive to viscosity, and it presented the largest differences in fluorescence detected upon binding to HEWL *vs* BI. This might suggest that probes with limited sensitivity to viscosity perform better in discriminating between different types of amyloids, where different mechanisms influencing FQY play the main role.

We also investigated the two-photon properties of the dyes and proved the importance of measuring 2PA cross sections of dyes both in a solution and after amyloid binding. Measuring 2PA cross sections in solvents may show a trend but may not be sufficient for the prediction of two-photon properties of a dye upon binding to amyloids. The measurements of σ_2 in organic solvents did not provide a reliable estimation of the difference in two-photon-excited fluorescence intensity between bound and unbound probes in water solutions, which is crucial for the observation of amyloid-bound dyes with no background fluorescence. Moreover, the evaluation of σ_2 in amyloids gave us important information about the factors that contribute to the highest differences in two-photon properties between bound and unbound dyes. Such an approach can be used for a better comparison of various probes designed for amyloid imaging by two-photon microscopy.

■ ASSOCIATED CONTENT

Supporting Information

The Supporting Information is available free of charge at https://pubs.acs.org/doi/10.1021/acsabm.3c00815.

AFM images of HEWL and BI amyloids; details of one-photon optical properties of dyes in different solvents; comparison of the fluorescence emissions with monomers of peptides and amyloids; fluorescence lifetime data; summary of radiative and nonradiative decay pathways; comparison of the fluorescence emission with HEWL amyloids and BI amyloids. partition coefficient (log *P*) of dyes; effective two-photon absorption cross sections; and results of computer simulations (PDF)

■ AUTHOR INFORMATION

Corresponding Author

Joanna Olesiak-Bańska − *Faculty of Chemistry, Wrocław University of Science and Technology, PL-50-370 Wrocław,*

https://doi.org/10.1021/acsabm.3c00815
ACS Appl. Bio Mater. 2023, 6, 5676−5684

Poland; orcid.org/0000-0002-7226-0077; Email: joanna.olesiak-banska@pwr.edu.pl

Authors

Agata Hajda – *Faculty of Chemistry, Wroclaw University of Science and Technology, PL-50-370 Wroclaw, Poland*

Manuela Grelich-Mucha – *Faculty of Chemistry, Wroclaw University of Science and Technology, PL-50-370 Wroclaw, Poland*; orcid.org/0000-0002-8591-9387

Patryk Rybczyński – *Faculty of Chemistry, Nicolaus Copernicus University, Toruń PL-87-100, Poland*

Borys Ośmiałowski – *Faculty of Chemistry, Nicolaus Copernicus University, Toruń PL-87-100, Poland*; orcid.org/0000-0001-9118-9264

Robert Zaleśny – *Faculty of Chemistry, Wroclaw University of Science and Technology, PL-50-370 Wroclaw, Poland*; orcid.org/0000-0001-8998-3725

Complete contact information is available at: https://pubs.acs.org/10.1021/acsabm.3c00815

Notes

The authors declare no competing financial interest.

■ ACKNOWLEDGMENTS

This work was supported by the National Science Centre OPUS project (project no. 2021/43/B/ST5/00753). The authors acknowledge computational resources generously provided by the Wroclaw Centre for Networking and Supercomputing.

■ REFERENCES

(1) Iadanza, M. G.; Jackson, M. P.; Hewitt, E. W.; Ranson, N. A.; Radford, S. E. A new era for understanding amyloid structures and disease. *Nat. Rev. Mol. Cell Biol.* **2018**, *19* (12), 755−773.

(2) Tipping, K. W.; van Oosten-Hawle, P.; Hewitt, E. W.; Radford, S. E. Amyloid Fibres: Inert End-Stage Aggregates or Key Players in Disease? *Trends Biochem. Sci.* **2015**, *40* (12), 719−727.

(3) Yanagisawa, D.; Taguchi, H.; Ibrahim, N. F.; Morikawa, S.; Shiino, A.; Inubushi, T.; Hirao, K.; Shirai, N.; Sogabe, T.; Tooyama, I. Preferred Features of a Fluorine-19 MRI Probe for Amyloid Detection in the Brain. *J. Alzheimer's Dis.* **2014**, *39*, 617−631.

(4) Mathis, C. A.; Mason, N. S.; Lopresti, B. J.; Klunk, W. E. Development of Positron Emission Tomography *β*-Amyloid Plaque Imaging Agents. *Semin. Nucl. Med.* **2012**, *42* (6), 423−432.

(5) Gyasi, Y. I.; Pang, Y. P.; Li, X. R.; Gu, J. X.; Cheng, X. J.; Liu, J.; Xu, T.; Liu, Y. Biological applications of near infrared fluorescence dye probes in monitoring Alzheimer's disease. *Eur. J. Med. Chem.* **2020**, *187*, No. 111982.

(6) Larson, A. M. Multiphoton microscopy. *Nat. Photonics* **2011**, *5* (1), No. 1.

(7) Kobat, D.; Durst, M. E.; Nishimura, N.; Wong, A. W.; Schaffer, C. B.; Xu, C. Deep tissue multiphoton microscopy using longer wavelength excitation. *Opt. Express* **2009**, *17* (16), 13354−13364.

(8) Chen, C.; Liang, Z.; Zhou, B.; Li, X.; Lui, C.; Ip, N. Y.; Qu, J. Y. In Vivo Near-Infrared Two-Photon Imaging of Amyloid Plaques in Deep Brain of Alzheimer's Disease Mouse Model. *ACS Chem. Neurosci.* **2018**, *9* (12), 3128−3136.

(9) Korzhova, V.; Marinković, P.; Njavro, J. R.; Goltstein, P. M.; Sun, F.; Tahirovic, S.; Herms, J.; Liebscher, S. Long-term dynamics of aberrant neuronal activity in awake Alzheimer's disease transgenic mice. *Commun. Biol.* **2021**, *4* (1), 1368.

(10) Mora, A. K.; Murudkar, S.; Alamelu, A.; Singh, P. K.; Chattopadhyay, S.; Nath, S. Benzothiazole-Based Neutral Ratiometric Fluorescence Sensor for Amyloid Fibrils. *Chem. - Eur. J.* **2016**, *22* (46), 16505−16512.

(11) Vus, K.; Trusova, V.; Gorbenko, G.; Sood, R.; Kinnunen, P. Thioflavin T derivatives for the characterization of insulin and lysozyme amyloid fibrils in vitro: Fluorescence and quantum-chemical studies. *J. Lumin.* **2015**, *159*, 284−293.

(12) Sundaram, G. S.; Garai, K.; Rath, N. P.; Yan, P.; Cirrito, J. R.; Cairns, N. J.; Lee, J. M.; Sharma, V. Characterization of a brain permeant fluorescent molecule and visualization of Abeta parenchymal plaques, using real-time multiphoton imaging in transgenic mice. *Org. Lett.* **2014**, *16* (14), 3640−3643.

(13) Ono, M.; Watanabe, H.; Kimura, H.; Saji, H. BODIPY-based molecular probe for imaging of cerebral beta-amyloid plaques. *ACS Chem. Neurosci.* **2012**, *3* (4), 319−324.

(14) Tonali, N.; Dodero, V. I.; Kaffy, J.; Hericks, L.; Ongeri, S.; Sewald, N. Real-Time BODIPY-Binding Assay To Screen Inhibitors of the Early Oligomerization Process of Abeta1−42 Peptide. *ChemBioChem* **2020**, *21* (8), 1129−1135.

(15) Sen, A.; Mora, A. K.; Koli, M.; Mula, S.; Kundu, S.; Nath, S. Sensing lysozyme fibrils by salicylaldimine substituted BODIPY dyes - A correlation with molecular structure. *Int. Biol. Macromol.* **2022**, *220*, 901−909.

(16) Ran, C.; Xu, X.; Raymond, S. B.; Ferrara, B. J.; Neal, K.; Bacskai, B. J.; Medarova, Z.; Moore, A. Design, Synthesis, and Testing of Difluoroboron-Derivatized Curcumins as Near-Infrared Probes for in Vivo Detection of Amyloid-*β* Deposits. *J. Am. Chem. Soc.* **2009**, *131* (42), 15257−15261.

(17) Liu, K.; Guo, T. L.; Chojnacki, J.; Lee, H. G.; Wang, X.; Siedlak, S. L.; Rao, W.; Zhu, X.; Zhang, S. Bivalent ligand containing curcumin and cholesterol as fluorescence probe for Abeta plaques in Alzheimer's disease. *ACS Chem. Neurosci.* **2012**, *3* (2), 141−146.

(18) Kelley, M.; Sant'Anna, R.; Fernandes, L.; Palhano, F. L. Pentameric Thiophene as a Probe to Monitor EGCG's Remodeling Activity of Mature Amyloid Fibrils: Overcoming Signal Artifacts of Thioflavin T. *ACS Omega* **2021**, *6* (12), 8700−8705.

(19) Calvo-Rodriguez, M.; Hou, S. S.; Snyder, A. C.; Dujardin, S.; Shirani, H.; Nilsson, K. P. R.; Bacskai, B. J. In vivo detection of tau fibrils and amyloid beta aggregates with luminescent conjugated oligothiophenes and multiphoton microscopy. *Acta Neuropathol. Commun.* **2019**, *7* (1), 171.

(20) Liu, H.; Kim, C.; Haldiman, T.; Sigurdson, C. J.; Nystrom, S.; Nilsson, K. P. R.; Cohen, M. L.; Wisniewski, T.; Hammarstrom, P.; Safar, J. G. Distinct conformers of amyloid beta accumulate in the neocortex of patients with rapidly progressive Alzheimer's disease. *J. Biol. Chem.* **2021**, *297* (5), No. 101267.

(21) Stsiapura, V. I.; Maskevich, A. A.; Kuzmitsky, V. A.; Uversky, V. N.; Kuznetsova, I. M.; Turoverov, K. K. Thioflavin T as a Molecular Rotor: Fluorescent Properties of Thioflavin T in Solvents with Different Viscosity. *J. Phys. Chem. B* **2008**, *112*, 15893.

(22) Kim, D.; Moon, H.; Baik, S. H.; Singha, S.; Jun, Y. W.; Wang, T.; Kim, K. H.; Park, B. S.; Jung, J.; Mook-Jung, I.; Ahn, K. H. Two-Photon Absorbing Dyes with Minimal Autofluorescence in Tissue Imaging: Application to in Vivo Imaging of Amyloid-*β* Plaques with a Negligible Background Signal. *J. Am. Chem. Soc.* **2015**, *137* (21), 6781−6789.

(23) Cao, K.; Farahi, M.; Dakanali, M.; Chang, W. M.; Sigurdson, C. J.; Theodorakis, E. A.; Yang, J. Aminonaphthalene 2-Cyanoacrylate (ANCA) Probes Fluorescently Discriminate between Amyloid-*β* and Prion Plaques in Brain. *J. Am. Chem. Soc.* **2012**, *134* (42), 17338−17341.

(24) Wang, Y.-L.; Fan, C.; Xin, B.; Zhang, J.-P.; Luo, T.; Chen, Z.-Q.; Zhou, Q.-Y.; Yu, Q.; Li, X.-N.; Huang, Z.-L.; Li, C.; Zhu, M.-Q.; Tang, B. Z. AIE-based super-resolution imaging probes for -amyloid plaques in mouse brains. *Mater. Chem. Front.* **2018**, *2* (8), 1554−1562.

(25) Rybczyński, P.; Bousquet, M. H. E.; Kaczmarek-Kędziera, A.; Jędrzejewska, B.; Jacquemin, D.; Ośmialowski, B. Controlling the fluorescence quantum yields of benzothiazole-difluoroborates by optimal substitution. *Chem. Sci.* **2022**, *13* (45), 13347−13360.

(26) Loudet, A.; Burgess, K. BODIPY Dyes and Their Derivatives: Syntheses and Spectroscopic Properties. *Chem. Rev.* **2007**, *107* (11), 4891−4932.
(27) Liu, M.; Ma, S.; She, M.; Chen, J.; Wang, Z.; Liu, P.; Zhang, S.; Li, J. Structural modification of BODIPY: Improve its applicability. *Chin. Chem. Lett.* **2019**, *30* (10), 1815−1824.
(28) Bednarska, J.; Zaleśny, R.; Wielgus, M.; Jędrzejewska, B.; Puttreddy, R.; Rissanen, K.; Bartkowiak, W.; Ågren, H.; Ośmiałowski, B. Two-photon absorption of BF2-carrying compounds: insights from theory and experiment. *Phys. Chem. Chem. Phys.* **2017**, *19* (8), 5705−5708.
(29) Chen, Y.; Ouyang, Q.; Li, Y.; Zeng, Q.; Dai, B.; Liang, Y.; Chen, B.; Tan, H.; Cui, M. Evaluation of N, O-Benzamide difluoroboron derivatives as near-infrared fluorescent probes to detect beta-amyloid and tau tangles. *Eur. J. Med. Chem.* **2022**, *227*, No. 113968.
(30) Chen, Y.; Yuan, C.; Xie, T.; Li, Y.; Dai, B.; Zhou, K.; Liang, Y.; Dai, J.; Tan, H.; Cui, M. N,O-Benzamide difluoroboron complexes as near-infrared probes for the detection of beta-amyloid and tau fibrils. *Chem. Commun.* **2020**, *56* (53), 7269−7272.
(31) Drobizhev, M.; Makarov, N. S.; Tillo, S. E.; Hughes, T. E.; Rebane, A. Two-photon absorption properties of fluorescent proteins. *Nat. Methods* **2011**, *8* (5), 393−399.
(32) Doan, P. H.; Pitter, D. R.; Kocher, A.; Wilson, J. N.; Goodson, T., 3rd Two-Photon Spectroscopy as a New Sensitive Method for Determining the DNA Binding Mode of Fluorescent Nuclear Dyes. *J. Am. Chem. Soc.* **2015**, *137* (29), 9198−9201.
(33) Magde, D.; Wong, R.; Seybold, P. G. Fluorescence Quantum Yields and Their Relation to Lifetimes of Rhodamine 6G and Fluorescein in Nine Solvents: Improved Absolute Standards for Quantum Yields. *Photochem. Photobiol.* **2002**, *75* (4), 327−334.
(34) Sulatskaya, A. I.; Maskevich, A. A.; Kuznetsova, I. M.; Uversky, V. N.; Turoverov, K. K. Fluorescence quantum yield of thioflavin T in rigid isotropic solution and incorporated into the amyloid fibrils. *PLoS One* **2010**, *5* (10), No. e15385.
(35) Needham, L.-M.; Weber, J.; Varela, J. A.; Fyfe, J. W. B.; Do, D. T.; Xu, C. K.; Tutton, L.; Cliffe, R.; Keenlyside, B.; Klenerman, D.; Dobson, C. M.; Hunter, C. A.; Müller, K. H.; O'Holleran, K.; Bohndiek, S. E.; Snaddon, T. N.; Lee, S. F. ThX − a next-generation probe for the early detection of amyloid aggregates. *Chem. Sci.* **2020**, *11* (18), 4578−4583.
(36) Needham, L.-M.; Weber, J.; Pearson, C. M.; Do, D. T.; Gorka, F.; Lyu, G.; Bohndiek, S. E.; Snaddon, T. N.; Lee, S. F. A Comparative Photophysical Study of Structural Modifications of Thioflavin T-Inspired Fluorophores. *J. Phys. Chem. Lett.* **2020**, *11* (19), 8406−8416.
(37) Jędrzejewska, B.; Skotnicka, A.; Laurent, A. D.; Pietrzak, M.; Jacquemin, D.; Ośmiałowski, B. Influence of the Nature of the Amino Group in Highly Fluorescent Difluoroborates Exhibiting Intramolecular Charge Transfer. *J. Org. Chem.* **2018**, *83*, 7779−7788.
(38) Wielgus, M.; Michalska, J.; Samoć, M.; Bartkowiak, W. Two-photon solvatochromism III: Experimental study of the solvent effects on two-photon absorption spectrum of p-nitroaniline. *Dyes Pigm.* **2015**, *113*, 426−434.
(39) Nag, A.; Goswami, D. Solvent effect on two-photon absorption and fluorescence of rhodamine dyes. *J. Photochem. Photobiol., A* **2009**, *206* (2), 188−197.
(40) Cao, Q.; Boyer, D. R.; Sawaya, M. R.; Abskharon, R.; Saelices, L.; Nguyen, B. A.; Lu, J.; Murray, K. A.; Kandeel, F.; Eisenberg, D. S. Cryo-EM structures of hIAPP fibrils seeded by patient-extracted fibrils reveal new polymorphs and conserved fibril cores. *Nat. Struct. Mol. Biol.* **2021**, *28* (9), 724−730.
(41) Li, B.; Ge, P.; Murray, K. A.; Sheth, P.; Zhang, M.; Nair, G.; Sawaya, M. R.; Shin, W. S.; Boyer, D. R.; Ye, S.; Eisenberg, D. S.; Zhou, Z. H.; Jiang, L. Cryo-EM of full-length α-synuclein reveals fibril polymorphs with a common structural kernel. *Nat. Commun.* **2018**, *9* (1), No. 3609.
(42) Drobizhev, M.; Tillo, S.; Makarov, N. S.; Hughes, T. E.; Rebane, A. Color Hues in Red Fluorescent Proteins Are Due to Internal Quadratic Stark Effect. *J. Phys. Chem. B* **2009**, *113* (39), 12860−12864.
(43) Bairu, S.; Ramakrishna, G. Two-photon absorption properties of chromophores in micelles: electrostatic interactions. *J. Phys. Chem. B* **2013**, *117* (36), 10484−10491.
(44) Grelich-Mucha, M.; Lipok, M.; Różycka, M.; Samoć, M.; Olesiak-Bańska, J. One- and Two-Photon Excited Autofluorescence of Lysozyme Amyloids. *J. Phys. Chem. Lett.* **2022**, *13* (21), 4673−4681.
(45) Makarov, N. S.; Drobizhev, M.; Rebane, A. Two-photon absorption standards in the 550−1600 nm excitation wavelength range. *Opt. Express* **2008**, *16* (6), 4029−4047.
(46) Chung, L. W.; Sameera, W. M. C.; Ramozzi, R.; Page, A. J.; Hatanaka, M.; Petrova, G. P.; Harris, T. V.; Li, X.; Ke, Z.; Liu, F.; Li, H.-B.; Ding, L.; Morokuma, K. The ONIOM Method and Its Applications. *Chem. Rev.* **2015**, *115* (12), 5678−5796.
(47) Frisch, M. J.; Trucks, G. W.; Schlegel, H. B.; Scuseria, G. E.; Robb, M. A.; Cheeseman, J. R.; Scalmani, G.; Barone, V.; Petersson, G. A.; Nakatsuji, H.; Li, X.; Caricato, M.; Marenich, A. V.; Bloino, J.; Janesko, B. G.; Gomperts, R.; Mennucci, B.; Hratchian, H. P.; Ortiz, J. V.; Izmaylov, A. F.; Sonnenberg, J. L.; Williams-Young, D.; Ding, F.; Lipparini, F.; Egidi, F.; Goings, J.; Peng, B.; Petrone, A.; Henderson, T.; Ranasinghe, D.; Zakrzewski, V. G.; Gao, J.; Rega, N.; Zheng, G.; Liang, W.; Hada, M.; Ehara, M.; Toyota, K.; Fukuda, R.; Hasegawa, J.; Ishida, M.; Nakajima, T.; Honda, Y.; Kitao, O.; Nakai, H.; Vreven, T.; Throssell, K.; Montgomery, J. A., Jr.; Peralta, J. E.; Ogliaro, F.; Bearpark, M. J.; Heyd, J. J.; Brothers, E. N.; Kudin, K. N.; Staroverov, V. N.; Keith, T. A.; Kobayashi, R.; Normand, J.; Raghavachari, K.; Rendell, A. P.; Burant, J. C.; Iyengar, S. S.; Tomasi, J.; Cossi, M.; Millam, J. M.; Klene, M.; Adamo, C.; Cammi, R.; Ochterski, J. W.; Martin, R. L.; Morokuma, K.; Farkas, O.; Foresman, J. B.; Fox, D. J. *Gaussian 16*, revision C.01; Gaussian, Inc.: Wallingford CT, 2016.
(48) Grimme, S.; Antony, J.; Ehrlich, S.; Krieg, H. A consistent and accurate ab initio parameterization of density functional dispersion correction (DFT-D) for the 94 elements H-Pu. *J. Chem. Phys.* **2010**, *132*, No. 154104.
(49) Cornell, W. D.; Cieplak, P.; Bayly, C. I.; Gould, I. R.; Merz, K. M., Jr.; Ferguson, D. M.; Spellmeyer, D. C.; Fox, T.; Caldwell, J. W.; Kollman, P. A. A second generation force-field for the simulation of proteins, nucleic-acids, and organic-molecules. *J. Am. Chem. Soc.* **1995**, *117*, 5179−5197.
(50) TURBOMOLE V7.2 2017, a development of University of Karlsruhe and Forschungszentrum Karlsruhe GmbH: 1989−2007, TURBOMOLE GmbH, since 2007; available from http://www.turbomole.com.
(51) Friese, D. H.; Hättig, C.; Ruud, K. Calculation of two-photon absorption strengths with the approximate coupled cluster singles and doubles model CC2 using the resolution-of-identity approximation. *Phys. Chem. Chem. Phys.* **2012**, *14*, 1175−1184.

https://doi.org/10.1021/acsabm.3c00815
ACS Appl. Bio Mater. 2023, 6, 5676−5684

Supporting Information

BF_2-functionalized benzothiazole amyloid markers: the effect of donor substituents on one- and two-photon properties

Agata Hajda[1], Manuela Grelich-Mucha[1], Patryk Rybczyński[2], Borys Ośmiałowski[2], Robert Zaleśny[1], Joanna Olesiak-Bańska[1*]

1.Faculty of Chemistry, Wroclaw University of Science and Technology, Wybrzeże Wyspiańskiego 27, 50-370 Wroclaw, Poland

2. Faculty of Chemistry, Nicolaus Copernicus University, Gagarina Street 7, Toruń, PL-87-100, Poland

a)

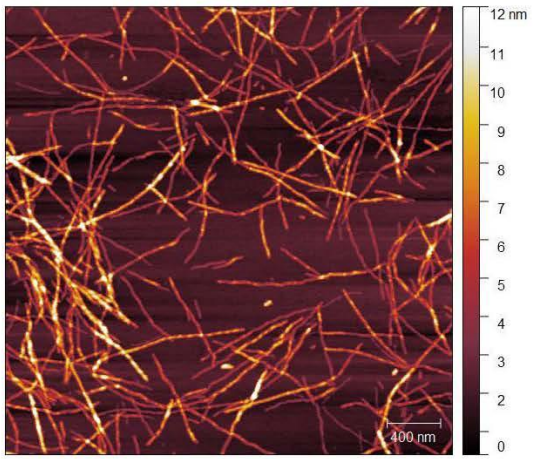

b)

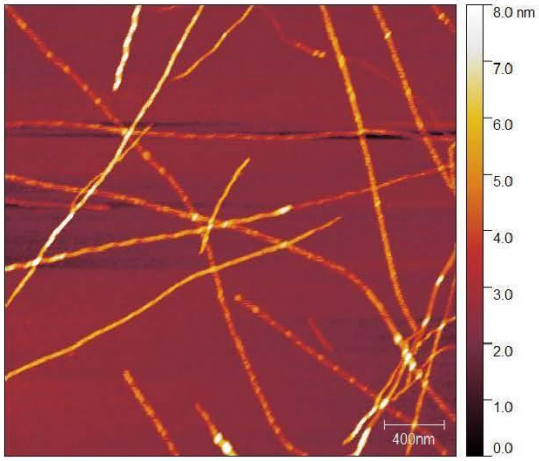

Figure S1. (a) Amyloids of BI deposited on mica (b) Amyloids of HEWL deposited on mica.

Table S1. One-photon optical properties of dyes in different solvents.

Probe	Solvent	Φ [%]	λ_{em}[nm]	λ_{abs} [nm]
DA-	H_2O/DMSO	1.1	515	361.0
	$CHCl_3$	0.9	458.5	361.0
	DMSO	-	512.0	365.0
	Glycerol	11.4	491.5	-
	Amyloids	27.5	485	364
-AD	H_2O/DMSO	12.7	430.0	364.0
	$CHCl_3$	75.6	419.5	364.0
	DMSO	-	428.0	366.0
	Glycerol	73.3	426.5	-
	Amyloids	94.4	424	366
DAD	H_2O/DMSO	1.3	502.5	373.0
	$CHCl_3$	13.1	454.5	368.0
	DMSO	-	501.0	375.0
	Glycerol	28.3	482.0	-
	Amyloids	75.2	470	380

For $CHCl_3$ and glycerol data taken from: Rybczynski, P.; Bousquet, M. H. E.; Kaczmarek-Kedziera, A.; Jedrzejewska, B.; Jacquemin, D.; Osmialowski, B., Controlling the fluorescence quantum yields of benzothiazole-difluoroborates by optimal substitution. *Chem Sci* **2022,** *13* (45), 13347-13360.

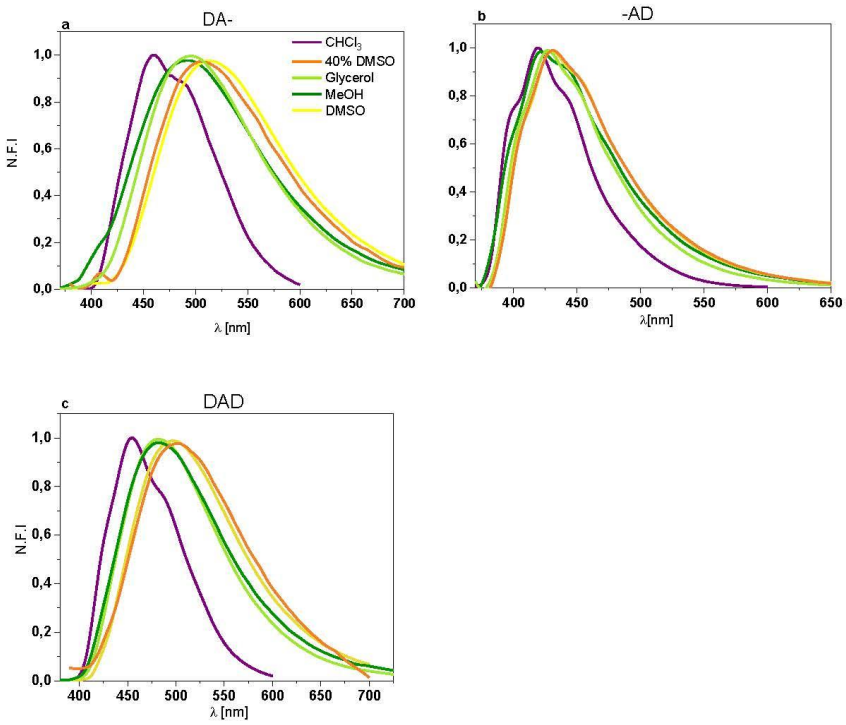

Figure S2. (a) DA- normalized fluorescence emission in different solvents (b) -AD normalized fluorescence emission in different solvents (c) DAD normalized fluorescence emission in different solvents.

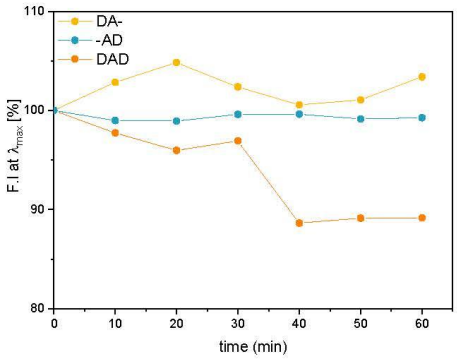

Figure S3. Photostability examination under irradiation using Xenon Lamp at 370nm. Fluorescence intesity at maximum emission wavelength before irradiation and during irradiation was monitored. Changes in intesity were recalculated to procentage for better visualization of data.

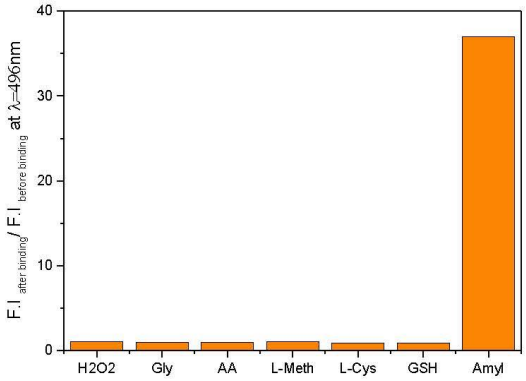

Figure S4. Fluorescence increasement of 2.5uM dye DAD upon mixing with various endogenous biomolecules – 100uM H_2O_2, 5mM Glycine (Gly), 10mM Ascorbic Acid(AA), 5mM L-Methionine(L-Meth), 5mM L-Cysteine (L-Cys), 1mM L-Gluthiahione (GSH) and comapred to increasment upon binding to 82uM amyloids from bovine insulin.

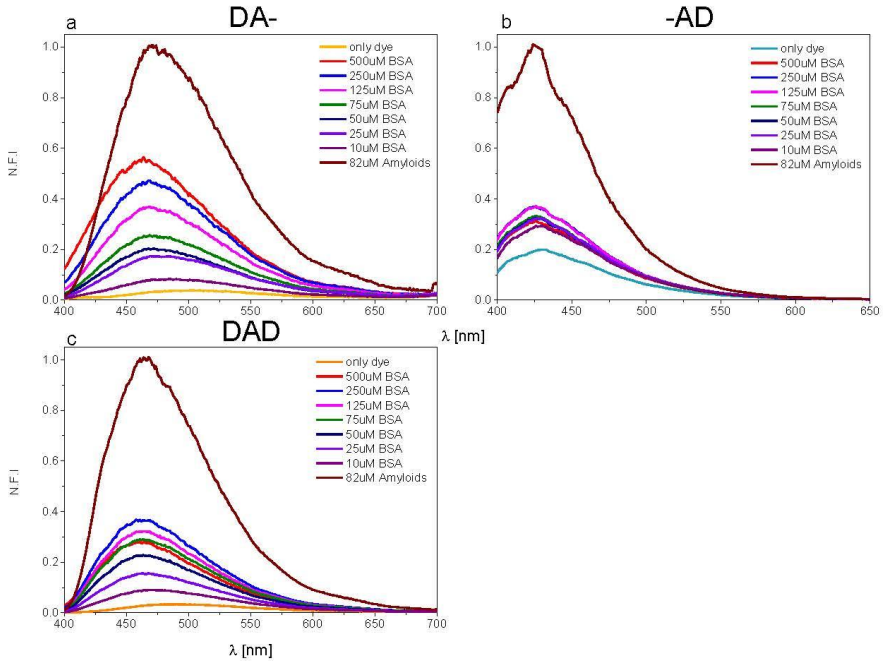

Figure S5 . Comparison of fluorescence intensity changes upon binding of dyes (c=2.5uM) to various concentrations of BSA. Comparison of fluorescence emission was taken before and after binding for maximum emission wavelength upon binding to BSA and to enhancement upon binding 82uM bovine amyloids.

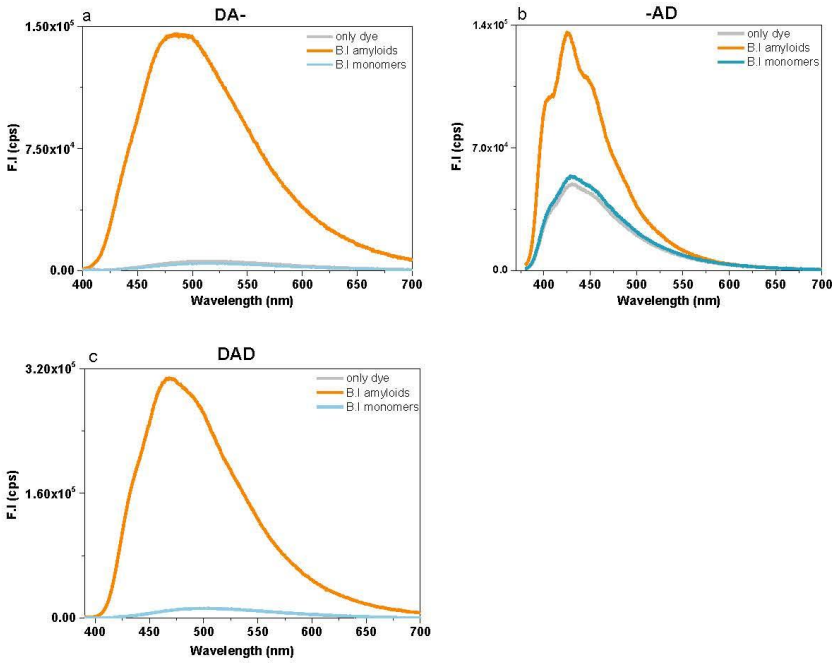

Figure S6. (a) comparison of F.I for dye (DA-) upon adding amyloids and monomers of bovine insulin (20uM); (b) comparison of F.I for dye (-AD) upon adding amyloids and monomers of bovine insulin (20uM); (c) comparison of F.I for dye (DAD) upon adding amyloids and monomers of bovine insulin (20uM).

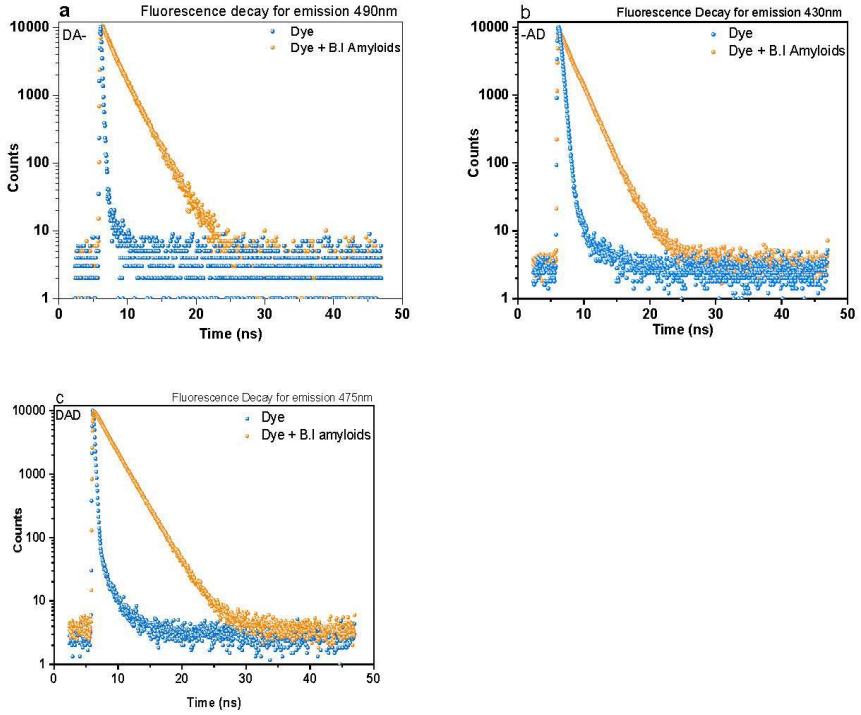

Figure S7. Fluorescence lifetime fitting for dyes with maximal amyloid F.I increment (a) DA- (b) -AD (c) DAD dye.

Tabel S2. Fluorescence lifetime details for water/dmso mixture and amyloid solution (maximal F.I enhancement concentration).

Probe	**solution**	τ_1 **[ns]**	a%	τ_2 **[ns]**	b%	τ_{avr} **[ns]**
DA-	40%DMSO	0.157	99.7	1.013	0.3	0.16
	Amyloid	1.509	56%	2.489	44%	1.93
-AD	40%DMSO	0.419	100%			0.42
	Amyloid	1.982	100%	-	-	1.98
DAD	40%DMSO	0.201	99,7%	1.827	0.3%	0.21
	Amyloid	2.445	100%	-	-	2.45

Table S3. Summary of radiative and non-radiative decay pathways

DYE	Solution	Φ [%]	τ_{avr}[ns]	k_{nr} (*10^8) [s^{-1}]	k_r (*10^8) [s^{-1}]
DA-	H_2O/DMSO	1.1	0.16	61.2	0.7
	Amyloids	27.5	1.93	3.7	1.4
	MeOH[1]	0.4	0.12	84.5	0.4
	Glycerol[1]	11.4	1.08	8.2	1.1
	$CHCl_3$[1]	0.9	0.13	78.7	0.7
-AD	H_2O/DMSO	12.7	0.42	20.7	3.0
	Amyloids	94.4	1.98	0.3	4.8
	MeOH[1]	26.5	0.68	10.8	3.9
	Glycerol[1]	73.3	1.58	1.7	4.6
	$CHCl_3$[1]	75.6	1.71	1.4	4.4
DAD	H_2O/DMSO	1.33	0.21	47.1	0.7
	Amyloids	75.3	2.45	1.0	3.2
	MeOH[1]	2.4	0.14	72.3	1.8
	Glycerol[1]	28.4	1.15	6.2	2.5
	$CHCl_3$[1]	13.1	0.46	18.9	2.85

[1] Data taken from: Rybczynski, P.; Bousquet, M. H. E.; Kaczmarek-Kedziera, A.; Jedrzejewska, B.; Jacquemin, D.; Osmialowski, B., Controlling the fluorescence quantum yields of benzothiazole-difluoroborates by optimal substitution. *Chem. Sci.* 2022, 13 (45), 13347-13360.

Table S4. Partition Coefficient (LogP) - Calculated using the online ALOGPS 2.1 program

DYE	logP
DA-	4.88
-AD	4.93
DAD	4.94

HEWL amyloid experiments

Fluorescence emissions of compounds upon addition of amyloids formed from hen egg white lysozyme (HEWL) was evaluated (Figure S4). Presence of HEWL amyloids was confirmed by AFM imaging (Figure S1b). All probes with HEWL amyloids presented smaller fluorescence intensity compared to BI amyloids. F.I for -**AD** with HEWL was smaller than for the dye without amyloids, which suggests fluorescence quenching mechanism upon binding. Increasing concentration of amyloids caused further quenching (Figure S5). Amyloids, besides their structural similarities, differ according to the amino acids content. Unique microenvironment, coming from amino acids residues, is used to distinguish amyloids by fluorescent probes.[2] It is known phenomenon for ThT[3] and Nile Red[4] that binding to HEWL amyloids results in smaller emission enhancement compared to BI amyloids. Since ThT is a charged molecule, electrostatic interactions play an important role influencing binding to amyloids. The molecules studied in this Letter are neutral; therefore, the electrostatic interactions do not prevail over other interaction components and we thus do not include them in our considerations. HEWL amyloids have higher hydrophobicity and contain more aromatic moieties within the groove than bovine insulin amyloids.[5] The arene groups play important role, since HEWL have six Tryptophan (Trp) residues in the sequence whereas BI have none. Quenching of dyes luminescence caused by Trp in well-known phenomenon.[6] The π-π interaction creating various microenvironment of studied amyloids grooves, including Trp presence, may be responsible for different optical properties of probes. This finding also supports our previous divagation about interaction of dyes with amino acids residues. **DAD** and **DA**- both have higher dependence of fluorescence on viscosity than -**AD** and for these dyes HEWL amyloids induced the increase in F.I upon binding.

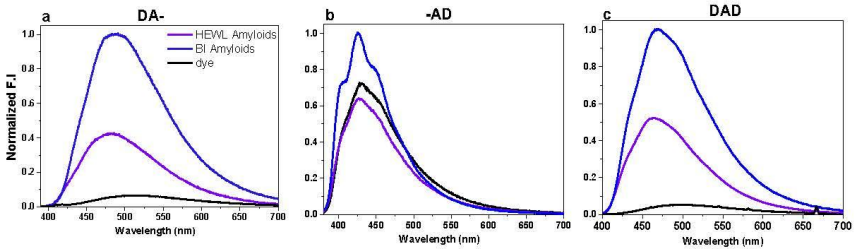

Figure S8. Comparison of Normalized Fluorescence Intensity (N.F.I) of dyes upon binding to amyloids of HEWL and BI. Both had concentration 20uM. Normalization was done using the highest Fluorescence intensity as 1.

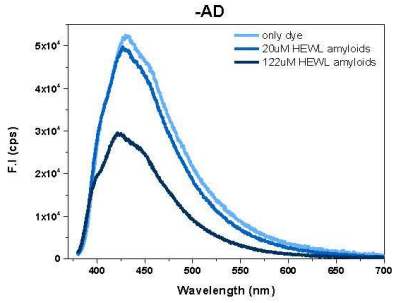

Figure S9. Fluorescence emission of -AD (2.5uM) upon binding to HEWL amyloids.

Table S5. Summarizing table of emission properties of dyes with 20uM of HEWL amyloids.

DYE	λ_{em} [nm]	Fold
DA-	482	8
-AD	427	decrease
DAD	462	15

Fold – the increase of fluorescence intensity upon binding with amyloids

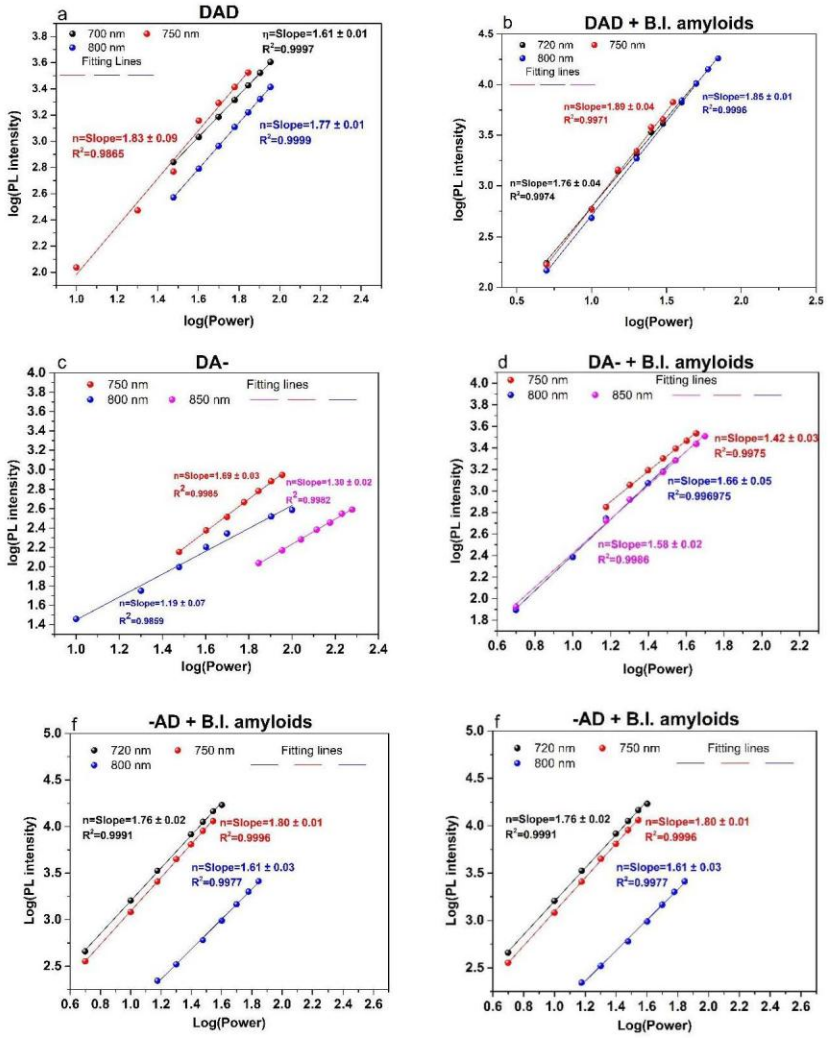

Figure S10. Log of the measured photoluminescence intensity (Log(PL intensity)) values plotted versus log of the incident laser power (log(Power)) for the studied free dyes: DAD (a), DA- (c), -AD (e) and upon the binding of bovine insulin (B.I.) amyloids to: DAD (b), DA- (d), and -AD (f).

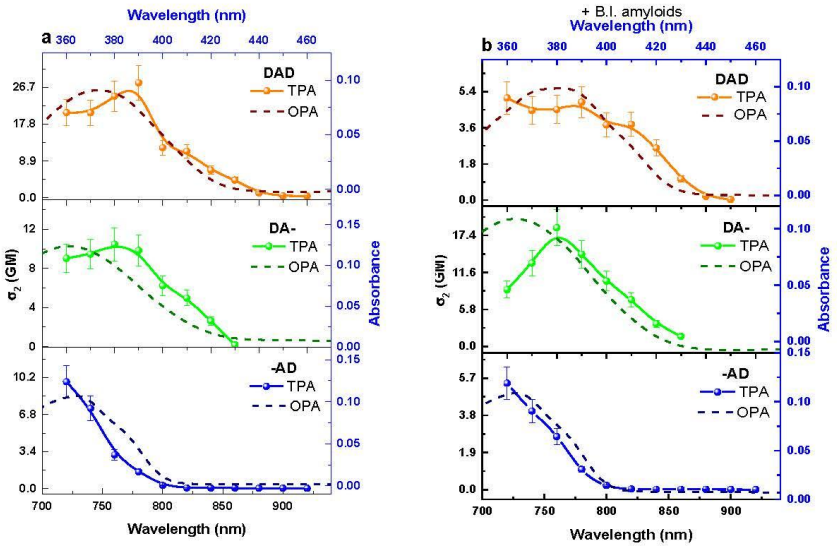

Figure S11. Two-photon absorption spectra with the corresponding one-photon absorption (1PA) spectra (a) free dyes in H_2O/DMSO mixture, (b) dyes with BI amyloids. Concentration of amyloids was chosen to provide the strongest one-photon fluorescence enhancement of each dye.

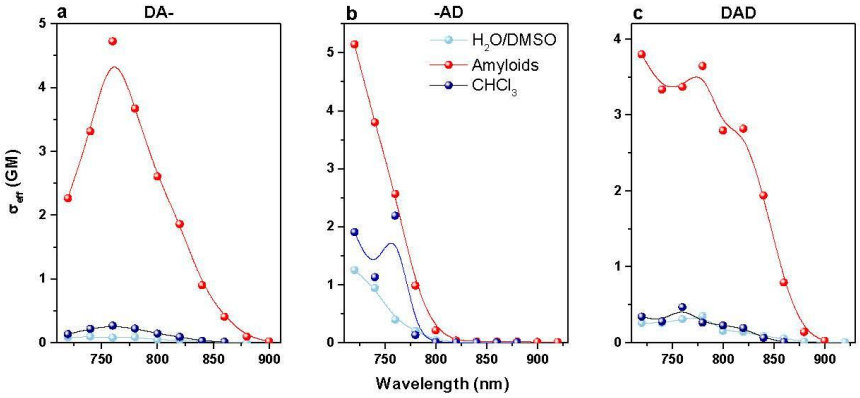

Figure S12. Effective two photon absorption cross-section for dyes in different solutions: $CHCl_3$, H_2O/DMSO, Amyloids. Concentration of amyloids was chosen to provide the strongest one-photon fluorescence enhancement of each dye. Uncertainty of values ±15%

Table S6. Calculated two-photon absorption cross sections (σ_2, [GM]). Two-photon absorption wavelengths (λ, [nm]) are given in parentheses. The results correspond to $S_0 \rightarrow S_1$ electronic transition.

DYE	σ_2[GM] (λ [nm]) chloroform	σ_2 [GM] (λ [nm]) water
DA-	47 (687)	57 (699)
-AD	12 (664)	29 (690)
DAD	5 (690)	11 (684)

References:

(1) Rybczynski, P.; Bousquet, M. H. E.; Kaczmarek-Kedziera, A.; Jedrzejewska, B.; Jacquemin, D.; Osmialowski, B. Controlling the fluorescence quantum yields of benzothiazole-difluoroborates by optimal substitution. *Chemical Science* **2022**, *13* (45), 13347-13360. DOI: 10.1039/d2sc05044g.

(2) Ran, C.; Wang, P.; Yang, J.; Zhu, B. Differentiating Aβ40 and Aβ42 with a small-molecule fluorescence probe. *Alzheimer's & Dementia* **2020**, *16* (S4), e041227. DOI: 10.1002/alz.041227

(3) Kuznetsova, I. M.; Sulatskaya, A. I.; Uversky, V. N.; Turoverov, K. K. Analyzing Thioflavin T Binding to Amyloid Fibrils by an Equilibrium Microdialysis-Based Technique. *PLOS ONE* **2012**, *7* (2), e30724. DOI: 10.1371/journal.pone.0030724.

(4) Mishra, R.; Sjölander, D.; Hammarström, P. Spectroscopic characterization of diverse amyloid fibrilsin vitro by the fluorescent dye Nile red. *Molecular BioSystems* **2011**, *7* (4), 1232-1240, DOI: 10.1039/C0MB00236D.

(5) Tokunaga, Y.; Sakakibara, Y.; Kamada, Y.; Watanabe, K.-i.; Sugimoto, Y. Analysis of Core Region from Egg White Lysozyme Forming Amyloid Fibrils. *International Journal of Biological Sciences* **2013**, *9* (2), 219-227, DOI: 10.7150/ijbs.5380.

(6) Vaiana, A. C.; Neuweiler, H.; Schulz, A.; Wolfrum, J.; Sauer, M.; Smith, J. C. Fluorescence Quenching of Dyes by Tryptophan: Interactions at Atomic Detail from Combination of Experiment and Computer Simulation. *Journal of the American Chemical Society* **2003**, *125* (47), 14564-14572. DOI: 10.1021/ja036082j.

Chapter 4. TWO-PHOTON BRIGHTNESS OF NIR-EMITTING, ATOMICALLY PRECISE DNA-STABILIZED SILVER NANOCLUSTERS.

4.1 Research purpose:

In this work, my aim was to investigate σ_2 by 2PEL technique of 4 representatives of Ag_N-DNA nanoclusters. Atomically precise silver or gold nanoclusters (Ag/Au NCs) were reported as strong two-photon absorbers with σ_2 ranging from 10^2 GM to 10^5 GM.[92, 94-95, 212] However, Ag/Au NCs stabilized by thioles show low Photoluminescence Quantum Yield (PLQY), which results in low $\sigma_{2,B}$ limiting their application in 2PFM. As mentioned in the chapter "DNA templated silver nanoclusters ", early studies on 2PA of Ag_N-DNAs presented their high values of σ_2. Nevertheless, these studies were performed on heterogeneous samples, without atomically precise size and with unknown chemical compositions. **Based on the literature, the 2PA of atomically precise Ag_N-DNAs has not been evaluated before.** Taking into account the advantages of these nanoclusters like high PLQY for NIR-emission, water-solubility and other properties which overcome limitations of organic chromophores, Ag_N-DNAs seem to be interesting materials to study in the context of two-photon properties and consequently evolve as potential probes for 2PFM. For this purpose I selected four far-red and NIR emitting Ag_N-DNAs from the study by Guha, *et al*[71]., which reported four distinct structural/compositional groups of HPLC-purified Ag_N-DNA. Four Ag_N-DNAs groups were characterized by: (1) 8-electron clusters stabilized by two DNA oligomer copies; (2) 6-electron clusters with two oligomer copies; (3) 6-electron clusters with three oligomer copies, (4) 6-electron clusters with two oligomer copies with additional chlorido ligands. In total 19 Ag_N-DNAs were presented and their emission, absorption and circular dichroism (CD) were characterized, each nanocluster composition was confirmed by ESI-MS[71].

Table 1. Composition and optical properties of Ag_N-DNAs, selected from a previous study.[68] n_s: number of ssDNA template stabilizing the Ag_N-DNA, N_0: effective valence electrons of Ag_N-DNAs, 1PA: one-photon absorption, FQY: fluorescence quantum yield, 1PEL: one-photon excited photoluminescence.

Name	Molecular Formula	DNA sequence (5′ to 3′)	x_s and no. of Cl^- ligands	N_0	1PA (nm)	1PEL (nm)	FQY [%]	Stokes shift (eV)
Ag_{15}-DNA	$(DNA)_2[Ag_{15}]^{9+}$	ACCAATGACC	2 and 0	6	550	652	11	0.35
Ag_{21}-DNA	$(DNA)_3[Ag_{21}]^{15+}$	CCCGGAGAAG	3 and 0	6	640	721	73 (Ref [11])	0.22
Ag_{16}-DNA-Cl_2	$(DNA)_2[Ag_{16}Cl_2]^{8+}$	CACCTAGCGA	2 and 2	6	525	744	26 (Ref[31])	0.70
Ag_{19}-DNA	$(DNA)_2[Ag_{19}]^{11+}$	GCGCAAGATG	2 and 0	8	480, 615	730	16	0.31

From each group one representative was chosen with different molecular formula, including total number of Ag atoms, effective valence electron count (N_0), DNA oligomers sequence, the numbers of DNA oligomer ligands (x_s) and presence of additional chlorido ligands: $(DNA)_2[Ag_{15}]^{9+}$; $(DNA)_3[Ag_{21}]^{15+}$; $(DNA)_2[Ag_{16}Cl_2]^{8+}$; $(DNA)_2[Ag_{19}]^{11+}$, which will be called in short as: Ag_{15}-DNA, Ag_{21}-DNA, Ag_{16}-DNA-Cl_2 and Ag_{19}-DNA, respectively.

4.2 Results:

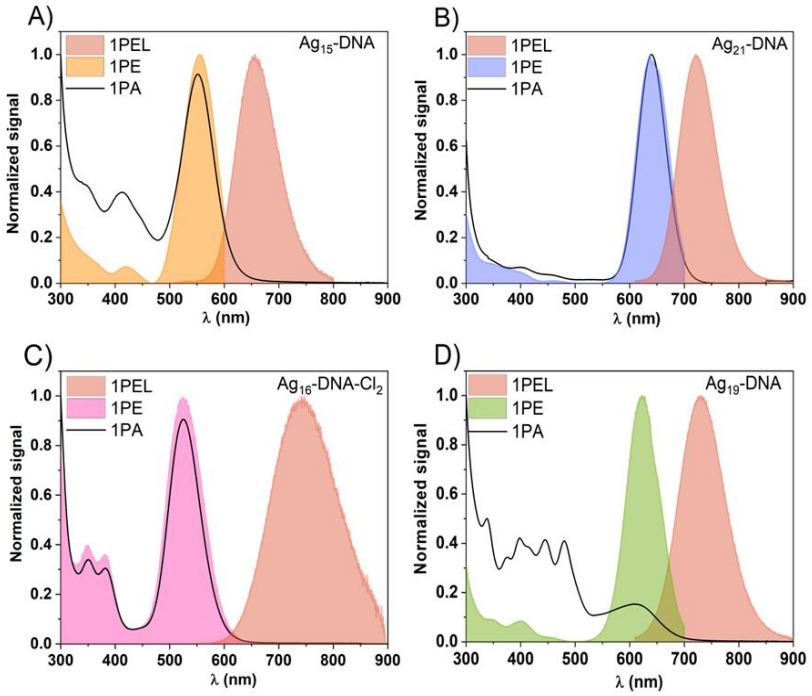

Figure 16. *Comparison between 1PE (one-photon excitation), 1PA (one-photon absorption), and 1PEL (one-photon excited luminescence) spectra of (A) Ag_{15}-DNA, (B) Ag_{21}-DNA, (C) Ag_{16}-DNA-Cl_2; (D) Ag_{19}-DNA. Figure reproduced from [A. Hajda, R. Guha, S. M. Copp and J. Olesiak-Bańska, Chem. Sci., 2025, 16, 1737 DOI: 10.1039/D4SC05853D].*

Ag_N-DNAs were synthesized by Rweetuparna Guha and Prof. Stacy Copp at the University of California, Irvine, USA. They were purified on HPLC and their molecular masses were confirmed by ESI-MS, which is presented in article's SI on page 95 and 96. Firstly, one-photon properties were evaluated like FQY, fluorescence, 1PA and 1PE. Some studies, such as emission and absorption spectra measurements, confirmed previous observations by Guha, et al[71]. However, 1PE spectra of these nanoclusters were reported for the first time in my work, as well as FQY for Ag_{15}-DNA (11%) and Ag_{19}-DNA (16%). Comparison of 1PA, 1PE and one-photon excited luminescence (1PEL) spectra of measured nanoclusters can be seen in Figure 16. After characterization of one-photon properties, I measured 2PA of the Ag_N-DNA species by 2PEL technique for a wide wavelength range from 810 to 1400 nm. Two-photon nature of observed emission was confirmed based on the quadratic dependence of photoluminescence intensity (PL intensity) on the incident laser power. If the slop of the log(PL intensity), in a function of log(laser power) is near 2.0, it indicates two-photon process. For Ag_{21}-DNA the slops had lower values than 1.7 for excitation <850nm, which indicates contributions from one-photon excitation process.

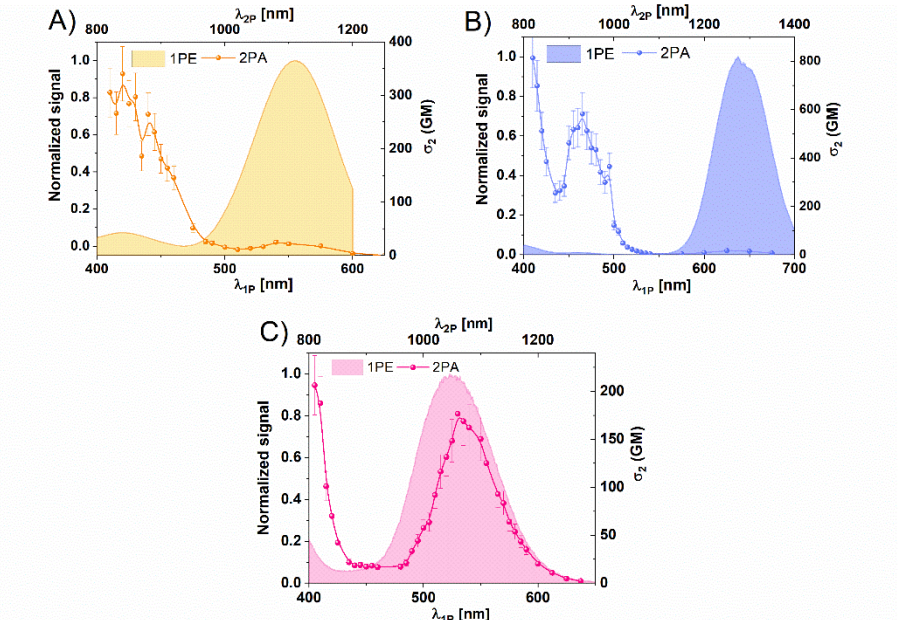

Figure 17. *Comparison between 1PE and 2PA of (A) Ag_{15}-DNA, (B)Ag_{21}-DNA, (C) Ag_{16}-DNA-Cl_2. Figure reproduced from [A. Hajda, R. Guha, S. M. Copp and J. Olesiak-Bańska, Chem. Sci., 2025, 16, 1737 DOI: 10.1039/D4SC05853D].*

Consequently, it should be stated that σ_2 values determined for 810 nm and 820 nm might be overestimated. Ag_{19}DNA had significant one-photon processes contribution at wavelengths below 980 nm, for 810 nm excitation the slop value equaled ~1.2. Due to this fact, Ag_{19}DNA was excluded from the main discussion of 2PA properties and data collected for this nanocluster should be considered as qualitative. Ag_{15}-DNA and Ag_{16}-DNA-Cl_2 were proven to have pure two-photon excitation. All log-log plots of the PL intensity are presented in article's SI on page 99. In Figure 17, σ_2 values were compared to 1PE spectra, due to the fact that for Ag_N-DNA 1PA differs from 1PE spectrum. Below 950 nm excitation, σ_2 had the highest values for all Ag_N-DNA, on the order of several hundred GM. Two distinct types of σ_2 trends are distinguished at lower-energy transitions (longer wavelengths). Ag_{15}-DNA and Ag_{21}-DNA showed a pronounced decrease in σ_2 values > 1000 nm, which corresponds to the dominant $S_0 \rightarrow S_1$ transition observed in this range. On the other hand, Ag_{16}-DNA-Cl_2 have two transitions at 800 nm and 1050 nm, with similar σ_2 values. In contrast to Ag_{21}-DNA and Ag_{15}-DNA, Ag_{16}-DNA-Cl_2 has σ_2 values one order of magnitude higher at longer wavelengths, which is discussed in details below.

In order to assess the relative strength of 2P versus 1P transitions, I compared the ratio of their transition intensities. In the case of Ag_{15}-DNA, the intensity ratio of 1PE at 420 nm and at 550 nm is approximately 1:20, whereas for σ_2 at 840 nm and at 1100 nm, the ratio is 17:1. This indicates an inversion in transition intensities between 2P and 1P excitation. For Ag_{21}-DNA, I also observed that transition $S_0 \rightarrow S_1$ is not the most prominent in 2P regime. The highest values of σ_2 were determined for 820 nm and 940 nm excitation, which correspond to low-intensity peaks in the 1PE spectrum. There were 3 transitions in 1P and 2P regime with ratio ~3 : 1 : 67 for 410/460/635 nm and 50 : 35 : 1 for double the wavelengths - 820/920/1270 nm. However, it is important to note that the lack of crystal structure for

Ag_{19}DNA, Ag_{21}DNA and Ag_{15}DNA and consequently the lack of theoretical calculations, energy diagrams significantly limits the interpretation of results.

Since Ag_{16}-DNA-Cl_2 had significantly higher σ_2 for $S_0 \rightarrow S_1$ transitions, I looked for the explanation of this phenomenon. Ag_{16}-DNA-Cl_2 is known for complex emission properties, since it has two components with nanosecond and microsecond lifetimes at liquid nitrogen temperature and in D_2O solvent.[213] To decode its excited state dynamics transient absorption (TA) spectroscopy was used.[214] It reveled, that fraction of fluorescent state can transitions to a microsecond-lived state, which is observed with a decay time of ca. 70 µs. TA spectra showed a positive signal between 1000–1200 nm. As the crystal structure of Ag_{16}-DNA-Cl_2 is known, theoretical calculations can support experiments. TA spectra calculated by Malola, *et al*[90] presented a broad positive peak between 1100–1400 nm related to S_1 and T_1 transitions, which supported experimental TA data. This range overlaps with the 2PA bands of Ag_{16}-DNA-Cl_2. In 2PEL measurements was used fs laser with 80 MHz repetition rate - 12.5 ns window between consecutive pulses. Taking this information into account, a possible contribution of long-lived T1 state in 2PA in NIR-II ranges was considered. Thus, I evaluated σ_2 by 2PEL technique using fs laser with 1 kHz repetition rate, which gives 1 ms window between pulses. Comparison of σ_2 values obtained by excitation by 1 kHz and 80 MHz laser showed no meaningful differences, which can be seen on Figure S8 in article's SI on page 98.

Table 2. Comparison of optical properties of Ag_N-DNAs (measured in 10 mM ammonium acetate solution, pH 7) with commercially available and water-soluble fluorescent probes with λ_{EM} above 600 nm (measured in H_2O).

Probe	σ_2 [GM]	$\sigma_{2,B}$[GM]	λ_{EM} [nm]	Excitation Window
mCherry[215]	25	5.5	610	NIR-II
tdTomato[215]	108	60	581	NIR-II
Alexa Fluor[216] 647	133	44	671	NIR-II
Cy5[216]	143	40	670	NIR-II
Cy7[216]	200	60	779	NIR-II
Alexa Fluor[216] 680	203	73	704	NIR-II
ICG[217]	210	6.3	813	NIR-II
Cy5.5[216]	286	60	695	NIR-II
Ag_{21}-DNA	582	425	>700	NIR-I
	17	12		NIR-II
Ag_{16}-DNA-Cl_2	211	54	>700	NIR-I
	176	45		NIR-II
Ag_{15}-DNA	340	37	650	NIR-II
	25	3		NIR-I

Lastly, $\sigma_{2,B}$ for measured nanoclusters was calculated and compared with commercially available NIR-emitting fluorescent probes used for 2PFM, which are water-soluble – see Table 2. Based on comparison of $\sigma_{2,B}$ Ag_N-DNAs have comparable $\sigma_{2,B}$ in the NIR-II excitation window for the best commercially available probes, but they outperform commercial probes in NIR-I window.

4.3 Summary:

I evaluated σ_2 and $\sigma_{2,B}$ of four distinct atomically precise Ag_{N-} DNAs. They present high values of σ_2 in <900 nm wavelengths range, corresponding to transitions which have lower intensity in 1P regime. In the longer wavelengths range, corresponding to the most prominent 1P transitions, 2PA is low for most of the studied nanoclusters. The most pronounced difference is for Ag_{16}-DNA-Cl_2, which have one order of magnitude higher σ_2 above 1000 nm, than the other studied Ag_{N-} DNAs. Understanding of this difference needs further investigation, also in the frame of theoretical calculations. Nevertheless, performed experiments confirmed the **hypothesis 3** "Atomically-precise nanoclusters Ag_N-DNA can have high σ_2 and $\sigma_{2,B}$, exceeding 50 GM, which will make them potential probes for bioimaging". I met the **goal 3** "Proposing new NIR-emitting nanoparticles, which are water-soluble two-photon absorbers and confirm their optical properties".

4.4 Research contribution of PhD candidate:

Contribution of PhD candidate

Agata Hajda
Institute of Advanced Materials
Wroclaw University of Science and Technology
ul. Gdańska 7/9
50-344 Wrocław

Author Contribution Statement

I, Agata Hajda hereby declare that in the article: Two photon brightness of NIR-emitting, atomically precise DNA-stabilized silver nanoclusters. *Chemical Science. 2025, vol. 16, nr 4, s. 1737-1745.*, I was responsible for:

- Methodology
- Investigation
  - One-photon measurements of nanoclusters: absorption, emission, excitation, fluorescence quantum yield, photostability, selectivity studies.
  - Two-photon measurements: two-photon excited fluorescence, power dependent studies, two-photon brightness
- Data analysis
- Writing– orginal draft

Agata Hajda

4.5 Article and supporting information:

Chemical Science

ROYAL SOCIETY OF CHEMISTRY

EDGE ARTICLE

View Article Online
View Journal | View Issue

Cite this: *Chem. Sci.*, 2025, **16**, 1737

All publication charges for this article have been paid for by the Royal Society of Chemistry

Two-photon brightness of NIR-emitting, atomically precise DNA-stabilized silver nanoclusters†

Agata Hajda, [a] Rweetuparna Guha, [b] Stacy Marla Copp [bcde] and Joanna Olesiak-Bańska *[a]

Received 31st August 2024
Accepted 16th December 2024

DOI: 10.1039/d4sc05853d

rsc.li/chemical-science

Near-infrared (NIR) emitters with high two-photon absorption (2PA) cross-sections are of interest to enable *in vivo* imaging in the tissue transparency windows. This study explores the potential of DNA-stabilized silver nanoclusters (Ag_N-DNAs) as water-soluble two-photon absorbers. We investigate 2PA of four different atomically precise Ag_N-DNA species with far-red to NIR emission and varying nanocluster and ligand compositions. 2PA cross-sections, σ_2, were determined by two-photon excited luminescence (2PEL) technique for a wide wavelength range from 810 to 1400 nm. The Ag_N-DNAs exhibited reversed strength of corresponding transitions in the two-photon regime, as compared to one-photon, which further demonstrates the complex photophysics of these emitters. Maximal 2PA cross-section value (~582 GM) was observed for $(DNA)_3[Ag_{21}]^{15+}$, which is stabilized by 3 DNA oligomers. $(DNA)_2[Ag_{16}Cl_2]^{8+}$ presented distinct 2PA behavior from the Ag_N-DNAs without chlorido ligands, with a high 2PA of 176 GM at 1050 nm. Our findings support the potential of Ag_N-DNAs as NIR-to-NIR two-photon probes that are both excited and emit in the NIR. Their high σ_2 and fluorescence quantum yield values result in superior two-photon brightness on the order of $\sim 10^2$ GM, significantly higher than water-soluble organic fluorophores.

Introduction

DNA-stabilized silver nanoclusters (Ag_N-DNAs) are an emerging class of biocompatible fluorescent nanomaterials with sequence-tuned optical properties.[1–3] These ultrasmall emitters have unique and diverse photoluminescence properties that span visible and near-infrared (NIR) wavelengths. The optical properties of Ag_N-DNAs depend strongly on the size, shape, and effective valence electron count of the nanocluster core, which are governed by the nucleobase sequence of the DNA oligomer template.[4–6] Thus, DNA oligomer selection enables tunable design of Ag_N-DNA properties,[7,8] making Ag_N-DNAs promising and versatile emitters to meet the needs of bioimaging.

Recent tandem efforts to harness machine learning-guided experiments and to prepare and investigate atomically precise Ag_N-DNA species have accelerated the discovery of Ag_N-DNAs.[9–11] Many recently discovered Ag_N-DNAs emit at NIR-I and NIR-II wavelengths (700–1000 nm and 1000–1300 nm, respectively)[12–15] with high fluorescence quantum yields[16] (FQY, ϕ) compared to other NIR emitters, such as organic dyes. Water soluble NIR emitting probes are highly desirable for optical imaging of biological samples because scattering, absorption, and autofluorescence of tissues are significantly reduced at NIR wavelengths compared to visible wavelengths.[17,18] The remarkably high FQY and inherent water solubility of NIR Ag_N-DNAs make these promising emitters for overcoming the issue of low FQY of NIR-emitting organic fluorophores, which limit *in vivo* fluorescence imaging.

In contrast to their one-photon (1P) properties, the nonlinear optical (NLO) properties of Ag_N-DNAs have been far less explored. Two-photon absorption (2PA) is a third order NLO phenomenon that occurs upon simultaneous absorption of two photons, each with half the excitation energy of the chromophore, thereby exciting an electron from the ground state to the excited state. This excitation process requires high-intensity pulsed laser irradiation and is induced at long wavelengths, which are more favorable for deeper penetration into biological samples. 2PA can be followed by two-photon excited fluorescence (2PEF), which enables two-photon fluorescence microscopy (2PFM). 2PFM at NIR-I or NIR-II wavelengths[19] presents multiple advantages compared to the standard 1P fluorescence microscopy, such as deeper sample penetration, reduced phototoxicity and photobleaching, 3D imaging within tissues, selective excitation of femtoliter-scale volumes, and visualization over long time periods (longitudinal imaging).[20–25]

[a]*Institute of Advanced Materials, Wroclaw University of Science and Technology, Wroclaw, Poland. E-mail: joanna.olesiak-banska@pwr.edu.pl*

[b]*Department of Materials Science and Engineering, University of California, Irvine, CA 92697, USA*

[c]*Department of Chemistry, University of California, Irvine, CA 92697, USA*

[d]*Department of Physics and Astronomy, University of California, Irvine, CA 92697, USA*

[e]*Department of Chemical and Biomolecular Engineering, University of California, Irvine, CA 92697, USA*

† Electronic supplementary information (ESI) available. See DOI: https://doi.org/10.1039/d4sc05853d

Atomically precise silver or gold nanoclusters (Ag/Au NCs) were reported as strong two-photon absorbers.[26–30] 2PA cross-section (σ_2, expressed in Goeppert-Mayer units, GM) for Ag/Au NCs varies from $\sim 10^2$ GM to $\sim 10^5$ GM and is dictated by nanocluster properties, such as the number of metal atoms, protecting ligands, and doping with other metal atoms.[26–28] However, Ag/Au NCs generally display low ϕ and low two-photon brightness (defined as $\sigma_{2,b} = \phi \times \sigma_2$), limiting their relevance in 2PFM. Early studies of 2PA of Ag_N-DNAs suggested the promise of these emitters for 2PFM, but these studies preceded the robust development of purification strategies to produce Ag_N-DNA emitters with defined chemical compositions.[31,32] While the 2PA of atomically precise Ag_N-DNAs has not been explored in detail, application of this effect is now emerging.[33]

To advance *in vivo* fluorescence imaging, it is a major goal to develop water-soluble, 2PEF probes that both excite and emit at NIR wavelengths with high FQY and high two-photon brightness ($\sigma_{2,b}$ above 50 GM).[34,35] In this study, we investigate 2PA of four different atomically precise Ag_N-DNAs with far-red to NIR emission, which were recently investigated by Guha, *et al.*[5] We find that 2PA spectra of the four Ag_N-DNAs, measured from 810 nm to 1400 nm, show significant differences between 1P and two-photon (2P) response. We then present a detailed analysis of NLO properties (specifically two-photon absorption) of the NIR-emissive Ag_N-DNA with chlorido ligands and known X-ray crystal structure, $(DNA)_2[Ag_{16}Cl_2]^{8+}$. Finally, we compare the 2P brightness of Ag_N-DNAs to organic fluorophores and commercially used NIR markers, demonstrating their utility for applications in NIR-to-NIR 2P bioimaging.

Results and discussion

To investigate the NLO properties of far red and NIR emitting Ag_N-DNAs, we selected four Ag_N-DNAs with different molecular compositions, including total number of Ag atoms, effective valence electron count (N_0), and the numbers of DNA oligomer ligands (n_s) and chlorido ligands (Table 1). Emitters were selected from a recent study by Guha, *et al.*, which reported the molecular compositions and one-photon absorbance (1PA) and emission spectra of four distinct structural/compositional groups of HPLC-purified far-red to NIR emitting Ag_N-DNAs.[5] One emitter from each group was selected to study the breadth of possible 2PE properties of far red and NIR emitting Ag_N-DNAs. To ensure agreement with past studies,[5] molecular compositions were confirmed by negative-ion mode electrospray ionization mass spectrometry (see Experimental methods and ESI†), and 1P optical properties of the Ag_N-DNAs (absorption and emission) were measured to ensure consistency with prior reports. For the first time, we present one-photon excitation (1PE) spectra of these clusters (Fig. 1). 1PA and 1PEL maxima, FQY, and Stokes shifts are reported in Table 1, and Fig. 1 presents 1P properties of the four Ag_N-DNAs.

Fig. 1 shows that the most prominent Ag_N-DNA excitation peaks are Gaussian-shaped bands located at the longest wavelength transition in 1PA, indicating that these emitters follow Kasha's rule. We observe no difference in shape or intensity of peaks in 1PA and one-photon excitation (1PE) spectra for **Ag_{21}-DNA** (Fig. 1b) and **Ag_{16}-DNA-Cl_2** (Fig. 1c). For **Ag_{15}-DNA**, the peak bands in 1PA and 1PE occur at the same wavelength, but the ratio of the longest-wavelength band and the band located between 400 and 450 nm is significantly higher in 1PE than in 1PA (Fig. 1a). The most significant deviations between 1PA and 1PE are observed for **Ag_{19}-DNA** (Fig. 1d). This emitter's 1PE spectrum contains four distinct peaks (347 nm, 401 nm, 450 nm, and 620 nm), while far more peaks are observed in the 1PA spectrum, as previously reported.[5] This suggests that absorption at certain wavelengths does not result in radiative recombination and fluorescence emission for **Ag_{19}-DNA**. **Ag_{15}-DNA**, **Ag_{21}-DNA**, **Ag_{19}-DNA** exhibit Stokes shifts between 0.2 and 0.3 eV whereas, **Ag_{16}-DNA-Cl_2** displays a Stokes shift of 0.7 eV (Table 1).[15] Comparison with FQY shows that energy gap law does not hold for these nanoclusters. **Ag_{21}-DNA** displays a high 73% FQY at room temperature in aqueous solution,[16] which is unprecedented for NIR emitters, however it displays the lowest Stokes shift.

Ag_{16}-DNA-Cl_2 has molecular composition $(DNA)_2[Ag_{16}Cl_2]^{8+}$; *i.e.* the species is stabilized by two copies of the ssDNA template and two additional chlorido ligands, which significantly contribute to nanocluster stability and optical properties.[9] **Ag_{16}-DNA-Cl_2** is the only Ag_N-DNA in this study with a reported high-resolution X-ray crystal structure (and one of only two Ag_N-DNA species with high-resolution structural information about both nanocluster core and ligand shell reported to date).[36] This emitter has 26% FQY and a high Stokes shift of 0.7 eV, implicating a large energy difference between the Franck–Condon excited state and the S_1–S_0 transition (fluorescence). The emitter has been well-studied by the Vosch group.[15,37–40] Theoretical analysis of its 1PA properties identified silver → silver, silver → base and base → silver electronic transitions.[41]

Table 1 Composition and optical properties of Ag_N-DNAs, selected from a previous study.[5] n_s: number of ssDNA template stabilizing the Ag_N-DNA, N_0: effective valence electrons of Ag_N-DNAs, 1PA: one-photon absorption, FQY: fluorescence quantum yield, 1PEL: one-photon excited luminescence

Name	Molecular formula	DNA sequence (5′ to 3′)	n_s and no. of Cl^- ligands	N_0	1PA (nm)	1PEL (nm)	FQY, ϕ [%]	Stokes shift (eV)
Ag_{15}-DNA	$(DNA)_2[Ag_{15}]^{9+}$	ACCAATGACC	2 and 0	6	550	652	11	0.35
Ag_{21}-DNA	$(DNA)_3[Ag_{21}]^{15+}$	CCCGGAGAAG	3 and 0	6	640	721	73 (ref. 16)	0.22
Ag_{16}-DNA-Cl_2	$(DNA)_2[Ag_{16}Cl_2]^{8+}$	CACCTAGCGA	2 and 2	6	525	744	26 (ref. 15)	0.70
Ag_{19}-DNA	$(DNA)_2[Ag_{19}]^{11+}$	GCGCAAGATG	2 and 0	8	480, 615	730	16	0.31

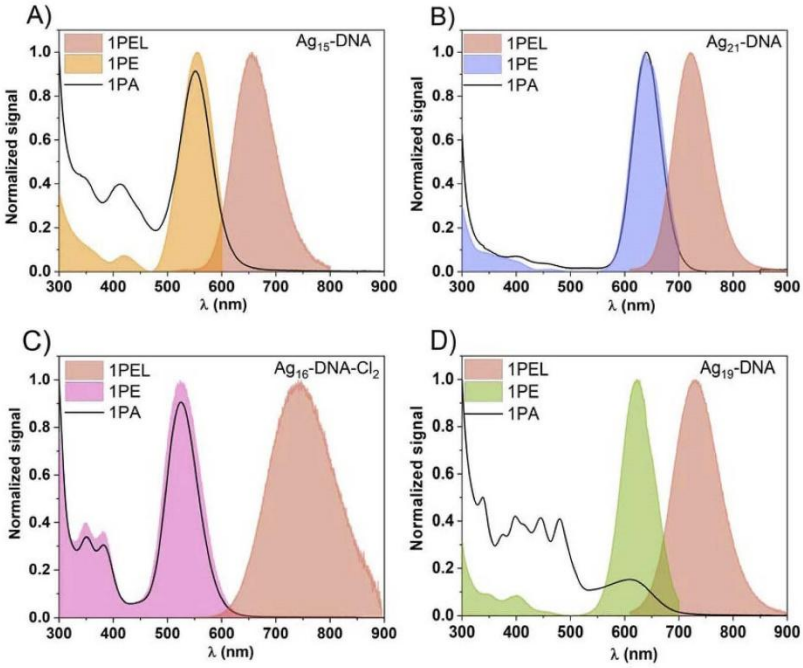

Fig. 1 Comparison between 1PE (one-photon excitation), 1PA (one-photon absorption, black curve), and 1PEL (one-photon excited luminescence) spectra of (A) **Ag_{15}-DNA**, (B) **Ag_{21}-DNA**, (C) **Ag_{16}-DNA-Cl_2**, and (D) **Ag_{19}-DNA**.

Finally, **Ag_{19}-DNA** has molecular composition $(DNA)_2[Ag_{19}]^{11-}$ and contains 8 effective valence electrons ($N_0 = 8$), unlike the $N_0 = 6$ of the rest of the Ag_N-DNAs studied here. Because $N_0 = 8$ is a magic number for spherical superatoms,[42] and due to its distinctly different absorption and circular dichroism spectra, **Ag_{19}-DNA** has been hypothesized to possess spheroidal nanocluster geometry[43] rather than the rod-shaped structures of $N_0 = 6$ Ag_N-DNAs.[44]

After characterization of one-photon properties, we measured the NLO properties of the Ag_N-DNA species. The 2PA cross-sections, σ_2, of Ag_N-DNAs and reference samples (Styryl 9M or LDS-698) were evaluated by two-photon excited luminescence (2PEL) technique using femtosecond pulsed laser excitation in a wide range of wavelengths (see Experimental section).[45] As a luminescence-based technique, 2PEL provides information about 2PA cross-section values only for wavelengths at which 2PE leads to luminescence.[26] In systems for which absorption perfectly overlaps with excitation, 2PA spectrum determined with 2PEL can be directly compared with 1PA. However, in systems for which absorption differs from excitation, the measured 2PA spectrum should be compared with the 1PE spectrum. Because excitation and absorption spectra differ for **Ag_{15}-DNA** and **Ag_{19}-DNA** (Fig. 1), we compare 2PA cross-sections to 1PE spectrum. Wavelength ranges were selected such that emission wavelengths do not interfere with the excitation wavelength range. Moreover, the 2P nature of the observed processes was determined based on the quadratic dependence of photoluminescence intensity (PL intensity) on the incident laser power, P, which indicates a two-photon process in Ag_N-DNAs (the slope of log(PL intensity) *vs.* log(P) plots equal ~2.0, Fig. S7†).[46] The values of ~1.9 support a 2P process (small deviations from 2.0 were also seen for reference organic dyes with known 2P behaviour). In case of lower values, contributions from upconversion may be present, as is observed for **Ag_{21}-DNA** for excitation <850 nm (Fig. S7b†). Therefore, it should be noted that σ_2 values for **Ag_{21}DNA** at 810 and 820 nm may have contributions from 1P processes. **Ag_{19}DNA** seems to have significant one-photon process contribution at wavelengths below 980 nm (Fig. S7†), nevertheless transitions involving higher energy states are the most prominent under fs laser excitation. Due to this fact, we present results for **Ag_{19}DNA** in the ESI,† and the measured 2PA spectra for **Ag_{19}DNA** presented in Fig. S8† need to be considered as qualitative. Taking into account, that there is no other experimental or theoretical data for this nanocluster, its response under fs laser illumination needs extended studies, out of the scope of this manuscript. **Ag_{19}-DNA** will be excluded from further comparisons with the other nanoclusters. We ensure lack of photobleaching by using low laser power ~10 mW and a short 5 s exposure time,

with samples exposed to laser irradiation only during signal collection.

Fig. 2 compares the σ_2 values of Ag_N-DNAs to their 1PE spectra. Ag_N-DNAs exhibit maximum σ_2 values of several hundred GM at <950 nm, which corresponds to one-photon transitions at <475 nm. At longer wavelengths, two different types of σ_2 behavior are observed. **Ag_{15}-DNA** and **Ag_{21}-DNA** exhibit significantly lower σ_2 above *ca.* 1000 nm, in the range of the most prominent $S_1 \rightarrow S_0$ transitions in the 1P regime. In contrast, the 2PA spectrum of **Ag_{16}-DNA-Cl_2** is distinctly different, with similar σ_2 values at 800 nm and 1050 nm (Fig. 2c).

1PE and 2PA spectra can be compared using the ratio of intensity of higher energy to lower energy transitions in 1PE and 2PA spectra. For **Ag_{15}-DNA**, the ratio between 1PE transitions at 420/550 nm is ~1 : 20. In contrast, the 2PA ratio at 840/1100 nm is 17 : 1. Thus, this emitter displays a reversal of the intensities of 2P transitions compared to 1P transitions.

For **Ag_{21}-DNA**, σ_2 is largest for 820 nm and 940 nm excitation, which overlap with low-intensity peaks in the 1PE spectrum (Fig. 2b). The 2PA is nearly zero between 1000 and 1150 nm, similar to 1PE in the 500–550 nm range. However, as mentioned before, the dominant 1PE peak at 640 nm is not the most prominent in 2PA (Fig. 2b). A closer look at 1PE between 400–500 nm (Fig. S2†) shows that high σ_2 bands correlate with very weak 1P $S_0 \rightarrow S_n$ transitions (where $n > 1$). The ratio of 1P transition intensity at 410/460/635 nm is ~3 : 1 : 67, while for 2PA (at double wavelength) the ratio is 50 : 35 : 1.

For **Ag_{16}-DNA-Cl_2**, the locations of 2PA transitions are well-aligned with 1PE transitions (Fig. 2c). Surprisingly, however, the 2PA band at longer wavelengths has one order of magnitude higher σ_2 value than the other three Ag_N-DNA species. This **Ag_{16}-DNA-Cl_2** is discussed in more detail later.

A trend of opposite strength of 1PE and 2PA bands is observed in **Ag_{15}-DNA**, **Ag_{21}-DNA** and **Ag_{16}-DNA-Cl_2**. Past studies of unpurified Ag_N-DNAs by Patel, *et al.*[32] reported a similar phenomenon where two-photon excitation (2PE) was more prominent at shorter wavelengths. Thus, such opposite strength of 1PA and 2PE bands could be a more general observation for this type of nanostructures could be a more general observation for this type of nanostructures. 1P and 2P transitions may follow distinct selection rules and resonant enhancements of selected transitions in 2PA, thus giving rise to the possibility of such phenomena. Generally, in molecules with more complex energy landscapes like porphyrins[47] or fluorescent proteins,[48] resonance effects with various electronic or vibrational states contribute to the enhancement of certain 2P transitions. In fluorescent proteins, 2PA corresponding to $S_0 \rightarrow S_1$ transition is often less prominent than for transitions at shorter wavelengths, which gain intensity due to the resonant enhancement effect related to the proximity of virtual state energy (at 1/2 transition energy) and real S_n state.[49] Such a phenomenon may exist in Ag_N-DNAs.

Ag_{16}-DNA-Cl_2 has one order of magnitude higher σ_2 at longer wavelengths than the other Ag_N-DNAs. **Ag_{16}-DNA-Cl_2** is distinct for containing chlorido ligands. As one of the most

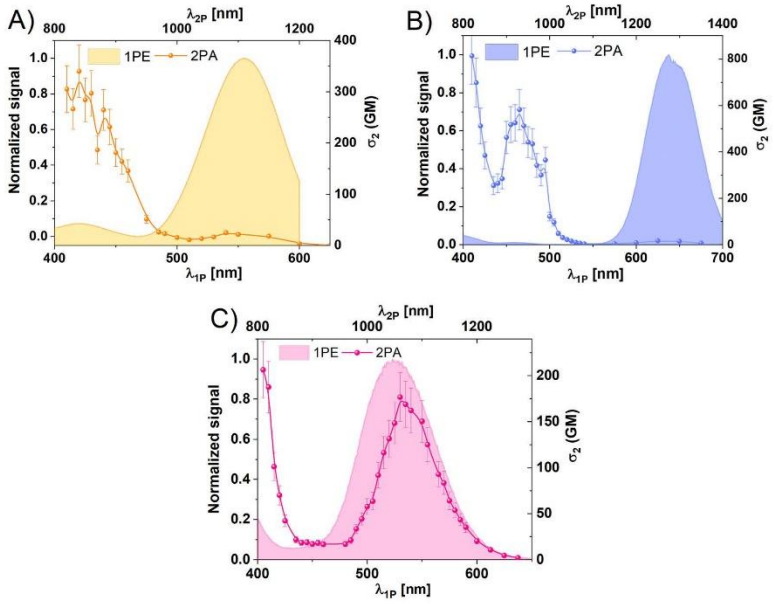

Fig. 2 Comparison between one photon excitation (1PE, filled bands) and two photon absorption (2PA, points and lines) of (A) Ag_{15}-DNA, (B) Ag_{21}-DNA, (C) Ag_{16}-DNA-Cl_2.

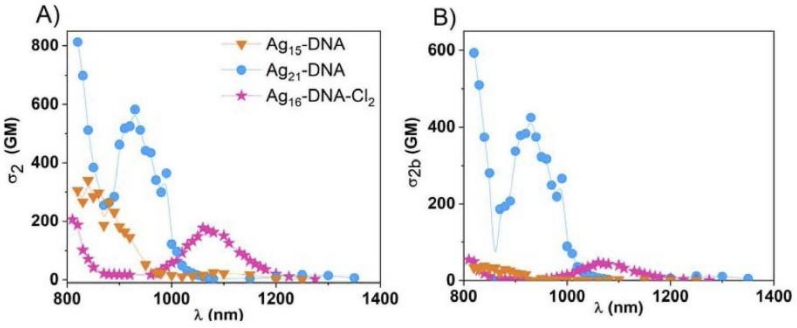

Fig. 3 Comparison of (A) two-photon absorption (2PA) cross-section (σ_2) and (B) 2PA brightness, $\sigma_{2,b}$ of Ag_{15}-DNA (orange inverted triangles), Ag_{21}-DNA (blue circles), Ag_{16}-DNA-Cl_2 (pink stars). The standard deviation of presented values is estimated to be ± 15%, not included in figures for more clarity.

electronegative atoms, chlorine influences electron density, electric transition dipole moment and increases the inter- and intra-molecular charge-transfer effects. Indeed, computational modelling[41] shows that chloridos modulate electron density and optical properties of **Ag_{16}-DNA-Cl_2**, stabilizing the electronic structure by reducing the electron density in the metal core and thereby leading to shifts in the nanocluster energy levels, affecting both the HOMO (highest occupied molecular orbital) and LUMO (lowest unoccupied molecular orbital) energies. Calculations also revealed that the experimentally observed absorbance peak at 525 nm consists only of a HOMO-to-LUMO molecular transition (S_0–S_1*) located at the silver core of **Ag_{16}-DNA-Cl_2**,[41] while higher energy transitions also contain contributions from silver–base and base–silver transitions, making these transitions more complex. **Ag_{16}-DNA-Cl_2** presents also complex emission, with nanosecond and microsecond components. In previous reports, excited state dynamics was probed by transient absorption (TA) spectroscopy for **Ag_{16}-DNA-Cl_2**, revealing that upon excitation, electrons are transferred to the Franck–Condon state and then rapidly depopulate to vibrationally hot levels of the fluorescent state within 100 fs.[51] Hot vibrational levels thermalize on a timescale of 6.2 ps. Radiative relaxation (emission) to the ground state occurs with a lifetime of 4.7 ns. In a fraction of cases, the transition to a microsecond-lived state is observed with a decay time of *ca.* 70 μs. TA spectra showed a positive signal between 1000–1200 nm, which blue-shifts over several ns.[51] Recently, the simulated TA spectra by Malola, *et al.* presented a broad peak between 1100–1400 nm related to S_1 and T_1 transitions with absorption maxima at 1244 nm and 1181 nm, respectively.[50] Because this range of wavelengths overlaps with the 2PA band of **Ag_{16}-DNA-Cl_2**, a possible contribution of transitions in a long-lived T_1 state in measurements at NIR wavelengths were considered. Therefore, we investigated the optical properties of **Ag_{16}-DNA-Cl_2** in more detail. Standard 2PEL measurements involve the use of fs lasers with 80 MHz repetition rate, corresponding to a 12.5 ns window between consecutive pulses. Because the long-lived state in **Ag_{16}-DNA-Cl_2** has 70 μs lifetime, we also performed 2PEL measurements using a laser system with a 1 kHz repetition rate (1 ms window between pulses) Fig. S6† compares 2PA spectra obtained at 1 kHz and 80 MHz laser repetition rates, which show no significant changes in σ_2 value or maximum wavelength. We do observe a slight alteration in the shape of the 2PA band at 1000–1150 nm, with higher values of σ_2 at 980–1060 nm.

Finally, 2P brightness ($\sigma_{2,b} = \phi \times \sigma_2$) of each Ag_N-DNA species was calculated and compared with commercially available probes to evaluate the potential of Ag_N-DNAs for 2PFM.[52–54] Fig. 3a and b present σ_2 and $\sigma_{2,b}$ of the Ag_N-DNA species, respectively, over a range of 810–1400 nm, which spans the NIR-I and NIR-II biological tissue transparency windows. Most notably, **Ag_{21}-DNA** has both high σ_2 and exceptionally high FQY compared to commonly used NIR-emitting fluorophores, resulting in the highest value of 2P brightness in the NIR-I window (*ca.* 582 GM at 930 nm, Fig. 3b). **Ag_{16}-DNA-Cl_2**

Table 2 Comparison of optical properties of Ag_N-DNAs (measured in 10 mM ammonium acetate solution, pH 7) with commercially available and water-soluble fluorescent probes with emission wavelength above 600 nm (measured in H_2O). [σ_2: 2PA cross-section, $\sigma_{2,b}$: two-photon brightness]

Probe	σ_2 [GM]	$\sigma_{2,b}$ [GM]	Emission [nm]	Excitation window
mCherry[58]	25	5.5	610	NIR-II
tdTomato[58]	108	60	581	NIR-II
Alexa Fluor (ref. 21) 647	133	44	671	NIR-II
Cy5 (ref. 21)	143	40	670	NIR-II
Cy7 (ref. 21)	200	60	779	NIR-II
Alexa Fluor (ref. 21) 680	203	73	704	NIR-II
ICG[59]	210	6.3	813	NIR-II
Cy5.5 (ref. 21)	286	60	695	NIR-II
Ag_{21}-DNA	582	425	>700	NIR-I
	17	12		NIR-II
Ag_{16}-DNA-Cl_2	211	54	>700	NIR-I
	176	45		NIR-II
Ag_{15}-DNA	340	37	650	NIR-II
	25	3		NIR-I

exhibits high $\sigma_{2,b}$ in the NIR-II window. Moreover, the combined use of **Ag_{15}-DNA** with other emitters could enable two-color, 2P imaging,[55,56] as the emission of this species is blue-shifted by 50 to 100 nm from the other three Ag_N-DNAs, which would enable simultaneous 2PE of two distinct probes using a single laser line.

There is a major need for water-soluble NIR-emitting probes with 2PE > 1000 nm, which currently are scarce because most available probes are insoluble in water due to the presence of highly hydrophobic units. Table 2 compares the NLO properties of the four Ag_N-DNA species with commercially available water-soluble dyes and fluorescent proteins used in 2PFM. σ_2 and 2P brightness values of Ag_N-DNAs are comparable or significantly greater than the commercial fluorescent probes. The ability of Ag_N-DNAs to combine water solubility with NIR-I emission, high 2P brightness, low toxicity, and functionalization *via* click-chemistry for applications such as targeted staining of certain cell lines[57] positions Ag_N-DNA as promising emitters to address the shortage of probes that are suitable for 2PFM.

Conclusions

We investigated the 2P properties of four atomically precise Ag_N-DNAs with far-red to NIR-I emission. These four species present distinct ligand compositions and valence electron counts, enabling us to probe the diversity of optical properties that may vary with nanocluster composition and structure. Ag_N-DNA species were measured with the same optical setup and the use of HPLC purification and ESI-MS allowed us to accurately estimate nanocluster concentration, an essential property for accurate σ_2 calculation. Thus, our results provide quantitative information to advance understanding of structure–optical properties relationship of these nanoclusters. For **Ag_{15}-DNA** and **Ag_{16}-DNA-Cl_2**, the same transitions take part in 1PA and radiative relaxation (1PA and 1PE spectra overlap). In contrast, some excited states are not involved in radiative relaxation for **Ag_{21}-DNA** and **Ag_{19}-DNA**, which results in differences in 1PA and 1PE spectra, particularly in case of **Ag_{19}-DNA**. All nanocluster species present high 2PA cross-sections. For **Ag_{15}-DNA** and **Ag_{21}-DNA**, maximum σ_2 values are obtained at the low-wavelength transitions, contrary to 1PA. In case of **Ag_{16}-DNA-Cl_2**, strong 2PA is also present at NIR-II wavelengths. For **Ag_{19}-DNA**, one-photon process contributes to excitation under fs laser illumination, and further studies on this cluster are needed to fully understand its nonlinear optical properties. At present, the relationship between nanocluster structure and two-photon properties still remains poorly understood, and additional Ag_N-DNA crystal structures are needed to enable theoretical studies that investigate how chemical composition and structure relate to observed 2P properties. However, our findings confirm that Ag_N-DNAs are a new class of promising markers for NIR imaging and 2PFM, presenting high values of two-photon brightness together with other properties beneficial for bioimaging, such as NIR emission, large Stokes shifts, and water solubility. Our findings further identify the optimal excitation wavelengths to achieve a strong 2P fluorescence signal from these emitters. A deeper understanding of their photophysics and NLO properties could enable rational design of these unique emitters for advanced two-photon deep tissue bioimaging applications.

Methods

Synthesis and purification of Ag_N-DNAs

An aqueous solution of single stranded DNA oligomer and $AgNO_3$ in 10 mM ammonium acetate (pH 7) was prepared and incubated at room temperature for 15 minutes, followed by reduction by a freshly prepared aqueous solution of sodium borohydride (more details in ESI and Table S1†). The solution was stored in the dark at 4 °C for several days to allow the fluorescent Ag_N-DNA to form. Each Ag_N-DNA was then purified by high-performance liquid chromatography (HPLC) to obtain atomically precise Ag_N-DNAs. The molecular compositions of HPLC-purified Ag_N-DNAs were determined using negative-ion mode electrospray ionization mass spectrometry (ESI-MS). The ESI-MS methods and the mass spectra of the Ag_N-DNAs studied are shown in Fig. S1–S4.† The concentrations of HPLC-purified Ag_N-DNAs were estimated using the sample's absorption at 260 nm, the known molar extinction coefficient of the ssDNA oligomer template, and the number of DNA oligomers per nanocluster (Table 1). Detailed synthesis procedures (including concentrations of DNA oligomer and $AgNO_3$, and storage conditions), HPLC chromatograms, and mass spectra of Ag_N-DNAs are reported in ref. 5.

One-photon measurements

All measurements were carried out in 10 mM ammonium acetate solution (pH 7). Absorption spectra were recorded using a Jasco V-670 spectrophotometer. Excitation and fluorescence spectra using an FS5 Spectrofluorometer (Edinburgh Instruments) equipped with a Xenon lamp.

FQY measurements

First, the FQY of the LDS-698 in $CHCl_3$ was determined using an integrating sphere (FS5 Spectrofluorometer) and by the comparative method. The standard in the comparative method was DCM (4-(dicyanomethylene)-2-methyl-6-(4-dimethylaminostyryl)-4*H*-pyran) in EtOH with FQY = 43.5%.[60] Finally, the FQY (ϕ) was determined using the following formula:

$$\phi_s = \phi_r \frac{f_r(\lambda_{ex})}{f_s(\lambda_{ex})} \frac{\int_{\lambda_{em}} F_s(\lambda_{em})}{\int_{\lambda_{em}} F_r(\lambda_{em})} \frac{{n_s}^2}{{n_r}^2}$$

$$f_s(\lambda_{ex}) = 1 - 10^{-A_s(\lambda_{ex})}$$

where, s and r stand for the sample and reference, respectively, ϕ is the quantum yield, and n is the refractive index of the solvent, $\int_{\lambda_{em}} F(\lambda_{em})$ corresponds to the fluorescence integral of the sample or reference, and $f_i(\lambda_{ex})$ refers to the corresponding absorption factor at the excitation wavelength. The results

obtained using the comparative method and the integrating sphere were almost identical, within the standard deviation margin for the integrating sphere (2%). FQY of LDS-698 in $CHCl_3$ was 14% for the absolute method and 15.5% for the comparative method. Hence, LDS-698 was used as a standard to determine the quantum yield for **Ag_{15}-DNA** and **Ag_{19}-DNA**. For **Ag_{21}-DNA** and **Ag_{16}-DNA-Cl_2**, FQY values were taken from previous reports.[15,16]

NLO measurements

Two-photon excited photoluminescence (2PEL) was measured using a custom-built multiphoton setup. The excitation source was femtosecond mode-locked Ti:Sapphire laser (~100 fs, 80 MHz, Chameleon, Coherent Inc. with a wavelength range 680 to 1080 nm), combined with an optical parametric oscillator Chameleon OPO (Coherent Inc., applied in 1100–1600 nm range). The signal was collected, and emission spectra were measured with a spectrograph – Shamrock 303i (Andor) with an iDUS camera (Andor). Depending on excitation wavelength ranges, optical filters were also used: FELH0950 – Ø 25.0 mm Longpass Filter (Thorlabs), FELH0800 – Ø 25.0 mm Longpass Filter (Thorlabs). The power of the laser irradiating the sample was measured and calibrated for each wavelength. Laser power was kept at ~10 mW for most measured wavelengths, to ensure quality signal of detectors and no photobleaching. Samples were irradiated only at the time of signal collection to avoid photobleaching. The sample and reference dye were always measured at the same excitation power. 2PA cross-sections were calculated with the following equation.[45,61]

$$\sigma_{2,s} = \frac{F_{2,s} C_r \phi_r {n_r}^2}{F_{2,r} C_s \phi_s {n_s}^2} \sigma_{2,r}$$

where, r and s denote reference and sample, respectively. ϕ_r and ϕ_s is the fluorescence quantum yield. $F_{2,s}$ and $F_{2,r}$ is the integrated two-photon fluorescence intensity at a particular excitation wavelength, n is the refractive index of the solvent. C_s and C_r is the concentration of the sample and reference, respectively. Styryl 9M and LDS-698 in $CHCl_3$ were used as a reference. FQY of Styryl was taken from literature.[27] FQY of LDS-698 in $CHCl_3$ was measured for this work and is described in the FQY measurements section. 2PA cross-sections of Styryl 9M and LDS-698 were obtained from previously reported literature.[45,61] Laser system employed in additional measurements of **Ag_{16}-DNA-Cl_2** was a Coherent Ti: Sapphire Astrella regenerative amplifier combined with an OPA TOPAS Prime (Coherent) optical parametric amplifier providing tunable ~60 fs pulses at 1 kHz.

Two-photon brightness ($\sigma_{2,b}$) was calculated using the equation:

$$\sigma_{2,b} = \sigma_2 \times \phi$$

Power dependence of luminescence intensity

To confirm the two-photon nature of the observed fluorescence excited by laser pulses, we measured fluorescence intensity *vs.* incident laser excitation power and determined the power exponent, n. 2PEL was collected by photon-counting avalanche photodiode (IDQ id100) or spectrograph – Shamrock 303i (Andor) with an iDUS camera (Andor). To avoid photobleaching, we recorded three separate spectra at each power or recorded for 30 s on an avalanche photodiode to detect any change in intensity. The power exponent was calculated using the equation:

$$n = \frac{\log(\text{PL intensity})}{\log(P)}$$

where PL intensity is a 2P excited photoluminescence intensity and P is the average incident laser power.

Data availability

The data that support the findings of this study are available within the article and ESI.†

Author contributions

A. H. conducted optical experiments and analysed the data. R. G. prepared and characterized atomically precise nanocluster solutions. S. M. C. and J. O. B. supervised the research, analyzed the data and acquired the funding. All authors took part in writing and editing the manuscript.

Conflicts of interest

There are no conflicts to declare.

Acknowledgements

This work was supported by the Sonata Bis project from National Science Centre (2019/34/E/ST5/00276). R. G. and S. M. C. acknowledge support from the Hellman Faculty Fellowship and grant 2024-337801 from the Chan Zuckerberg Initiative DAF, an advised fund of the Silicon Valley Community Foundation. The authors acknowledge Anna Gonzàlez-Rosell for preparing one of the nanoclusters used in this study.

References

1 J. T. Petty, J. Zheng, N. V. Hud and R. M. Dickson, DNA-Templated Ag Nanocluster Formation, *J. Am. Chem. Soc.*, 2004, **126**(16), 5207–5212.
2 Y. Chen, M. L. Phipps, J. H. Werner, S. Chakraborty and J. S. Martinez, DNA Templated Metal Nanoclusters: From Emergent Properties to Unique Applications, *Acc. Chem. Res.*, 2018, **51**(11), 2756–2763.
3 A. Gonzàlez-Rosell, C. Cerretani, P. Mastracco, T. Vosch and S. M. Copp, Structure and luminescence of DNA-templated silver clusters, *Nanoscale Adv.*, 2021, **3**(5), 1230–1260.
4 S. M. Copp, D. Schultz, S. Swasey, J. Pavlovich, M. Debord, A. Chiu, K. Olsson and E. Gwinn, Magic Numbers in DNA-Stabilized Fluorescent Silver Clusters Lead to Magic Colors, *J. Phys. Chem. Lett.*, 2014, **5**(6), 959–963.

5 R. Guha, A. Gonzàlez-Rosell, M. Rafik, N. Arevalos, B. B. Katz and S. M. Copp, Electron count and ligand composition influence the optical and chiroptical signatures of far-red and NIR-emissive DNA-stabilized silver nanoclusters, *Chem. Sci.*, 2023, **14**(41), 11340–11350.
6 A. Gonzàlez-Rosell and S. M. Copp, An Atom-Precise Understanding of DNA-Stabilized SilverNanoclusters, *Acc. Chem. Res.*, 2024, **57**, 2117–2129.
7 A. V. Pinheiro, D. Han, W. M. Shih and H. Yan, Challenges and opportunities for structural DNA nanotechnology, *Nat. Nanotechnol.*, 2011, **6**(12), 763–772.
8 S. M. Copp and A. Gonzàlez-Rosell, Large-scale investigation of the effects of nucleobase sequence on fluorescence excitation and Stokes shifts of DNA-stabilized silver clusters, *Nanoscale*, 2021, **13**, 4602–4613.
9 A. Gonzàlez-Rosell, S. Malola, R. Guha, N. R. Arevalos, M. F. Matus, M. E. Goulet, E. Haapaniemi, B. B. Katz, T. Vosch, J. Kondo, H. Häkkinen and S. M. Copp, Chloride Ligands on DNA-Stabilized Silver Nanoclusters, *J. Am. Chem. Soc.*, 2023, **145**(19), 10721–10729.
10 R. Guha and S. M. Copp, 12 Nucleic Acid-Templated Metal Nanoclusters, in *Modern Avenues in Metal-Nucleic Acid Chemistry*, ed. Müller, J. and Lippert, B., CRC Press, 2023, pp. 291–342.
11 P. Mastracco and S. M. Copp, Beyond nature's base pairs: machine learning-enabled design of DNA-stabilized silver nanoclusters, *Chem. Commun.*, 2023, **59**, 10360–10375.
12 M. B. Liisberg, Z. Shakeri Kardar, S. M. Copp, C. Cerretani and T. Vosch, Single-Molecule Detection of DNA-Stabilized Silver Nanoclusters Emitting at the NIR I/II Border, *J. Phys. Chem. Lett.*, 2021, **12**(4), 1150–1154.
13 J. T. Petty, C. Fan, S. P. Story, B. Sengupta, M. Sartin, J.-C. Hsiang, J. W. Perry and R. M. Dickson, Optically Enhanced, Near-IR, Silver Cluster Emission Altered by Single Base Changes in the DNA Template, *J. Phys. Chem. B*, 2011, **115**(24), 7996–8003.
14 J. T. Petty, C. Fan, S. P. Story, B. Sengupta, A. St. John Iyer, Z. Prudowsky and R. M. Dickson, DNA Encapsulation of 10 Silver Atoms Producing a Bright, Modulatable, Near-Infrared-Emitting Cluster, *J. Phys. Chem. Lett.*, 2010, **1**(17), 2524–2529.
15 S. A. Bogh, M. R. Carro-Temboury, C. Cerretani, S. M. Swasey, S. M. Copp, E. G. Gwinn and T. Vosch, Unusually large Stokes shift for a near-infrared emitting DNA-stabilized silver nanocluster, *Methods Appl. Fluoresc.*, 2018, **6**(2), 024004.
16 V. A. Neacşu, C. Cerretani, M. B. Liisberg, S. M. Swasey, E. G. Gwinn, S. M. Copp and T. Vosch, Unusually large fluorescence quantum yield for a near-infrared emitting DNA-stabilized silver nanocluster, *Chem. Commun.*, 2020, **56**(47), 6384–6387.
17 R. Weissleder, A clearer vision for *in vivo* imaging, *Nat. Biotechnol.*, 2001, **19**(4), 316–317.
18 J. V. Frangioni, *In vivo* near-infrared fluorescence imaging, *Curr. Opin. Chem. Biol.*, 2003, **7**(5), 626–634.
19 A. M. Smith, M. C. Mancini and S. Nie, Second window for *in vivo* imaging, *Nat. Nanotechnol.*, 2009, **4**(11), 710–711.
20 S. E. Crowe and G. C. R. Ellis-Davies, Longitudinal *in vivo* two-photon fluorescence imaging, *J. Comp. Neurol.*, 2014, **522**(8), 1708–1727.
21 D. Kobat, M. E. Durst, N. Nishimura, A. W. Wong, C. B. Schaffer and C. Xu, Deep tissue multiphoton microscopy using longer wavelength excitation, *Opt. Express*, 2009, **17**(16), 13354–13364.
22 D. Kobat, N. Horton and C. Xu, *In vivo* two-photon microscopy to 1.6-mm depth in mouse cortex, *J. Biomed. Opt.*, 2011, **16**(10), 106014.
23 K. W. Dunn and P. A. Young, Principles of Multiphoton Microscopy, *Nephron Exp. Nephrol.*, 2006, **103**(2), e33–e40.
24 C. Xu, W. Zipfel, J. B. Shear, R. M. Williams and W. W. Webb, Multiphoton fluorescence excitation: new spectral windows for biological nonlinear microscopy, *Proc. Natl. Acad. Sci. U.S.A.*, 1996, **93**(20), 10763–10768.
25 W. R. Zipfel, R. M. Williams and W. W. Webb, Nonlinear magic: multiphoton microscopy in the biosciences, *Nat. Biotechnol.*, 2003, **21**(11), 1369–1377.
26 J. Olesiak-Banska, M. Waszkielewicz, P. Obstarczyk and M. Samoc, Two-photon absorption and photoluminescence of colloidal gold nanoparticles and nanoclusters, *Chem. Soc. Rev.*, 2019, **48**(15), 4087–4117.
27 A. Pniakowska, K. Kumaranchira Ramankutty, P. Obstarczyk, M. Perić Bakulić, Ž. Sanader Maršić, V. Bonačić-Koutecký, T. Bürgi and J. Olesiak-Bańska, Gold-Doping Effect on Two-Photon Absorption and Luminescence of Atomically Precise Silver Ligated Nanoclusters, *Angew. Chem., Int. Ed.*, 2022, **61**(43), e202209645.
28 V. Bonačić-Koutecký and R. Antoine, Enhanced two-photon absorption of ligated silver and gold nanoclusters: theoretical and experimental assessments, *Nanoscale*, 2019, **11**(26), 12436–12448.
29 J. Olesiak-Banska, M. Waszkielewicz, K. Matczyszyn and M. Samoc, A closer look at two-photon absorption, absorption saturation and nonlinear refraction in gold nanoclusters, *RSC Adv.*, 2016, **6**(101), 98748–98752.
30 A. S. Reyna, I. Russier-Antoine, F. Bertorelle, E. Benichou, P. Dugourd, R. Antoine, P.-F. Brevet and C. B. de Araújo, Nonlinear Refraction and Absorption of Ag29 Nanoclusters: Evidence for Two-Photon Absorption Saturation, *J. Phys. Chem. C*, 2018, **122**(32), 18682–18689.
31 S. H. Yau, N. Abeyasinghe, M. Orr, L. Upton, O. Varnavski, J. H. Werner, H.-C. Yeh, J. Sharma, A. P. Shreve, J. S. Martinez and T. Goodson Iii, Bright two-photon emission and ultra-fast relaxation dynamics in a DNA-templated nanocluster investigated by ultra-fast spectroscopy, *Nanoscale*, 2012, **4**(14), 4247–4254.
32 S. A. Patel, C. I. Richards, J.-C. Hsiang and R. M. Dickson, Water-Soluble Ag Nanoclusters Exhibit Strong Two-Photon-Induced Fluorescence, *J. Am. Chem. Soc.*, 2008, **130**(35), 11602–11603.
33 X. Wang, M. B. Liisberg, G. L. Nolt, X. Fu, C. Cerretani, L. Li, L. A. Johnson, T. Vosch and C. I. Richards, DNA-AgNC Loaded Liposomes for Measuring Cerebral Blood Flow

Using Two-Photon Fluorescence Correlation Spectroscopy, *ACS Nano*, 2023, **17**(13), 12862–12874.

34 H. J. Chun, E. S. Kim and B. R. Cho, Scope and limitation of label-free multiphoton microscopy and probe-labeled two-photon microscopy for the endomicroscopic diagnosis, *Scanning*, 2014, **36**(4), 462–464.

35 H. M. Kim and B. R. Cho, Small-Molecule Two-Photon Probes for Bioimaging Applications, *Chem. Rev.*, 2015, **115**(11), 5014–5055.

36 C. Cerretani, H. Kanazawa, T. Vosch and J. Kondo, Crystal structure of a NIR-Emitting DNA-Stabilized Ag16 Nanocluster, *Angew. Chem., Int. Ed.*, 2019, **58**(48), 17153–17157.

37 C. Cerretani, M. B. Liisberg, V. Rück, J. Kondo and T. Vosch, The effect of inosine on the spectroscopic properties and crystal structure of a NIR-emitting DNA-stabilized silver nanocluster, *Nanoscale Adv.*, 2022, **4**(15), 3212–3217.

38 C. Cerretani, G. Palm-Henriksen, M. B. Liisberg and T. Vosch, The effect of deuterium on the photophysical properties of DNA-stabilized silver nanoclusters, *Chem. Sci.*, 2021, **12**(48), 16100–16105.

39 V. Rück, C. Cerretani and T. Vosch, How Inert is Single-Stranded DNA Towards DNA-Stabilized Silver Nanoclusters? A Case Study, *ChemPhotoChem*, 2024, e202400014.

40 C. Cerretani, J. Kondo and T. Vosch, Removal of the A10 adenosine in a DNA-stabilized Ag16 nanocluster, *RSC Adv.*, 2020, **10**(40), 23854–23860.

41 S. Malola, M. F. Matus and H. Häkkinen, Theoretical Analysis of the Electronic Structure and Optical Properties of DNA-Stabilized Silver Cluster Ag16Cl2 in Aqueous Solvent, *J. Phys. Chem. C*, 2023, **127**(33), 16553–16559.

42 H. Häkkinen, Atomic and electronic structure of gold clusters: understanding flakes, cages and superatoms from simple concepts, *Chem. Soc. Rev.*, 2008, **37**(9), 1847–1859.

43 A. Gonzàlez-Rosell, R. Guha, C. Cerretani, V. Rück, M. B. Liisberg, B. B. Katz, T. Vosch and S. M. Copp, DNA Stabilizes Eight-Electron Superatom Silver Nanoclusters with Broadband Downconversion and Microsecond-Lived Luminescence, *J. Phys. Chem. Lett.*, 2022, **13**(35), 8305–8311.

44 S. M. Copp, D. Schultz, S. M. Swasey, A. Faris and E. G. Gwinn, Cluster Plasmonics: Dielectric and Shape Effects on DNA-Stabilized Silver Clusters, *Nano Lett.*, 2016, **16**(6), 3594–3599.

45 N. S. Makarov, M. Drobizhev and A. Rebane, Two-photon absorption standards in the 550–1600 nm excitation wavelength range, *Opt. Express*, 2008, **16**(6), 4029–4047.

46 C. Li, *Nonlinear Optics. Principles and Applications*. 1 edn, Springer Singapore, 2016, vol. XVII, p. 386.

47 M. Drobizhev, F. Meng, A. Rebane, Y. Stepanenko, E. Nickel and C. W. Spangler, Strong Two-Photon Absorption in New Asymmetrically Substituted Porphyrins: Interference between Charge-Transfer and Intermediate-Resonance Pathways, *J. Phys. Chem. B*, 2006, **110**(20), 9802–9814.

48 M. Drobizhev, N. S. Makarov, T. Hughes and A. Rebane, Resonance Enhancement of Two-Photon Absorption in Fluorescent Proteins, *J. Phys. Chem. B*, 2007, **111**(50), 14051–14054.

49 M. Drobizhev, N. S. Makarov, S. E. Tillo, T. E. Hughes and A. Rebane, Two-photon absorption properties of fluorescent proteins, *Nat. Methods*, 2011, **8**(5), 393–399.

50 S. Malola and H. Häkkinen, On transient absorption and dual emission of the atomically precise, DNA-stabilized silver nanocluster Ag16Cl2, *Chem. Commun.*, 2024, **60**(24), 3315–3318.

51 J. Chen, A. Kumar, C. Cerretani, T. Vosch, D. Zigmantas and E. Thyrhaug, Excited-State Dynamics in a DNA-Stabilized Ag16 Cluster with Near-Infrared Emission, *J. Phys. Chem. Lett.*, 2023, **14**(17), 4078–4083.

52 S. Wang, B. Li and F. Zhang, Molecular Fluorophores for Deep-Tissue Bioimaging, *ACS Cent. Sci.*, 2020, **6**(8), 1302–1316.

53 S. Pascal, S. David, C. Andraud and O. Maury, Near-infrared dyes for two-photon absorption in the short-wavelength infrared: strategies towards optical power limiting, *Chem. Soc. Rev.*, 2021, **50**(11), 6613–6658.

54 P. A. Shaw, E. Forsyth, F. Haseeb, S. Yang, M. Bradley and M. Klausen, Two-Photon Absorption: An Open Door to the NIR-II Biological Window?, *Front. Chem.*, 2022, **10**, 921354.

55 H. Kawano, T. Kogure, Y. Abe, H. Mizuno and A. Miyawaki, Two-photon dual-color imaging using fluorescent proteins, *Nat. Methods*, 2008, **5**(5), 373–374.

56 S. E. Tillo, T. E. Hughes, N. S. Makarov, A. Rebane and M. Drobizhev, A new approach to dual-color two-photon microscopy with fluorescent proteins, *BMC Biotechnol.*, 2010, **10**(1), 6.

57 V. Rück, N. K. Mishra, K. K. Sørensen, M. B. Liisberg, A. B. Sloth, C. Cerretani, C. B. Mollerup, A. Kjaer, C. Lou, K. J. Jensen and T. Vosch, Bioconjugation of a Near-Infrared DNA-Stabilized Silver Nanocluster to Peptides and Human Insulin by Copper-Free Click Chemistry, *J. Am. Chem. Soc.*, 2023, **145**(30), 16771–16777.

58 M. Drobizhev, S. Tillo, N. S. Makarov, T. E. Hughes and A. Rebane, Absolute Two-Photon Absorption Spectra and Two-Photon Brightness of Orange and Red Fluorescent Proteins, *J. Phys. Chem. B*, 2009, **113**(4), 855–859.

59 M. Y. Berezin, C. Zhan, H. Lee, C. Joo, W. J. Akers, S. Yazdanfar and S. Achilefu, Two-Photon Optical Properties of Near-Infrared Dyes at 1.55 μm Excitation, *J. Phys. Chem. B*, 2011, **115**(39), 11530–11535.

60 K. Rurack and M. Spieles, Fluorescence Quantum Yields of a Series of Red and Near-Infrared Dyes Emitting at 600–1000 nm, *Anal. Chem.*, 2011, **83**(4), 1232–1242.

61 N. S. Makarov, J. Campo, J. M. Hales and J. W. Perry, Rapid, broadband two-photon-excited fluorescence spectroscopy and its application to red-emitting secondary reference compounds, *Opt. Mater. Express*, 2011, **1**(4), 551–563.

Supporting Information

Two-photon brightness of NIR-emitting, atomically precise DNA-stabilized silver nanoclusters

Agata Hajda,[1] Rweetuparna Guha,[2] Stacy Marla Copp,[2,3,4,5] Joanna Olesiak-Bańska[1]

[1] *Institute of Advanced Materials, Wroclaw University of Science and Technology, Wrocław, Poland*

[2] *Department of Materials Science and Engineering, University of California, Irvine, CA 92697, USA*

[3] *Department of Chemistry, University of California, Irvine, CA 92697, USA*

[4] *Department of Physics and Astronomy, University of California, Irvine, CA 92697, USA*

[5] *Department of Chemical and Biomolecular Engineering, University of California, Irvine, CA 92697, USA*

Contents

1. Synthesis and purification of DNA-stabilized silver nanoclusters (Ag_N-DNAs).

A stoichiometric amount of $AgNO_3$ (Sigma Aldrich) was added to the ssDNA oligomer (Integrated DNA Technologies, standard desalting) in 10 mM ammonium acetate (pH 7.0) to form the Ag^+–DNA complex. After 15 minutes, a freshly prepared aqueous solution of $NaBH_4$ ($[BH_4^-]/[Ag^+] = 0.5$) was added to the Ag^+–DNA complex. Samples were stored at 4 °C in the dark for 3 to 5 days, allowing sufficient time for the Ag_N-DNA formation, followed by purification using ion-paired reverse-phase high-performance liquid chromatography (RP-HPLC). The stoichiometry for Ag^+:DNA was optimized for each Ag_N-DNA to achieve maximum chemical yield (**Table S1**). No additional chloride source was added to synthesize chlorido-protected **Ag_{16}-DNA-Cl_2.**[1] The HPLC chromatograms of the four Ag_N-DNA species are previously reported in Ref. 2.[2]

Table S1. The experimental conditions used for synthesis of Ag_N-DNAs.

Name	[DNA]/ μM	[$AgNO_3$]/ μM
Ag_{15}-DNA	25	125
Ag_{21}-DNA	20	100
Ag_{16}-DNA-Cl_2	25	187.5
Ag_{19}-DNA	25	187.5

2. Mass spectrometry

HPLC-purified Ag_N-DNAs were solvent exchanged to 10 mM ammonium acetate (pH 7) and were directly injected at 100 μL/min in negative ion mode with a 2 kV capillary voltage, 30 V cone voltage, and no collision energy. Spectra were collected from 1000 to 4000 *m/z* and integrated for 1 s. Unless otherwise stated, the source and desolvation temperatures were 80 and 150 °C respectively. Gas flows were 45 L/h for the cone and 450 L/h for the desolvation. Samples were injected with 50 mM NH_4OAc – MeOH (80:20) solution at pH 7.

2.1 Molecular composition determination of Ag_N-DNAs using mass spectrometry.

HPLC-purified Ag_N-DNAs were directly injected to obtain mass spectra using negative-ion mode electrospray ionization mass spectrometry (ESI-MS). The molecular composition of Ag_N-DNA such as the number of ssDNA oligomers (n_s) and the presence of additional chlorido ligands, total number of silver atoms (N) were first determined. Then the number of effective valence electrons (N_0) of each Ag_N-DNA species was determined by fitting the calculated isotopic distribution of the Ag_N-DNA to the experimental spectra. Detailed explanation formulae used for the calculation of N and N_0 have been reported previously.[1-3] The molecular formula of Ag_N-DNA is denoted as $(DNA)_{ns}\,(Ag_NCl_X)^{Qc}$, where Q_c is the nanocluster charge that matches the isotope pattern. In the absence of Cl^- ligands, N_+ equals Q_c, whereas, in the presence of Cl^- ligands, $Q_c = N_+ - x$. The nanocluster size and charge were determined by fitting the calculated isotopic distribution of the Ag_N-DNA to the experimental spectra. Calculated isotopic distributions were obtained from MassLynx using the chemical formula and corrected for the nanocluster's overall positive charge (oxidation state) cluster. The Ag_N-DNA composition and charge were determined by fitting the calculated isotopic distribution of the Ag_N-DNA to the experimental spectra. To confirm the overall charge of the nanocluster (Q_c), we compared the best fit with the two observed charge states peaks, z = 4− (dark blue curve) and z = 5− (light blue curve) as shown in the insets of **Fig. S1** to **S4**.

2.2 Mass spectra of Ag_N-DNAs.

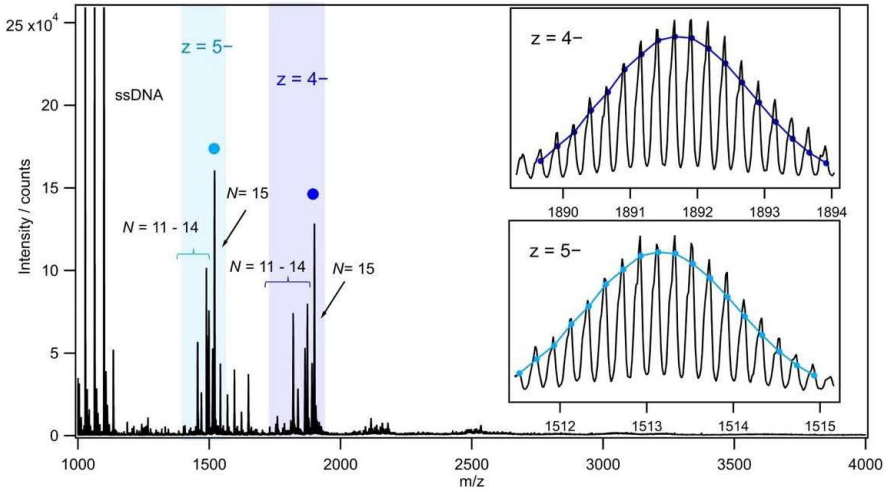

Fig. S1 Mass spectra of **Ag_{15}-DNA**. Experimental isotopic distributions (black curves) for all peaks of **Ag_{15}-DNA** mass spectra. Insets show isotopic distributions aligned with experimental peaks for $(DNA)_2[Ag_{15}]^{9+}$ at z = 5− (light blue) and z = 4− (dark blue). Isotopic distributions were calculated using the chemical formula $C_{192}H_{244}N_{78}O_{110}P_{18}Ag_{15}$.

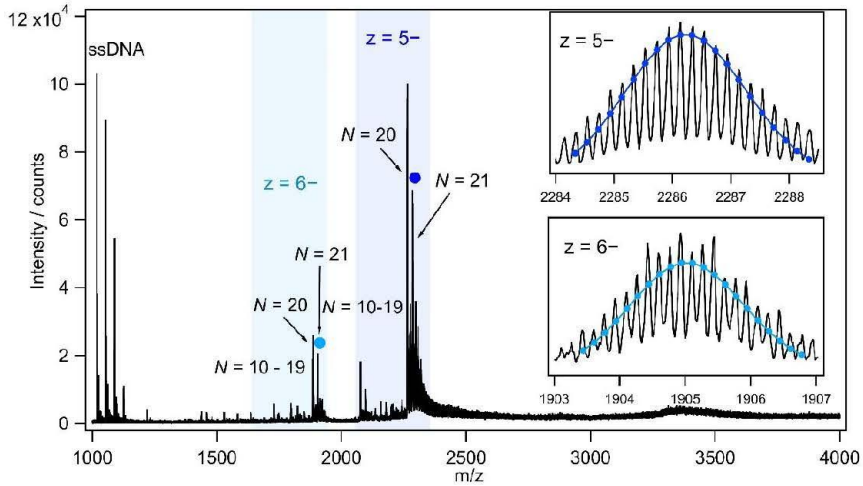

Fig. S2 Mass spectra of **Ag_{21}-DNA**. Experimental isotopic distributions (black curves) for all peaks of **Ag_{21}-DNA** mass spectra. Insets show isotopic distributions aligned with experimental peaks for $(DNA)_3[Ag_{21}]^{15+}$ at z = 6− (light blue) and z = 5− (dark blue). Isotopic distributions were calculated using the chemical formula $C_{291}H_{363}N_{132}O_{165}P_{27}Ag_{21}$.

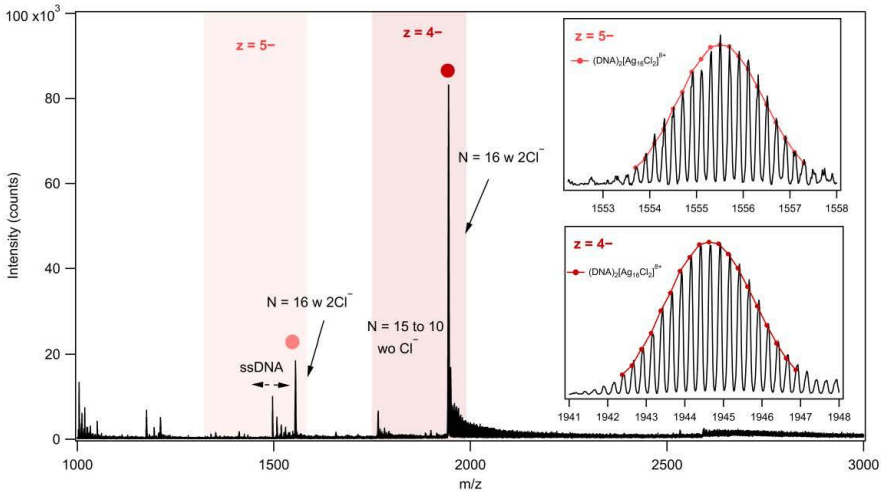

Fig. S3 Mass spectra of **Ag_{16}-DNA-Cl_2**. Experimental isotopic distributions (black curves) for all peaks of **Ag_{16}-DNA-Cl_2** mass spectra. Insets show isotopic distributions aligned with experimental peaks for $(DNA)_2[Ag_{16}Cl_2]^{8+}$ at z = 6− (light red) and z = 5− (dark red). Isotopic distributions were calculated using the chemical formula $C_{192}H_{244}N_{78}O_{112}P_{18}Cl_2Ag_{16}$.

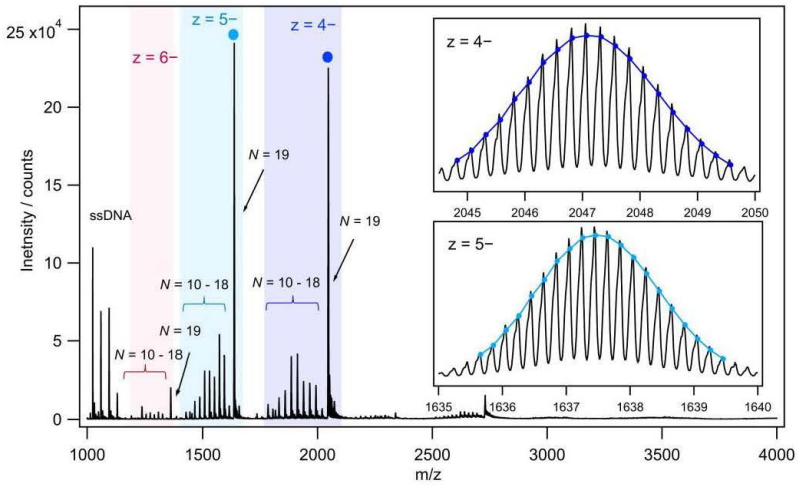

Fig. S4 Mass spectra of **Ag_{19}-DNA**. Experimental isotopic distributions (black curves) for peaks of **Ag_{19}-DNA** mass spectra. Insets show isotopic distributions aligned with experimental peaks for $(DNA)_2[Ag_{19}]^{11+}$ at z = 5− (light blue) and z = 4− (dark blue), as indicated by circles. Isotopic distributions were calculated using the chemical formula $C_{196}H_{244}N_{86}O_{112}P_{18}Ag_{19}$.

3. Two-photon spectra measurements of Ag_N-DNAs.

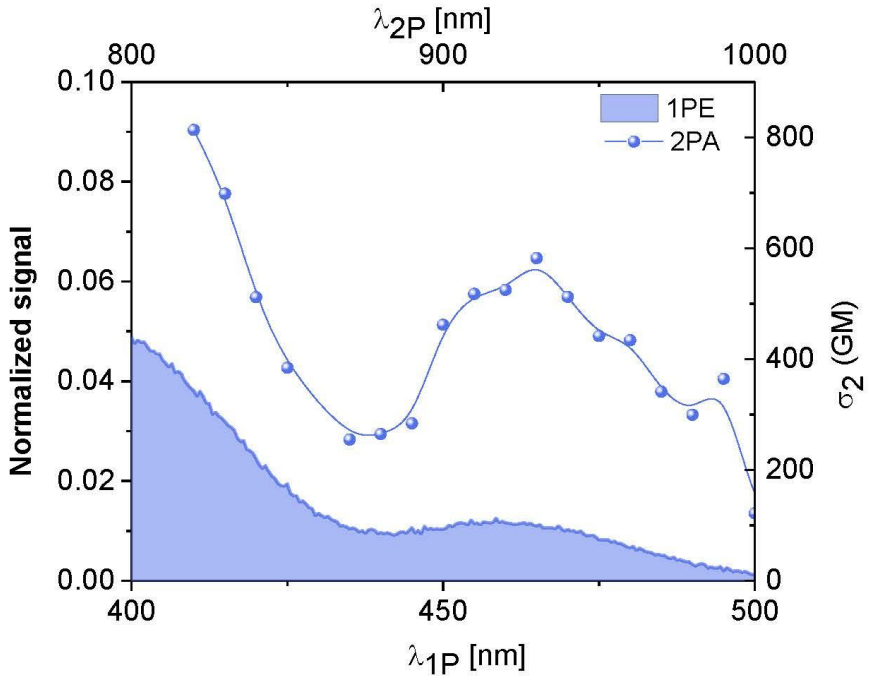

Fig. S5 Zoomed-in comparison of one-photon excitation (1PE, filled blue band) and two-photon absorbance (2PA, blue circles and lines) for **Ag_{21}-DNA.**

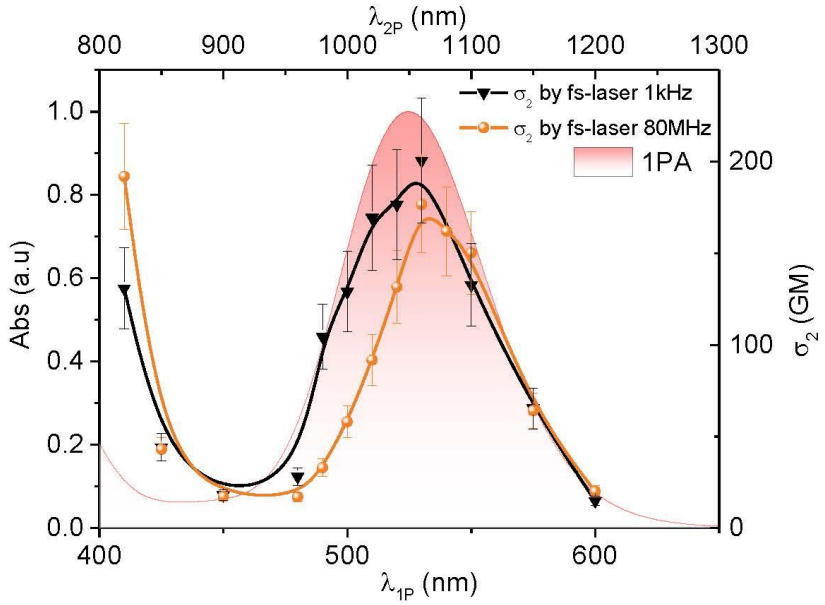

Fig. S6 Comparison of one-photon excitation (1PE, filled red band) and two-photon absorption (2PA) spectra of **Ag_{16}-DNA-Cl_2** obtained with fs lasers at repetition rates of 1 kHz (black lines with inverted triangles) and 80 MHz (orange line with circles).

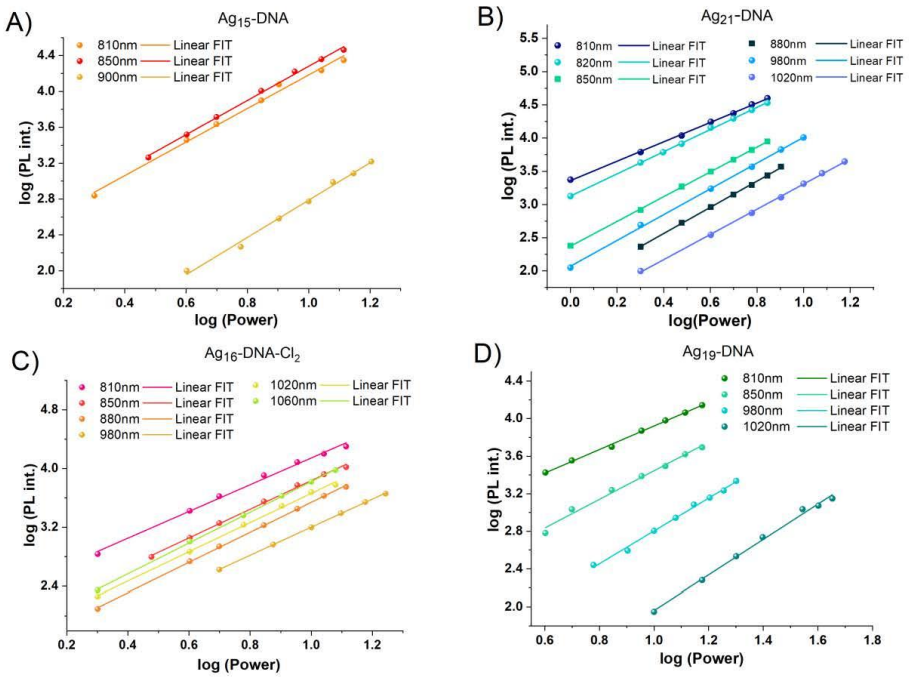

Legend for Log-log plots of the PL intensity. Power exponent (n) is shown for all measured wavelengths.			
Ag_{15}-DNA	**Ag_{21}-DNA**	**Ag_{16}-DNA-Cl_2**	**Ag_{19}-DNA**
n_{810}: 1.87±0.07 n_{850}: 1.91±0.04 n_{900}: 2.08±0.07	n_{810}: 1.48±0.02 n_{820}: 1.67±0.02 n_{850}: 1.86±0.01 n_{880}: 1.97±0.02 n_{980}: 2.07±0.07 n_{1020}: 1.90±0.01	n_{810}: 1.82±0.06 n_{850}: 1.95±0.04 n_{880}: 2.04±0.02 n_{980}: 1.91±0.01 n_{1020}: 1.98±0.04 n_{1060}: 2.09±0.02	n_{810}: 1.19±0.02 n_{850}: 1.52±0.07 n_{980}: 1.75±0.04 n_{1020}: 1.88±0.06

Fig. S7 Log-log plot of the PL intensity of (A) **Ag_{15}-DNA**, (B) **Ag_{21}-DNA**, (C) **Ag_{16}-DNA-Cl_2**, and (D) **Ag_{19}-DNA**. Slopes indicate power exponent (n).

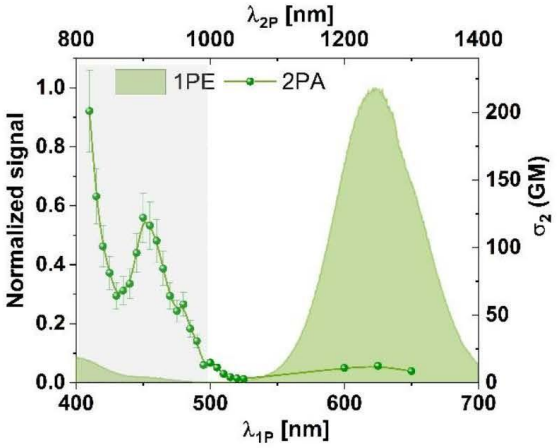

Fig. S8 Comparison between one-photon excitation (1PE, filled bands) and two-photon absorption (2PA, points and lines) of **Ag_{19}-DNA**. Grey shaded area implies a high contribution of one-photon processes based on power exponent.

4. References

1. A. Gonzàlez-Rosell, S. Malola, R. Guha, N. R. Arevalos, M. F. Matus, M. E. Goulet, E. Haapaniemi, B. B. Katz, T. Vosch, J. Kondo, H. Häkkinen and S. M. Copp, *J. Am. Chem. Soc.*, 2023, **145**, 10721-10729.
2. R. Guha, A. Gonzàlez-Rosell, M. Rafik, N. Arevalos, B. B. Katz and S. M. Copp, *Chem. Sci.*, 2023, **14**, 11340-11350.
3. R. Guha, S. Malola, M. Rafik, M. Khatun, A. Gonzàlez-Rosell, H. Häkkinen and S. M. Copp, *Nanoscale*, 2024, DOI: 10.1039/D4NR03533J.

Chapter 5. Novel O,N,O-coordinated organofluoroboron probe for amyloid detection: insight from experiment and theory.

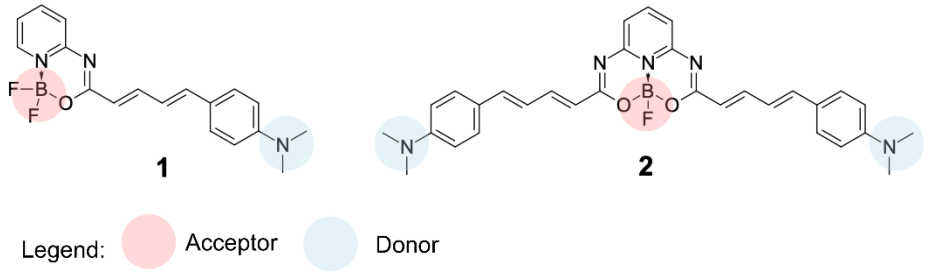

Figure 18. *Structures of studied dye 1 and dye 2 with DA- and DAD architecture, respectively. Blue circles indicates electron donor groups; red circles indicates electron acceptor groups.*

5.1 Research purpose:

To propose a new amyloid marker for 2PFM with improved optical properties, I proposed novel O,N,O-coordinated organofluoroboron-based dye of D–A–D topology (**dye 2**) (IUPAC name - (p-[(1E,3E)-4-[(2Z,7Z)-3-(1E,3E)-4-[p-(Dimethylamino)phenyl]-1,3-butadienyl-5-fluoro-4λ2-fluora-6-oxa2,8,13-triaza-5-borabicyclo[7.3.1]trideca-1(13),2,7,9,11-pentaen-7-yl]-1,3-butadienyl](dimethylamino)benzene)). As it was mentioned in theoretical introduction, 2PFM is a technique, which can be used to monitor formation of amyloid. For this purpose staining probe have to be used to obtain fluorescent signal from amyloid plaques. In terms of potential *in vivo* imaging excitation and emission in biological windows provides collection of a signal from deeper laying structure. Multiparameter optimization of optical properties of a fluorophore, like shifting emission into NIR-I window, enhancing FQY and σ_2, simultaneously with targeting amyloids is a challenging task. Research presents how extension of electronic architecture already described for **dye 1**, with D-A topology, can be used in optical multiparameter optimization for amyloid detection[190-191]. Additionally, I evaluated novel compound 2 in comparison to two-photon standard in amyloid staining, called methoxy-X04 (MeO-X04), derivative of Congo red and Chrysamine-G, which was described in the chapter "Fluorescent probes for Amyloids in 2PFM", structure is presented in Figure 11. MeO-X04 optical properties are far from perfect for *in vivo* measurements. My goal was to focus on proposing a dye with **improved optical properties compared to MeO-X04 upon binding to amyloids and present novel scaffold for potential application in 2PFM.**

5.2 Results:

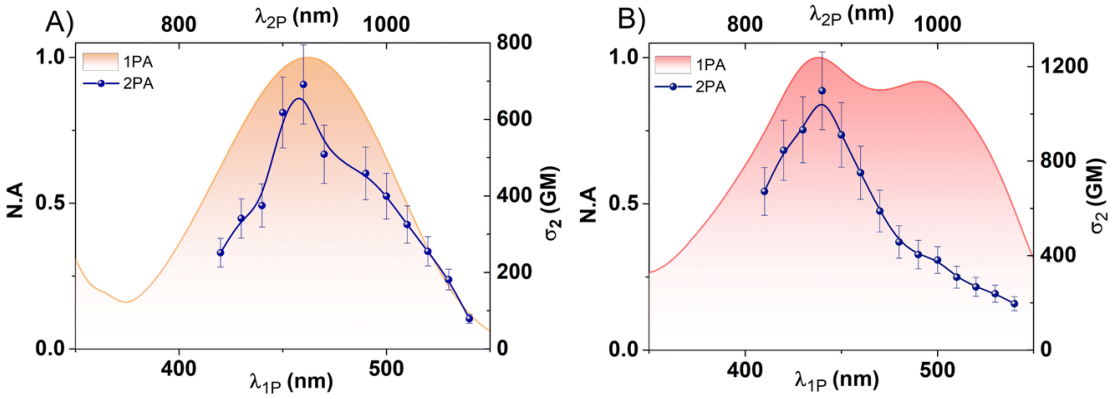

***Figure 19**. Normalized one-photon absorption (N.A) spectra and two-photon absorption spectra expressed in σ_2 (in GM) of dyes **1** (A) and **2** (B). Reproduced from [A. Hajda, E. F. Petrusevich, R. Zaleśny, B. Ośmiałowski and J. Olesiak-Bańska, Chem. Commun., 2025, 61, 3990 DOI: 10.1039/D5CC00243E].*

Organoboron complexes carrying BF/BF2 moieties were synthesized by Prof. Borys Ośmiałowski from University of Mikołaj Kopernik from Toruń. Dyes had dipolar architecture with a strong acceptor of electrons (BF/BF2 groups), combined with electron-donating moieties (N,N-dimethylaniline group ($PhNMe_2$)), architecture appropriate for efficient 2PA with excellent remaining photophysical properties like red-shift of fluorescence emission, increasing FQY. Presented studies were inspired by previous findings by Chen *et al.*[190-191], which studied BF_2-carrying donor–acceptor (D–A) dyes in amyloid-β and tau tangle staining. One of the molecules was selected from his work (**dye 1,** in Figure 18) with dipolar non-centrosymmetric architecture, which is a commonly used architecture for 2P absorbers. The second dye: dye 2 was symmetric twin of dye 1, with two identical terminal groups. Both of the dyes exhibited ICT upon electronic excitation, which provides sensitivity of fluorescence to microenvironment. It is often used in fluorescent probes also for amyloid staining[218-219]. Firstly, one-photon properties like 1PA, 1PEF, FQY, and fluorescence lifetime of both dyes were studied in $CHCl_3$. Extension of electronic architecture of **dye 2** resulted in a red-shift of λ_{EM} compared to **dye 1** (620 nm versus 595nm). FQY also increased from 9.8% for **dye 1** to 22.0% for **dye 2**. Later, 2PA in $CHCl_3$ was evaluated by 2PEL technique. Changed electronic architecture also impacted 2PA of studied molecules. **Dye 1** at 920 nm reached the highest σ_2 values = 700 GM, and the position of the 2PA maximum overlaps with 1PA maximum at corresponding wavelengths – see Figure 19A. **Dye 2** presented two absorption maxima in 1PA,

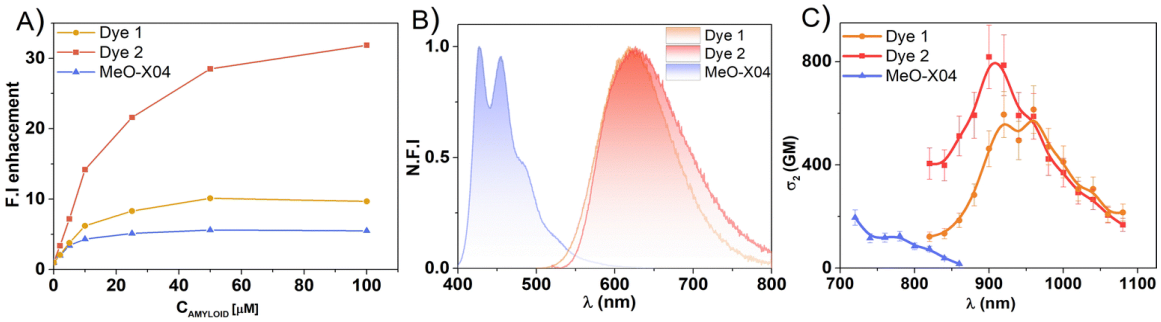

Figure 20. *(A) Increase in fluorescence intensity upon adding bovine insulin amyloids; (B) comparison of normalized 1PEF for all dyes with the same concentration of insulin amyloids. The same solutions were taken for 2PEL measurements; (C) comparison of σ_2 for all dyes in the same concentration. Figure reproduced from [A. Hajda, E. F. Petrusevich, R. Zaleśny, B. Ośmiałowski and J. Olesiak-Bańska, Chem. Commun., 2025, 61, 3990 DOI: 10.1039/D5CC00243E]*

in contrary to **dye 1,** which can be seen in Figure 19. These transitions are also visible in 2PA spectrum at 880 nm and 1020 nm with the σ_2 value 1101 GM and 400 GM, respectively.

Further, I tested dye–amyloid interactions. As previously reported, **dye 1** has been tested as a fluorescent probe for amyloid detection and exhibited distinct responses when interacting with Aβ and tau fibrils[190]. Since one- and two-photon properties of **dye 2** measured in organic solvent were improved – higher FQY, red-shifted emission, higher σ_2 than for **dye 1**, evaluation of **dye 2** as a fluorescent probe for amyloid detection was performed. In addition, **MeO-X04** was used as a reference, as it is a standard fluorescent probe for amyloid staining. I measured photophysical parameters of dyes upon binding to bovine insulin amyloids (1PA, 1PEF, 1PE and σ_2). I confirmed the formation of amyloids by AFM and TEM imaging, which is presented in SI of the article on the page 120. Firstly, fluorescence changes of dyes within increasing amyloid concentration were measured. In Figure 19A comparison of fluorescence intensity enhancement is presented, which was the highest for **dye 2**. Fluorescence spectra of **dye 1** (λ_{EM} at 623 nm) and **dye 2** (λ_{EM} at 627 nm) are significantly bathochromically shifted from the spectrum of MeO-X04, which presents several λ_{EM} below 500 nm (427 nm; 454 nm; 484 nm) – see Figure 19B. Fluorescence in these parts of the electromagnetic spectrum overlaps with regions where tissue absorption, autofluorescence, and scattering are predominant, which was shown to significantly affect performance during imaging procedure of amyloids.[202, 220] **Dye 2** presents the bathochromic shift of λ_{EM} in the solvents with increasing polarity (see Figure S12 in article's SI on page 121). Position of emission peak in the amyloids suggests that the fluorophore is located in a more hydrophobic microenvironment within the amyloid fibrils. FQY of **dye 2** in amyloids (~10%) is significantly higher than in DMSO (0.6%), which supports this hypothesis. Enhancement of observed emission might come also from restricted conformational freedom of -NMe_2 groups at the end of molecule upon binding to amyloids.

Additional experiments for **dye 2** were conducted to evaluate its potential as a probe for amyloid detection. I observed the lack of enhancement of fluorescence emission upon adding insulin monomers, which proves interaction only with amyloid aggregates. Saturation binding assay based on fluorescence was performed to obtain affinity of **dye 2** (K_d) to insulin amyloids,

which had value 229 ± 12 nM. Lastly, selectivity measurements showed the highest fluorescence intensity upon binding to insulin amyloids, as compared to solutions with other bio-molecules – data presented in SI on the page 123. Furthermore, σ_2 for all compounds upon binding to amyloids was evaluated by 2PEL technique. This represents **one of the innovative aspects** of my doctoral thesis: evaluating σ_2 of dyes in solvents as well as bound with amyloids. **Dye 2** had the highest 2PA among all dyes upon binding to amyloids (Figure 19C), which corresponds to trends for **dye 2** in $CHCl_3$. On the other hand, MeO-X04 had the lowest values of σ_2 (~200 GM) and above 860nm excitation of 2PL was not possible (Figure 19A). In summary, MeO-X04 had the lowest values of σ_2 and the shortest window of 2PE. **Dye 2** and **1** had long ranges of 2PE, exceeded even 1000 nm, which corresponds to NIR-II biological window.

5.3 Summary:

Newly presented **dye 2** has optical properties more optimized for amyloid detection than MeO-X04 standard and **dye 1**: it has higher fluorescence enhancement upon binding with amyloids, λ_{EM} above 600 nm and its tail above 700 nm, higher values of σ_2, and broader excitation range, also possibility to be excited in NIR-II biological window. Presented results also confirms **hypothesis 2** "2PA of fluorophores bound to amyloids is different than the one of free molecules and can be modulated based on their chemical and consequently electronic structure". These results fulfil two **goal 1** of the thesis "Prove that new fluorophore scaffold based on BF moiety interact with amyloids and have improved optical properties (red-shifted absorption, emission and values of σ_2), as compared to commercially available standard Methoxy-X04.". Branched electronic architecture of **dye 2** provides a scaffold for further studies and modifications, in order to increase FQY even more, and shift the emission toward NIR region, increase selectivity and biological compatibility for application in bioimaging, like Brain-Blood-Barrier (BBB) entry. In the literature on amyloid probes, it is often the case to present at first the scaffold of a molecule, which can be then optimized in terms of optical and biological properties.[221-222] Additionally, for the first time σ_2 of MeO-X04 upon binding to amyloids was evaluated, which may be impactful for the optimization of excitation wavelength, as the probe is broadly used in bioimaging.

5.4 Research contribution of PhD candidate:

Contribution of PhD candidate

Agata Hajda
Institute of Advanced Materials
Wroclaw University of Science and Technology
ul. Gdańska 7/9
50-344 Wrocław

Author Contribution Statement

I, Agata Hajda hereby declare that in the article: Novel O,N,O-coordinated organofluoroboron probe for amyloid detection: insight from experiment and theory. Chemical Communications. 2025, vol. 61, nr 20, s. 3990-3993, I was responsible for

- Methodology
- Investigation
  - Incubation and characterization of amyloids.
  - Fluorescence od dyes in various solvent.
  - One-photon measurements of dyes with amyloids: absorption, emission, fluorescence lifetime, fluorescence quantum yield, selectivity studies.
  - Two-photon measurements: two-photon excited fluorescence, power dependent studies, two-photon brightness.
- Data analysis
- Writing– orginal draft

Agata Hajda

5.5 Article and supporting information :

ChemComm

COMMUNICATION

View Article Online
View Journal | View Issue

Cite this: Chem. Commun., 2025, 61, 3990

Received 14th January 2025,
Accepted 21st January 2025

DOI: 10.1039/d5cc00243e

rsc.li/chemcomm

A novel *O,N,O*-coordinated organofluoroboron probe for amyloid detection: insight from experiment and theory†

Agata Hajda, [a] Elizaveta F. Petrusevich, [b] Robert Zaleśny, *[a] Borys Ośmiałowski *[c] and Joanna Olesiak-Bańska *[a]

This work presents the results of photophysical studies for a newly synthesized BF-based organoboron dye of D–A–D topology. The one- and two-photon properties of the dye are compared with the D–A parent compound and commercially available amyloid marker: methoxy-X04. We demonstrate that the new dye exhibits better optical properties upon binding to amyloids than methoxy-X04, including emission above 600 nm, higher values of 2PA cross section, broader excitation range and higher increment of emission intensity upon binding to amyloids. All these data demonstrate that the new probe is an interesting scaffold for application in two-photon microscopy and amyloid staining.

Fluorescent probes exhibiting red and near infra-red (NIR) excitation and emission are in high demand due to their potential in bioimaging. The irradiation wavelengths corresponding to biological windows (>700 nm) provide deeper penetration into the sample, improve contrast and safeguard lower phototoxicity.[1,2] A viable route to use irradiation wavelengths matching biological windows is two-photon microscopy (2PM), as this technique relies on the simultaneous absorption of two photons. In the case of degenerate two-photon absorption (2PA) process photon energies are equal so in 2PM the excitation occurs at two times longer wavelengths in comparison to a one-photon absorption process.[3] The design of fluorophores, which might serve as potential novel two-photon probes, is by far a nontrivial process as the tuning of the photophysical properties (fluorescence quantum yield (FQY, Φ), excitation/emission wavelength ($\lambda_{EX}/\lambda_{EM}$), and 2PA cross-section (σ_2)) needs to be addressed in a holistic way (multiparameter optimization). 2PM is a widely used technique in the imaging of complex deep-laying structures, *e.g.*, in the detection of amyloid plaques in the brain.[4–6] The mentioned amyloids are aggregates of misfolded proteins and peptides. Their presence can be associated with various diseases, especially neurodegenerative ones, such as Alzheimer's disease, but also type 2 diabetes. The palette of fluorescent probes for amyloid detection used in 2PM is much more narrow, compared to one-photon microscopy (1PM). Recently, several imaging agents specifically designed for 2PM have been developed, featuring red/NIR emission, appropriate σ_2 values, and high affinity for amyloids.[7,8] There is a piece of evidence[9–12] that probes with improved properties (high FQY and σ_2, λ_{EM} > 600 nm) can provide additional information, compared to the widely used two-photon standard in amyloid staining, such as methoxy-X04 (MeO-X04), in which λ_{EM} is shorter than 550 nm.[12,13] However, progress in the development of two-photon probes for amyloids remains limited compared to one-photon probes, making each proposed 2PM agent a valuable research tool.

A promising platform for the design of two-photon-excited fluorescent probes for 2PM is the one composed of organoboron complexes carrying BF/BF_2 moieties. Since the (bis)fluoroborate group is a strong acceptor of electrons, it can be combined with electron-donating moieties, yielding dipolar (non-centrosymmetric) or quadrupolar (centrosymmetric) dyes suitable for efficient 2PA with excellent remaining photophysical properties.[14] Dyes exhibiting intramolecular charge transfer (ICT) upon electronic excitation that are sensitive to environment or structural changes are natural candidates as fluorescent probes, *e.g.*, for amyloid staining. In this work we rely on the previous findings by Chen *et al.*, demonstrating the usefulness of BF_2-carrying donor–acceptor (D–A) dyes in β-amyloid and tau tangle staining,[15,16] and propose the D–A to D–A–D topology extension (see Fig. 1). In doing so, we aim at the red-shift of the emission wavelength and the enhancement of the interaction with bio-molecules by two *N,N*-dimethylamino (NMe_2) groups, as the interaction *via* an amino moiety was proven to be responsible for binding with amyloid fibrils.[17]

[a] Faculty of Chemistry, Wroclaw University of Science and Technology, Wybrzeże Wyspiańskiego 27, 50-370 Wrocław, Poland. E-mail: robert.zalesny@pwr.edu.pl, joanna.olesiak-banska@pwr.edu.pl
[b] Faculty of Chemistry, University of Gdańsk, Fahrenheit Union of Universities in Gdańsk, Wita Stwosza 63, 80-308 Gdańsk, Poland
[c] Faculty of Chemistry, Nicolaus Copernicus University, Gagarina 7, PL-87100 Toruń, Poland. E-mail: borys.osmialowski@umk.pl

† Electronic supplementary information (ESI) available. See DOI: https://doi.org/10.1039/d5cc00243e

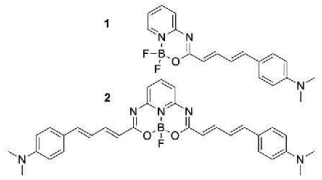

Fig. 1 The structure of molecules studied in the present work.

Table 1 Experimental spectroscopic data for dyes in $CHCl_3$ – extinction coefficient (ε), absorption (λ_{ABS}) and emission (λ_{EM}) wavelength, fluorescence quantum yield (FQY), fluorescence lifetime (τ) and its amplitude (α)

Dye	ε [M^{-1} cm^{-1}]	λ_{ABS} [nm]	λ_{EM} [nm]	FQY [%]	τ [ns]
1	48 000	460.5	595	9.8	0.641[a]
2	47 800	436, 494	620	22.0	0.829

[a] τ_{ave}: τ_1 = 0.055 ns, α = 12.91; τ_2 = 0.728 ns, α = 87.09.

Note that heterocyclic cores in **1** and **2** are substituted with identical terminal moieties ("arms"). We will compare the effectiveness of staining model amyloids obtained from bovine insulin by these two dyes.

Synthesis, experimental and computational details are described in the ESI† (see, *e.g.*, Fig. S1–S5). One-photon properties (1P) like 1PA (Fig. 2), one-photon excited fluorescence (1PEF), FQY, and fluorescence lifetimes (τ) of both dyes in $CHCl_3$ were acquired, which is summarized in Table 1 (for **1** in agreement with previous data[18]) and more detailed data are presented in the ESI.† Spectra of 1PEF in $CHCl_3$, and additionally in DMSO are presented in Fig. S6 in the ESI.† The absorption and the emission spectra of **1** (see Fig. 2A and Fig. S6A, ESI†) present mirror-like images, suggesting a relatively limited geometrical relaxation of the Franck–Condon singlet excited state. However, in the case of **2** (see Fig. 2B and Fig. S6B, ESI†) the mirror-image rule does not hold (similarly to the smaller molecule carrying the same core[18]) because two, close in energy bands in the absorption spectra between 400–600 nm correspond to two electronic states (see below for the analysis of electronic-structure calculations). For 1PA and 1PEF, a bathochromic shift of the broadened bands, caused by the flexibility of π-conjugated arms, was observed for **2** as compared to **1**. This phenomenon is accompanied by an over double increase in FQY (Table 1). Enhancement of FQY is highly beneficial for fluorophores with red-shifted emission. According to the energy-gap rule, the emission efficiency drops down as the energy between the ground and excited state decreases, which means that the far-red emitting dyes are usually much less efficient in comparison with their counterparts showing emission in the blue part of the spectrum. The radiative (k_r) rate constant for **2** (2.65×10^8 s^{-1}) is higher than that for **1** (1.53×10^8 s^{-1}); conversely, the non-radiative (k_{nr}) rate constant for **1** (1.41×10^9 s^{-1}) is larger than that for **2** (9.41×10^8 s^{-1}), which can be linked with the topologies of BF/BF_2-carrying cores (compare ref. 18). We measured the 2PA spectra using the two-photon excited fluorescence (2PEF) method, and we further supported these measurements by electronic-structure calculations. The palette of simulated properties (*vide infra*) encompasses excitation energies, oscillator strengths, Ciofini's charge transfer diagnostics, electronic density difference plots and two-photon transition strengths (see the ESI,† Fig. S20–S24 and Tables S2, S3). The non-linear nature of the observed processes was determined based on the quadratic dependence of photoluminescence intensity on the incident laser power confirming two-photon absorption (Fig. S7C and D, ESI†). For dye **1**, the 2PA band matches the 1PA band (Fig. 2A). The peak values of σ_2 for **1** at 920 nm reach 700 GM and the band maxima are red-shifted compared to the results of the simulations (Table 2), which comes as no surprise given the predictive power of the employed coupled-cluster model. The results of electronic-structure calculations demonstrate higher values of σ_2 for $S_0 \rightarrow S_1$, than for $S_0 \rightarrow S_2$, which comes from the larger difference in dipole moment between the excited and the ground state. It should be noted that the calculated 2PA cross section for the $S_0 \rightarrow S_1$ transition satisfactorily matches the value measured experimentally (Fig. 2A). Note that the estimation of 2PA experimentally in the regime of higher energy transition ($S_0 \rightarrow S_2$) was unsuccessful, due to the emission wavelength overlapping with the excitation wavelength. Molecule **2** presents two absorption maxima in 1PA, which is also visible in the 2PA spectrum (Fig. 2B). However, the σ_2 value at 880 nm with 1101 GM is much more prominent than the value of σ_2 equal to 400 GM at 1020 nm. The results of calculations demonstrate that the σ_2 value for $S_0 \rightarrow S_2$ is roughly 20 times larger than that calculated for $S_0 \rightarrow S_1$. Note that due to close proximity of the absorption bands, the experiment-theory comparison of σ_2 for $S_0 \rightarrow S_1$ is difficult as both transitions contribute to the 2PA cross section value at

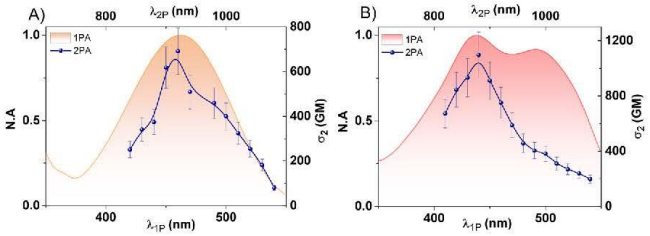

Fig. 2 Normalized one-photon absorption spectra and two-photon absorption spectra (in GM) of molecules **1** (A) and **2** (B).

Table 2 Spectroscopic properties (one-photon excitation energy (ΔE) and wavelength (λ), dipole moment (μ), two-photon transition strength (δ^{2PA})) and two-photon absorption cross section (σ_2) calculated at the RI-CC2/def2-TZVP/EE level of theory for **1** and **2** in $CHCl_3$

	Transition	ΔE [eV]	λ [nm]	f	$\Delta\mu$ [D]	$\mu(S_n)$ [D]	δ^{2PA} [a.u.]	σ_2 [GM]
1	$S_0 \rightarrow S_1$	3.00	414	1.85	14.1	23.6	188×10^3	494
	$S_0 \rightarrow S_2$	4.04	307	0.04	4.8	14.3	37×10^3	176
2	$S_0 \rightarrow S_1$	2.84	437	3.04	3.8	8.8	32×10^3	75
	$S_0 \rightarrow S_2$	3.17	392	0.40	4.2	9.2	492×10^3	1442

1020 nm (*cf.* Fig. 2B and Table 2). Comparing both dyes, one finds that maximal two-photon absorption action cross-section $\sigma_{2,eff}$ ($\sigma_2 \times \Phi$) is higher for **2**, which implies greater potential in imaging applications. A closer look at two-photon excitation above 1000 nm shows $\sigma_{2,eff} > 50$ GM, which is still an effective value for application of **2** as a fluorescent probe in the NIR-II window.[19]

In order to further understand the two-photon activity of **1** and **2** we performed the analysis based on the generalized few-state model for theories with a non-Hermitian structure.[20] The summary of these calculations is shown in Fig. 3, which presents the two-photon transition strengths (δ^{2PA}) computed by response theory as well as based on two- and three-state models. Note that δ^{2PA} is a purely molecular parameter and it is proportional to σ_2 (see eqn (S3) in the ESI†). In more detail, we aimed at explaining the differences in two-photon absorption activity between **1** ($S_0 \rightarrow S_1$) and **2** ($S_0 \rightarrow S_2$). In the case of **1**, the two-state model yields the values of two-photon $S_0 \rightarrow S_1$ transition strengths similar to that from response theory calculations and the extension to the three-state model (by including S_2 state as the intermediate) leads to insignificant improvement. In other words, the parameters of the ground and final state (energy difference, transition strength and dipole moment difference) determine the two-photon $S_0 \rightarrow S_1$ activity of molecule **1**. On the other hand, the same is not true for two-photon $S_0 \rightarrow S_2$ transition for **2**, *i.e.*, the two-state model (including ground and the final state S_2) fails to reproduce the two-photon $S_0 \rightarrow S_2$ transition strength. It is necessary to go beyond the two-state model to reproduce the response theory value. The three-state model that yields satisfactory agreement with response theory includes the ground, final (S_2) and intermediate state (S_1). One may thus conclude that the differences in two-photon absorption activity between **1** ($S_0 \rightarrow S_1$) and **2** ($S_0 \rightarrow S_2$) are due to very different physical mechanisms and the latter property depends on the coupling between S_1 and S_2 states.

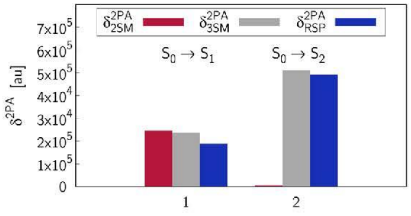

Fig. 3 Two-photon transition strengths predicted by response theory (RSP), and the two- (2SM) and three-state model (3SM) for **1** and **2**.

Dye **1** was previously evaluated as a fluorescent probe for amyloid staining and showed various responses upon binding to Aβ and tau amyloids.[15] Therefore, studying interaction with amyloids for dye **2** seems well justified, especially since it has λ_{EM} shifted towards the red part of the spectrum and high $\sigma_{2,eff}$ in the NIR-I (700–950 nm) and NIR-II (>1000 nm) biological windows. Here, we compared the optical properties of dye **1**, dye **2** and MeO-X04 – a fluorescent standard commonly used for amyloid staining in 2PM[13,21,22] – upon binding to bovine insulin amyloids. Insulin serves as a good model system since it forms uniform fibrils, which was confirmed by atomic force microscopy (AFM) and transmission electron microscopy (TEM) analysis (see Fig. S9 and S10, ESI†). Photophysical parameters of MeO-X04 upon binding to amyloids like 1PA, 1PEF, 1PE (one-photon excitation) and σ_2 are rarely discussed in the literature.[12] Our experiments can also shed light on the 1P and 2P properties of this probe. For all considered molecules (dye **1**, dye **2** and MeO-X04), fluorescence was measured as a function of increasing amyloid concentration (Fig. S11 in ESI†). The highest fluorescence enhancement was observed for dye **2**, while the lowest one for MeO-X04, which is presented in Fig. 4A. λ_{EM} with amyloids of dye **1** (623 nm) and dye **2** (627 nm) are significantly bathochromically shifted from the spectra of MeO-X04, which presents several maxima due to the vibrational fine structure (427 nm; 454 nm; 484 nm) of Fig. 4B. The emission between 400–500 nm falls into ranges where autofluorescence, absorption and scattering of tissues dominates, which can significantly influence its performance, which was proven during *in vivo* imaging analysis.[11,23] It is worth pointing

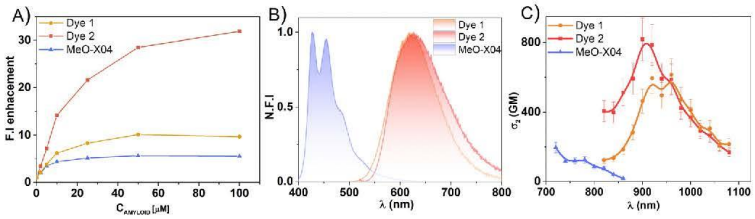

Fig. 4 (A) Increase in fluorescence maximum upon adding bovine insulin amyloids; all dyes had 0.5 μM, and the solvent was 5% DMSO. Point "zero" was the dye in 5% DMSO without amyloids; (B) comparison of normalized 1PEF for all dyes (1 μM) with 50 μM of bovine insulin amyloids. The same solutions were taken for 2PEF measurements; (C) comparison of σ_2 with 50 μM of amyloids.

out that dye **2** has even more prominent emission above 700 nm than dye **1**, which can be seen in Fig. 4B. The bathochromic shift in λ_{EM} of the dye **2** observed in solvents with increasing polarity (see Fig. S12 in ESI†) suggests that the molecule is located in the more hydrophobic regions of the amyloid fibrils. It is also supported by the value of FQY in amyloids (10%), which is much higher than in polar DMSO (0.6%) – see Table S1 in the ESI.† Additionally, dye **2** is substituted by NMe_2 groups at both arms and it contains single C–C bonds that can easily rotate or kink leading to non-radiative energy dissipation. Upon binding to amyloids, NMe_2 groups can have restricted conformational freedom, which is observed as fluorescence enhancement. We can observe a significant difference in 1PE upon increasing the amyloid concentration for dye **2** (see Fig. S13 in the ESI†). 1PE changes the shape of the spectrum; the band around 450 nm starts to vanish, and a new band around 550 nm starts to appear. No changes in 1PE were observed for dye **1**. In addition, we measured 1PE for MeO-X04, which is presented in Fig. S13C in the ESI.† Additional experiments for dye **2** were conducted due to its novelty. Lack of observed changes in emission between the solution of **2** and upon mixing with insulin monomers, proves interaction with fibrils and not with the native peptide (Fig. S14, ESI†). The affinity of dye **2** (K_d) to insulin amyloids was measured by saturation binding assay. The K_d value was determined to be 229 ± 12 nM (Fig. S15, ESI†). Furthermore, selectivity measurements of dye **2** show the highest fluorescence intensity upon binding to insulin amyloids (Fig. S16, ESI†) compared to other bio-molecules.

The evaluation of the 1P properties was followed by studies of σ_2 upon binding to amyloids. We confirmed the two-photon nature of the observed process (see Fig. S17C and D, ESI†). No alteration in λ_{EM} was observed upon two-photon excitation (2PE) compared to 1PE for dye **1** and dye **2** (Fig. S18, ESI†) indicating relaxation from the same energy state. Evaluation of σ_2 revealed that dye **2** upon binding has the highest 2PA among all dyes (Fig. 4C), which is in line with the trend in $CHCl_3$. The lowest values of 2PA are found for MeO-X04, and these were measured within the 720–860 nm range (Fig. 4C). At longer wavelengths of 2PE, no emission was detected in the used experimental conditions. On the other hand, 2PE for dye **1** and dye **2** have a much broader range overlapping with both the NIR-I and NIR-II biological window, which is beneficial from an application point of view. The detailed comparison of 1PA and 2PA upon binding is presented in the ESI† (Fig. S19).

To sum up, newly synthesized dye **2** has better optical properties upon binding to amyloids than MeO-X04, including emission spectra above 600 nm, higher values of 2PA cross section, and broader excitation range in both the NIR-I and NIR-II biological window. We also proved that the branched architecture (D–A–D) has higher σ_2 upon binding to amyloids, compared to their unsymmetrical parent compound (D–A). The newly synthesized compound **2** also exhibits a higher increment of emission intensity upon binding to amyloids. All these data demonstrate that the new probe is an interesting scaffold for further development for applications in 2PM and amyloid detection.

B. O. and R. Z. thank the National Science Centre (Poland) for financial support (grant no. 2019/35/B/ST5/00656). The computational resources were provided by Wroclaw Centre for Networking and Supercomputing. The authors acknowledge the resources provided by the Electron Microscopy Laboratory at WUST and the help from MSc Olga Kaczmarczyk who performed amyloid imaging using TEM.

Data availability

The data supporting this article have been included as part of the ESI.†

Conflicts of interest

There are no conflicts of interest.

Notes and references

1 G. Hong, A. L. Antaris and H. Dai, *Nat. Biomed. Eng.*, 2017, **1**, 0010.
2 R. Weissleder, *Nat. Biotechnol.*, 2001, **19**, 316–317.
3 A. M. Larson, *Nat. Photon.*, 2011, **5**, 1.
4 S. Burgold, S. Filser, M. M. Dorostkar, B. Schmidt and J. Herms, *Acta Neuropathol. Commun.*, 2014, **2**, 30.
5 P. d'Errico, S. Ziegler-Waldkirch, V. Aires, P. Hoffmann, C. Mezö, D. Erny, L. S. Monasor, S. Liebscher, V. M. Ravi, K. Joseph, O. Schnell, K. Kierdorf, O. Staszewski, S. Tahirovic, M. Prinz and M. Meyer-Luehmann, *Nat. Neurosci.*, 2022, **25**, 20–25.
6 S. Burgold, T. Bittner, M. M. Dorostkar, D. Kieser, M. Fuhrmann, G. Mitteregger, H. Kretzschmar, B. Schmidt and J. Herms, *Acta Neuropathol.*, 2011, **121**, 327–335.
7 L. Li, Z. Lv, Z. Man, Z. Xu, Y. Wei, H. Geng and H. Fu, *Chem. Sci.*, 2021, **12**, 3308–3313.
8 M. Chen, Z. Zhang, Z. Shi, J. Sun and F. Gao, *Cell Rep. Phys. Sci.*, 2024, **5**, 101810.
9 D. Kim, H. Moon, S. H. Baik, S. Singha, Y. W. Jun, T. Wang, K. H. Kim, B. S. Park, J. Jung, I. Mook-Jung and K. H. Ahn, *J. Am. Chem. Soc.*, 2015, **137**, 6781–6789.
10 J.-W. Choi, Y. H. Ju, Y. Choi, S. J. Hyeon, C. G. Gadhe, J.-H. Park, M. S. Kim, S. Baek, Y. Kim, K. D. Park, A. N. Pae, H. Ryu, C. J. Lee and B. R. Cho, *ACS Chem. Neurosci.*, 2020, **11**, 1801–1810.
11 C. Chen, Z. Liang, B. Zhou, X. Li, C. Lui, N. Y. Ip and J. Y. Qu, *ACS Chem. Neurosci.*, 2018, **9**, 3128–3136.
12 C. H. Heo, K. H. Kim, H. J. Kim, S. H. Baik, H. Song, Y. S. Kim, J. Lee, I. Mook-jung and H. M. Kim, *Chem. Commun.*, 2013, **49**, 1303–1305.
13 W. E. Klunk, B. J. Bacskai, C. A. Mathis, S. T. Kajdasz, M. E. McLellan, M. P. Frosch, M. L. Debnath, D. P. Holt, Y. Wang and B. T. Hyman, *J. Neuropathol. Exp. Neurol.*, 2002, **61**, 797–805.
14 M. Pawlicki, H. Collins, R. Denning and H. Anderson, *Angew. Chem., Int. Ed.*, 2009, **48**, 3244–3266.
15 Y. Chen, Q. Ouyang, Y. Li, Q. Zeng, B. Dai, Y. Liang, B. Chen, H. Tan and M. Cui, *Eur. J. Med. Chem.*, 2022, **227**, 113968.
16 Y. Chen, C. Yuan, T. Xie, Y. Li, B. Dai, K. Zhou, Y. Liang, J. Dai, H. Tan and M. Cui, *Chem. Commun.*, 2020, **56**, 7269–7272.
17 K. J. Robbins, G. Liu, G. Lin and N. D. Lazo, *J. Phys. Chem. Lett.*, 2011, **2**, 735–740.
18 A. M. Grabarz, A. D. Laurent, B. Jędrzejewska, A. Zakrzewska, D. Jacquemin and B. Ośmiałowski, *J. Org. Chem.*, 2016, **81**, 2280–2292.
19 H. M. Kim and B. R. Cho, *Chem. Rev.*, 2015, **115**, 5014–5055.
20 M. T. P. Beerepoot, M. M. Alam, J. Bednarska, W. Bartkowiak, K. Ruud and R. Zaleśny, *J. Chem. Theory Comput.*, 2018, **14**, 3677–3685.
21 D. S. Whittaker, L. Akhmetova, D. Carlin, H. Romero, D. K. Welsh, C. S. Colwell and P. Desplats, *Cell Metab.*, 2023, **35**, 1704–1721.
22 M. Meyer-Luehmann, T. L. Spires-Jones, C. Prada, M. Garcia-Alloza, A. de Calignon, A. Rozkalne, J. Koenigsknecht-Talboo, D. M. Holtzman, B. J. Bacskai and B. T. Hyman, *Nature*, 2008, **451**, 720–724.
23 J. Shin, P. Verwilst, H. Choi, S. Kang, J. Han, N. H. Kim, J. G. Choi, M. S. Oh, J. S. Hwang, D. Kim, I. Mook-Jung and J. S. Kim, *Angew. Chem., Int. Ed.*, 2019, **58**, 5648–5652.

Supplementary Information (SI) for Chemical Communications.

Novel O,N,O-coordinated organofluoroboron probe for amyloid detection: Insight from experiment and theory

SUPPORTING INFORMATION

Agata Hajda,[a] Elizaveta F. Petrusevich,[a] Robert Zaleśny,[*,a] Borys Ośmiałowski,[*,b] Joanna Olesiak-Bańska,[*,a]

[a] *Faculty of Chemistry, Wroclaw University of Science and Technology, Wybrzeże Wyspiańskiego 27, 50-370 Wrocław, Poland*
[b] *Faculty of Chemistry, University of Gdańsk, Fahrenheit Union of Universities in Gdańsk, Wita Stwosza 63, 80-308 Gdańsk, Poland*
[c] *Faculty of Chemistry, Nicolaus Copernicus University, Gagarina 7, PL-87100 Toruń, Poland*
[*]*E-mail: robert.zalesny@pwr.edu.pl (R.Z.), borys.osmialowski@umk.pl (B.O.), joanna.olesiak-banska@pwr.edu.pl (J.O.-B.)*

The ester, namely ethyl (2E,4E)-5-(4-(dimethylamino)phenyl)penta-2,4-dienoate, introducing two double bonds and 1,4-phenylene as a conjugated spacer between donor and acceptor was obtained as described elsewhere.[1] The synthesis of amide and dye **2** was guided as described in previous publication by some of authors of the current manuscript.[2] The NMR spectra were recorded in DMSO-d_6 for amide used in the synthesis of **2** or $CDCl_3$, for **2**, as solvents. The dye **1** was previously described elsewhere.[3]

Amide (N-(6-(1E,3E)-4-[p-(Dimethylamino)phenyl]-1,3-butadienylcarbonylamino-2-pyridyl)-(2E,4E)-5-[p-(dimethylamino)phenyl]-2,4-pentadienamide):

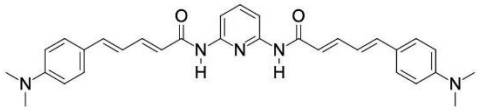

^{1}H (400 MHz, DMSO-d_6, TMS), 10.15 (s, 2H), 7.88 (d, 2H, J=7.98 Hz), 7.75 (m, 1H), 7.43 (d, 4H, J=8.9 Hz), 7.38 (dd, 2H, overlapped), 6.95 (d, 2H, J=15.4 Hz), 6.83 (dd, 2H, J=15.4, 10.9 Hz), 6.71 (d, 4H, J=8.9 Hz), 6.45 (d, 2H, J=14.9 Hz), 2.96 (s, 12H). ^{13}C (100 MHz, DMSO-d_6, TMS) 165.2, 151.2, 143.2, 141.1, 140.2, 130.9, 129.0, 124.3, 122.2, 122.1, 112.5, 112.4, 109.6, 40.25 (overlapped with solvent). HRMS 506.2558, cal. ($C_{31}H_{32}N_5O_2$) 506.2556.

Dye **2** (p-[(1E,3E)-4-[(2Z,7Z)-3-(1E,3E)-4-[p-(Dimethylamino)phenyl]-1,3-butadienyl-5-fluoro-4λ2-fluora-6-oxa-2,8,13-triaza-5-borabicyclo[7.3.1]trideca-1(13),2,7,9,11-pentaen-7-yl]-1,3-butadienyl](dimethylamino)benzene):

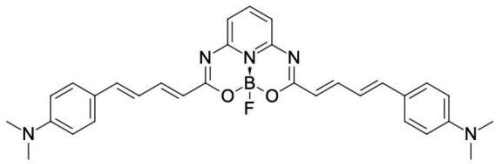

^{1}H (400 MHz, $CDCl_3$, TMS), 7.92 (t, 1H, J=8.2 Hz), 7.80 (dd, 2H, J= 14.9, 11.1 Hz), 7.44 (d, 4H, J = 8.9 Hz), 7.09 (d, 2H, J=8.0 Hz), 6.98 (d, 2H, J=15.2 Hz), 6.86 (dd, 2H, J=15.2, 11.1 Hz), 6.75 (broadened d, 4H, J=8.5 Hz), 6.26 (d, 2H, J=14.9 Hz), 3.06 (s, 12H). ^{11}B 0.53 (d, J=33 Hz). ^{13}C (150 MHz, $CDCl_3$, TMS), 166.1, 151.1, 150.4, 146.1, 144.3, 142.0, 129.0, 124.3, 122.5, 122.0, 115.8, 112.1, 40.2. HRMS 536.2646, cal. ($C_{31}H_{32}BN_5O_2F$) 536.2633.

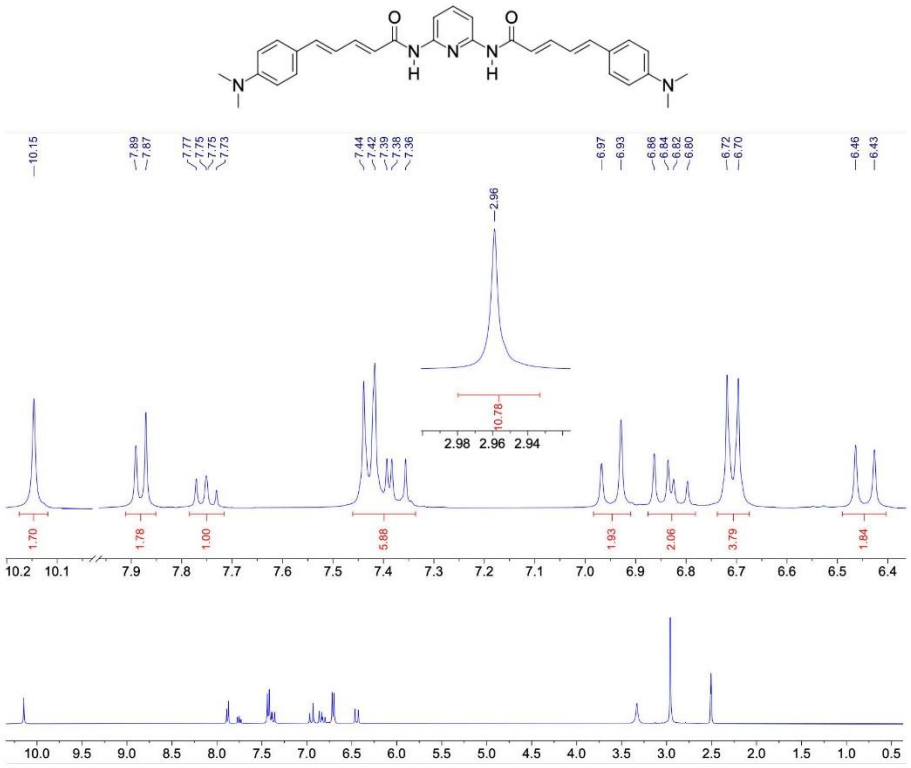

Figure S1: ^{1}H NMR spectrum (in DMSO-d_6) of amide used in the synthesis of **2**

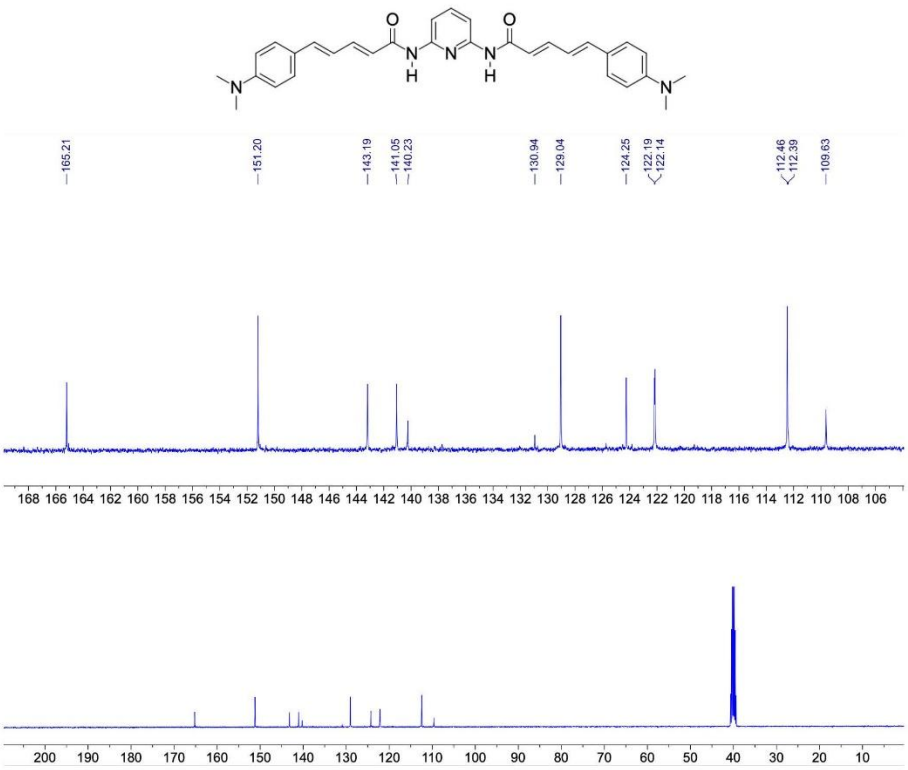

Figure S2: ^{13}C NMR spectrum (DMSO-d_6) of amide used in the synthesis of **2**

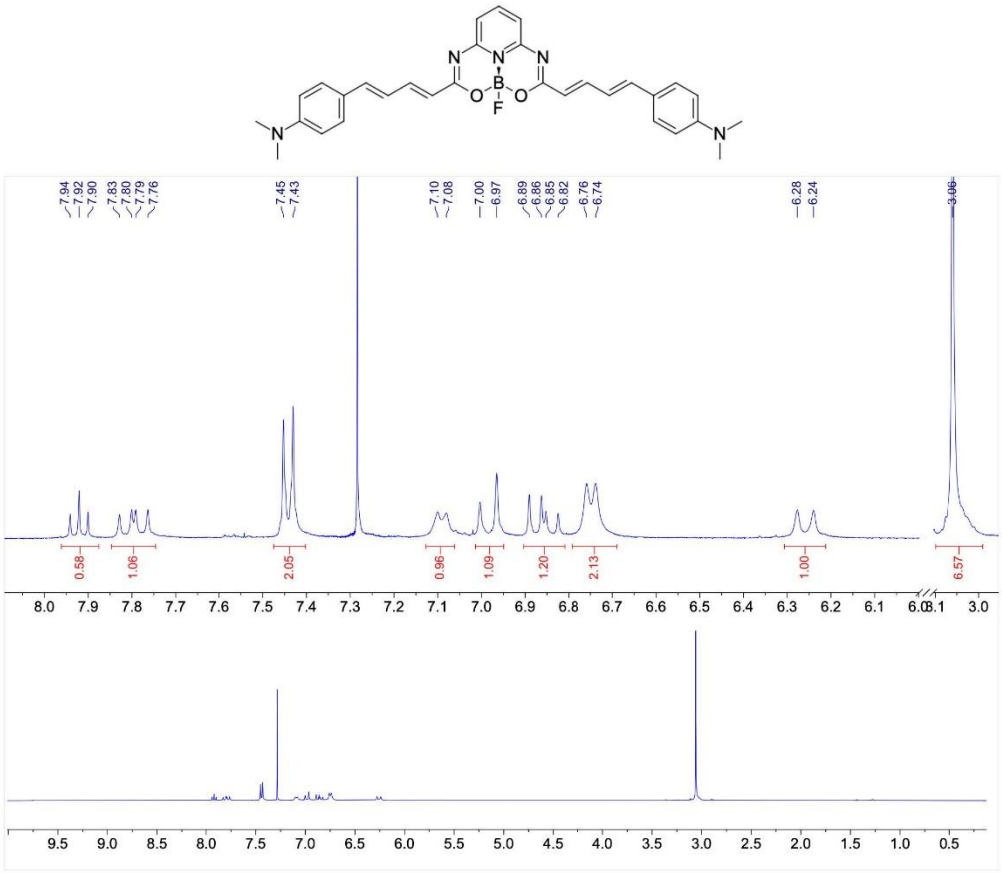

Figure S3: ^{1}H NMR spectrum (in $CDCl_3$) of **2**

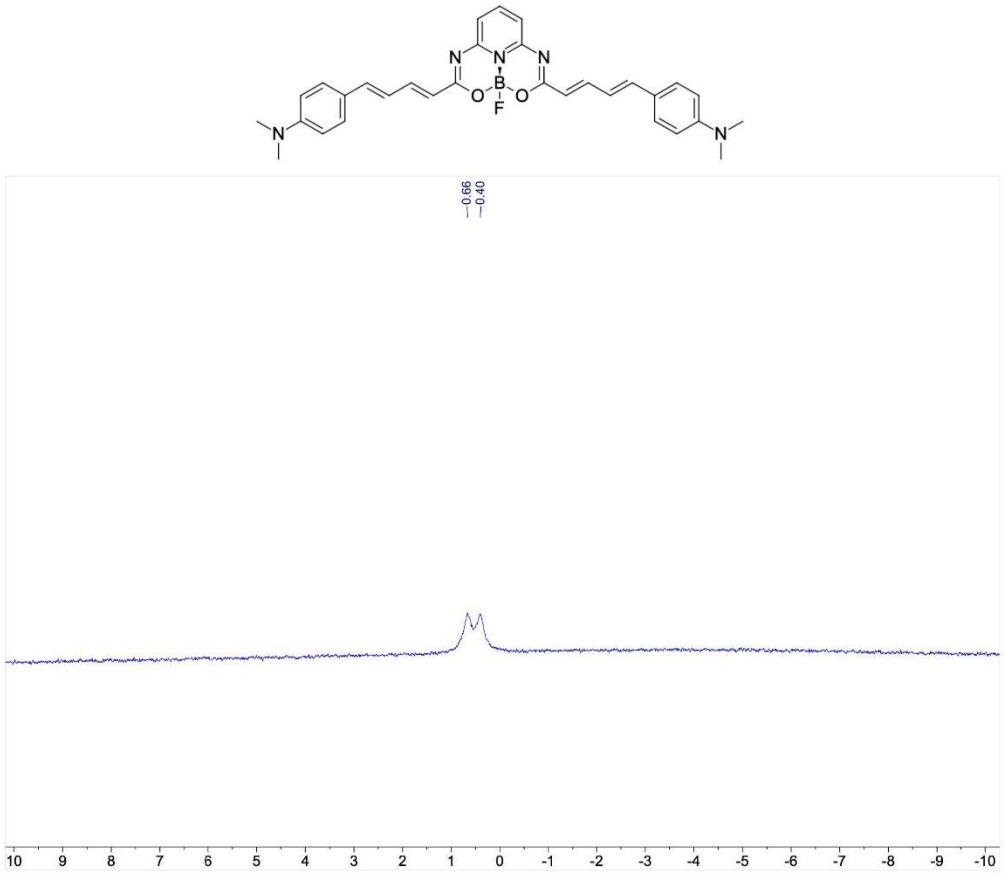

Figure S4: ^{11}B NMR spectrum (in $CDCl_3$) of **2**

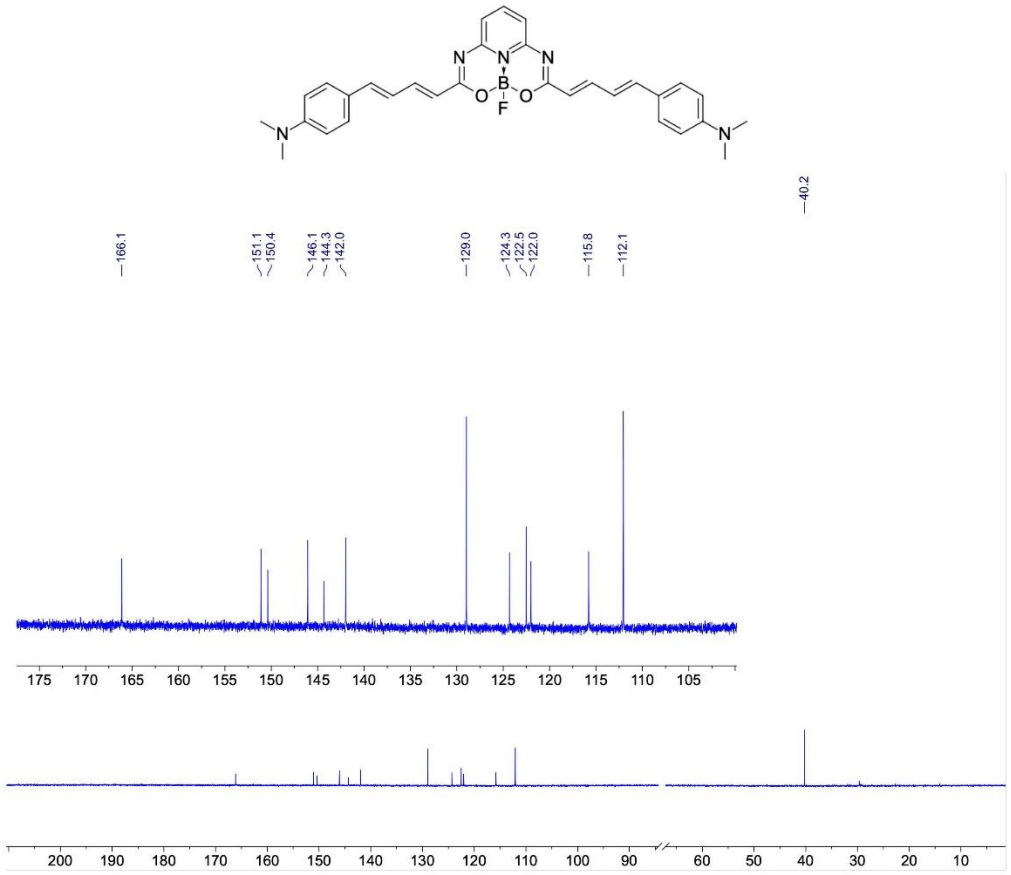

Figure S5: ^{13}C NMR spectrum (in $CDCl_3$) of **2**

One-photon measurements
Absorption spectra were recorded using a Jasco V-670 spectrophotometer, while excitation and fluorescence spectra using an FS5 Spectrofluorometer (Edinburgh Instruments) equipped with a Xenon lamp. Fluorescence lifetimes were measured using time-correlated single-photon counting technique using the same FS5 spectrometer. Samples were excited at 510 nm using a laser diode, while fluorescence decays were fitter using FAST software (Edinburgh Instruments). Chloroform for one-photon measurements was spectral grade.

Two-photon measurements
Two-photon excited photoluminescence (2PEL) was measured using a custom-built multiphoton setup. The excitation source was femtosecond mode-locked Ti:Sapphire laser (100 fs, 80 MHz, Chameleon, Coherent Inc.) with a wavelength range 680 to 1080 nm. The emission spectra were measured with a spectrograph - Shamrock 303i (Andor) with an iDUS camera (Andor). Optical filters were also used: FELH0800 - ϕ 25.0 mm Longpass Filter (Thorlabs). Stability of laser power was checked for all experimental time by power-meter (Thorlabs). The sample and reference dye were always measured at the same excitation power. 2PA cross-sections were calculated with the following equation:

$$\sigma_{2,s} = \frac{F_{2,s} C_r \phi_r n_r^2}{F_{2,r} C_s \phi_s n_s^2} \sigma_{2,r} \tag{1}$$

where r and s denote reference and sample, respectively. ϕ_r and ϕ_s is the fluorescence quantum yield. $F_{2,s}$ and $F_{2,r}$ is the integrated two-photon fluorescence intensity at a particular excitation wavelength, n is the refractive index of the solvent. C_s and C_r is the concentration of the sample and reference, respectively. LDS-698 in $CHCl_3$ was used as a reference. 2PA cross-sections of LDS-698 was obtained from previous reports.[4] FQY of LDS-698 in $CHCl_3$ was taken from Ref. 5.

Power dependence of photolumiescence intensity
To confirm the two-photon nature of the observed photoluminescence excited by laser pulses, we measured photoluminescence intensity vs incident laser excitation power and determined the power exponent, n. 2PEL was collected. For each power two spectra were collected to observed if photobleaching does not occur upon increasing laser power. The power exponent was calculated using the equation:

$$n = \frac{\log(\text{PL intensity})}{\log(\text{P})} \tag{2}$$

where PL intensity is a 2PE photoluminescence intensity and P is the average incident laser power.

Incubation of bovine insulin amyloids
Bovine insulin was purchased from Sigma-Aldrich (I5500) and dissolved in HCl solution (pH $\sim$1.5), yielding the final concentration of 2 mg/mL. The samples were incubated in an Eppendorf ThermoMixer C for 48h at 45 °C, with agitation set to 500 rpm.

Characterization of amyloids on Atomic Force Microscope (AFM)
The full procedure is described elsewhere.[6] In brief, samples were 100x diluted from stock solution (2 mg/ml). The droplets of the samples were deposited on a mica layer, rinsed with Milli-Q water after 5 min, and dried. Measurements were conducted using a Veeco Dimension V AFM in tapping mode with the SuperSharpSilicon probe mounted (Manufacturer: NANOSENSORS). Analysis of height was done in Nanoscope software for over 50 fibrils. Histogram with distibution was plotted in program OriginPro 9.0.

Characterization of amyloids on Transmission Electron Microscopy (TEM)
The solution from same sample was used as for AFM imaging to provide reliable results. 2 μL solution was placed on clean standard TEM carbon on plasma cleaned copper grids (Agar Scientific) fo 30 seconds and stained with 2 μL of uranyl acetate for additional 30 seconds. The samples were studied using Talos F200i transmission electron microscope (Thermofisher Scientific) at 200 kV accelerating voltage. Analysis of sizes was done in imageJ program fo over 50 fibrils. Histogram with distibution was plotted in program OriginPro 9.0.

Preparation of dye and amyloid samples for optical measurements (one- and two-photon)
One-photon absorption spectra were measured with a Jasco V-670 spectrophotometer in quartz cuvettes within the range of 280–700 nm. Stock solutions of dyes were prepared by dissolution in DMSO (500 μM for dye **1** and **2**; 200 μM for MeOX-4), and all solutions were prepared before use. Then, the appropriate volume of the stock solution was withdrawn and diluted so the volume of DMSO was 5% in final volume. Then appropriate amount of amyloids solution were added.

Fluorescence quantum yield of dyes
The FQY was measured by using the SC-30 Integrating Sphere Module for an FS5 spectrofluorometer from Edinburgh Instruments. **For dyes with amyloids:** The concentration of dyes was set to obtain a high signal on a two-photon microscope, as the FQY is used to calculate the 2PA cross section. The final concentration of dyes was 1 μM, and amyloid 50 μM in 5% of DMSO. Reference solution for integrating sphere was 50 μM of amyloids in 5% DMSO, to provide the same scattering.

Selectivity studies
Measurements of fluorescence changes of dye **2** (1 μM) upon binding to bioanalytes (100 μM) were measured on a clarioSTAR Plus plate reader in a 96-well black plate. Fluorescence spectra were measured 30 min after the incubation of dyes with biomolecules at 37^{o} C. To compare changes before and after binding, the fluorescence intensity (F.I) at maximum wavelength before and after binding in the same solvent were divided by each other (FI after binding / FI dye alone).

Saturation binding assay
To a solution of dye **2** the solution of insulin amyloids was added and incubated for 30 min at 37 °C. The binding solutions were measured in quartz cuvette on FS5 Spectrofluorometer (Edinburgh Instruments). For each concentration was tested in triplicate. Mean value with standard deviation was calculated and Michaelis-Menten curve was fitted in OrginPro 9.0.

Table S1: FQY of dye **2** in solvents and bovine amyloid solution (50 µM).

solvent	FQY [%]
$CHCl_3$	22
DMSO	0.6
Amyloids	10

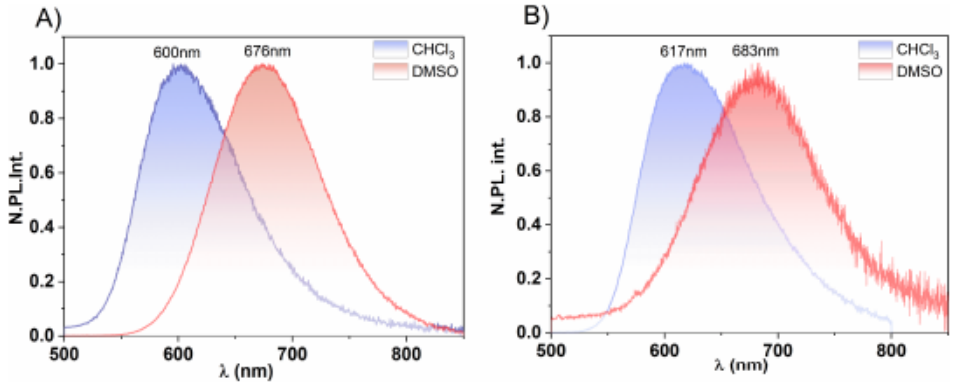

Figure S6: Normalized photoluminescence intensity (N. PL.Int.) in DMSO and $CHCl_3$ (A) dye **1** (B) dye **2**.

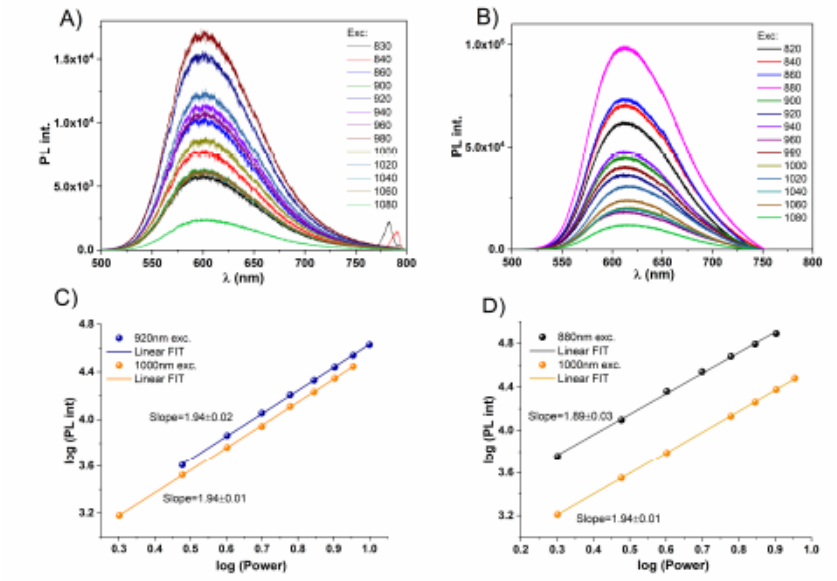

Figure S7: Two-photon excited luminescence in $CHCl_3$ of (A) dye **1** (B) dye **2**. Plots C i D shows photoluminescence intensity (PL int.) dependence on laser power for (C) dye **1** (D) dye **2**.

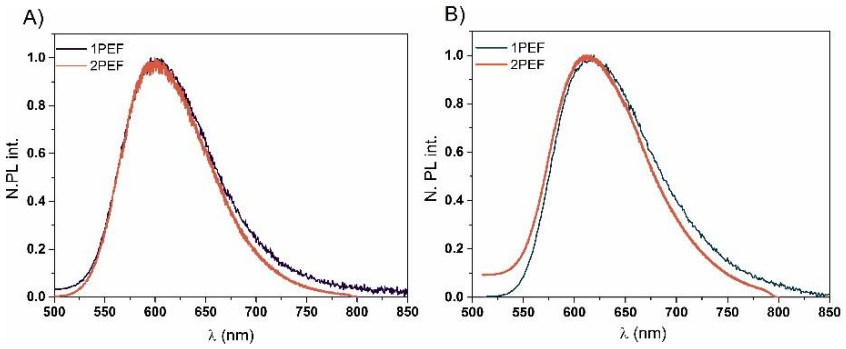

Figure S8: Normalized photoluminescence intensity (N. PL.Int.). Comparison of one-photon excited fluorescence (1PEF) vs two-photon excited fluorescence (2PEF) (A) dye **1** (B) dye **2**.

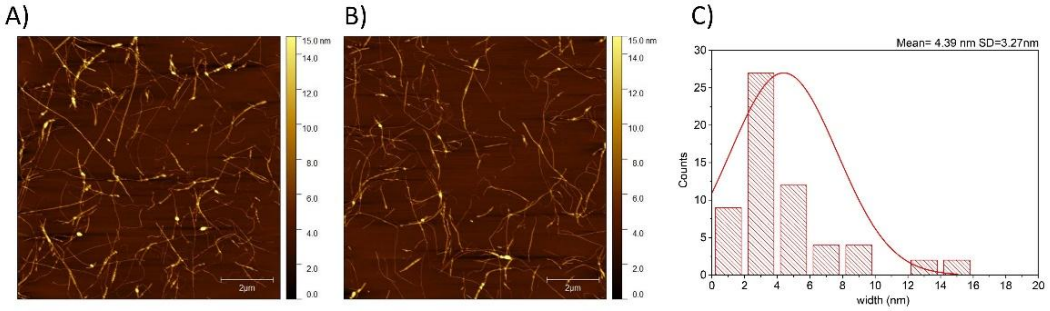

Figure S9: Atomic Forme Microscope (AFM) images of bovine insulin amyloids (A) size of scan 10x10 µm (B) size of scan 10x10 µm (C) Histogram with normal distribution of height with mean and standard deviation.

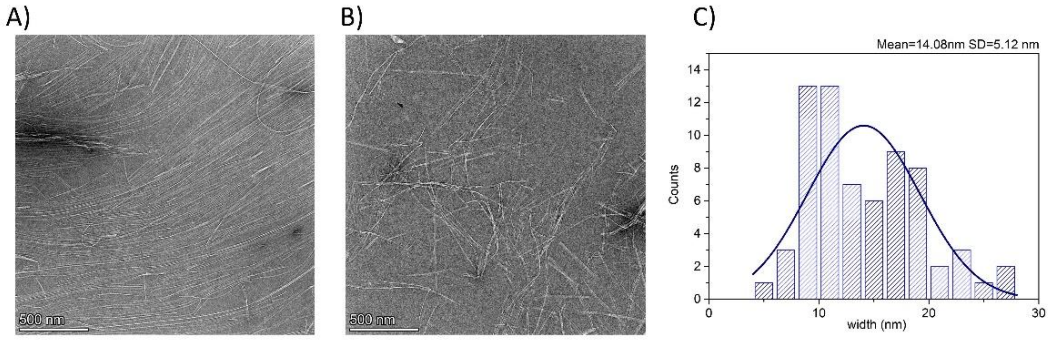

Figure S10: A) and B) TEM images of bovine insulin amyloids on two different places on grid, scale 500nm for both images; C) Histogram with normal distribution of width with mean and standard deviation.

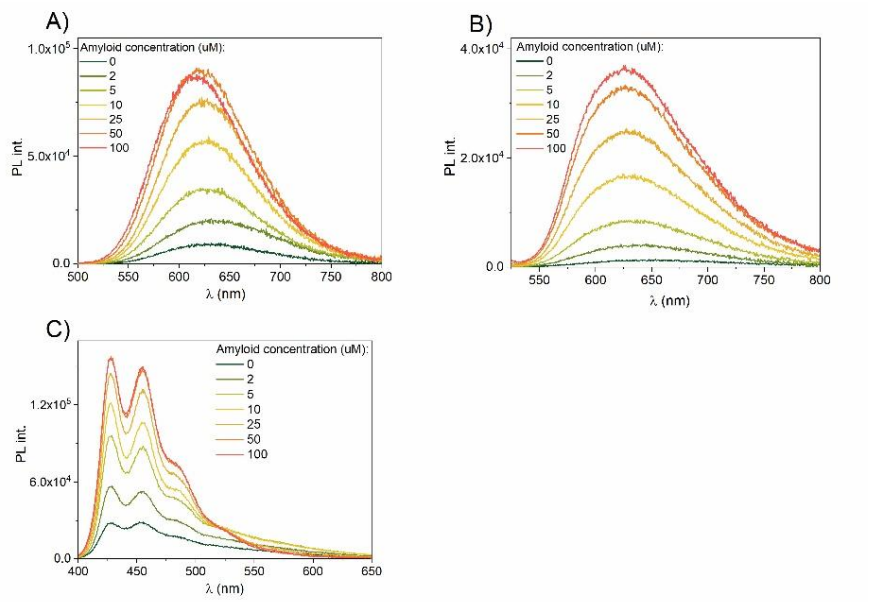

Figure S11: Spectrum of one-photon excited emission in increasing bovine insulin amyloid concentration. All solutions were 5% DMSO in water, dyes concentration was 0.5μM. (A) dye **1**; (B) dye **2** (C) MeO-X04

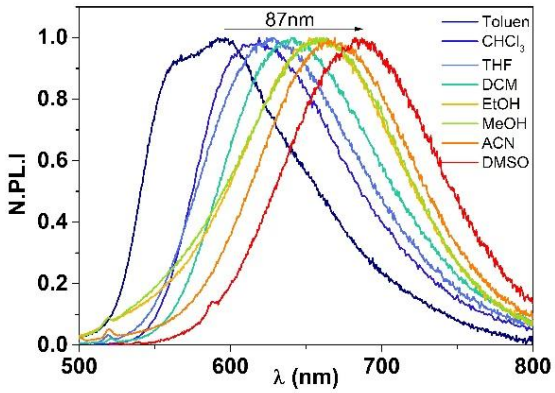

Figure S12: Emission spectrum of dye **2** in solvent with various polarity and static electric permittivity.

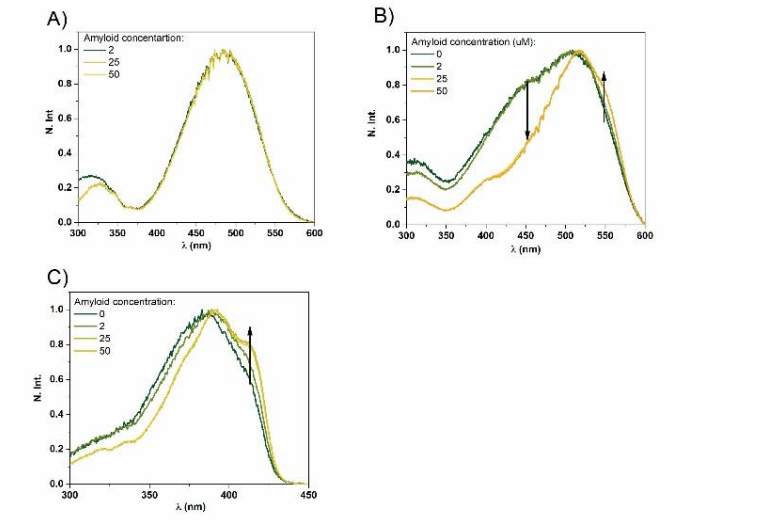

Figure S13: Spectrum of one-photon excitation in increasing bovine insulin amyloid concentration. All solutions were 5% DMSO in water, dyes concentration was 0.5µM. (A) dye **1**; (B) dye **2** (C) MeO-X04

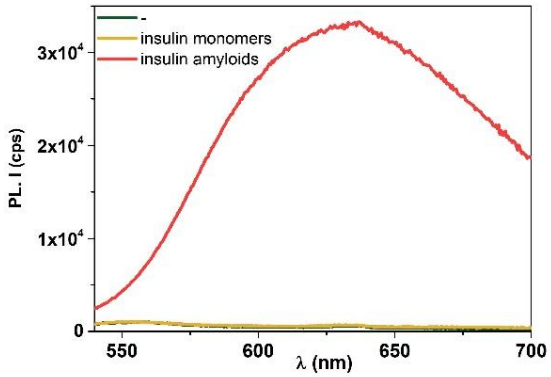

Figure S14: Emission spectrum of dye **2** only in 5% DMSO in water, upon addition of insulin monomers and insulin amyloids. Concetartion of monomers and amyloids were equal.

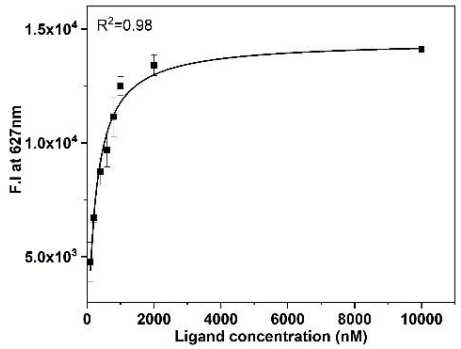

Figure S15: Saturation binding curves for ligand (dye **2**) to insulin amyloids (10 μM).

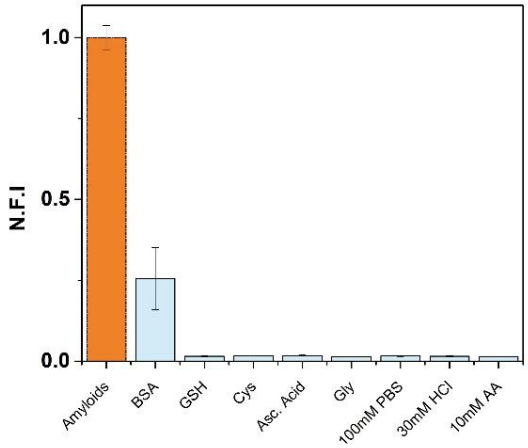

Figure S16: Selectivity studies of dye **2** (1 μM) toward potential competitive biomolecules (100 μM of Gluthation-GSH , L-cystein-Cys, Ascorbic Acid, Glycine-Gly and three different solvents: PBS pH=7.4, 10mM Ammonium Acetate pH=7.0, aqueous solution of 30mM HCl pH=1.5), different buffers and insulin aggregates (100 μM).N.F.I stands or normalized fluorescence intensity at maxima.

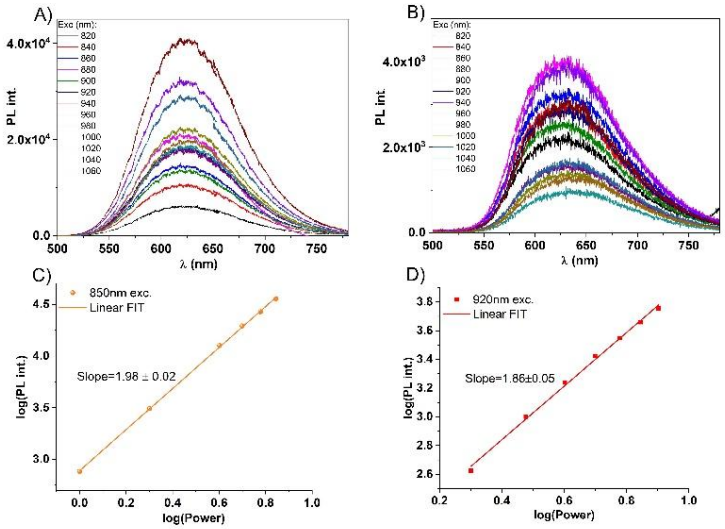

Figure S17: Two-photon excited luminescence with 50 μM of amyloids of (A) dye **1** (B) dye **2**. Plots C i D shows photoluminescence intensity (PL int.) dependence on laser power for (C) dye **1** (D) dye **2**

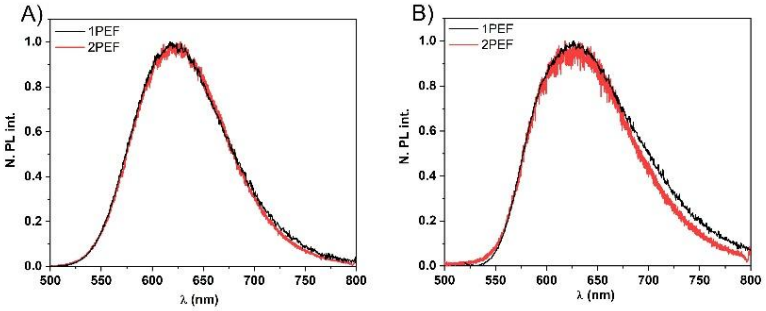

Figure S18: Normalized photoluminescence intensity (N. PL.Int.). Comparison of one-photon excited fluorescence (1PEF) vs two-photon excited fluorescence (2PEF) (A) dye **1** (B) dye **2** with 50μM of amyloids.

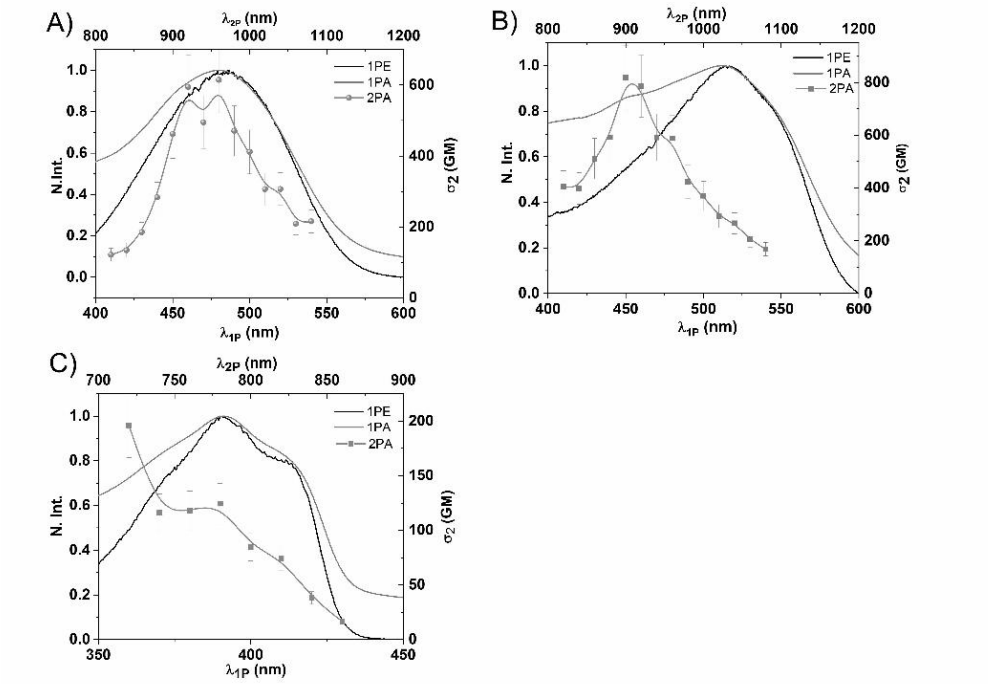

Figure S19: Experimental 2PA cross-sections compared to 1PA and 1PE of the same solution of amyloids (50 μM) with dyes (1 μM) (A) dye **1**; (B) dye **2**; (C) MeOX-04.

Two-photon absorption of dyes bound to amyloids

In our previous work we proved that 2PA can change upon interaction with protein aggregates[6] and measurements only in solvents may not give full perspective on 2PA characteristics of dyes bound to amyloid fibrils. To accurately compare two-photon and one-photon effects in dyes upon binding to amyloids, we plotted one-photon absorption (1PA), one-photon excitation (1PE) and two-photon absorption, which is represented by measured experimentally σ_2 for the same solutions (Figure S14). Normalized 1PA spectra have higher background due to scattering of amyloid solution. For dye **1** 1PA and 1PE are in line and maximum of σ_2 is around double wavelength of 1PA and 1PE. More complex story is shown in graph S14 B, which represents data for dye **2**. In 1PA peak at 515 nm dominates, however around 450 nm there is still visible peak, which is also presented in 1PA of dye **2** in $CHCl_3$ (Figure 4). In increasing amyloid concentration this peak starts to slowly vanish in 1PA. However, in the same concentration of amyloids in 1PE this peak starts to disappear more prominently, which indicates dramatic changes in one-photon radiative pathways. On the other hand 2PA has maximum around 900 nm, which corresponds to peak in one-photon regime, which decreases upon amyloid binding. It shows that 2PA of dyes maintain its shape upon binding to amyloids, as compared to measurements in $CHCl_3$, in contrast to the trend observed in 1PA and 1PE. This may be due to different selection rules for one-photon and two-photon absorption. In Figure S14 C is MeOX-4, two maxima (390, 413 nm) are present in 1PA and 1PE, which are in line with 2PA results.

Computational details

The ground state geometry optimization was performed for the studied dyes at the MN15/def2-TZVP level of theory.[7–9] Solvent environment was taken into account using the polarizable continuum model in the integral equation formalism (IEF-PCM).[10] Additionally, we confirmed that the obtained geometry corresponds to a minimum on the potential energy surface by evaluation of Hessian. In order to get insights into the electronic structure of the studied dyes, we calculated Ciofini's charge transfer diagnostic[11] and electronic density difference plots ($\Delta\rho(r) = \rho^{S_n}(r) - \rho^{S_0}(r)$) for the $S_0 \rightarrow S_1$, $S_0 \rightarrow S_2$, and $S_0 \rightarrow S_3$ transitions. The MN15/def2-TZVP/IEF-PCM level of theory was used for these analyses using Gaussian 16 program.[12]

For the further analyses of two-photon absorption we included the discrete representation of solvent environment. Studied systems were represented by the ground state geometry placed inside of the chloroform box ($50 \times 50 \times 50$ Å, 930 chloroform molecules). Molecular dynamics (MD) simulations of studied systems were performed using periodic boundary conditions. In these simulations the geometry of dye was kept rigid, while solvent molecules remained flexible. NAMD program was used to that end.[13] Subsequently, we extracted 100 "solute–solvent" snapshots per dye from the resulting MD trajectories. Approximate coupled cluster singles and doubles model using the resolution-of-identity approximation (RI-CC2)[14] and the def2-SVPP basis set[15,16] were used to simulate 2PA properties of studied systems. In these calculations electrostatic embedding model was used to include the influence of the discrete solvent environment. The described RI-CC2/def2-SVPP/EE electronic structure calculations were performed using TURBOMOLE 7.3 program.[17]

The results of RI-CC2/def2-SVPP/EE calculations for the full set of snapshots were used to determine the single snapshot (for each dye molecule) with $S_0 \rightarrow S_1$ excitation energy closest to the average over 100 solute–solvent snapshots. These two snapshots, for **1** and **2**, were subsequently used in more refined calculations at the RI-CC2/def2-TZVP/EE level of theory. In more details, we determined excitation energies, excited state dipole moments, two-photon transition strengths and all parameters required for generalized few-state model calculations.[18] These results, corresponding to RI-CC2/def2-TZVP/EE level of theory, are reported in Table 2 in the accompanying manuscript.

Two-photon absorption cross section was computed assuming Lorentzian broadening (with Γ_f equal to 0.25 eV) according to the following formula:

$$\sigma_2(\omega = \frac{1}{2}\omega_f) = \frac{8\pi^2 \alpha a_0^5 \omega^2}{c\Gamma_f}\delta^{2\mathrm{PA}} \tag{3}$$

where $\hbar\omega$ is photon energy, c is speed of light, a_0 is Bohr radius and α is fine structure constant.

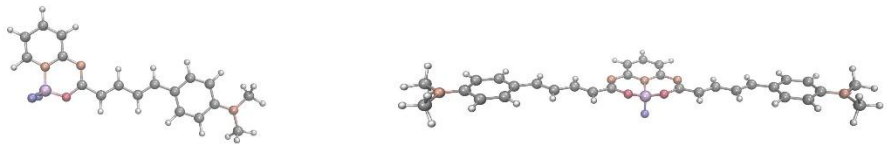

Figure S20: Ground state geometries of studied dyes determined at MN15/def2-TZVP/IEF-PCM level of theory (in chloroform). Geometry of **2** belongs to C_s symmetry point group.

Table S2: Electronic-structure parameters simulated at MN15/def2-TZVP/IEF-PCM level of theory (in chloroform): excitation energy ΔE, excitation wavelength λ, oscillator strength f, and Ciofini's charge transfer diagnostic D^{CT}.

	transition	ΔE [eV]	λ [nm]	f	D^{CT} [Å]	dominant orbital transitions
1	$S_0 \rightarrow S_1$	2.7321	453.81	1.9088	4.391	HOMO→LUMO(0.67)
	$S_0 \rightarrow S_2$	3.8919	318.57	0.0138	4.429	HOMO-1→LUMO(0.46)
	$S_0 \rightarrow S_3$	4.1362	299.75	0.1368	5.456	HOMO-1→LUMO(0.47)
						HOMO→LUMO+1(0.45)
2	$S_0 \rightarrow S_1$	2.6114	474.77	3.1577	1.085	HOMO→LUMO(0.57)
	$S_0 \rightarrow S_2$	2.8411	436.40	0.3811	1.451	HOMO-1→LUMO(0.49)
						HOMO→LUMO+1(0.48)
	$S_0 \rightarrow S_3$	3.4160	362.95	0.2733	1.122	HOMO-1→LUMO+1(0.47)

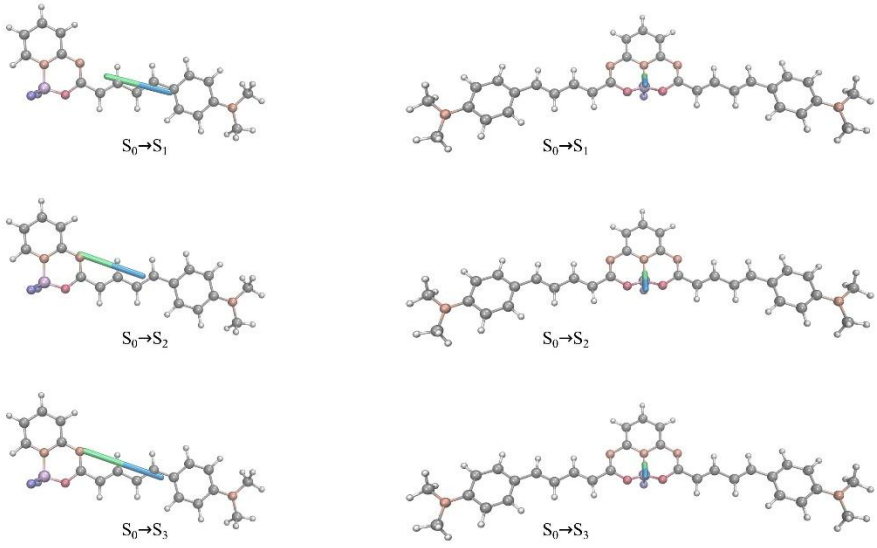

Figure S 21: Graphical representation of Ciofini's charge transfer diagnostic D^{CT} determined at MN15/def2-TZVP/IEF-PCM level of theory (in chloroform)

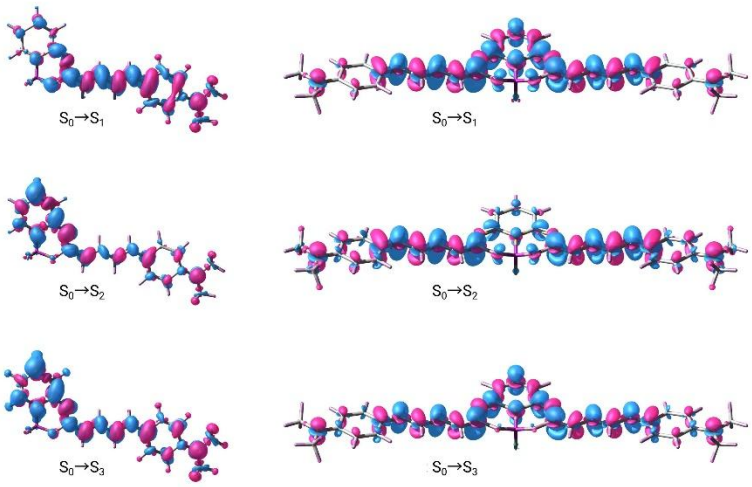

Figure S22: Electronic density difference plots corresponding to the $S_0 \rightarrow S_1$, $S_0 \rightarrow S_2$, and $S_0 \rightarrow S_3$ transitions ($\Delta\rho(r) = \rho^{S_n}(r) - \rho^{S_0}(r)$) determined at the MN15/def2-TZVP/IEF-PCM level of theory (in chloroform). Density contour value 0.001 was used.

Table S3: 1PA and 2PA properties calculated at the RI-CC2/def2-SVPP/EE level of theory (in chloroform): one-photon excitation energy ΔE, one-photon excitation wavelength λ, oscillator strength f, 2PA transition strength δ^{2PA}). In the case of each dye, the reported values correspond to a single snapshot with $S_0 \rightarrow S_1$ excitation energy closest to the average over 100 solute–solvent snapshots.

	transition	ΔE [eV]	λ [nm]	f	δ^{2PA} [a.u.]
1	$S_0 \rightarrow S_1$	3.11	399	1.85	182×10^3
	$S_0 \rightarrow S_2$	4.17	297	0.05	44×10^3
	$S_0 \rightarrow S_3$	4.43	280	0.03	21×10^3
2	$S_0 \rightarrow S_1$	2.94	421	2.99	32×10^3
	$S_0 \rightarrow S_2$	3.29	377	0.40	487×10^3
	$S_0 \rightarrow S_3$	3.68	337	0.35	37×10^3

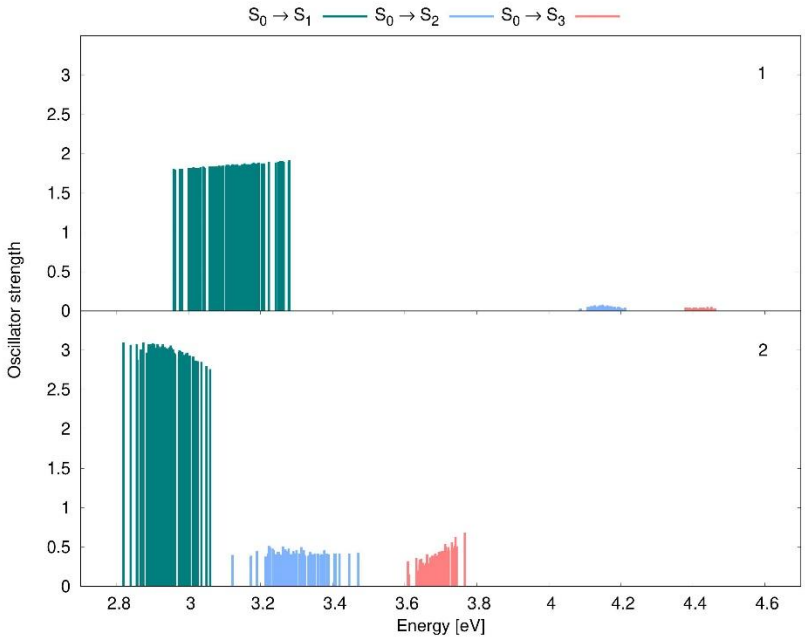

Figure S23: 1PA properties (excitation energies ΔE and oscillator strengths f) simulated for 100 snapshots at the RI-CC2/def2-SVPP/EE level of theory (in chloroform).

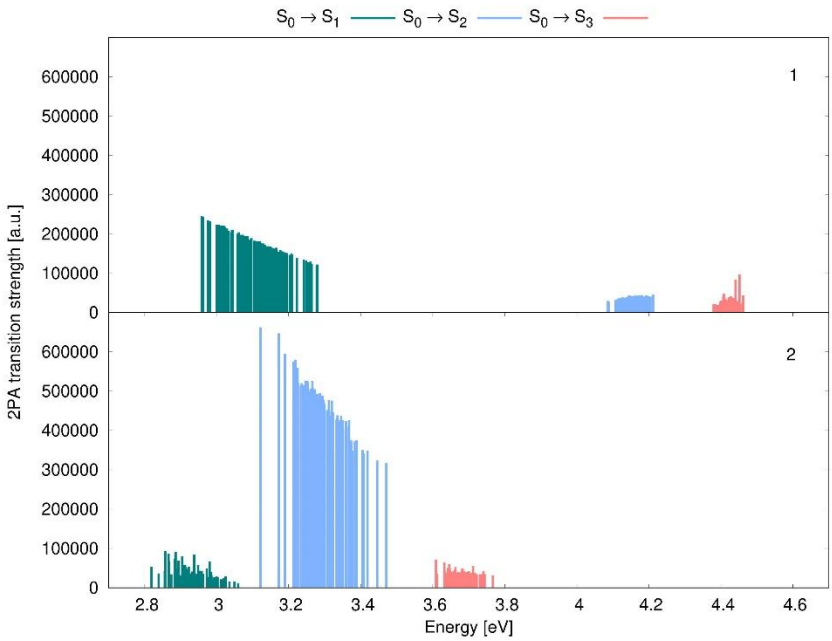

Figure S24: 2PA properties (excitation energies ΔE and 2PA transition strengths δ^{2PA}) simulated for 100 snapshots at the RI-CC2/def2-SVPP/EE level of theory (in chloroform).

References

[1] S. Iwano, R. Obata, C. Miura, M. Kiyama, K. Hama, M. Nakamura, Y. Amano, S. Kojima, T. Hirano, S. Maki and H. Niwa, *Tetrahedron*, 2013, **69**, 3847–3856.

[2] A. M. Grabarz, A. D. Laurent, B. Jędrzejewska, A. Zakrzewska, D. Jacquemin and B. Ośmiałowski, *J. Org. Chem.*, 2016, **81**, 2280–2292.

[3] B. Ośmiałowski, B. Dziuk, K. Ejsmont, L. Checińska and L. Dobrzańska, *Acta Crystallogr. C*, 2021, **77**, 807–813.

[4] N. S. Makarov, J. Campo, J. M. Hales and J. W. Perry, *Opt. Mater. Express*, 2011, **1**, 551–563.

[5] A. Hajda, R. Guha, S. M. Copp and J. Olesiak-Bańska, *Chem. Sci.*, 2025, **16**, 1737–1745.

[6] A. Hajda, M. Grelich-Mucha, P. Rybczyński, B. Ośmiałowski, R. Zaleśny and J. Olesiak-Bańska, *ACS Appl. Bio Mater.*, 2023, **6**, 5676–5684.

[7] H. S. Yu, X. He, S. L. Li and D. G. Truhlar, *Chem. Sci.*, 2016, **7**, 5032–5051.

[8] F. Weigend and R. Ahlrichs, *Phys. Chem. Chem. Phys.*, 2005, **7**, 3297–3305.

[9] F. Weigend, *Phys. Chem. Chem. Phys.*, 2006, **8**, 1057–1065.

[10] J. Tomasi, B. Mennucci and E. Cancès, *J. Mol. Struct. (Theochem)*, 1999, **464**, 211–226.

[11] T. Le Bahers, C. Adamo and I. Ciofini, *J. Chem. Theory Comput.*, 2011, **7**, 2498–2506.

[12] M. J. Frisch, G. W. Trucks, H. B. Schlegel, G. E. Scuseria, M. A. Robb, J. R. Cheeseman, G. Scalmani, V. Barone, G. A. Petersson, H. Nakatsuji, X. Li, M. Caricato, A. V. Marenich, J. Bloino, B. G. Janesko, R. Gomperts, B. Mennucci, H. P. Hratchian, J. V. Ortiz, A. F. Izmaylov, J. L. Sonnenberg, D. Williams-Young, F. Ding, F. Lipparini, F. Egidi, J. Goings, B. Peng, A. Petrone, T. Henderson, D. Ranasinghe, V. G. Zakrzewski, J. Gao, N. Rega, G. Zheng, W. Liang, M. Hada, M. Ehara, K. Toyota, R. Fukuda, J. Hasegawa, M. Ishida, T. Nakajima, Y. Honda, O. Kitao, H. Nakai, T. Vreven, K. Throssell, J. A. Montgomery, Jr., J. E. Peralta, F. Ogliaro, M. J. Bearpark, J. J. Heyd, E. N. Brothers, K. N. Kudin, V. N. Staroverov, T. A. Keith, R. Kobayashi, J. Normand, K. Raghavachari, A. P. Rendell, J. C. Burant, S. S. Iyengar, J. Tomasi, M. Cossi, J. M. Millam, M. Klene, C. Adamo, R. Cammi, J. W. Ochterski, R. L. Martin, K. Morokuma, O. Farkas, J. B. Foresman and D. J. Fox, *Gaussian 16 Revision C.01*, 2016, Gaussian Inc. Wallingford CT.

[13] J. C. Phillips, R. Braun, W. Wang, J. Gumbart, E. Tajkhorshid, E. Villa, C. Chipot, R. D. Skeel, L. Kale and K. Schulten, *J. Comput. Chem.*, 2005, **26**, 1781–1802.

[14] D. H. Friese, C. Hättig and K. Ruud, *Phys. Chem. Chem. Phys.*, 2012, **14**, 1175–1184.

[15] A. Schäfer, H. Horn and R. Ahlrichs, *J. Chem. Phys.*, 1992, **97**, 2571–2577.

[16] F. Weigend, M. Häser, H. Patzelt and R. Ahlrichs, *Chem. Phys. Lett.*, 1998, **294**, 143–152.

[17] *TURBOMOLE V7.3 2018, a development of University of Karlsruhe and Forschungszentrum Karlsruhe GmbH, 1989-2007, TURBOMOLE GmbH, since 2007; available from* `http://www.turbomole.com`.

[18] M. T. P. Beerepoot, M. M. Alam, J. Bednarska, W. Bartkowiak, K. Ruud and R. Zaleśny, *J. Chem. Theory Comput.*, 2018, **14**, 3677–3685.

IV. SUMMARY AND PERSPECTIVES

In the 1st article, detailed information regarding modulation of optical properties of BF_2-functionalized benzothiazoles with structural core inspired by ThT was presented. σ_2 of the studied probes was not sufficient for bioimaging application, but incorporation of a stronger electron donor group in the structure would be beneficial in increasing charge-transfer character and σ_2 of the dyes. Indeed, it was already presented in our other work.[223] Presence of amines as donor groups resulted in σ_2 values between 200-700 GM. Next, more general aspect is modulation of 2PA in amyloids. As it was presented in the first article, 2PA changes as the dye binds to amyloids. Exploring this topic could be a starting point to thoughtfully design 2PA modulation upon binding. Selective enhancement or decrease of 2PA upon binding to certain amyloids could be a new approach in the detection of certain analytes.

In the 2nd article, Ag_N- DNAs was confirmed as interesting probes for 2PFM. In my opinion, evaluation of a bigger set of Ag_N-DNA nanoclusters is needed for understanding the connections between structure and 2PA, since there are many variables like DNA sequence, number of DNA oligomers per nanocluster, number of silver atoms, values of N_0. In order to asses dependencies, large scale investigation have to be done, as in the case of one-photon properties for Ag_N-DNAs[68]. However, due to the time consuming experiments on 2PA evaluation, similar investigation in two-photon regime would be extremely difficult and extended in time.

Another aspect is deeper understanding of 2PA of Ag_{16}-DNA-Cl_2, since it has more pronounced σ_2 above 1000 nm. This nanocluster, as the only one evaluated, has chloride atoms, which have an impact on electron distribution in the structure. Interesting approach would be to replace chlorine atoms for other representatives of halogen atoms like e.g bromine. In the work of Anna Gonzàlez-Rosell *et al*.[85], it was demonstrated that an exchange of chlorine for bromine atoms is possible. This sophisticated change in the structure could show how 2PA is impacted by the change in electronegativity of the additional atoms. If the change would be visible, then it introduces additional ligands – Cl atoms – as an important factor in the modulation of σ_2. Theoretical simulations of energy diagrams are also required, since without them the explanation of the observed processes is highly limited.

3rd article is a foundation for further studies regarding O,N,O-coordinated organofluoroboron-based dye of D–A–D structure. It can serve as a scaffold for further development as amyloid-binding probe for 2PFM. The crucial aspect for potential investigation is the evaluation of this dye *in vivo*. It would show if the dye needs to be modified to meet biological criteria of amyloid staining in transgenic mice or in postmortem tissues. Based on this, its derivatives can be obtained to e.g improve water solubility or increase FQY. Studies show, that there is still a room for improvement of probes for amyloid detection.

I want to address more general perspectives, which came to my mind after years of research, during preparation of this thesis and literature review. Measurements of 2PA are time consuming, sometimes they have to be repeated several times. They cannot be performed routinely on a large set of compounds. Building the experimental setup, which could be partially robotized and operated more by programmable software than by humans, may be the answer to this limitation. Use of ML approaches and Artificial Intelligence (AI) in science is more and more visible with each year[224-226], and it helps to uncover problems, which were not possible before. This was also reflected in the Nobel Prize in Chemistry awarded in 2024, which went to David Baker **for computational protein design**, and to Demis Hassabis and John Jumper **for protein structure prediction**. However, ML or AI need large number of data to be useful, which is often not possible to be produced only by hands in the labolatory.[227] Idea of robotized 2PA measurements combined with ML could give information about designing of efficient two-photon absorbers, e.g. in case of Ag_N-DNAs. Construction of such a setup would require the involvement of scientists from various fields. In my opinion, fully automatic 2PEL measurements, operated by programs and robots is not yet possible at university laboratories, but minimalizing human participation would make high-throughput screening of set of chromophores possible. Staying in the topic of large scale investigation and ML, article presented in Nature Chemistry in 2025[104], which shows high-throughput screening in the evaluation of fluorophores for the detection of certain polymorphs of Tau might be an answer to problems in the detection of polymorphs of amyloids. Polymorphism impact on diseases is undeniable, which was presented in the chapter “introduction”. Proposing large number of selective dyes for certain polymorphs could be one of the solutions in explanation of amyloids role in various pathologies. My studies also show, that there is a need for more research regarding evaluation of the structure - optical properties - amyloid binding relationships. If these three aspects are not addressed simultaneously, it is difficult to talk about “intelligent” design of fluorophores for a given application.

V. REFERENCES

1. Kaiser, W.; Garrett, C. G. B., Two-Photon Excitation in CaF2:Eu2+. *Physical Review Letters* **1961,** *7* (6), 229-231.
2. Pawlicki, M.; Collins, H. A.; Denning, R. G.; Anderson, H. L., Two-Photon Absorption and the Design of Two-Photon Dyes. *Angewandte Chemie International Edition* **2009,** *48* (18), 3244-3266.
3. Birge, R. R.; Pierce, B. M., Semiclassical time-dependent theory of two-photon spectroscopy. The effect of dephasing in the virtual level on the two-photon excitation spectrum of isotachysterol. *International Journal of Quantum Chemistry* **1986,** *29* (4), 639-656.
4. Makarov, N. S.; Drobizhev, M.; Rebane, A., Two-photon absorption standards in the 550–1600 nm excitation wavelength range. *Optics Express* **2008,** *16* (6), 4029-4047.
5. Wang, S.; Ren, W. X.; Hou, J.-T.; Won, M.; An, J.; Chen, X.; Shu, J.; Kim, J. S., Fluorescence imaging of pathophysiological microenvironments. *Chemical Society Reviews* **2021,** *50* (16), 8887-8902.
6. Grimm, J. B.; English, B. P.; Chen, J.; Slaughter, J. P.; Zhang, Z.; Revyakin, A.; Patel, R.; Macklin, J. J.; Normanno, D.; Singer, R. H.; Lionnet, T.; Lavis, L. D., A general method to improve fluorophores for live-cell and single-molecule microscopy. *Nature Methods* **2015,** *12* (3), 244-250.
7. Benaissa, H.; Ounoughi, K.; Aujard, I.; Fischer, E.; Goïame, R.; Nguyen, J.; Tebo, A. G.; Li, C.; Le Saux, T.; Bertolin, G.; Tramier, M.; Danglot, L.; Pietrancosta, N.; Morin, X.; Jullien, L.; Gautier, A., Engineering of a fluorescent chemogenetic reporter with tunable color for advanced live-cell imaging. *Nature Communications* **2021,** *12* (1), 6989.
8. Grimm, J. B.; Muthusamy, A. K.; Liang, Y.; Brown, T. A.; Lemon, W. C.; Patel, R.; Lu, R.; Macklin, J. J.; Keller, P. J.; Ji, N.; Lavis, L. D., A general method to fine-tune fluorophores for live-cell and in vivo imaging. *Nature Methods* **2017,** *14* (10), 987-994.
9. Liu, D.; He, Z.; Gao, W.; Shang, J.; Yang, Y.; Zhang, X.; Li, X.; Ma, H.; Shi, W., Near-infrared II cyanine fluorophores with large stokes shift engineered by regulating respective absorption and emission. *Nature Communications* **2025,** *16* (1), 4911.
10. Cheong, W. F.; Prahl, S. A.; Welch, A. J., A review of the optical properties of biological tissues. *IEEE Journal of Quantum Electronics* **1990,** *26* (12), 2166-2185.
11. Diao, S.; Hong, G.; Antaris, A. L.; Blackburn, J. L.; Cheng, K.; Cheng, Z.; Dai, H., Biological imaging without autofluorescence in the second near-infrared region. *Nano Research* **2015,** *8* (9), 3027-3034.
12. Li, C.; Chen, G.; Zhang, Y.; Wu, F.; Wang, Q., Advanced Fluorescence Imaging Technology in the Near-Infrared-II Window for Biomedical Applications. *Journal of the American Chemical Society* **2020,** *142* (35), 14789-14804.
13. Cheng, H.; Tong, S.; Deng, X.; Liu, H.; Du, Y.; He, C.; Qiu, P.; Wang, K., Deep-brain 2-photon fluorescence microscopy in vivo excited at the 1700 nm window. *Opt. Lett.* **2019,** *44* (17), 4432-4435.

14. Dong, N.-N.; Pedroni, M.; Piccinelli, F.; Conti, G.; Sbarbati, A.; Ramírez-Hernández, J. E.; Maestro, L. M.; Iglesias-de la Cruz, M. C.; Sanz-Rodriguez, F.; Juarranz, A.; Chen, F.; Vetrone, F.; Capobianco, J. A.; Solé, J. G.; Bettinelli, M.; Jaque, D.; Speghini, A., NIR-to-NIR Two-Photon Excited CaF2:Tm3+,Yb3+ Nanoparticles: Multifunctional Nanoprobes for Highly Penetrating Fluorescence Bio-Imaging. *ACS Nano* **2011,** *5* (11), 8665-8671.
15. Denk, W.; Strickler, J. H.; Webb, W. W., Two-Photon Laser Scanning Fluorescence Microscopy. *Science* **1990,** *248* (4951), 73-76.
16. Luu, P.; Fraser, S. E.; Schneider, F., More than double the fun with two-photon excitation microscopy. *Communications Biology* **2024,** *7* (1), 364.
17. Miller, D. R.; Hassan, A. M.; Jarrett, J. W.; Medina, F. A.; Perillo, E. P.; Hagan, K.; Shams Kazmi, S. M.; Clark, T. A.; Sullender, C. T.; Jones, T. A.; Zemelman, B. V.; Dunn, A. K., In vivo multiphoton imaging of a diverse array of fluorophores to investigate deep neurovascular structure. *Biomed. Opt. Express* **2017,** *8* (7), 3470-3481.
18. Burgold, S.; Filser, S.; Dorostkar, M. M.; Schmidt, B.; Herms, J., In vivo imaging reveals sigmoidal growth kinetic of β-amyloid plaques. *Acta Neuropathologica Communications* **2014,** *2* (1), 30.
19. Shih, A. Y.; Driscoll, J. D.; Drew, P. J.; Nishimura, N.; Schaffer, C. B.; Kleinfeld, D., Two-Photon Microscopy as a Tool to Study Blood Flow and Neurovascular Coupling in the Rodent Brain. *Journal of Cerebral Blood Flow & Metabolism* **2012,** *32* (7), 1277-1309.
20. Alberto, D.; Giberto, C.; Federico, F.; Fabio, C.; Sabrina, B.; Mauro, R.; Francesca, O.; Paola, R., Two-photon microscopy and spectroscopy based on a compact confocal scanning head. *Journal of Biomedical Optics* **2001,** *6* (3), 300-310.
21. Diaspro, A.; Corosu, M.; Ramoino, P.; Robello, M., Adapting a compact confocal microscope system to a two-photon excitation fluorescence imaging architecture. *Microscopy Research and Technique* **1999,** *47* (3), 196-205.
22. Christie, R. H.; Bacskai, B. J.; Zipfel, W. R.; Williams, R. M.; Kajdasz, S. T.; Webb, W. W.; Hyman, B. T., Growth arrest of individual senile plaques in a model of Alzheimer's disease observed by in vivo multiphoton microscopy. *JOURNAL OF NEUROSCIENCE* **2001,** *21* (3), 858-864.
23. Hefendehl, J. K.; Wegenast-Braun, B. M.; Liebig, C.; Eicke, D.; Milford, D.; Calhoun, M. E.; Kohsaka, S.; Eichner, M.; Jucker, M., Long-Term Imaging of β-Amyloid Plaque Appearance and Growth in a Mouse Model of Cerebral β-Amyloidosis. *The Journal of Neuroscience* **2011,** *31* (2), 624.
24. Burgold, S.; Bittner, T.; Dorostkar, M. M.; Kieser, D.; Fuhrmann, M.; Mitteregger, G.; Kretzschmar, H.; Schmidt, B.; Herms, J., In vivo multiphoton imaging reveals gradual growth of newborn amyloid plaques over weeks. *Acta Neuropathologica* **2011,** *121* (3), 327-335.
25. Liebscher, S.; Meyer-Luehmann, M., A Peephole into the Brain: Neuropathological Features of Alzheimer's Disease Revealed by in vivo Two-Photon Imaging. *Frontiers in Psychiatry* **2012,** *3*.
26. Subramanian, J.; Savage, J. C.; Tremblay, M.-È., Synaptic Loss in Alzheimer's Disease: Mechanistic Insights Provided by Two-Photon in vivo Imaging of Transgenic Mouse Models. *Frontiers in Cellular Neuroscience* **2020,** *14*.

27. Lu, Y.; Wei, X.; Li, W.; Wu, X.; Chen, C.; Li, G.; Huang, Z.; Li, Y.; Zhang, Y.; Gan, W.-B., Large-volume and deep brain imaging in rabbits and monkeys using COMPACT two-photon microscopy. *Scientific Reports* **2022,** *12* (1), 17736.
28. Korzhova, V.; Marinković, P.; Njavro, J. R.; Goltstein, P. M.; Sun, F.; Tahirovic, S.; Herms, J.; Liebscher, S., Long-term dynamics of aberrant neuronal activity in awake Alzheimer's disease transgenic mice. *Communications Biology* **2021,** *4* (1), 1368.
29. Algamal, M.; Russ, A. N.; Miller, M. R.; Hou, S. S.; Maci, M.; Munting, L. P.; Zhao, Q.; Gerashchenko, D.; Bacskai, B. J.; Kastanenka, K. V., Reduced excitatory neuron activity and interneuron-type-specific deficits in a mouse model of Alzheimer's disease. *Communications Biology* **2022,** *5* (1), 1323.
30. Chapleau, M.; Iaccarino, L.; Soleimani-Meigooni, D.; Rabinovici, G. D., The Role of Amyloid PET in Imaging Neurodegenerative Disorders: A Review. *Journal of Nuclear Medicine* **2022,** *63* (Supplement 1), 13S.
31. Condeelis, J.; Weissleder, R., In Vivo Imaging in Cancer. *COLD SPRING HARBOR PERSPECTIVES IN BIOLOGY* **2010,** *2* (12).
32. Skoch, J.; Hyman, B. T.; Bacskai, B. J., Preclinical characterization of amyloid imaging probes with multiphoton microscopy. *J Alzheimers Dis* **2006,** *9* (3 Suppl), 401-7.
33. Zong, W.; Obenhaus, H. A.; Skytøen, E. R.; Eneqvist, H.; de Jong, N. L.; Vale, R.; Jorge, M. R.; Moser, M.-B.; Moser, E. I., Large-scale two-photon calcium imaging in freely moving mice. *Cell* **2022,** *185* (7), 1240-1256.e30.
34. Zong, W.; Wu, R.; Li, M.; Hu, Y.; Li, Y.; Li, J.; Rong, H.; Wu, H.; Xu, Y.; Lu, Y.; Jia, H.; Fan, M.; Zhou, Z.; Zhang, Y.; Wang, A.; Chen, L.; Cheng, H., Fast high-resolution miniature two-photon microscopy for brain imaging in freely behaving mice. *Nature Methods* **2017,** *14* (7), 713-719.
35. Han, J.; Zhou, F.; Zhao, Z.; Zhang, D.; Chen, X.; Wang, L.; Zhao, T.; Ye, W.; Gu, X.; Fang, H.; Zhang, J.; Zhang, L.; Cheng, H., 24-hour simultaneous mPFC's miniature 2-photon imaging, EEG-EMG, and video recording during natural behaviors. *Scientific Data* **2025,** *12* (1), 1226.
36. McNulty, P.; Wu, R.; Yamaguchi, A.; Heckscher, E. S.; Haas, A.; Nwankpa, A.; Skanata, M. M.; Gershow; Marc, Closed-loop two-photon functional imaging in a freely moving animal. *Nature Communications* **2025,** *16* (1), 5950.
37. Fan, J. L.; Rivera, J. A.; Sun, W.; Peterson, J.; Haeberle, H.; Rubin, S.; Ji, N., High-speed volumetric two-photon fluorescence imaging of neurovascular dynamics. *Nature Communications* **2020,** *11* (1), 6020.
38. Meng, G.; Zhong, J.; Zhang, Q.; Wong, J. S. J.; Wu, J.; Tsia, K. K.; Ji, N., Ultrafast two-photon fluorescence imaging of cerebral blood circulation in the mouse brain in vivo. *Proceedings of the National Academy of Sciences* **2022,** *119* (23), e2117346119.
39. Schmid, F.; Barrett, M. J. P.; Obrist, D.; Weber, B.; Jenny, P., Red blood cells stabilize flow in brain microvascular networks. *PLOS Computational Biology* **2019,** *15* (8), e1007231.
40. Kim, H. M.; Cho, B. R., Two-photon materials with large two-photon cross sections. Structure-property relationship. *CHEMICAL COMMUNICATIONS* **2009,** (2), 153-164.

41. Pascal, S.; David, S.; Andraud, C.; Maury, O., Near-infrared dyes for two-photon absorption in the short-wavelength infrared: strategies towards optical power limiting. *Chemical Society Reviews* **2021,** *50* (11), 6613-6658.
42. Knysh, I.; Jassar, M. B.; Ośmiałowski, B.; Zaleśny, R.; Jacquemin, D., In Silico Screening of Two-Photon Absorption Properties of a Large Set of Bis-Difluoroborate Dyes. *ChemPhotoChem* **2022,** *6* (10), e202200137.
43. Kim, H. M.; Cho, B. R., Small-Molecule Two-Photon Probes for Bioimaging Applications. *Chemical Reviews* **2015,** *115* (11), 5014-5055.
44. Lakowicz, J. R., *Principles of Fluorescence Spectroscopy*. 3 ed.; Springer New York, NY: 2007; p XXVI, 954.
45. Dipold, J.; Romero, E. E.; Donnelly, J.; Calheiro, T. P.; Bonacorso, H. G.; Iglesias, B. A.; Siqueira, J. P.; Hernandez, F. E.; Boni, L. D.; Mendonca, C. R., Two-photon absorption properties of BODIPY-like compounds based on BF2–naphthyridine complexes. *Physical Chemistry Chemical Physics* **2019,** *21* (12), 6662-6671.
46. Ośmiałowski, B.; Petrusevich, E. F.; Nawrot, K. C.; Paszkiewicz, B. K.; Nyk, M.; Zielak, J.; Jędrzejewska, B.; Luis, J. M.; Jacquemin, D.; Zaleśny, R., Tailoring the nonlinear absorption of fluorescent dyes by substitution at a boron center. *Journal of Materials Chemistry C* **2021,** *9* (19), 6225-6233.
47. Yang, J.; Cai, F.; Desbois, N.; Huang, L.; Gros, C. P.; Bolze, F.; Fang, Y.; Wang, S.; Xu, H.-J., Synthesis, spectroscopic characterization, one and two-photon absorption properties and electrochemistry of π-expanded BODIPYs dyes. *Dyes and Pigments* **2020,** *175*, 108173.
48. Yang, J.; Jiang, H.; Desbois, N.; Zhu, G.; Gros, C. P.; Fang, Y.; Bolze, F.; Wang, S.; Xu, H.-J., Synthesis, spectroscopic characterization, one and two-photon absorption properties, and electrochemistry of truxene π-expanded BODIPYs dyes. *Dyes and Pigments* **2020,** *176*, 108183.
49. Li, P.; Sun, D.; Liu, N.; Fang, Y.; Gros, C. P.; Bolze, F.; Xu, H.-J., Synthesis, spectroscopic characterization and one and two-photon absorption properties of π-expanded thiophene and truxene BODIPYs dyes. *Dyes and Pigments* **2021,** *192*, 109418.
50. Treibs, A.; Kreuzer, F.-H., Difluorboryl-Komplexe von Di- und Tripyrrylmethenen. *Justus Liebigs Annalen der Chemie* **1968,** *718* (1), 208-223.
51. Kowada, T.; Maeda, H.; Kikuchi, K., BODIPY-based probes for the fluorescence imaging of biomolecules in living cells. *Chemical Society Reviews* **2015,** *44* (14), 4953-4972.
52. Bumagina, N. A.; Antina, E. V.; Ksenofontov, A. A.; Antina, L. A.; Kalyagin, A. A.; Berezin, M. B., Basic structural modifications for improving the practical properties of BODIPY. *Coordination Chemistry Reviews* **2022,** *469*, 214684.
53. Ulrich, G.; Ziessel, R.; Harriman, A., The chemistry of fluorescent bodipy dyes: versatility unsurpassed. *Angew Chem Int Ed Engl* **2008,** *47* (7), 1184-201.
54. Boens, N.; Leen, V.; Dehaen, W., Fluorescent indicators based on BODIPY. *Chem Soc Rev* **2012,** *41* (3), 1130-72.
55. Frath, D.; Azizi, S.; Ulrich, G.; Retailleau, P.; Ziessel, R., Facile Synthesis of Highly Fluorescent Boranil Complexes. *Organic Letters* **2011,** *13* (13), 3414-3417.

56. Rybczynski, P.; Bousquet, M. H. E.; Kaczmarek-Kedziera, A.; Jedrzejewska, B.; Jacquemin, D.; Osmialowski, B., Controlling the fluorescence quantum yields of benzothiazole-difluoroborates by optimal substitution. *Chem Sci* **2022,** *13* (45), 13347-13360.
57. Gonzàlez-Rosell, A.; Cerretani, C.; Mastracco, P.; Vosch, T.; Copp, S. M., Structure and luminescence of DNA-templated silver clusters. *Nanoscale Advances* **2021,** *3* (5), 1230-1260.
58. Rajeev, A.; Bhatia, D., DNA-templated fluorescent metal nanoclusters and their illuminating applications. *Nanoscale* **2024,** *16* (40), 18715-18731.
59. Gonzàlez-Rosell, A.; Copp, S. M., An Atom-Precise Understanding of DNA-Stabilized Silver Nanoclusters. *Accounts of Chemical Research* **2024,** *57* (15), 2117-2129.
60. Petty, J. T.; Zheng, J.; Hud, N. V.; Dickson, R. M., DNA-Templated Ag Nanocluster Formation. *Journal of the American Chemical Society* **2004,** *126* (16), 5207-5212.
61. Richards, C. I.; Choi, S.; Hsiang, J.-C.; Antoku, Y.; Vosch, T.; Bongiorno, A.; Tzeng, Y.-L.; Dickson, R. M., Oligonucleotide-Stabilized Ag Nanocluster Fluorophores. *Journal of the American Chemical Society* **2008,** *130* (15), 5038-5039.
62. Ritchie, C. M.; Johnsen, K. R.; Kiser, J. R.; Antoku, Y.; Dickson, R. M.; Petty, J. T., Ag Nanocluster Formation Using a Cytosine Oligonucleotide Template. *The Journal of Physical Chemistry C* **2007,** *111* (1), 175-181.
63. Sengupta, B.; Ritchie, C. M.; Buckman, J. G.; Johnsen, K. R.; Goodwin, P. M.; Petty, J. T., Base-Directed Formation of Fluorescent Silver Clusters. *The Journal of Physical Chemistry C* **2008,** *112* (48), 18776-18782.
64. Vosch, T.; Antoku, Y.; Hsiang, J.-C.; Richards, C. I.; Gonzalez, J. I.; Dickson, R. M., Strongly emissive individual DNA-encapsulated Ag nanoclusters as single-molecule fluorophores. *Proceedings of the National Academy of Sciences* **2007,** *104* (31), 12616-12621.
65. Patel, S. A.; Richards, C. I.; Hsiang, J.-C.; Dickson, R. M., Water-Soluble Ag Nanoclusters Exhibit Strong Two-Photon-Induced Fluorescence. *Journal of the American Chemical Society* **2008,** *130* (35), 11602-11603.
66. Schultz, D.; Gwinn, E. G., Silver atom and strand numbers in fluorescent and dark Ag:DNAs. *Chemical Communications* **2012,** *48* (46), 5748-5750.
67. Petty, J. T.; Fan, C.; Story, S. P.; Sengupta, B.; St. John Iyer, A.; Prudowsky, Z.; Dickson, R. M., DNA Encapsulation of 10 Silver Atoms Producing a Bright, Modulatable, Near-Infrared-Emitting Cluster. *The Journal of Physical Chemistry Letters* **2010,** *1* (17), 2524-2529.
68. Copp, S. M.; Swasey, S. M.; Gorovits, A.; Bogdanov, P.; Gwinn, E. G., General Approach for Machine Learning-Aided Design of DNA-Stabilized Silver Clusters. *Chemistry of Materials* **2020,** *32* (1), 430-437.
69. Copp, S. M.; Gorovits, A.; Swasey, S. M.; Gudibandi, S.; Bogdanov, P.; Gwinn, E. G., Fluorescence Color by Data-Driven Design of Genomic Silver Clusters. *ACS Nano* **2018,** *12* (8), 8240-8247.

70. Copp, S. M.; Bogdanov, P.; Debord, M.; Singh, A.; Gwinn, E., Base Motif Recognition and Design of DNA Templates for Fluorescent Silver Clusters by Machine Learning. *Advanced Materials* **2014,** *26* (33), 5839-5845.
71. Guha, R.; Gonzàlez-Rosell, A.; Rafik, M.; Arevalos, N.; Katz, B. B.; Copp, S. M., Electron count and ligand composition influence the optical and chiroptical signatures of far-red and NIR-emissive DNA-stabilized silver nanoclusters. *Chemical Science* **2023,** *14* (41), 11340-11350.
72. Romolini, G.; Kanazawa, H.; Mollerup, C. B.; Liisberg, M. B.; Lind, S. W.; Huang, Z.; Cerretani, C.; Kondo, J.; Vosch, T., Shining Bright at 960 nm: A 28-Silver-Atom Nanorod Stabilized by DNA. *Small Structures* **2025,** *n/a* (n/a), 2500022.
73. Liisberg, M. B.; Shakeri Kardar, Z.; Copp, S. M.; Cerretani, C.; Vosch, T., Single-Molecule Detection of DNA-Stabilized Silver Nanoclusters Emitting at the NIR I/II Border. *The Journal of Physical Chemistry Letters* **2021,** *12* (4), 1150-1154.
74. Neacşu, V. A.; Cerretani, C.; Liisberg, M. B.; Swasey, S. M.; Gwinn, E. G.; Copp, S. M.; Vosch, T., Unusually large fluorescence quantum yield for a near-infrared emitting DNA-stabilized silver nanocluster. *Chemical Communications* **2020,** *56* (47), 6384-6387.
75. Krause, S.; Carro-Temboury, M. R.; Cerretani, C.; Vosch, T., Anti-Stokes fluorescence microscopy using direct and indirect dark state formation. *Chemical Communications* **2018,** *54* (36), 4569-4572.
76. Fleischer, B. C.; Petty, J. T.; Hsiang, J.-C.; Dickson, R. M., Optically Activated Delayed Fluorescence. *The Journal of Physical Chemistry Letters* **2017,** *8* (15), 3536-3543.
77. Krause, S.; Cerretani, C.; Vosch, T., Disentangling optically activated delayed fluorescence and upconversion fluorescence in DNA stabilized silver nanoclusters. *Chemical Science* **2019,** *10* (20), 5326-5331.
78. Rück, V.; Mishra, N. K.; Sørensen, K. K.; Liisberg, M. B.; Sloth, A. B.; Cerretani, C.; Mollerup, C. B.; Kjaer, A.; Lou, C.; Jensen, K. J.; Vosch, T., Bioconjugation of a Near-Infrared DNA-Stabilized Silver Nanocluster to Peptides and Human Insulin by Copper-Free Click Chemistry. *Journal of the American Chemical Society* **2023,** *145* (30), 16771-16777.
79. Wang, X.; Liisberg, M. B.; Nolt, G. L.; Fu, X.; Cerretani, C.; Li, L.; Johnson, L. A.; Vosch, T.; Richards, C. I., DNA-AgNC Loaded Liposomes for Measuring Cerebral Blood Flow Using Two-Photon Fluorescence Correlation Spectroscopy. *ACS Nano* **2023,** *17* (13), 12862-12874.
80. Huard, D. J. E.; Demissie, A.; Kim, D.; Lewis, D.; Dickson, R. M.; Petty, J. T.; Lieberman, R. L., Atomic Structure of a Fluorescent Ag8 Cluster Templated by a Multistranded DNA Scaffold. *Journal of the American Chemical Society* **2019,** *141* (29), 11465-11470.
81. Cerretani, C.; Kanazawa, H.; Vosch, T.; Kondo, J., Crystal structure of a NIR-Emitting DNA-Stabilized Ag16 Nanocluster. *Angewandte Chemie International Edition* **2019,** *58* (48), 17153-17157.

82. Sapnik, A. F.; Romolini, G.; Cerretani, C.; Vosch, T.; Jensen, K. M. Ø., Structure of a DNA-Stabilized Ag16Cl2 Nanocluster in Solution. *Angewandte Chemie International Edition* **2025,** *n/a* (n/a), e202422432.
83. Häkkinen, H., Atomic and electronic structure of gold clusters: understanding flakes, cages and superatoms from simple concepts. *Chemical Society Reviews* **2008,** *37* (9), 1847-1859.
84. Copp, S. M.; Schultz, D.; Swasey, S.; Pavlovich, J.; Debord, M.; Chiu, A.; Olsson, K.; Gwinn, E., Magic Numbers in DNA-Stabilized Fluorescent Silver Clusters Lead to Magic Colors. *The Journal of Physical Chemistry Letters* **2014,** *5* (6), 959-963.
85. Gonzàlez-Rosell, A.; Malola, S.; Guha, R.; Arevalos, N. R.; Matus, M. F.; Goulet, M. E.; Haapaniemi, E.; Katz, B. B.; Vosch, T.; Kondo, J.; Häkkinen, H.; Copp, S. M., Chloride Ligands on DNA-Stabilized Silver Nanoclusters. *Journal of the American Chemical Society* **2023,** *145* (19), 10721-10729.
86. Hooley, E. N.; Carro-Temboury, M. R.; Vosch, T., Probing the Absorption and Emission Transition Dipole Moment of DNA Stabilized Silver Nanoclusters. *The Journal of Physical Chemistry A* **2017,** *121* (5), 963-968.
87. O'Neill, P. R.; Gwinn, E. G.; Fygenson, D. K., UV Excitation of DNA Stabilized Ag Cluster Fluorescence via the DNA Bases. *The Journal of Physical Chemistry C* **2011,** *115* (49), 24061-24066.
88. Krause, S.; Carro-Temboury, M. R.; Cerretani, C.; Vosch, T., Probing heterogeneity of NIR induced secondary fluorescence from DNA-stabilized silver nanoclusters at the single molecule level. *Physical Chemistry Chemical Physics* **2018,** *20* (24), 16316-16319.
89. Romolini, G.; Cerretani, C.; Mollerup, C. B.; Vosch, T., On the Chemical Stability of DNA-Stabilized Silver Nanoclusters. *ACS Omega* **2024,** *9* (47), 47248-47253.
90. Malola, S.; Häkkinen, H., On transient absorption and dual emission of the atomically precise, DNA-stabilized silver nanocluster Ag16Cl2. *Chemical Communications* **2024,** *60* (24), 3315-3318.
91. Malola, S.; Matus, M. F.; Häkkinen, H., Theoretical Analysis of the Electronic Structure and Optical Properties of DNA-Stabilized Silver Cluster Ag16Cl2 in Aqueous Solvent. *The Journal of Physical Chemistry C* **2023,** *127* (33), 16553-16559.
92. Olesiak-Banska, J.; Waszkielewicz, M.; Obstarczyk, P.; Samoc, M., Two-photon absorption and photoluminescence of colloidal gold nanoparticles and nanoclusters. *Chemical Society Reviews* **2019,** *48* (15), 4087-4117.
93. Reyna, A. S.; Russier-Antoine, I.; Bertorelle, F.; Benichou, E.; Dugourd, P.; Antoine, R.; Brevet, P.-F.; de Araújo, C. B., Nonlinear Refraction and Absorption of Ag29 Nanoclusters: Evidence for Two-Photon Absorption Saturation. *The Journal of Physical Chemistry C* **2018,** *122* (32), 18682-18689.
94. Pniakowska, A.; Kumaranchira Ramankutty, K.; Obstarczyk, P.; Perić Bakulić, M.; Sanader Maršić, Ž.; Bonačić-Koutecký, V.; Bürgi, T.; Olesiak-Bańska, J., Gold-Doping Effect on Two-Photon Absorption and Luminescence of Atomically Precise Silver Ligated Nanoclusters. *Angewandte Chemie International Edition* **2022,** *61* (43), e202209645.

95. Bonačić-Koutecký, V.; Antoine, R., Enhanced two-photon absorption of ligated silver and gold nanoclusters: theoretical and experimental assessments. *Nanoscale* **2019,** *11* (26), 12436-12448.
96. Buxbaum, J. N.; Linke, R. P., A Molecular History of the Amyloidoses. *Journal of Molecular Biology* **2012,** *421* (2), 142-159.
97. Sipe, J. D.; Cohen, A. S., Review: History of the Amyloid Fibril. *Journal of Structural Biology* **2000,** *130* (2), 88-98.
98. Kisilevsky, R.; Raimondi, S.; Bellotti, V., Historical and Current Concepts of Fibrillogenesis and In vivo Amyloidogenesis: Implications of Amyloid Tissue Targeting. *Frontiers in Molecular Biosciences* **2016,** *Volume 3 - 2016*.
99. Riek, R., The Three-Dimensional Structures of Amyloids. *Cold Spring Harb Perspect Biol* **2017,** *9* (2).
100. Sunde, M.; Blake, C., The Structure of Amyloid Fibrils by Electron Microscopy and X-Ray Diffraction. In *Advances in Protein Chemistry*, Richards, F. M.; Eisenberg, D. S.; Kim, P. S., Eds. Academic Press: 1997; Vol. 50, pp 123-159.
101. Sunde, M.; Serpell, L. C.; Bartlam, M.; Fraser, P. E.; Pepys, M. B.; Blake, C. C. F., Common core structure of amyloid fibrils by synchrotron X-ray diffraction. *Journal of Molecular Biology* **1997,** *273* (3), 729-739.
102. Lutter, L.; Aubrey, L. D.; Xue, W.-F., On the Structural Diversity and Individuality of Polymorphic Amyloid Protein Assemblies. *Journal of Molecular Biology* **2021,** *433* (20), 167124.
103. Jia, M.; Liu, Z.; Fan, X.; Ahmad, S.; Wang, Z.; Zhu, X.; Ai, H., Conformation-Dependent Binding Affinity of Small Molecules to Aβ42 Fibrils: Mechanistic Insights into Tracer Design. *The Journal of Physical Chemistry B* **2025,** *129* (34), 8700-8711.
104. Carroll, E. C.; Yang, H.; Powell, W. C.; Charvat, A. F.; Oehler, A.; Jones, J. G.; Montgomery, K. M.; Yung, A.; Millbern, Z.; Taylor, A. I. P.; Wilkinson, M.; Ranson, N. A.; Radford, S. E.; Vinueza, N. R.; DeGrado, W. F.; Mordes, D. A.; Condello, C.; Gestwicki, J. E., High-throughput discovery of fluoroprobes that recognize amyloid fibril polymorphs. *Nature Chemistry* **2025**.
105. Knowles, T. P. J.; Waudby, C. A.; Devlin, G. L.; Cohen, S. I. A.; Aguzzi, A.; Vendruscolo, M.; Terentjev, E. M.; Welland, M. E.; Dobson, C. M., An Analytical Solution to the Kinetics of Breakable Filament Assembly. *Science* **2009,** *326* (5959), 1533-1537.
106. Meisl, G.; Kirkegaard, J. B.; Arosio, P.; Michaels, T. C. T.; Vendruscolo, M.; Dobson, C. M.; Linse, S.; Knowles, T. P. J., Molecular mechanisms of protein aggregation from global fitting of kinetic models. *Nature Protocols* **2016,** *11* (2), 252-272.
107. Cohen, S. I. A.; Vendruscolo, M.; Dobson, C. M.; Knowles, T. P. J., From Macroscopic Measurements to Microscopic Mechanisms of Protein Aggregation. *Journal of Molecular Biology* **2012,** *421* (2), 160-171.
108. Knowles, T. P. J.; Vendruscolo, M.; Dobson, C. M., The amyloid state and its association with protein misfolding diseases. *Nature Reviews Molecular Cell Biology* **2014,** *15* (6), 384-396.
109. Törnquist, M.; Michaels, T. C. T.; Sanagavarapu, K.; Yang, X.; Meisl, G.; Cohen, S. I. A.; Knowles, T. P. J.; Linse, S., Secondary nucleation in amyloid formation. *Chemical Communications* **2018,** *54* (63), 8667-8684.

110. Arosio, P.; Knowles, T. P. J.; Linse, S., On the lag phase in amyloid fibril formation. *Physical Chemistry Chemical Physics* **2015,** *17* (12), 7606-7618.
111. Dear, A. J.; Michaels, T. C. T.; Meisl, G.; Klenerman, D.; Wu, S.; Perrett, S.; Linse, S.; Dobson, C. M.; Knowles, T. P. J., Kinetic diversity of amyloid oligomers. *Proceedings of the National Academy of Sciences* **2020,** *117* (22), 12087-12094.
112. Nguyen, P. H.; Ramamoorthy, A.; Sahoo, B. R.; Zheng, J.; Faller, P.; Straub, J. E.; Dominguez, L.; Shea, J.-E.; Dokholyan, N. V.; De Simone, A.; Ma, B.; Nussinov, R.; Najafi, S.; Ngo, S. T.; Loquet, A.; Chiricotto, M.; Ganguly, P.; McCarty, J.; Li, M. S.; Hall, C.; Wang, Y.; Miller, Y.; Melchionna, S.; Habenstein, B.; Timr, S.; Chen, J.; Hnath, B.; Strodel, B.; Kayed, R.; Lesné, S.; Wei, G.; Sterpone, F.; Doig, A. J.; Derreumaux, P., Amyloid Oligomers: A Joint Experimental/Computational Perspective on Alzheimer's Disease, Parkinson's Disease, Type II Diabetes, and Amyotrophic Lateral Sclerosis. *Chemical Reviews* **2021,** *121* (4), 2545-2647.
113. Tang, H.; Andrikopoulos, N.; Li, Y.; Ke, S.; Sun, Y.; Ding, F.; Ke, P. C., Emerging biophysical origins and pathogenic implications of amyloid oligomers. *Nature Communications* **2025,** *16* (1), 2937.
114. Jin, M.; Shepardson, N.; Yang, T.; Chen, G.; Walsh, D.; Selkoe, D. J., Soluble amyloid β-protein dimers isolated from Alzheimer cortex directly induce Tau hyperphosphorylation and neuritic degeneration. *Proceedings of the National Academy of Sciences* **2011,** *108* (14), 5819-5824.
115. Jansen, R.; Dzwolak, W.; Winter, R., Amyloidogenic Self-Assembly of Insulin Aggregates Probed by High Resolution Atomic Force Microscopy. *Biophysical Journal* **2005,** *88* (2), 1344-1353.
116. Cao, A.; Hu, D.; Lai, L., Formation of amyloid fibrils from fully reduced hen egg white lysozyme. *Protein Science* **2004,** *13* (2), 319-324.
117. Adamcik, J.; Jung, J.-M.; Flakowski, J.; De Los Rios, P.; Dietler, G.; Mezzenga, R., Understanding amyloid aggregation by statistical analysis of atomic force microscopy images. *Nature Nanotechnology* **2010,** *5* (6), 423-428.
118. Adamcik, J.; Mezzenga, R., Study of amyloid fibrils via atomic force microscopy. *Current Opinion in Colloid & Interface Science* **2012,** *17* (6), 369-376.
119. Aubrey, L. D.; Blakeman, B. J. F.; Lutter, L.; Serpell, C. J.; Tuite, M. F.; Serpell, L. C.; Xue, W.-F., Quantification of amyloid fibril polymorphism by nano-morphometry reveals the individuality of filament assembly. *Communications Chemistry* **2020,** *3* (1), 125.
120. Scheres, S. H. W.; Ryskeldi-Falcon, B.; Goedert, M., Molecular pathology of neurodegenerative diseases by cryo-EM of amyloids. *Nature* **2023,** *621* (7980), 701-710.
121. Zielinski, M.; Peralta Reyes, F. S.; Gremer, L.; Schemmert, S.; Frieg, B.; Schäfer, L. U.; Willuweit, A.; Donner, L.; Elvers, M.; Nilsson, L. N. G.; Syvänen, S.; Sehlin, D.; Ingelsson, M.; Willbold, D.; Schröder, G. F., Cryo-EM of Aβ fibrils from mouse models find tg-APPArcSwe fibrils resemble those found in patients with sporadic Alzheimer's disease. *Nature Neuroscience* **2023,** *26* (12), 2073-2080.
122. Li, B.; Ge, P.; Murray, K. A.; Sheth, P.; Zhang, M.; Nair, G.; Sawaya, M. R.; Shin, W. S.; Boyer, D. R.; Ye, S.; Eisenberg, D. S.; Zhou, Z. H.; Jiang, L., Cryo-EM of full-length α-synuclein reveals fibril polymorphs with a common structural kernel. *Nature Communications* **2018,** *9* (1), 3609.

123. Moran, S. D.; Zanni, M. T., How to Get Insight into Amyloid Structure and Formation from Infrared Spectroscopy. *The Journal of Physical Chemistry Letters* **2014,** *5* (11), 1984-1993.
124. Stelzmann, R. A.; Norman Schnitzlein, H.; Reed Murtagh, F., An english translation of alzheimer's 1907 paper, "über eine eigenartige erkankung der hirnrinde". *Clinical Anatomy* **1995,** *8* (6), 429-431.
125. Iadanza, M. G.; Jackson, M. P.; Hewitt, E. W.; Ranson, N. A.; Radford, S. E., A new era for understanding amyloid structures and disease. *Nature Reviews Molecular Cell Biology* **2018,** *19* (12), 755-773.
126. Fowler, D. M.; Koulov, A. V.; Balch, W. E.; Kelly, J. W., Functional amyloid - from bacteria to humans. *Trends in Biochemical Sciences* **2007,** *32* (5), 217-224.
127. Brown, A.; Török, M., Functional amyloids in the human body. *Bioorganic & Medicinal Chemistry Letters* **2021,** *40*, 127914.
128. Seuring, C.; Verasdonck, J.; Gath, J.; Ghosh, D.; Nespovitaya, N.; Walti, M. A.; Maji, S. K.; Cadalbert, R.; Guntert, P.; Meier, B. H.; Riek, R., The three-dimensional structure of human beta-endorphin amyloid fibrils. *Nat Struct Mol Biol* **2020,** *27* (12), 1178-1184.
129. Abedini, A.; Schmidt, A. M., Mechanisms of islet amyloidosis toxicity in type 2 diabetes. *FEBS Letters* **2013,** *587* (8), 1119-1127.
130. Spillantini, M. G.; Goedert, M., Tau pathology and neurodegeneration. *The Lancet Neurology* **2013,** *12* (6), 609-622.
131. Calabresi, P.; Mechelli, A.; Natale, G.; Volpicelli-Daley, L.; Di Lazzaro, G.; Ghiglieri, V., Alpha-synuclein in Parkinson's disease and other synucleinopathies: from overt neurodegeneration back to early synaptic dysfunction. *Cell Death & Disease* **2023,** *14* (3), 176.
132. Bates, G., Huntingtin aggregation and toxicity in Huntington's disease. *The Lancet* **2003,** *361* (9369), 1642-1644.
133. Hardy, J. A.; Higgins, G. A., Alzheimer's Disease: The Amyloid Cascade Hypothesis. *Science* **1992,** *256* (5054), 184-185.
134. Busche, M. A.; Hyman, B. T., Synergy between amyloid-β and tau in Alzheimer's disease. *Nature Neuroscience* **2020,** *23* (10), 1183-1193.
135. Muralidar, S.; Ambi, S. V.; Sekaran, S.; Thirumalai, D.; Palaniappan, B., Role of tau protein in Alzheimer's disease: The prime pathological player. *International Journal of Biological Macromolecules* **2020,** *163*, 1599-1617.
136. Bharadwaj, P.; Wijesekara, N.; Liyanapathirana, M.; Newsholme, P.; Ittner, L.; Fraser, P.; Verdile, G., The Link between Type 2 Diabetes and Neurodegeneration: Roles for Amyloid-β, Amylin, and Tau Proteins. *Journal of Alzheimer's Disease* **2017,** *59* (2), 421-432.
137. Chatterjee, S.; Mudher, A., Alzheimer's Disease and Type 2 Diabetes: A Critical Assessment of the Shared Pathological Traits. *Frontiers in Neuroscience* **2018,** *12*.
138. Kollmer, M.; Close, W.; Funk, L.; Rasmussen, J.; Bsoul, A.; Schierhorn, A.; Schmidt, M.; Sigurdson, C. J.; Jucker, M.; Fändrich, M., Cryo-EM structure and polymorphism of Aβ amyloid fibrils purified from Alzheimer's brain tissue. *Nature Communications* **2019,** *10* (1), 4760.

139. Wilkinson, M.; Xu, Y.; Thacker, D.; Taylor, A. I. P.; Fisher, D. G.; Gallardo, R. U.; Radford, S. E.; Ranson, N. A., Structural evolution of fibril polymorphs during amyloid assembly. *Cell* **2023,** *186* (26), 5798-5811.e26.
140. Liu, H.; Kim, C.; Haldiman, T.; Sigurdson, C. J.; Nyström, S.; Nilsson, K. P. R.; Cohen, M. L.; Wisniewski, T.; Hammarström, P.; Safar, J. G., Distinct conformers of amyloid beta accumulate in the neocortex of patients with rapidly progressive Alzheimer's disease. *Journal of Biological Chemistry* **2021,** *297* (5).
141. Koutarapu, S.; Ge, J.; Dulewicz, M.; Srikrishna, M.; Szadziewska, A.; Wood, J.; Blennow, K.; Zetterberg, H.; Michno, W.; Ryan, N. S.; Lashley, T.; Savas, J. N.; Schöll, M.; Hanrieder, J., Chemical imaging delineates Aβ plaque polymorphism across the Alzheimer's disease spectrum. *Nature Communications* **2025,** *16* (1), 3889.
142. Rasmussen, J.; Mahler, J.; Beschorner, N.; Kaeser, S. A.; Häsler, L. M.; Baumann, F.; Nyström, S.; Portelius, E.; Blennow, K.; Lashley, T.; Fox, N. C.; Sepulveda-Falla, D.; Glatzel, M.; Oblak, A. L.; Ghetti, B.; Nilsson, K. P. R.; Hammarström, P.; Staufenbiel, M.; Walker, L. C.; Jucker, M., Amyloid polymorphisms constitute distinct clouds of conformational variants in different etiological subtypes of Alzheimer's disease. *Proceedings of the National Academy of Sciences* **2017,** *114* (49), 13018-13023.
143. Shi, Y.; Zhang, W.; Yang, Y.; Murzin, A. G.; Falcon, B.; Kotecha, A.; van Beers, M.; Tarutani, A.; Kametani, F.; Garringer, H. J.; Vidal, R.; Hallinan, G. I.; Lashley, T.; Saito, Y.; Murayama, S.; Yoshida, M.; Tanaka, H.; Kakita, A.; Ikeuchi, T.; Robinson, A. C.; Mann, D. M. A.; Kovacs, G. G.; Revesz, T.; Ghetti, B.; Hasegawa, M.; Goedert, M.; Scheres, S. H. W., Structure-based classification of tauopathies. *Nature* **2021,** *598* (7880), 359-363.
144. Yang, Y.; Arseni, D.; Zhang, W.; Huang, M.; Lövestam, S.; Schweighauser, M.; Kotecha, A.; Murzin, A. G.; Peak-Chew, S. Y.; Macdonald, J.; Lavenir, I.; Garringer, H. J.; Gelpi, E.; Newell, K. L.; Kovacs, G. G.; Vidal, R.; Ghetti, B.; Ryskeldi-Falcon, B.; Scheres, S. H. W.; Goedert, M., Cryo-EM structures of amyloid-β 42 filaments from human brains. *Science* **2022,** *375* (6577), 167-172.
145. Pimplikar, S. W.; Nixon, R. A.; Robakis, N. K.; Shen, J.; Tsai, L.-H., Amyloid-Independent Mechanisms in Alzheimer's Disease Pathogenesis. *The Journal of Neuroscience* **2010,** *30* (45), 14946.
146. Chatanaka, M.; Sohaei, D.; Diamandis, E.; Prassas, I., Beyond the amyloid hypothesis: how current research implicates autoimmunity in Alzheimer's disease pathogenesis. *Critical Reviews in Clinical Laboratory Sciences* **2023,** *60*, 398-426.
147. Behl, C., In 2024, the amyloid-cascade-hypothesis still remains a working hypothesis, no less but certainly no more. *Frontiers in Aging Neuroscience* **2024,** *16*.
148. Kepp, K. P.; Robakis, N. K.; Høilund-Carlsen, P. F.; Sensi, S. L.; Vissel, B., The amyloid cascade hypothesis: an updated critical review. *Brain* **2023,** *146* (10), 3969-3990.
149. Tanzi, R. E.; Rose, J. P.; Kennedy, F., FDA Approval of Aduhelm Paves a New Path for Alzheimer's Disease. *Acs Chemical Neuroscience* **2021,** *12* (15), 2714-2715.
150. van Dyck, C. H.; Swanson, C. J.; Aisen, P.; Bateman, R. J.; Chen, C.; Gee, M.; Kanekiyo, M.; Li, D.; Reyderman, L.; Cohen, S.; Froelich, L.; Katayama, S.; Sabbagh, M.; Vellas, B.; Watson, D.; Dhadda, S.; Irizarry, M.; Kramer, L. D.; Iwatsubo, T., Lecanemab in Early Alzheimer's Disease. *New England Journal of Medicine* **2022,** *388* (1), 9-21.

151. Cummings, J.; Lee, G.; Nahed, P.; Kambar, M. E. Z. N.; Zhong, K.; Fonseca, J.; Taghva, K., Alzheimer's disease drug development pipeline: 2022. *Alzheimer's & Dementia: Translational Research & Clinical Interventions* **2022,** *8* (1), e12295.
152. Rogers, D. R., Screening for Amyloid with the Thioflavin-T Fluorescent Method. *American Journal of Clinical Pathology* **1965,** *44* (1), 59-61.
153. Krebs, M. R. H.; Bromley, E. H. C.; Donald, A. M., The binding of thioflavin-T to amyloid fibrils: localisation and implications. *Journal of Structural Biology* **2005,** *149* (1), 30-37.
154. Stsiapura, V. I.; Maskevich, A. A.; Kuzmitsky, V. A.; Uversky, V. N.; Kuznetsova, I. M.; Turoverov, K. K., Thioflavin T as a Molecular Rotor: Fluorescent Properties of Thioflavin T in Solvents with Different Viscosity. *The Journal of Physical Chemistry B* **2008,** *112* (49), 15893-15902.
155. Amdursky, N.; Erez, Y.; Huppert, D., Molecular Rotors: What Lies Behind the High Sensitivity of the Thioflavin-T Fluorescent Marker. *Acc. Chem. Res.* **2012,** *45*, 1548.
156. Stsiapura, V. I.; Maskevich, A. A.; Kuzmitsky, V. A.; Turoverov, K. K.; Kuznetsova, I. M., Computational Study of Thioflavin T Torsional Relaxation in the Excited State. *The Journal of Physical Chemistry A* **2007,** *111* (22), 4829-4835.
157. Stsiapura, V. I.; Maskevich, A. A.; Tikhomirov, S. A.; Buganov, O. V., Charge Transfer Process Determines Ultrafast Excited State Deactivation of Thioflavin T in Low-Viscosity Solvents. *The Journal of Physical Chemistry A* **2010,** *114* (32), 8345-8350.
158. Sulatskaya, A. I.; Maskevich, A. A.; Kuznetsova, I. M.; Uversky, V. N.; Turoverov, K. K., Fluorescence quantum yield of thioflavin T in rigid isotropic solution and incorporated into the amyloid fibrils. *PLoS One* **2010,** *5* (10), e15385.
159. Arosio, P.; Michaels, T. C. T.; Linse, S.; Månsson, C.; Emanuelsson, C.; Presto, J.; Johansson, J.; Vendruscolo, M.; Dobson, C. M.; Knowles, T. P. J., Kinetic analysis reveals the diversity of microscopic mechanisms through which molecular chaperones suppress amyloid formation. *Nature Communications* **2016,** *7* (1), 10948.
160. Cohen, S. I. A.; Linse, S.; Luheshi, L. M.; Hellstrand, E.; White, D. A.; Rajah, L.; Otzen, D. E.; Vendruscolo, M.; Dobson, C. M.; Knowles, T. P. J., Proliferation of amyloid-β42 aggregates occurs through a secondary nucleation mechanism. *Proceedings of the National Academy of Sciences* **2013,** *110* (24), 9758-9763.
161. Meisl, G.; Yang, X.; Hellstrand, E.; Frohm, B.; Kirkegaard, J. B.; Cohen, S. I. A.; Dobson, C. M.; Linse, S.; Knowles, T. P. J., Differences in nucleation behavior underlie the contrasting aggregation kinetics of the Aβ40 and Aβ42 peptides. *Proceedings of the National Academy of Sciences* **2014,** *111* (26), 9384-9389.
162. Groenning, M.; Norrman, M.; Flink, J. M.; van de Weert, M.; Bukrinsky, J. T.; Schluckebier, G.; Frokjaer, S., Binding mode of Thioflavin T in insulin amyloid fibrils. *J Struct Biol* **2007,** *159* (3), 483-97.
163. Kuznetsova, I. M.; Sulatskaya, A. I.; Uversky, V. N.; Turoverov, K. K., Analyzing Thioflavin T Binding to Amyloid Fibrils by an Equilibrium Microdialysis-Based Technique. *PLOS ONE* **2012,** *7* (2), e30724.
164. Frieg, B.; Gremer, L.; Heise, H.; Willbold, D.; Gohlke, H., Binding modes of thioflavin T and Congo red to the fibril structure of amyloid-β(1–42). *Chemical Communications* **2020,** *56* (55), 7589-7592.

165. Sulatskaya, A. I.; Rychkov, G. N.; Sulatsky, M. I.; Mikhailova, E. V.; Melnikova, N. M.; Andozhskaya, V. S.; Kuznetsova, I. M.; Turoverov, K. K. New Evidence on a Distinction between Aβ40 and Aβ42 Amyloids: Thioflavin T Binding Modes, Clustering Tendency, Degradation Resistance, and Cross-Seeding *International Journal of Molecular Sciences* [Online], 2022.
166. Sulatskaya, A. I.; Rodina, N. P.; Sulatsky, M. I.; Povarova, O. I.; Antifeeva, I. A.; Kuznetsova, I. M.; Turoverov, K. K. Investigation of α-Synuclein Amyloid Fibrils Using the Fluorescent Probe Thioflavin T *International Journal of Molecular Sciences* [Online], 2018.
167. Ziaunys, M.; Smirnovas, V., Additional Thioflavin-T Binding Mode in Insulin Fibril Inner Core Region. *J Phys Chem B* **2019,** *123* (41), 8727-8732.
168. Hudson, S. A.; Ecroyd, H.; Kee, T. W.; Carver, J. A., The thioflavin T fluorescence assay for amyloid fibril detection can be biased by the presence of exogenous compounds. *The FEBS Journal* **2009,** *276* (20), 5960-5972.
169. Mikalauskaite, K.; Ziaunys, M.; Sneideris, T.; Smirnovas, V., Effect of Ionic Strength on Thioflavin-T Affinity to Amyloid Fibrils and Its Fluorescence Intensity. *Int J Mol Sci* **2020,** *21* (23).
170. Sabaté, R.; Lascu, I.; Saupe, S. J., On the binding of Thioflavin-T to HET-s amyloid fibrils assembled at pH 2. *Journal of Structural Biology* **2008,** *162* (3), 387-396.
171. Hackl, E. V.; Darkwah, J.; Smith, G.; Ermolina, I., Effect of acidic and basic pH on Thioflavin T absorbance and fluorescence. *European Biophysics Journal* **2015,** *44* (4), 249-261.
172. Klunk, W. E.; Wang, Y.; Huang, G.-f.; Debnath, M. L.; Holt, D. P.; Mathis, C. A., Uncharged thioflavin-T derivatives bind to amyloid-beta protein with high affinity and readily enter the brain. *Life Sciences* **2001,** *69* (13), 1471-1484.
173. Hanczyc, P.; Rajchel-Mieldzioc, P.; Feng, B.; Fita, P., Identification of Thioflavin T Binding Modes to DNA: A Structure-Specific Molecular Probe for Lasing Applications. *J Phys Chem Lett* **2021,** *12* (22), 5436-5442.
174. Verma, S.; Ghuge, S. A.; Ravichandiran, V.; Ranjan, N., Spectroscopic studies of Thioflavin-T binding to c-Myc G-quadruplex DNA. *Spectrochimica Acta Part A: Molecular and Biomolecular Spectroscopy* **2019,** *212*, 388-395.
175. Sugimoto, S.; Arita-Morioka, K.; Mizunoe, Y.; Yamanaka, K.; Ogura, T., Thioflavin T as a fluorescence probe for monitoring RNA metabolism at molecular and cellular levels. *Nucleic Acids Res* **2015,** *43* (14), e92.
176. Xu, S.; Li, Q.; Xiang, J.; Yang, Q.; Sun, H.; Guan, A.; Wang, L.; Liu, Y.; Yu, L.; Shi, Y.; Chen, H.; Tang, Y., Thioflavin T as an efficient fluorescence sensor for selective recognition of RNA G-quadruplexes. *Scientific Reports* **2016,** *6* (1), 24793.
177. Zunbul, Z.; An, J.; Aziz, H.; Shin, J.; Lim, S.; Yu, L.; Kim, Y. K.; Kim, J. S., Tailoring Hydrophobicity of Thioflavin T to Optimize Aβ Fibril Bioimaging. *Advanced NanoBiomed Research* **2023,** *3* (6), 2200161.
178. Lavysh, A. V.; Sulatskaya, A. I.; Lugovskii, A. A.; Voropay, E. S.; Kuznetsova, I. M.; Turoverov, K. K.; Maskevich, A. A., Photophysical Properties of Trans-2-[4-(dimethylamino)styryl]-3-ethyl-1,3-benzothiazolium Perchlorate, a New Structural Analog of Thioflavin T. *Journal of Applied Spectroscopy* **2014,** *81* (2), 205-213.

179. Sulatskaya, A. I.; Sulatsky, M. I.; Antifeeva, I. A.; Kuznetsova, I. M.; Turoverov, K. K., Structural Analogue of Thioflavin T, DMASEBT, as a Tool for Amyloid Fibrils Study. *Anal Chem* **2019,** *91* (4), 3131-3140.
180. Lin, P. H.; Tsai, C. S.; Hsu, C. C.; Lee, I. R.; Shen, Y. X.; Fan, H. F.; Chen, Y. W.; Tu, L. H.; Liu, W. M., An environmentally sensitive molecular rotor as a NIR fluorescent probe for the detection of islet amyloid polypeptide. *Talanta* **2023,** *254*, 124130.
181. Gaur, P.; Galkin, M.; Kurochka, A.; Ghosh, S.; Yushchenko, D. A.; Shvadchak, V. V., Fluorescent Probe for Selective Imaging of alpha-Synuclein Fibrils in Living Cells. *ACS Chem Neurosci* **2021,** *12* (8), 1293-1298.
182. Needham, L.-M.; Weber, J.; Pearson, C. M.; Do, D. T.; Gorka, F.; Lyu, G.; Bohndiek, S. E.; Snaddon, T. N.; Lee, S. F., A Comparative Photophysical Study of Structural Modifications of Thioflavin T-Inspired Fluorophores. *The Journal of Physical Chemistry Letters* **2020,** *11* (19), 8406-8416.
183. Sutharsan, J.; Dakanali, M.; Capule, C. C.; Haidekker, M. A.; Yang, J.; Theodorakis, E. A., Rational Design of Amyloid Binding Agents Based on the Molecular Rotor Motif. *ChemMedChem* **2010,** *5* (1), 56-60.
184. Loving, G. S.; Sainlos, M.; Imperiali, B., Monitoring protein interactions and dynamics with solvatochromic fluorophores. *Trends in Biotechnology* **2010,** *28* (2), 73-83.
185. Li, L.; Lv, Z.; Man, Z.; Xu, Z.; Wei, Y.; Geng, H.; Fu, H., Polarity-active NIR probes with strong two-photon absorption and ultrahigh binding affinity of insulin amyloid fibrils. *Chem Sci* **2021,** *12* (9), 3308-3313.
186. Venkatesh, Y.; Marotta, N. P.; Lee, V. M. Y.; Petersson, E. J., Highly tunable bimane-based fluorescent probes: design, synthesis, and application as a selective amyloid binding dye. *Chemical Science* **2024,** *15* (16), 6053-6063.
187. Chang, W. M.; Dakanali, M.; Capule, C. C.; Sigurdson, C. J.; Yang, J.; Theodorakis, E. A., ANCA: A Family of Fluorescent Probes that Bind and Stain Amyloid Plaques in Human Tissue. *ACS Chem Neurosci* **2011,** *2* (5), 249-255.
188. Xu, M.; Li, R.; Li, X.; Lv, G.; Li, S.; Sun, A.; Zhou, Y.; Yi, T., NIR fluorescent probes with good water-solubility for detection of amyloid beta aggregates in Alzheimer's disease. *J Mater Chem B* **2019,** *7* (36), 5535-5540.
189. Cao, K.; Farahi, M.; Dakanali, M.; Chang, W. M.; Sigurdson, C. J.; Theodorakis, E. A.; Yang, J., Aminonaphthalene 2-cyanoacrylate (ANCA) probes fluorescently discriminate between amyloid-beta and prion plaques in brain. *J Am Chem Soc* **2012,** *134* (42), 17338-41.
190. Chen, Y.; Ouyang, Q.; Li, Y.; Zeng, Q.; Dai, B.; Liang, Y.; Chen, B.; Tan, H.; Cui, M., Evaluation of N, O-Benzamide difluoroboron derivatives as near-infrared fluorescent probes to detect beta-amyloid and tau tangles. *Eur J Med Chem* **2022,** *227*, 113968.
191. Chen, Y.; Yuan, C.; Xie, T.; Li, Y.; Dai, B.; Zhou, K.; Liang, Y.; Dai, J.; Tan, H.; Cui, M., N,O-Benzamide difluoroboron complexes as near-infrared probes for the detection of beta-amyloid and tau fibrils. *Chem Commun (Camb)* **2020,** *56* (53), 7269-7272.
192. Ran, C.; Xu, X.; Raymond, S. B.; Ferrara, B. J.; Neal, K.; Bacskai, B. J.; Medarova, Z.; Moore, A., Design, Synthesis, and Testing of Difluoroboron-Derivatized Curcumins as

Near-Infrared Probes for in Vivo Detection of Amyloid-β Deposits. *Journal of the American Chemical Society* **2009,** *131* (42), 15257-15261.
193. Klunk, W. E.; Bacskai, B. J.; Mathis, C. A.; Kajdasz, S. T.; McLellan, M. E.; Frosch, M. P.; Debnath, M. L.; Holt, D. P.; Wang, Y.; Hyman, B. T., Imaging Aβ Plaques in Living Transgenic Mice with Multiphoton Microscopy and Methoxy-X04, a Systemically Administered Congo Red Derivative. *Journal of Neuropathology & Experimental Neurology* **2002,** *61* (9), 797-805.
194. Heo, C. H.; Kim, K. H.; Kim, H. J.; Baik, S. H.; Song, H.; Kim, Y. S.; Lee, J.; Mook-jung, I.; Kim, H. M., A two-photon fluorescent probe for amyloid-β plaques in living mice. *Chemical Communications* **2013,** *49* (13), 1303-1305.
195. Heo, C. H.; Sarkar, A. R.; Baik, S. H.; Jung, T. S.; Kim, J. J.; Kang, H.; Mook-Jung, I.; Kim, H. M., A quadrupolar two-photon fluorescent probe for in vivo imaging of amyloid-β plaques. *Chemical Science* **2016,** *7* (7), 4600-4606.
196. Kim, D.; Moon, H.; Baik, S. H.; Singha, S.; Jun, Y. W.; Wang, T.; Kim, K. H.; Park, B. S.; Jung, J.; Mook-Jung, I.; Ahn, K. H., Two-Photon Absorbing Dyes with Minimal Autofluorescence in Tissue Imaging: Application to in Vivo Imaging of Amyloid-β Plaques with a Negligible Background Signal. *Journal of the American Chemical Society* **2015,** *137* (21), 6781-6789.
197. Zhang, X.; Tian, Y.; Yuan, P.; Li, Y.; Yaseen, M. A.; Grutzendler, J.; Moore, A.; Ran, C., A bifunctional curcumin analogue for two-photon imaging and inhibiting crosslinking of amyloid beta in Alzheimer's disease. *Chemical Communications* **2014,** *50* (78), 11550-11553.
198. Xueli Zhanga; Yanli Tiana; Can Zhange; Xiaoyu Tianf; Alana W. Rossa; Robert D. Moire; Hongbin Sunb; Rudolph E. Tanzie; Anna Moorea; Rana, C., Near-infrared fluorescence molecular imaging of amyloid beta species and monitoring therapy in animal models of Alzheimer's disease. *PNAS* **2015,** *112*, 9734–9739.
199. Calvo-Rodriguez, M.; Hou, S. S.; Snyder, A. C.; Dujardin, S.; Shirani, H.; Nilsson, K. P. R.; Bacskai, B. J., In vivo detection of tau fibrils and amyloid β aggregates with luminescent conjugated oligothiophenes and multiphoton microscopy. *Acta Neuropathologica Communications* **2019,** *7* (1), 171.
200. Klunk, W. E.; Engler, H.; Nordberg, A.; Wang, Y. M.; Blomqvist, G.; Holt, D. P.; Bergström, M.; Savitcheva, I.; Huang, G. F.; Estrada, S.; Ausén, B.; Debnath, M. L.; Barletta, J.; Price, J. C.; Sandell, J.; Lopresti, B. J.; Wall, A.; Koivisto, P.; Antoni, G.; Mathis, C. A.; Långström, B., Imaging brain amyloid in Alzheimer's disease with Pittsburgh Compound-B. *ANNALS OF NEUROLOGY* **2004,** *55* (3), 306-319.
201. Oakley, H.; Cole, S. L.; Logan, S.; Maus, E.; Shao, P.; Craft, J.; Guillozet-Bongaarts, A.; Ohno, M.; Disterhoft, J.; Van Eldik, L.; Berry, R.; Vassar, R., Intraneuronal β-Amyloid Aggregates, Neurodegeneration, and Neuron Loss in Transgenic Mice with Five Familial Alzheimer Disease Mutations: Potential Factors in Amyloid Plaque Formation. *The Journal of Neuroscience* **2006,** *26* (40), 10129.
202. Shin, J.; Verwilst, P.; Choi, H.; Kang, S.; Han, J.; Kim, N. H.; Choi, J. G.; Oh, M. S.; Hwang, J. S.; Kim, D.; Mook-Jung, I.; Kim, J. S., Harnessing Intramolecular Rotation To Enhance Two-photon Imaging of Aβ Plaques through Minimizing Background Fluorescence. *Angewandte Chemie International Edition* **2019,** *58* (17), 5648-5652.

203. Choi, J. W.; Ju, Y. H.; Choi, Y.; Hyeon, S. J.; Gadhe, C. G.; Park, J. H.; Kim, M. S.; Baek, S.; Kim, Y.; Park, K. D.; Pae, A. N.; Ryu, H.; Lee, C. J.; Cho, B. R., PyrPeg, a Blood-Brain-Barrier-Penetrating Two-Photon Imaging Probe, Selectively Detects Neuritic Plaques, Not Tau Aggregates. *ACS CHEMICAL NEUROSCIENCE* **2020,** *11* (12), 1801-1810.
204. Ju, Y. H.; Bhalla, M.; Hyeon, S. J.; Oh, J. E.; Yoo, S.; Chae, U.; Kwon, J.; Koh, W.; Lim, J.; Park, Y. M.; Lee, J.; Cho, I.-J.; Lee, H.; Ryu, H.; Lee, C. J., Astrocytic urea cycle detoxifies Aβ-derived ammonia while impairing memory in Alzheimer's disease. *Cell Metabolism* **2022,** *34* (8), 1104-1120.e8.
205. Neto, B. A. D.; Correa, J. R.; Spencer, J., Fluorescent Benzothiadiazole Derivatives as Fluorescence Imaging Dyes: A Decade of New Generation Probes. *Chemistry – A European Journal* **2022,** *28* (4), e202103262.
206. Chen, M.; Zhang, Z.; Shi, Z.; Sun, J.; Gao, F., A facile two-photon red-emission fluorescent marker with a large Stokes shift for in vivo brain imaging of amyloid-beta aggregates. *Cell Reports Physical Science* **2024,** *5* (2), 101810.
207. Schwarze, T.; Riemer, J.; Eidner, S.; Holdt, H.-J., A Highly K+-Selective Two-Photon Fluorescent Probe. *Chemistry – A European Journal* **2015,** *21* (32), 11306-11310.
208. Yu, F. T.; Huang, Z.; Yang, J. X.; Yang, L. M.; Xu, X. Y.; Huang, J. Y.; Kong, L., Two quinoline-based two-photon fluorescent probes for imaging of viscosity in subcellular organelles of living HeLa cells. *Spectrochim Acta A Mol Biomol Spectrosc* **2022,** *283*, 121769.
209. Hornum, M.; Reinholdt, P.; Zaręba, J. K.; Jensen, B. B.; Wüstner, D.; Samoć, M.; Nielsen, P.; Kongsted, J., One- and two-photon solvatochromism of the fluorescent dye Nile Red and its CF3, F and Br-substituted analogues. *Photochemical & Photobiological Sciences* **2020,** *19* (10), 1382-1391.
210. Doan, P. H.; Pitter, D. R.; Kocher, A.; Wilson, J. N.; Goodson, T., 3rd, Two-Photon Spectroscopy as a New Sensitive Method for Determining the DNA Binding Mode of Fluorescent Nuclear Dyes. *J Am Chem Soc* **2015,** *137* (29), 9198-201.
211. Drobizhev, M.; Makarov, N. S.; Tillo, S. E.; Hughes, T. E.; Rebane, A., Two-photon absorption properties of fluorescent proteins. *Nature Methods* **2011,** *8* (5), 393-399.
212. Olesiak-Banska, J.; Waszkielewicz, M.; Matczyszyn, K.; Samoc, M., A closer look at two-photon absorption, absorption saturation and nonlinear refraction in gold nanoclusters. *RSC Advances* **2016,** *6* (101), 98748-98752.
213. Cerretani, C.; Palm-Henriksen, G.; Liisberg, M. B.; Vosch, T., The effect of deuterium on the photophysical properties of DNA-stabilized silver nanoclusters. *Chemical Science* **2021,** *12* (48), 16100-16105.
214. Chen, J.; Kumar, A.; Cerretani, C.; Vosch, T.; Zigmantas, D.; Thyrhaug, E., Excited-State Dynamics in a DNA-Stabilized Ag16 Cluster with Near-Infrared Emission. *The Journal of Physical Chemistry Letters* **2023,** *14* (17), 4078-4083.
215. Drobizhev, M.; Tillo, S.; Makarov, N. S.; Hughes, T. E.; Rebane, A., Absolute Two-Photon Absorption Spectra and Two-Photon Brightness of Orange and Red Fluorescent Proteins. *The Journal of Physical Chemistry B* **2009,** *113* (4), 855-859.

216. Kobat, D.; Durst, M. E.; Nishimura, N.; Wong, A. W.; Schaffer, C. B.; Xu, C., Deep tissue multiphoton microscopy using longer wavelength excitation. *Optics Express* **2009,** *17* (16), 13354-13364.
217. Berezin, M. Y.; Zhan, C.; Lee, H.; Joo, C.; Akers, W. J.; Yazdanfar, S.; Achilefu, S., Two-Photon Optical Properties of Near-Infrared Dyes at 1.55 μm Excitation. *The Journal of Physical Chemistry B* **2011,** *115* (39), 11530-11535.
218. Das, A.; Dutta, T.; Gadhe, L.; Koner, A. L.; Saraogi, I., Biocompatible Fluorescent Probe for Selective Detection of Amyloid Fibrils. *Analytical Chemistry* **2020,** *92* (15), 10336-10341.
219. Fu, H.; Cui, M.; Zhao, L.; Tu, P.; Zhou, K.; Dai, J.; Liu, B., Highly Sensitive Near-Infrared Fluorophores for in Vivo Detection of Amyloid-β Plaques in Alzheimer's Disease. *Journal of Medicinal Chemistry* **2015,** *58* (17), 6972-6983.
220. Chen, C.; Liang, Z.; Zhou, B.; Li, X.; Lui, C.; Ip, N. Y.; Qu, J. Y., In Vivo Near-Infrared Two-Photon Imaging of Amyloid Plaques in Deep Brain of Alzheimer's Disease Mouse Model. *ACS Chemical Neuroscience* **2018,** *9* (12), 3128-3136.
221. Jun, Y. W.; Cho, S. W.; Jung, J.; Huh, Y.; Kim, Y.; Kim, D.; Ahn, K. H., Frontiers in Probing Alzheimer's Disease Biomarkers with Fluorescent Small Molecules. *ACS Central Science* **2019,** *5* (2), 209-217.
222. Su, D.; Diao, W.; Li, J.; Pan, L.; Zhang, X.; Wu, X.; Mao, W., Strategic Design of Amyloid-beta Species Fluorescent Probes for Alzheimer's Disease. *ACS Chem Neurosci* **2022,** *13* (5), 540-551.
223. Rybczyński, P.; Hajda, A.; Zaleśny, R.; Ośmiałowski, B.; Olesiak-Bańska, J., Thioflavin T Inspirations: On the Photophysical and Aggregation Properties of Fluorescent Difluoroborates Based on the Benzothiazole Core. *The Journal of Physical Chemistry A* **2025,** *129* (16), 3663-3671.
224. Jumper, J.; Evans, R.; Pritzel, A.; Green, T.; Figurnov, M.; Ronneberger, O.; Tunyasuvunakool, K.; Bates, R.; Žídek, A.; Potapenko, A.; Bridgland, A.; Meyer, C.; Kohl, S. A. A.; Ballard, A. J.; Cowie, A.; Romera-Paredes, B.; Nikolov, S.; Jain, R.; Adler, J.; Back, T.; Petersen, S.; Reiman, D.; Clancy, E.; Zielinski, M.; Steinegger, M.; Pacholska, M.; Berghammer, T.; Bodenstein, S.; Silver, D.; Vinyals, O.; Senior, A. W.; Kavukcuoglu, K.; Kohli, P.; Hassabis, D., Highly accurate protein structure prediction with AlphaFold. *Nature* **2021,** *596* (7873), 583-589.
225. Beker, W.; Roszak, R.; Wołos, A.; Angello, N. H.; Rathore, V.; Burke, M. D.; Grzybowski, B. A., Machine Learning May Sometimes Simply Capture Literature Popularity Trends: A Case Study of Heterocyclic Suzuki–Miyaura Coupling. *Journal of the American Chemical Society* **2022,** *144* (11), 4819-4827.
226. Back, S.; Aspuru-Guzik, A.; Ceriotti, M.; Gryn'ova, G.; Grzybowski, B.; Gu, G. H.; Hein, J.; Hippalgaonkar, K.; Hormázabal, R.; Jung, Y.; Kim, S.; Kim, W. Y.; Moosavi, S. M.; Noh, J.; Park, C.; Schrier, J.; Schwaller, P.; Tsuda, K.; Vegge, T.; von Lilienfeld, O. A.; Walsh, A., Accelerated chemical science with AI. *Digital Discovery* **2024,** *3* (1), 23-33.
227. Strieth-Kalthoff, F.; Hao, H.; Rathore, V.; Derasp, J.; Gaudin, T.; Angello, N. H.; Seifrid, M.; Trushina, E.; Guy, M.; Liu, J.; Tang, X.; Mamada, M.; Wang, W.; Tsagaantsooj, T.; Lavigne, C.; Pollice, R.; Wu, T. C.; Hotta, K.; Bodo, L.; Li, S.; Haddadnia, M.; Wołos, A.; Roszak, R.; Ser, C. T.; Bozal-Ginesta, C.; Hickman, R. J.; Vestfrid, J.; Aguilar-Granda, A.;

Klimareva, E. L.; Sigerson, R. C.; Hou, W.; Gahler, D.; Lach, S.; Warzybok, A.; Borodin, O.; Rohrbach, S.; Sanchez-Lengeling, B.; Adachi, C.; Grzybowski, B. A.; Cronin, L.; Hein, J. E.; Burke, M. D.; Aspuru-Guzik, A., Delocalized, asynchronous, closed-loop discovery of organic laser emitters. *Science 384* (6697), eadk9227.